Research Report

Drop-In Top Flange Connection

FINAL REPORT

AISC RESEARCH REPORT NO. AISC-IRR-NFS-2025-01
MARCH 2025

Project Title:	**Drop-In Top Flange Connection**
Primary Investigator(s):	**Matthew Yarnold, Ph.D, P.E.**
	Kadir Sener, Ph.D., P.E.
Research Organization(s):	**Auburn University**

DISCLAIMER

The material contained herein has been developed by researchers based on their research findings and is for general information only. The information in it should not be used without first securing competent advice with respect to its suitability for any given application. The publication of the information is not intended as a representation or warranty on the part of the American Institute of Steel Construction (AISC) or of any other person named herein, that the information is suitable for any general or particular use or of freedom from infringement of any patent or patents. Anyone making use of the information assumes all liability arising from such use.

PREFACE

The American Institute of Steel Construction (AISC), headquartered in Chicago, is a non-partisan, not-for-profit technical institute and trade association established in 1921 to serve the structural steel design community and construction industry in the United States. As part of its technical activities, AISC actively funds and supports research related to structural steel design and construction. AISC members primarily come from the structural steel construction community, including producers, fabricators, and engineers.

Many AISC members are engineers, so much of our research supports the engineering community, including maintaining and updating our technical publications such as Design Guides, The Steel Construction Manual, and our Specifications and Provisions. We distribute our specifications free for their use. The primary goal of those specifications is the reliability of structures and, through that, the safety of the public.

AISC does not use the results of research for profit, nor do we sell reports of the research or derivatives from it. Our work is performed in the interest of public safety. As such, we fund projects to, in part, support the development of next-generation steel systems for enhanced performance, safety, sustainability, and economy.

It is reasonably common for AISC research projects to receive additional direct, indirect, or in-kind support from external organizations such as federal or state agencies or member companies . As such, the partial or complete contents of this Report may also reside in the public domain of these external funding agencies.

Drop-In Top Flange Connection

Final Report

PI - Matthew Yarnold, Ph.D., P.E.
Auburn University, Director of the Advanced Structural Engineering Laboratory and
Associate Professor in the Department of Civil & Environmental Engineering

Co-PI - Kadir Sener, Ph.D., P.E.
Auburn University, Assistant Professor in the Department of Civil & Environmental Engineering

Researcher - Robel Alemayehu, Ph.D.
Auburn University, Postdoctoral Fellow in the Department of Civil & Environmental Engineering

Researcher - Emily Doody, E.I.
Auburn University, Graduate Student in the Department of Civil & Environmental Engineering

Presented to the American Institute of Steel Construction

Submission: March 7, 2025

Table of Contents

Abstract

Drop-in top flange shear connections were studied as an erector-friendly alternative to single plate connections (shear tabs), double-angle connections, and seated connections. The research and development of this novel connection included initial concept development, full-scale testing of 12 connections, and extensive numerical modeling. The study found that drop-in top flange connections are viable connections with adequate shear strength, rotational ductility, and stability for multi-story residential and commercial construction. As a result, design guidance was developed in the form of a design methodology, design tables, and design examples for future implementation.

Motivation and Scope

The American Institute of Steel Construction (AISC) has an ambitious program called "Need for Speed," which aims to make steel construction 50% faster by the end of 2025 (Huber and Colsia 2025). Structural steel frame buildings are commonly considered the faster alternative over reinforced concrete. The Need for Speed initiative doubles down on this aspect of steel construction. The intent is for developers to realize the economic benefit of opening a facility faster, subsequently choosing steel.

A critical aspect of structural steel buildings is the connections. This is in terms of structural performance as well as speed of erection. The focus area of this research study was to ***increase the erection speed of conventional shear connections for multi-story residential and commercial facilities while maintaining structural performance***. This research encompasses girder-column, beam-column, and steel-concrete wall connections. Extended beam-girder connections were identified as future research.

Concept

The most common shear connections in steel framing are single plate connections (or shear tabs). Shear tabs essentially connect two structural steel elements with a plate welded to one element and typically bolted to the other. Figure 1(a) illustrates a girder-column shear tab connection. Other common alternatives include double-angle and seated connections (outside the flanges).

The new concept developed as part of this study is a ***drop-in top flange connection*** where the girder/beam is seated on the bottom of the top flange, as shown in Figure 1(b). For drop-in top flange connections, angles are shop welded to a steel element (e.g., column), and the girder/beam is coped on the bottom flange to allow for a simple vertical drop-in erection. The final connection is made via vertical bolts (not horizontal), attaching the top flange of the girder/beam to the angles.

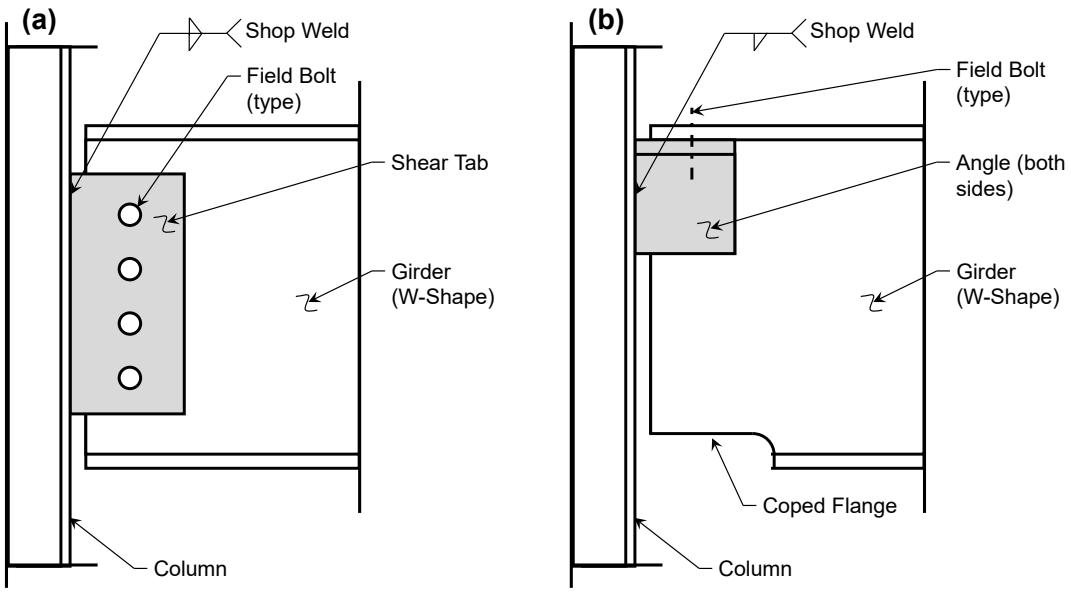

Figure 1: General Illustrative Comparison between a (a) Conventional Shear Tab Connection and (b) the Drop-In Top Flange Seated Connection

Research Goals

The overarching goal of this study is to fully develop the drop-in top flange connection, which aims to increase the erection speed of conventional shear connections (not including extended connections) while maintaining structural performance. The specific goals include:

1. Experimentally evaluate the drop-in connection structural performance through full-scale testing.
2. Numerically evaluate the drop-in connection further through refined finite element analysis (FEA). This includes stability analysis.
3. Develop a design methodology for drop-in connections.
4. Create detailed design examples for practicing engineers.
5. Develop design tables for practicing engineers.
6. Identify the advantages/disadvantages of drop-in connections over conventional alternatives to guide engineers on where they should be utilized.

Research Summary

The approach to accomplish the goals stated earlier was to divide the research study into four main phases. Phase 1 performed preliminary analysis and further developed the drop-in top flange connection concept. This information was utilized within Phase 2 where the experimental testing program was performed, which included 12 full-scale connection tests. Phase 3 focused on a refined analysis of drop-in connections where the experimental results were used to validate the modeling approach. Finally, Phase 4 developed design guidance for future engineers through a drop-in top flange connection design methodology, design examples, and design tables. Each phase of the research study is discussed in detail below.

Phase 1 - A-priori Analysis and Concept Development

Purpose and Approach

The primary purpose of this phase was to develop the initial details for the drop-in top flange connection concept. Critical parameters were identified for fabrication, fit-up, erection, and structural performance. Realistic member sizes, design loads, and dimensions were established for multi-story residential and commercial facilities by referencing a benchmark building. These parameters were utilized to design the experimental testing in the following phase.

Benchmark Designs

The benchmark building was selected from AISC's steel solutions center example, "*Conventional Steel Framing Study*" for office buildings (AISC 2018). Highlighted in Figure 2, a W24x68 girder with a span length of 30' and spacing of 45'-6'' was deemed appropriate for a drop-in connection. The loading provided in the AISC document resulted in factored girder-column and beam-column reactions of 78 kips and 39 kips, respectively. A column size of W14x82 was chosen from the design example.

The benchmark girder-column shear tab and drop-in top flange connections are provided in Figure 3. Elevation views are provided to scale to compare the shear tab and drop-in connection directly. In addition, Figure 4 shows further details for the drop-in top flange connection. Note that these connections were fabricated and tested in Phase 2 below.

The connections were designed using the AISC Steel Construction Manual (AISC 2017) and the ANSI/AISC 360-22 Specification (ANSI/AISC 2022). Since there was limited design guidance for drop-in connections, assumptions were made for several limit states. These assumptions proved to be conservative, resulting in relatively large angles. The final design guidance is provided later under Phase 4, which would produce a more efficient design for the reactions noted above.

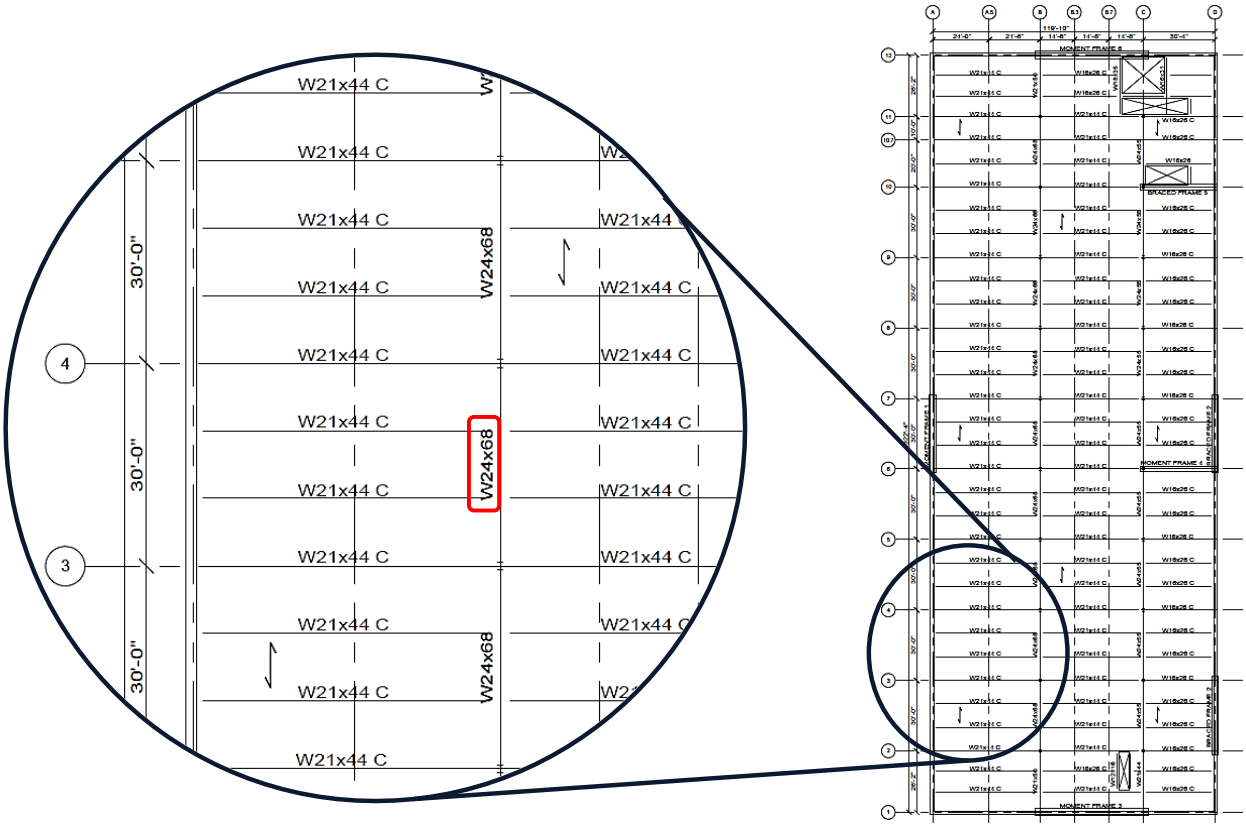

Figure 2: Girder Selected from the AISC Conventional Steel Framing Study for Office Buildings (AISC 2018)

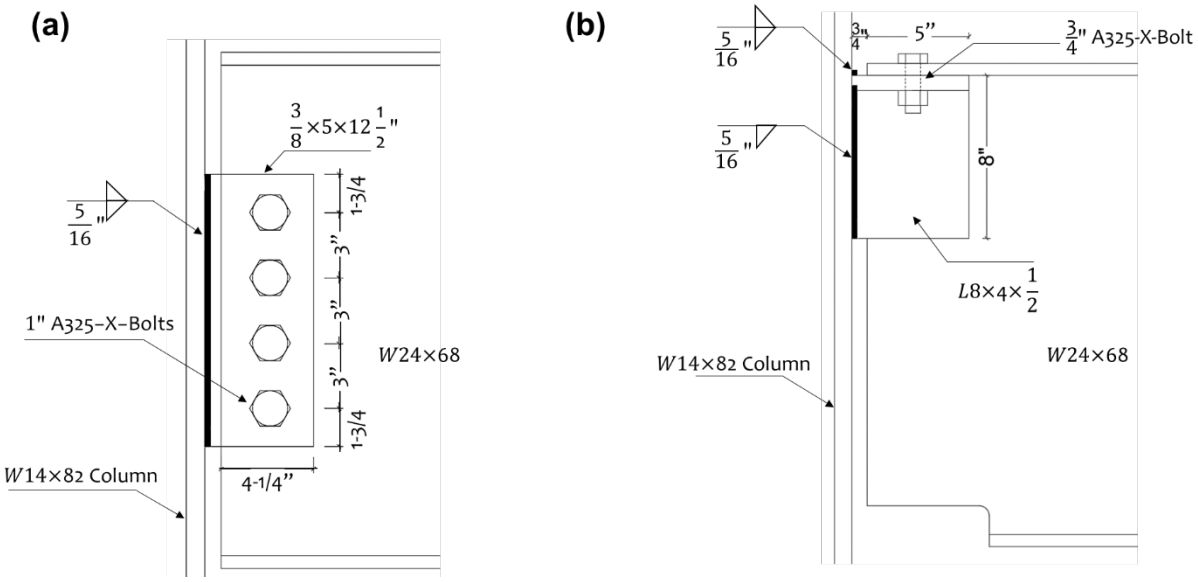

Figure 3: W24x68 Benchmark Designs for a Girder-Column (a) Shear Tab Connection and (b) Drop-In Top Flange Connection

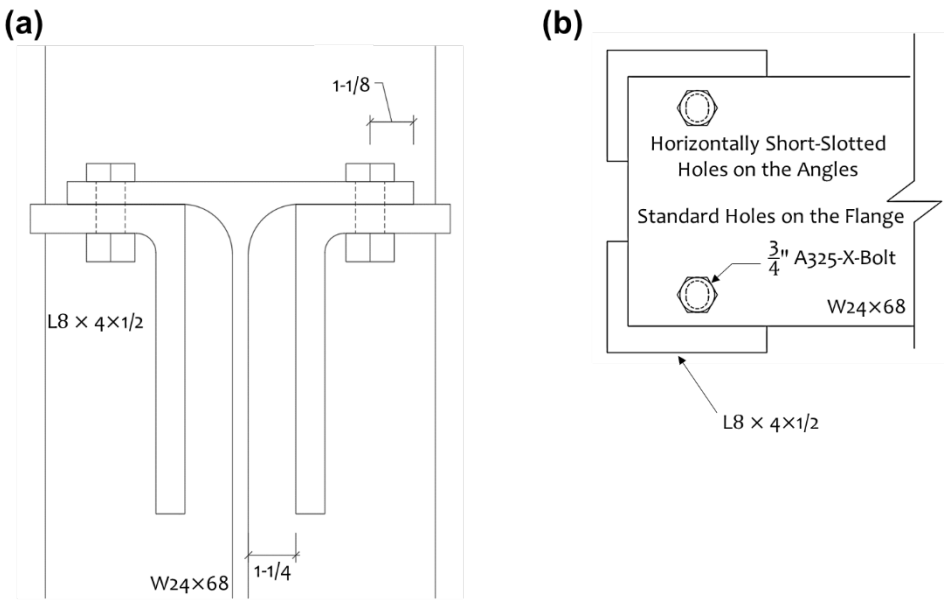

Figure 4: Benchmark Drop-In Top Flange Connection (a) Section View and (b) Plan View

Utilizing the same benchmark building design loads and a modified (smaller) building layout, a W16x36 girder with a spacing and span length of 30' was chosen to investigate a relatively small girder-column connection with a factored reaction of 52 kips. Figure 5 provides an elevation view of both benchmark connection designs. Note that only the drop-in top flange connection for the W16x36 girder was tested in Phase 2.

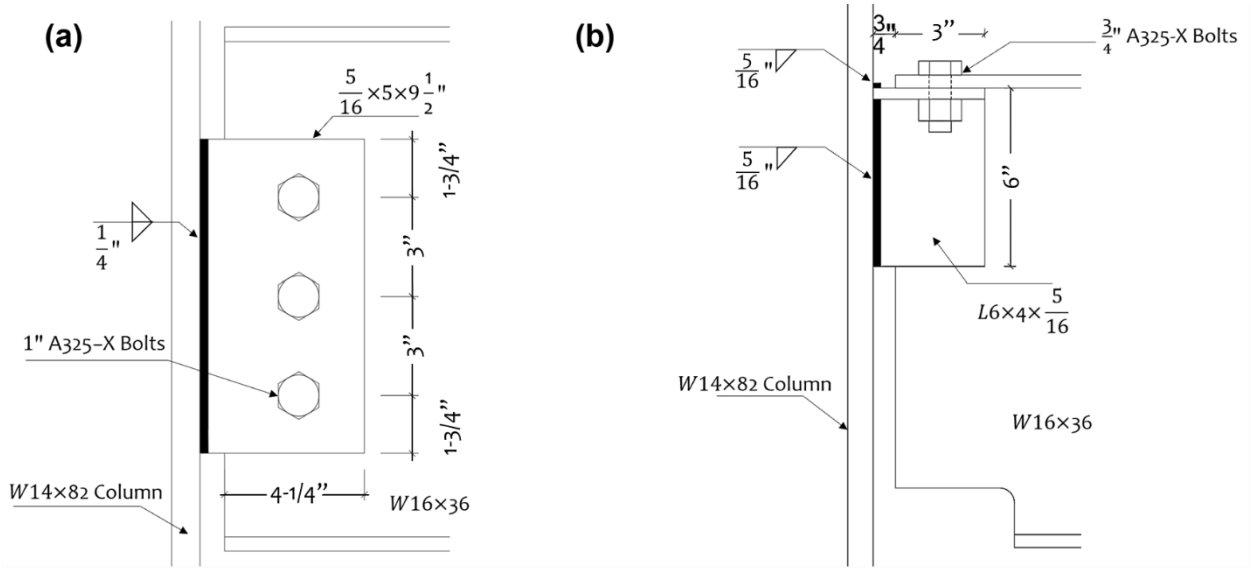

Figure 5: W16x36 Benchmark Designs for a Girder-Column (a) Shear Tab Connection and (b) Drop-In Top Flange Connection

The following critical parameters were identified after completing the drop-in design calculations and several meetings with the industry panel. These parameters were evaluated through experimental testing (Phase 2) and/or refined finite element analysis (Phase 3).

1. Angle size
2. Weld geometry and thickness
3. Bolt pretension
4. Beam/girder size
5. Angle orientation (mirrored)
6. Angle spacing
7. Angle length

Additional parameters discussed included the number of bolts (four bolts instead of two), end plate, top flange cover plate, web stiffener, and fabrication tolerances. These parameters were considered, but they were not explicitly included in the testing and modeling research program for various reasons.

Phase 2 - Full-Scale Testing Program

Purpose and Approach

This phase aimed to evaluate the true behavior of drop-in top flange connections. The intent was to test full-scale girder-column and beam-column connections for direct evaluation. In addition, the data was utilized for finite element model validation and parametric studies (part of Phase 3). This validated methodology can also be utilized in the future to study beam-girder connections (not included in this study).

The primary metrics for the evaluation of the connections tested included:

1. Shear strength
2. In-plane rotational stiffness
3. In-plane rotational ductility
4. Torsional stiffness
5. Failure mode

Experimental Testing

The scope of work for full-scale testing included the development of a test matrix, test setup design, fabrication, instrumentation, and experimental testing execution.

Test Matrix

The test matrix was developed to experimentally evaluate a number of the parameters of interest listed in Phase 1. There were six overall tests in which 12 connections were tested. Due to experimental circumstances, multiple tests had to be performed several times with varying accommodations (e.g., after retrofitting a failed connection to test further the connection on the other side of the girder/beam). The final test matrix is provided below in Table 1, which shows all the tests that were performed.

It should be noted that the minimum measured weld sizes on the outer vertical leg and top of the horizontal leg are reported in Table 1. In the table, H and V refer to the horizontal and vertical welds, respectively. The number proceeding H or V represents the number of weld lines per angle. Therefore, 1V means only a single weld line was provided along the outside face, but 2V indicates weld lines on both sides. ***Appendix A*** provides all the measured weld sizes for each connection. ***Appendix B*** provides the specified weld sizes.

Table 1: Test Matrix

Test	Conn Type	Conn. Name	Beam Size	Angle/Shear Tab Size	Size and No. of Bolts	Bearing Length (in.)	Weld Position	Vertical Weld Size (in.)	Horizontal Weld Size (in.)
1.1 & 1.2	Girder to Column	A	W24x68	L8x4x3/4	Two ¾"	5	2V&2H	3/4	1/4
		B		L8x4x3/4		5	2V&2H	3/8	5/16
2.1		C		L8x4x3/4		3	1V&2H	1/4	1/4
		D		L6x4x5/16		5	1V&1H	5/16	1/4
2.2		C		L8x4x3/4		3	1V&2H	1/4	1/4
		Retrofit		-	-	-	-	-	-
3.1 & 3.2		E		L8x4x1/2	Two ¾"	5	1V&2H	1/4	5/16
		F		3/8x5x12.5	Four 1"	-	2V	5/16	-
4.1		G	W16x36	L6x4x5/16	Two ¾"	3	1V&2H	1/4	1/4
		H		L4x3x1/2 (Flipped)		3	2V&2H	1/4	5/16
4.2		G		L6x4x5/16		3	1V&2H	1/4	1/4
		Retrofit		-	-	-	-	-	-
5.1 & 5.2		I	W24x68	L6x4x5/16	Two ¾"	5	2V&2H	5/16	1/4
		J		L4x3x1/2		3	2V&2H	5/16	5/16
5.3		I		L6x4x5/16		5	2V&2H	5/16	1/4
		Retrofit		-	-	-	-	-	-
6.1	Beam to Column	K		L6x4x5/16	Two ¾"	5	2V&2H	5/16	1/4
		L		L4x3x1/2		5	2V&2H	5/16	5/16

The intent of each connection is explained below:

- Connections A and B evaluated the general behavior of the girder top flange and drop-in connection angles, as well as indirectly assessed the torsional stiffness. The angles were oversized to induce a flange bending failure mode.
- Connection C evaluated the effect of a reduced bearing length while holding the same angle size as Connections A and B.
- Connection D evaluated the effect of a smaller angle size and reduced weld.
- Connections E and F were the benchmark drop-in connection and shear tab designs from Phase 1, serving as the baseline for the investigation.
- Connection G investigated the general behavior for a smaller girder and angle size.
- Connection H evaluated the effect of a mirrored angle orientation.
- Connection I was a modification of Connection D, where the weld geometry was improved. The torsional stiffness was evaluated for an unbraced girder, along with connection failure mode when the girder was braced.
- Connection J investigated the behavior of undersized angles.
- Connections K and L evaluated drop-in beam-column connections.

Test Setup

Several shear connection testing methods have been employed in the past, including a full-scale propped cantilever beam setup with the connection to be tested at one end and a rocker support at the opposite end (Richard, Gillett et al. 1980, Ellifritt and Sputo 1999), symmetrical double cantilever beams connected to and loaded via a central column (White 1965), and a cantilever beam shear connected to a rigid column with two actuators controlling the shear and rotation of the connection (Astaneh-Asl, Call et al. 1989). These different testing methods offer varying degrees of shear and rotation combinations that the connections experience during testing. As shear connections should accommodate the rotation demand in addition to having sufficient strength, testing connections under realistic shear and rotation combinations is crucial (Astaneh 1989). This study adopted a different test setup than those listed above, which also results in a realistic end rotation and shear.

The girder-column experimental setup is shown in Figure 6 (similar to the beam-column setup). The setup utilizes stub columns with shop-welded connections. Each column was utilized twice with a welded connection on both flanges. The girders were erected with an overhead crane to realistically evaluate the true construction process of this connection.

While the actual application of this connection is intended for composite construction, this test evaluated the girder without a composite slab to save time and resources. For realistic composite slab behavior, the beam span lengths were reduced for testing to provide reasonable combined shear and rotation at the connections. To avoid significantly altering the shear-rotation demand due to this simplification, the length of the beams and girders were reduced using Eqs. 1-1 and 1-2 where θ is the end rotation of a simply supported girder, k is a constant depending on the position and number of the applied loads, and P, L, E, and I

represent the applied load, span length, modulus of elasticity, and moment of inertia of the section, respectively.

$$\theta = k\frac{PL^2}{EI} \tag{1-1}$$

$$\frac{L_{Comp}}{L_{Non-Comp}} = \sqrt{\frac{EI_{Non-Comp}}{EI_{Comp}}} \tag{1-2}$$

Eq. 1-2 was reached by using Eq. 1-1 to equate the shear-to-rotation ratio of the composite benchmark section to that of the non-composite section used for testing. L_{Comp}, $L_{Non\text{-}Comp}$, I_{Comp}, and $I_{Non\text{-}Comp}$ represent the composite and non-composite length and the moment of inertia of the composite and non-composite sections, respectively. As well, bracing was provided at three locations to prevent lateral buckling and replicate the effects of a composite slab being present. The 30 ft. composite span of the W24×68 and W16×36 girder was reduced to 18 ft. and 14 ft. using Eq. 1-1 and rounding for the laboratory strong floor anchor hole spacing.

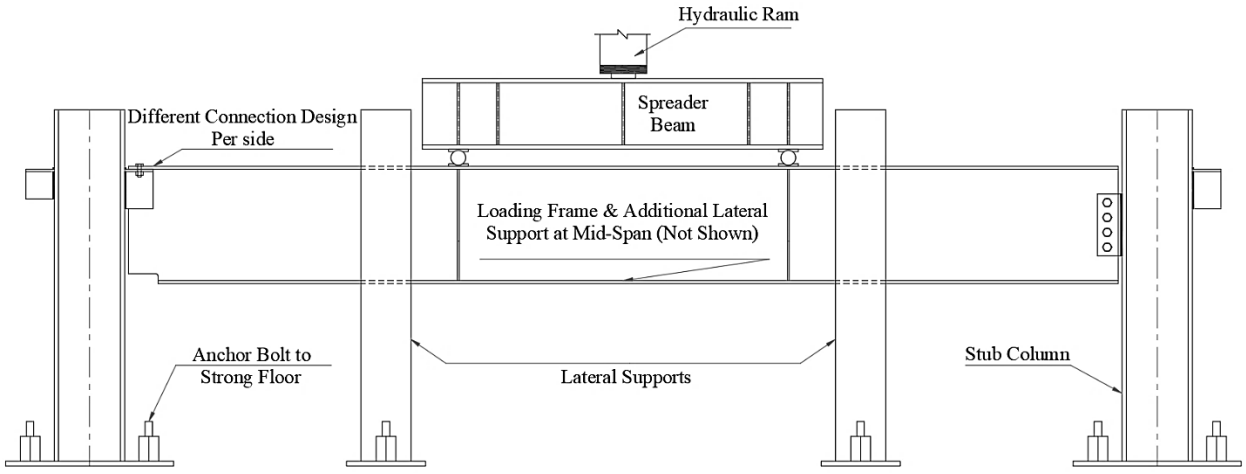

Figure 6: Girder-Column Test Setup (Elevation View)

A double-column load frame was utilized for the testing. A hydraulic ram (600-kip capacity) and 400-kip load cell (with a safe over-range of 150%) was mounted along the underside of the load frame headers. Figure 7 provides a rendering of the test setup.

Figure 7: Girder-Column Test Setup (Rendering)

Fabrication

The research team developed detailed drawings to fabricate the girders, connections, columns, and lateral braces. These drawings can be found in ***Appendix B***.

The steel rolled sections and plates were acquired by AISC from Sisken Steel & Supply. This included steel from Gerdau, Nucor, SSAB, and Steel Dynamics. Mill test reports were obtained for all the steel utilized in the study. The average material properties for the specimens are provided in Table 2.

Table 2: Mill Test Report Average Results

Shape	Grade	F_y (ksi)	F_u (ksi)	Elongation (%)
W24x68	A572/A992	55.9	72.4	23.7
W16x36	A572/A992	58.0	73.0	26.5
W14x82	A572/A992	55.1	71.1	24.7
L8x4x3/4	A572	54.6	75.3	26.1
L4x3x1/2	A36/50	55.1	73.5	29.0
L8x4x1/2	A36/572	56.5	73.0	26.0
L6x4x5/16	A36 (Meets A572 Gr.50)	57.9	76.1	25.0
3/8" Plate	A572 GR.50	67.0	77.7	31.0

The North Alabama Fabrication Company (NAFCO) graciously donated their time, facility, and personnel to fabricate the specimens. NAFCO developed official shop drawings, which were then reviewed by the research team. The fabrication was completed in October 2023 and shipped to the Advanced Structural Engineering Laboratory (ASEL) at Auburn University. Figure 8 provides a photo of two fabricated columns with drop-in angle connections at the NAFCO facility.

Figure 8: NAFCO Fabrication Photo (Provided by Doug Abernathy)

Instrumentation

The instrumentation design was performed in parallel with the fabrication process. This design aimed to capture the global and local behaviors of the specimens, along with loading information. Figure 9 provides an elevation view of the instrumentation design. ***Appendix C*** provides the full set of instrumentation drawings with different views.

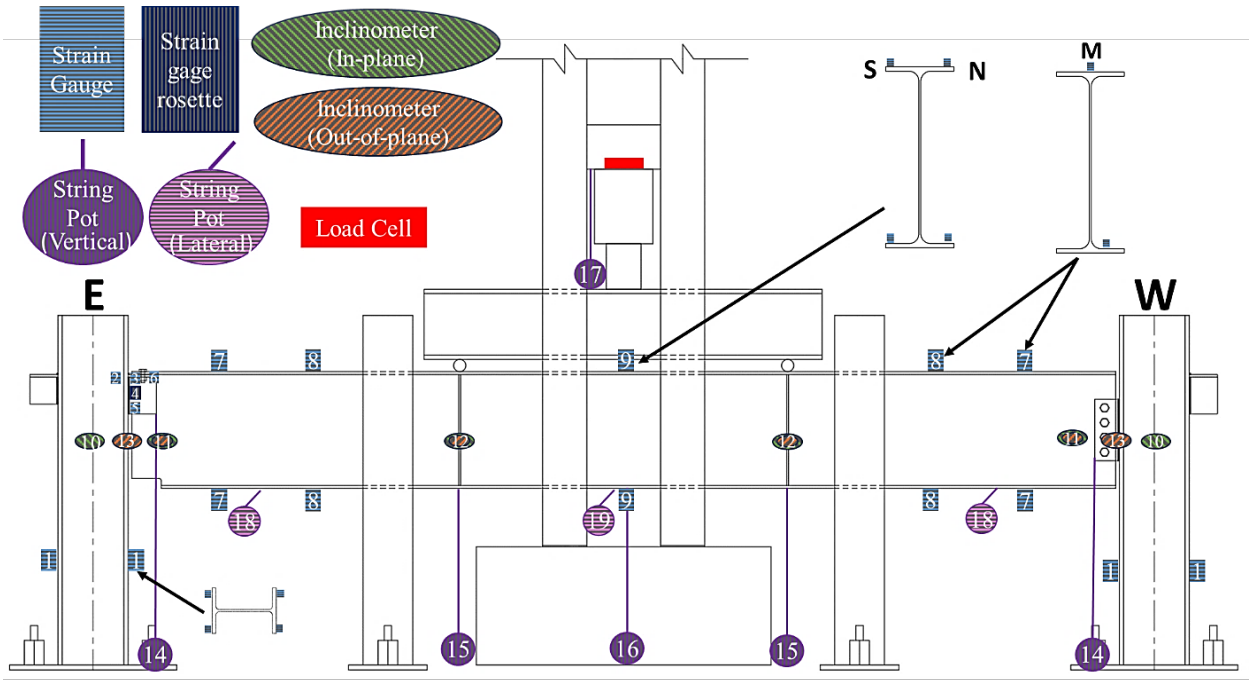

Figure 9: Instrumentation Design (Elevation View)

Global behavior in the form of force, displacements, and rotations were captured. The force was captured with a load cell connected to the hydraulic ram. Six vertical and two lateral displacement measurements were performed using string potentiometers. Rotations at the ends of the girder and center of the columns were measured with inclinometers. In addition, unbraced girder tests included out-of-plane rotation measurements.

The localized behavior was captured using two different methods. One method was to measure localized deformations with strain gauges. These gauges have been placed on the girders, angles, and columns. Figure 10 to Figure 12 provide photos of the strain gauge attachment.

Figure 10: Girders with Strain Gauges Attached

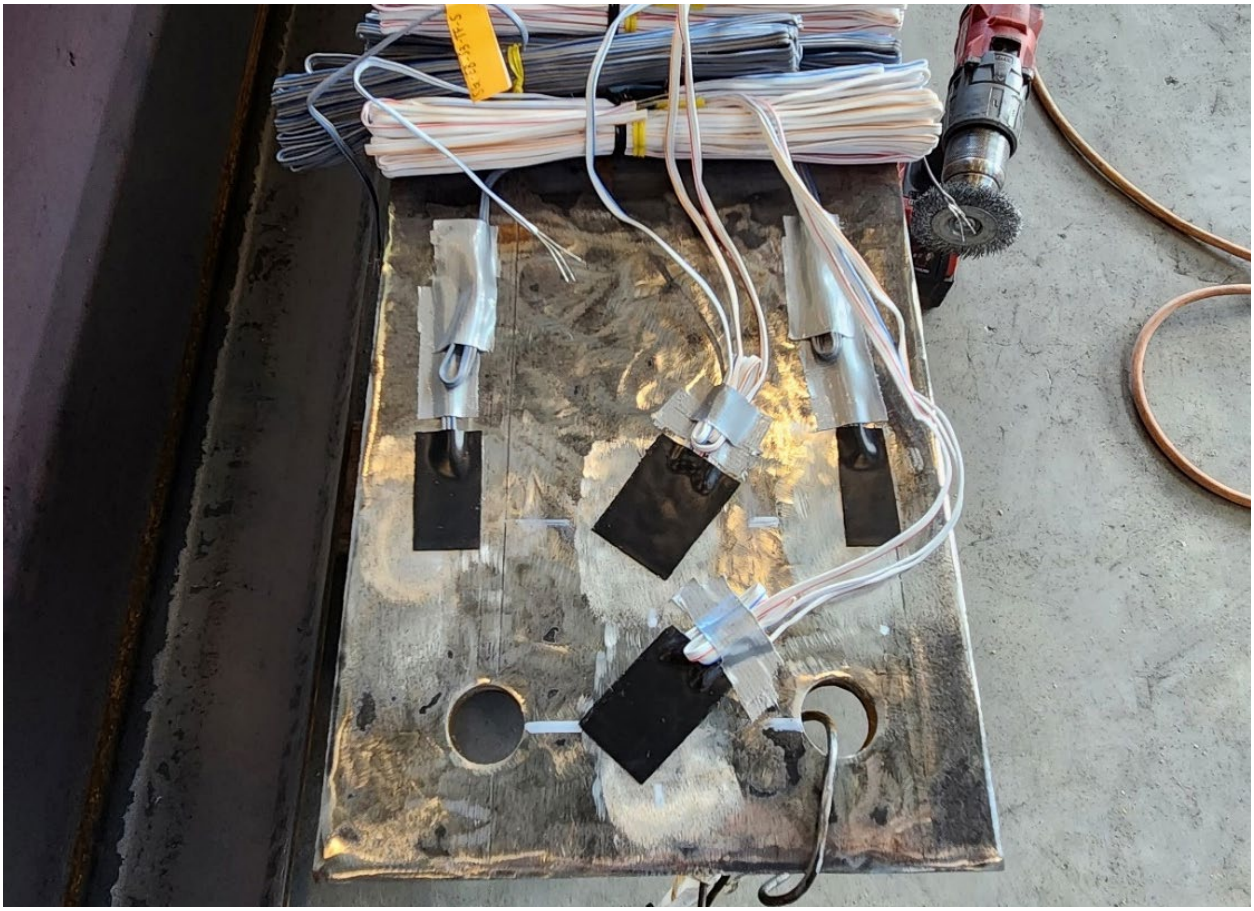

Figure 11: Girder Top Flange Strain Gauge Attachment

Figure 12: Drop-In Angles and Column Strain Gauge Attachment

The second measurement method was to capture a strain field using Digital Image Correlation (DIC) (Sutton, Orteu et al. 2009). While the data provided utilizing DIC is not as absolute as that of a strain gauge, it allows for a better visual understanding of the overall deformation. DIC data was recorded at different locations for the various tests. Figure 13 provides an example of a DIC setup for the testing.

Figure 13: DIC Setup Example

DIC was utilized in varying capacities for all tests to capture the yield lines and deformations in 2D or 3D. A 3D analysis of an area/member requires two cameras, while a 2D analysis requires only one camera. Due to a limited number of cameras (four total), tests were limited to the number of areas/members that could be captured via DIC. The potential locations to be investigated via DIC considered for each test were the girder/beam top flange, vertical angle leg, shear tab, and column web. Table 3 provides a summary of the DIC locations recorded for each test. While DIC was utilized in multiple rounds of each test, it is noted that all DIC data reported is a product of the first round of each test. For example, DIC was used in Test-1.1 and Test-1.2 but is only reported for Test-1.1 due to insignificant data provided in Test-1.2.

Table 3: DIC Locations

Test	Connection	2D or 3D		
		Girder/Beam Top Flange	Angle/Plate	Column Web
1	A	2D	-	-
	B	3D	2D	-
2	C	2D	2D	-
	D	2D	2D	-
3	E	3D	2D	-
	F	-	2D	-
4	G	-	2D	-
	H	3D	2D	-
5	I	-	3D	-
	J	-	3D	-
6	K	-	-	3D
	L	-	-	3D

To prepare the specimen, a thin layer of white spray paint was applied to create a uniform background. For all tests, excluding Test-2.1 and 2.2 (Connections C and D), the mill scale was carefully removed from the surface of the steel to allow for optimal bonding of the spray paint and minimize the likelihood of the paint flaking off during testing. A random speckle pattern with varying dot sizes (0.13" to 0.5") was applied on top of the white paint with black ink and a stamp/stamp roller. To achieve the desired 50/50 white/black color, a black fine-tipped marker was utilized to add more speckling. During testing, each camera captured a photo of the specimen and actuator load data at a rate of 1.0 Hz. In addition, sufficient lighting in the areas of interest was crucial to ensure that the entire speckled area's data could be processed. This lighting was provided via blue and/or white light lamps; the color of the lighting did not affect the data. Post-testing, these images were processed in Correlated Solutions' VIC-2D or VIC-3D software utilizing a recommended subset size to obtain the DIC figures and graphs.

Experimental Test Execution

Five girder-to-column tests and one beam-to-column test were conducted. In total, twelve connections were tested since two different connections were utilized in each test. If a connection failed before the connection on the opposite end of the girder/beam, the test was repeated after retrofitting the failed connection. The following sub-sections provide a summary of the tests conducted.

Test One

In Test One, Connections A and B, summarized in Table 1, were tested in the setup illustrated in Figure 14 (a). For Test-1.1, the three lateral supports were set back by approximately half an inch to examine the connections restraint against lateral torsional buckling of the girder.

The lateral support setback before the beginning of the test is illustrated in Figure 14 (b-d). Connections A and B (before testing) are shown in Figure 15.

a.

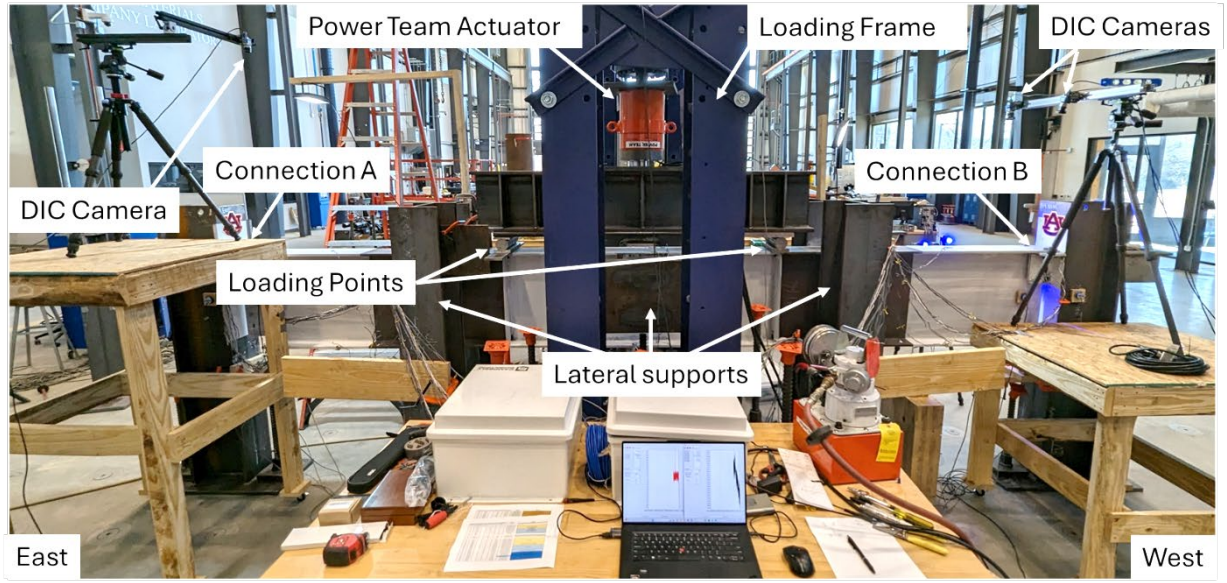

b.

c.

d.

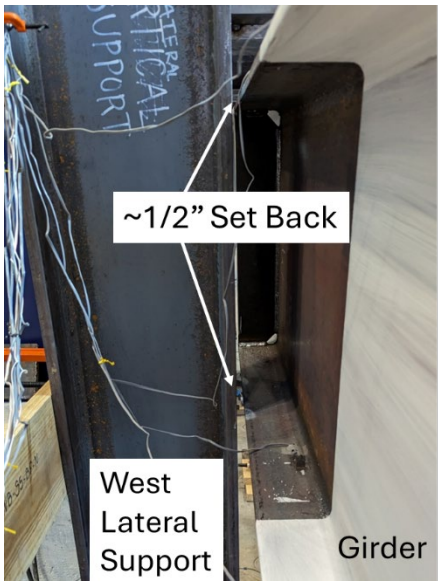

Figure 14: Test Setup Before Testing (a) Test Setup, (b) East Lateral Support Set Back, (c) Mid-Span Lateral Support Set Back, and (d) West Lateral Support Set Back

a. **b.**

Figure 15: Before Testing (a) Connection A and (b) Connection B

The girder and connections were loaded using a power team actuator. As shown in Figure 14 (a), a spreader beam distributes the load across two loading points. The loading points divide the W24x68 girder into three equal segments for Test-1.1. For Test-1.2, the loading points were shifted towards the center of the girder (explained further below). The resulting mid-span moment – mid-span displacement plot is shown in Figure 16. As can be seen from the figure, the applied load was well above the design load, and the maximum moment was between the yielding moment (M_y) and the plastic moment (M_p) of the girder. The yielding and plastic moments of the girder were calculated based on yield strength obtained from a mill test report.

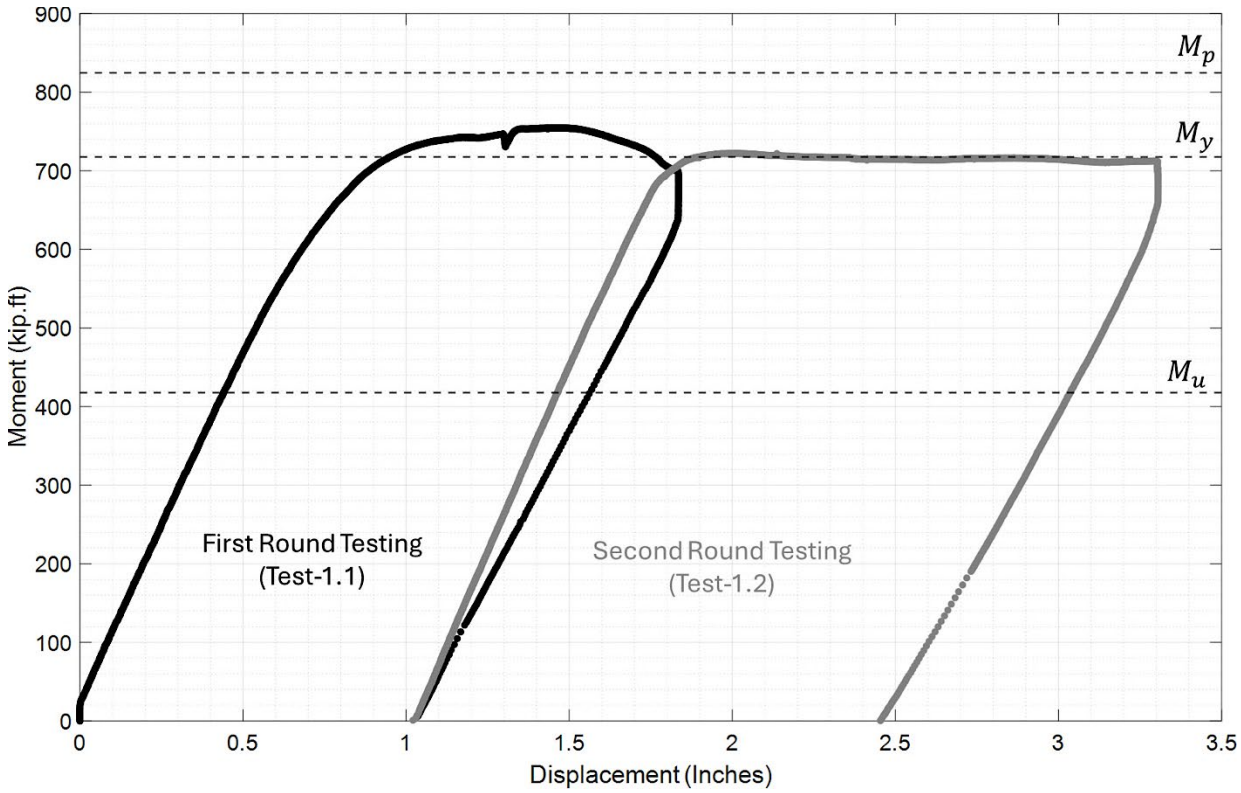

Figure 16: Mid-Span Moment – Mid-Span Displacement Curve

After about 1.5 inches of mid-span deflection, lateral displacement of the girder and spreader beam occurred (due to lateral-torsional buckling (LTB)), followed by local buckling of the girder top flange and web near the loading points. This phenomenon is depicted in Figure 17 (a-b). Figure 18 shows a plot of the measured lateral displacement against the mid-span moment. The lateral displacement was measured on the bottom flange 25 inches from Connection A. As can be seen from Figure 18, no appreciable lateral displacement was measured until the theoretical nominal moment (M_n) was exceeded (controlled by inelastic LTB). Moreover, the girder came in contact with the lateral supports after the theoretical unbraced nominal moment (M_n) was exceeded, implying that the drop-in connections provided sufficient LTB restraint. The LTB modification factor C_b=1.14 was used to calculate M_r and M_n. The C_b value corresponds to a four-point bending with lateral restraints only at the ends.

a.

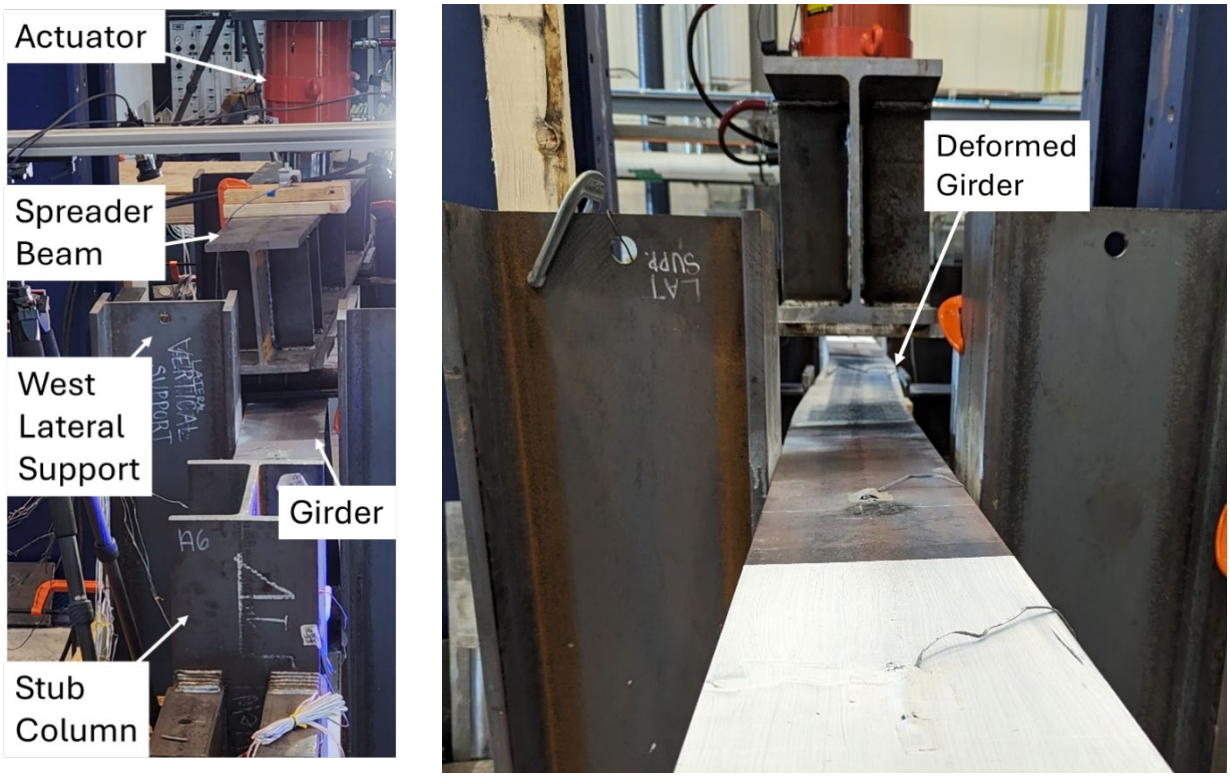

b.

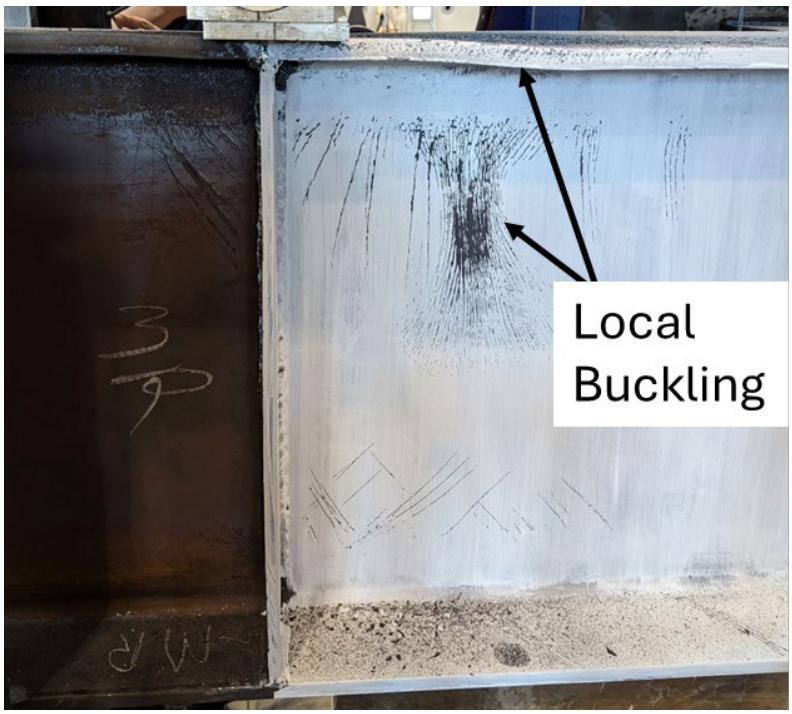

Figure 17: Test Setup after First Round Testing (1.1) (a) Girder and Spreader Beam Deformation (b) Local Buckling at the West Loading Points

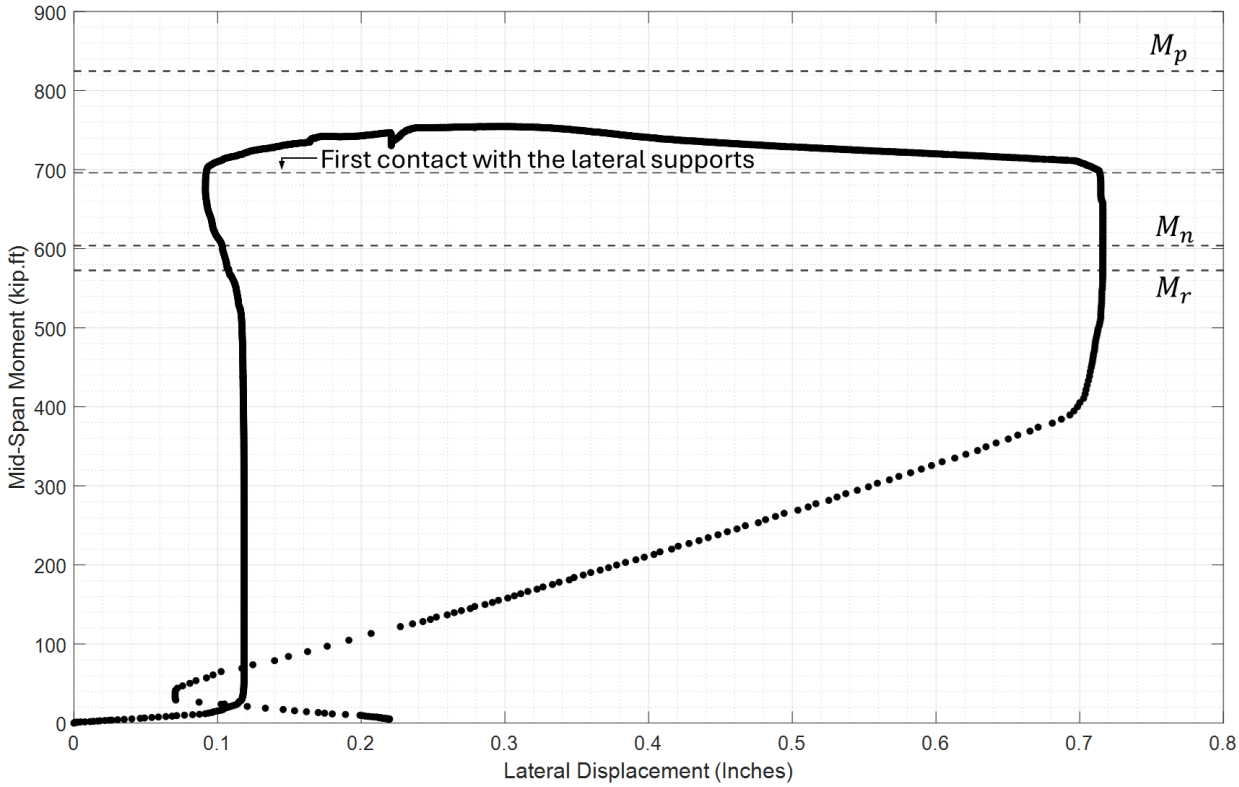

Figure 18: Mid-Span Moment – Girder Lateral Displacement Curve for Test-1.1

Further increasing the applied load during Test-1.1 resulted in large lateral displacement and instability in the spreader beam. As a result, the test was stopped, and the specimen was unloaded. Figure 19 (a and b) shows Connections A and B after unloading the test specimen. As evident from Figure 19, there was no significant plastic deformation or damage to the connections. Therefore, a second round of testing (Test-1.2) was continued after some modifications to the girder and spreader beam.

a. **b.**

Figure 19: After Test-1.1 (a) Connection A and (b) Connection B

In the second round of the testing process (Test-1.2), restraint plates were incorporated into the spreader beam to enhance its lateral stability. In addition, the loading points were moved closer to the mid-span to limit the maximum shear force and impart more rotational demand on the connections. This decision was made because the maximum load in the first round of testing was well above the design load, as shown in Figure 16 and Figure 20. The loading points were moved from 66.75 to 24 inches apart, and cross-laminated timber (CLT) stiffeners were added to the girder under the new loading points. The new loading points and CLT stiffeners are shown in Figure 21.

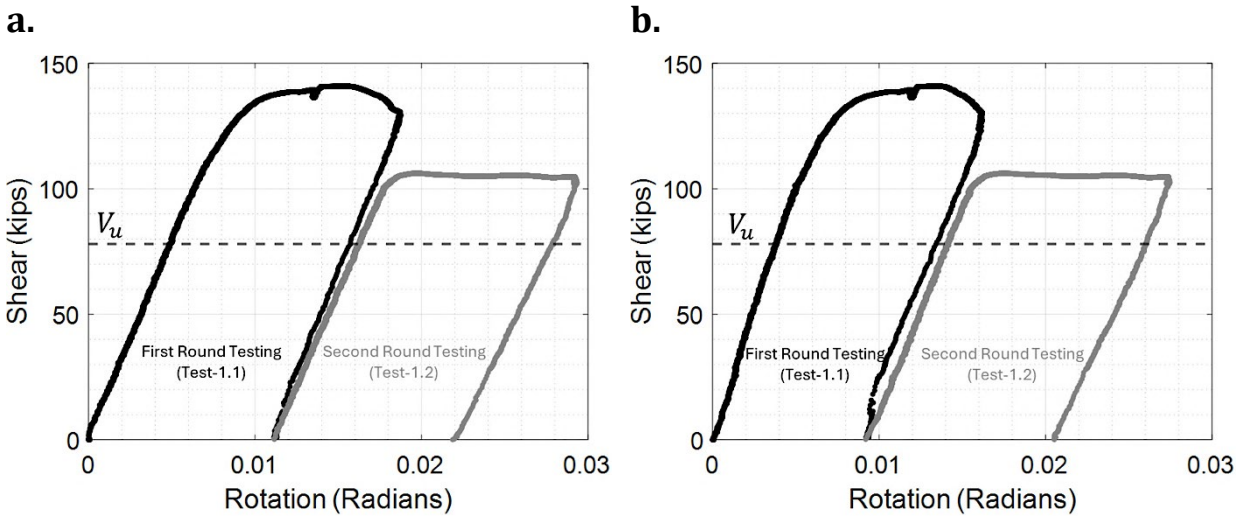

Figure 20: Connection Shear Force-Rotation Curve (a) Connection A and (b) Connection B

The second round of testing was continued until the connection rotation was approximately at the required connection rotation (0.03 radian). The connection rotation was calculated as the difference between the beam end and column rotation. As shown in the shear rotation plots of Figure 20, Connections A and B reached 0.03 and 0.028 radian rotation, respectively. Moreover, the connection shear at these rotation levels was above the design shear force V_u. The connections at their respective maximum rotation are shown in Figure 22 (a and b). It can be seen that most of the connection rotation is due to flange bending. The girder's local buckling and lateral displacement were more pronounced at the end of the second loading cycle, which also dictated the completion of the testing.

a. **b.**

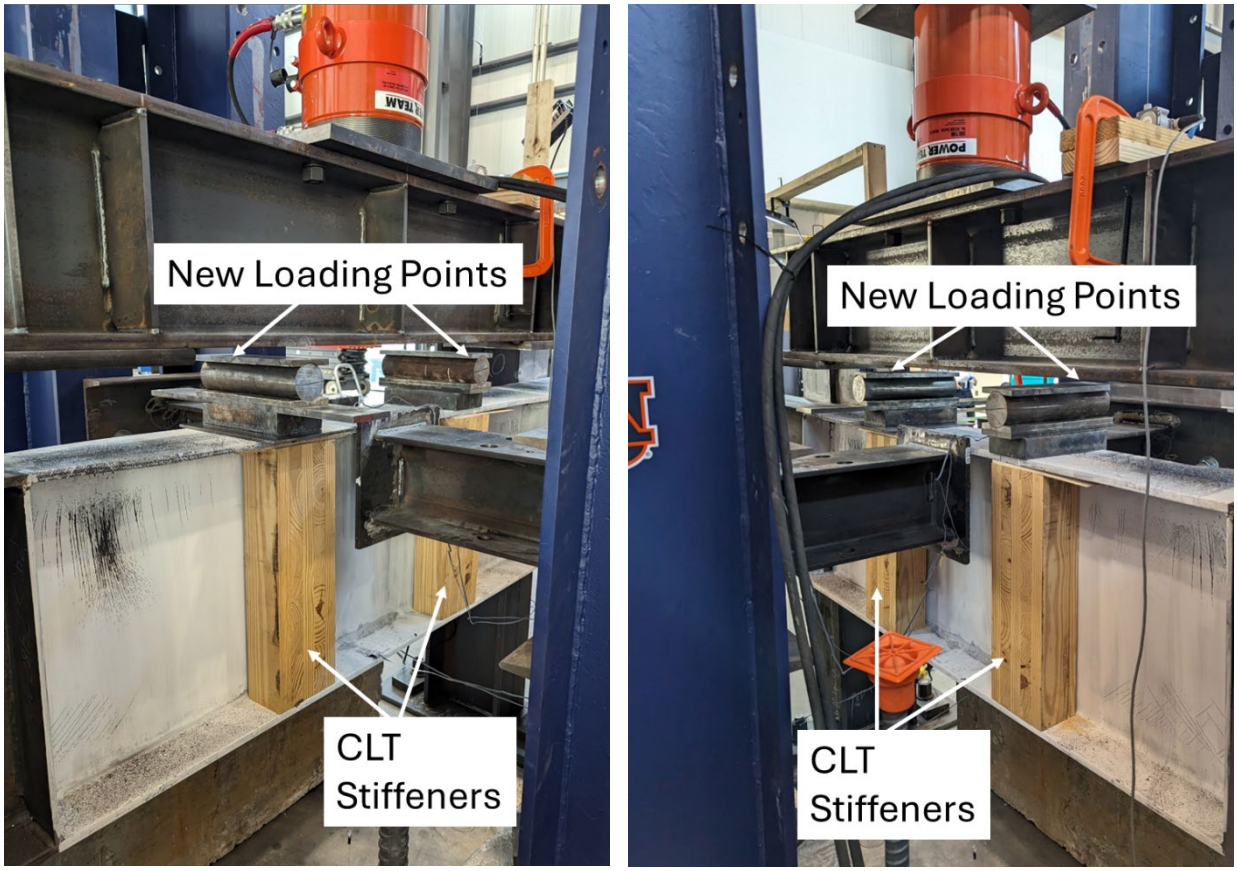

Figure 21: Loading Points and CLT Stiffeners for Test-1.2 (a) View from Connection B and (b) View from Connection A

a. **b.**

Figure 22: Test-1.2 (a) Connection A near 0.03-radian rotation and (b) Connection B near 0.028-radian rotation

The connection in-plane rotational stiffness and moment resistance were compared against the limits for simple connection. The support moments were calculated by projecting the girder moment on the column face. The girder moments were calculated using a set of strain gages symmetrically attached at mid-span and 20 and 40 inches from either end of the beam. The calculated mid-span moment was assumed to be constant between the loading points, and linear regression was used to estimate the bending moment in the remaining portions of the girder and the supports. The support moment was taken as the moment at the face of the column flanges. This process is illustrated in Figure 23(a) at the design load level and repeated for a range of load levels in Figure 23 (b). The illustrations shown in Figure 23 are based on data from the first round of testing (Test-1.1).

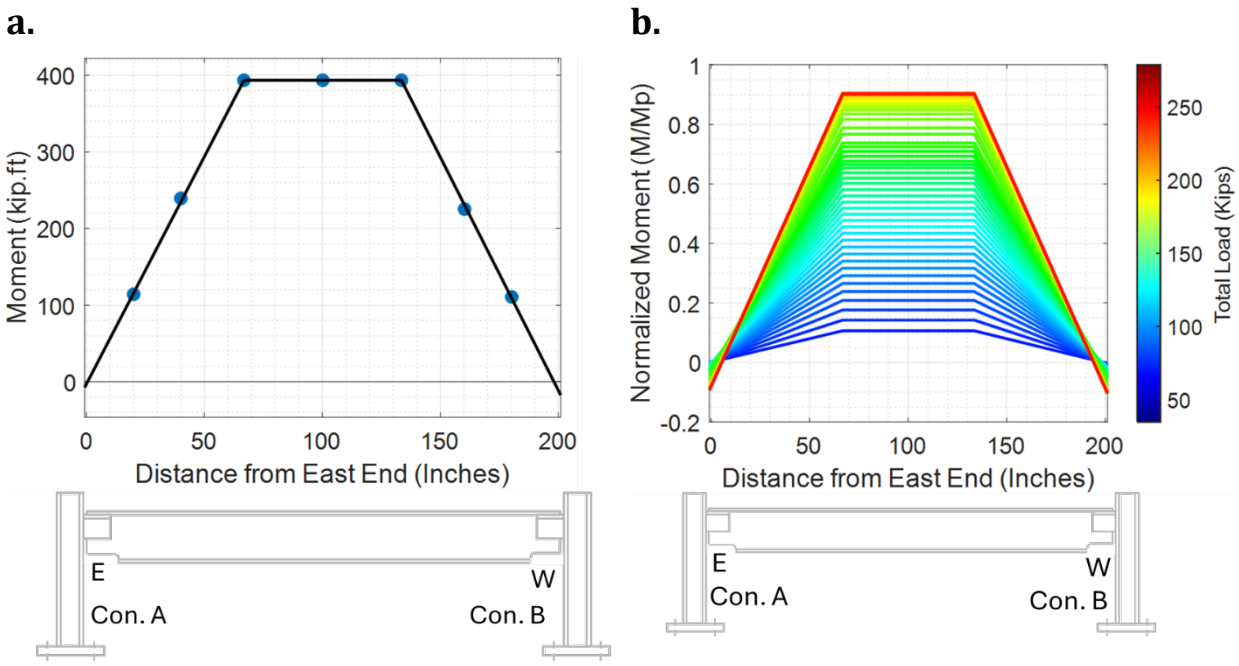

Figure 23: Girder Bending Moment Diagram (a) Girder Bending Moment Diagram at the Design Load and (b) Girder Bending Moment Diagram Over a Range of Loads

The calculated support moments were then plotted against the measured connection rotation to produce the normalized support moment-rotation curves shown in Figure 24. As can be seen from the graphs, the rotational stiffness of both connections was well below the 2EI/L limit in both rounds of testing. Furthermore, the support moment corresponding to 0.02 radian rotation was below the $0.2M_p$ limit.

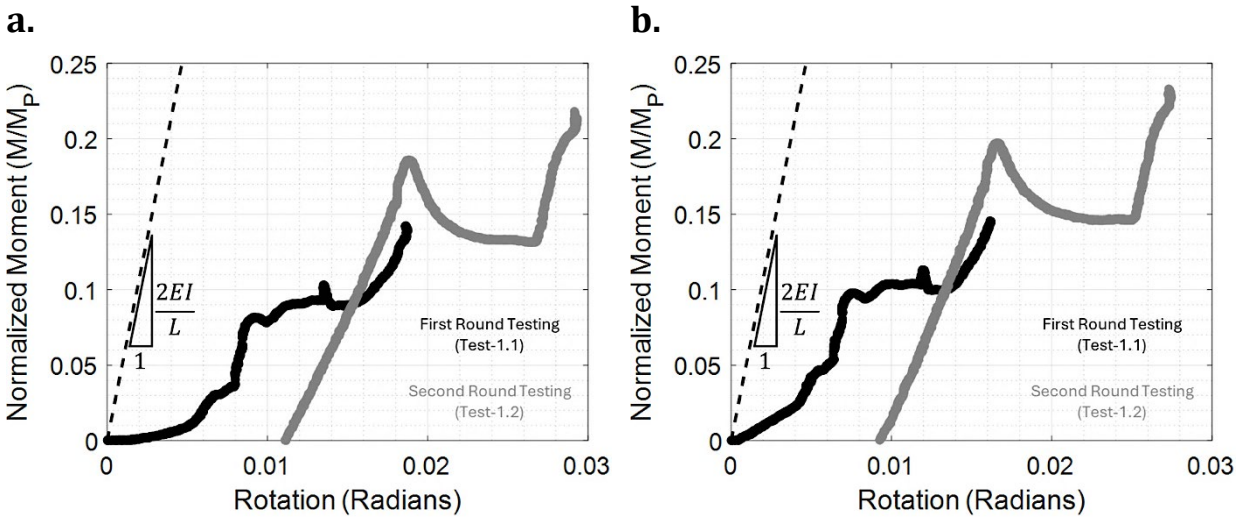

Figure 24: Normalized Support Moment – Rotation Curve (a) Connection A and (b) Connection B

As noted in the instrumentation section of this report, Digital Image Correlation (DIC) was utilized to capture various member behavior. Using all four available cameras in Test-1.1, Connection A girder top flange and Connection B angle were captured in 2D with one camera allocated to each; Connection B girder top flange was captured in 3D utilizing the two remaining cameras.

To investigate the Connection A top flange, an approximate area of 117 square inches (13 inches longitudinally by the width of the girder top flange) was prepared closest to the column face. Upon completion of the test, the captured images of Connection A were analyzed in VIC-2D. It is noted that due to the attached strain gauges on Connection A's top flange obstructing the camera's view of the underlying steel, the associated wires and tape were excluded from the defined AOI in the VIC-2D analysis. This area is seen in the middle and lower portions of the flange and remains white with black speckling in all progression images. Steel strain cannot be concluded in these areas and should be understood when looking at Connection A top flange figures. Also, due to out-of-plane movement during testing and monocular vision of the DIC system, a compression bias formed beyond the bearing length of the angles as the girder moved away from the sensor. While this area towards midspan is not suitable for conclusive evidence about strain magnitude, the flange area bearing on the angles stayed in relative original planar view, producing reliable data.

Figure 25 visualizes the girder's strain field progression, in microstrain units, with (a) Von Mises strains (ε_v), (b) transverse strains (ε_{xx}), and (c) longitudinal strains (ε_{yy}) for a connection shear (or reaction) of 40, 60, 80, 100, and 140 kips.

a.

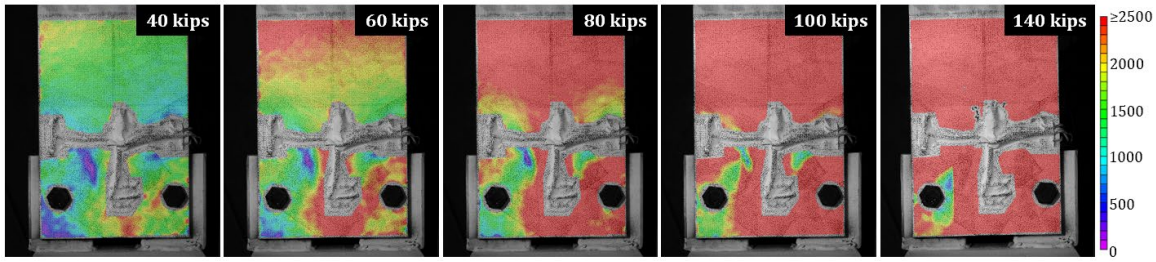

b.

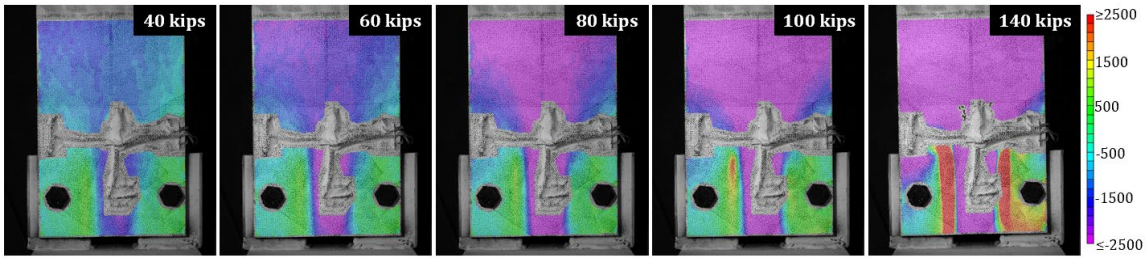

c.

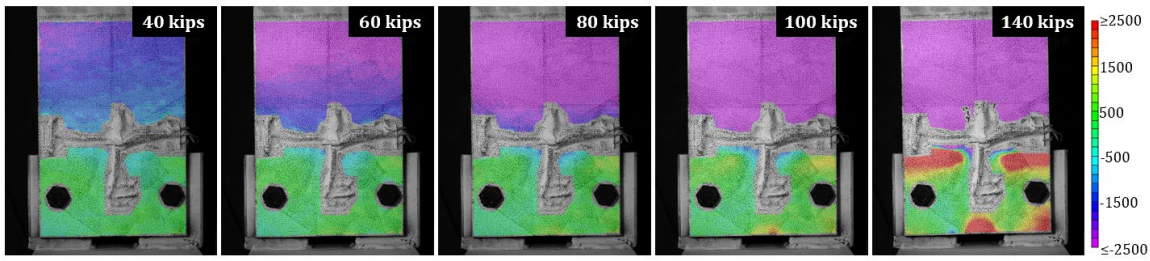

Figure 25: Connection A (Test-1.1) 2D DIC Flange Deformation Progression (a) Von Mises Strain (ε_v) (b) Transverse Strain (ε_{xx}) – Engineering, and (c) Longitudinal Strain (ε_{yy}) – Engineering

Figure 25 is oriented in such a way that the midspan of the girder is in the upper direction of the progression photo and the stub column/connection angles are in the lower portion of the photo. Shown by both Von Mises and transverse strains, a wide initial yield line begins to form on the centerline of the flange closest to the face of the column, in the region unsupported by the connection angles at a shear of 40 kips. It then gradually moves towards the midspan of the beam, eventually passing the transverse edge of the angles. Further insight and according to Figure 25 (b), the region between these initial yield lines is in compression. Though the magnitude of these yield lines cannot be concluded beyond the bearing length, the flaking of the speckle pattern, due to the deformation of the underlying steel, suggests that they extend approximately 2.5 inches beyond the supported region. This observation is further shown in Figure 26 in which the end of the bearing length and continuation of the yield lines (seen via flaking of paint) are noted. At a shear of 100 kips, a secondary set of yield lines is seen forming along the interior angle edges. Initially, the area

at the left-hand angle edge farthest from the column exhibits yielding, followed by complete yielding over both angle's interior edges at the maximum shear. These secondary yield lines encase an area of tension as the flange bends about the interior edge of each angle.

Figure 26: Connection A (Test-1.1) Yield Line Length According to Flaking of Paint

To further investigate the initial failure mode of flange bending about the interior longitudinal edges of the angles, a transverse cross-sectional cut was made approximately midway between the transverse edge of the angles and the bolt centerline at various shear forces, as shown in Figure 27. The theoretical centerline (CL) of the flange (with the edges of the flange web noted on each side) and the edge of the right-hand and left-hand angles (as seen from plan view with the midspan of the girder into the plane) are noted for reference in Figure 27. Maximum tensile strains of 0.023 and 0.014 are located approximately 0.12 in. (3 mm.) left of the left-hand angle and 0.38 in (9.6 mm) right of the right-hand angle. From the available data, a maximum compressive strain of 0.028 is revealed 0.34 in. (8.6 mm) left of the web edge, likely in or near the actual fillet of this girder. Conclusively, three (likely four, had the strain gauges not been present) plastic hinges formed across the width of the girder flange during this test. Again, due to LTB of the girder, these results are not symmetric.

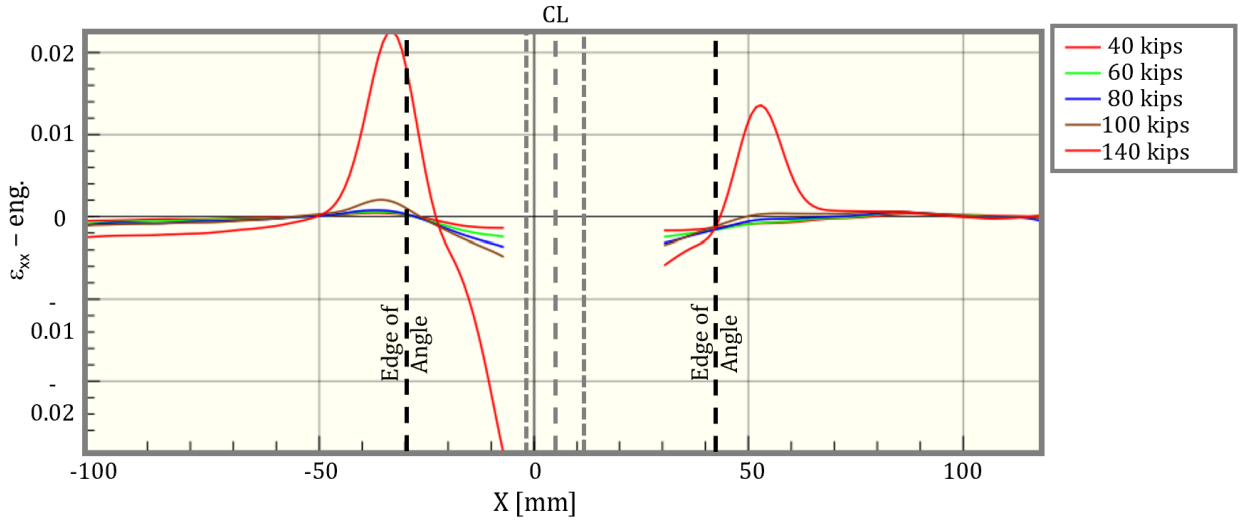

Figure 27: Connection A (Test-1.1) DIC Flange Section Cut Transverse Strain (ε_{xx}) Profile

The investigation of Connection B behavior included the analysis of the girder's top flange and the vertical angle leg via DIC. For the girder, an approximate area of 117 square inches (13 inches longitudinally by the width of the girder top flange) was prepared closest to the column face, and a rough area of 46 square inches (entire visible vertical angle face) was prepared for the angle. Figure 28 displays the girder's 2D strain field during testing, in microstrain units, with (a) Von Mises strains (ε_v), (b) transverse strains (ε_{xx}), and (c) longitudinal strains (ε_{xx}) for a connection shear of 40, 60, 80, 100, and 140 kips. It is noted that small areas of incomplete data seen in the lower middle portion of the flange are due to preliminary flaking of the spray paint on top of the flange beginning at a shear of 80 kips.

a.

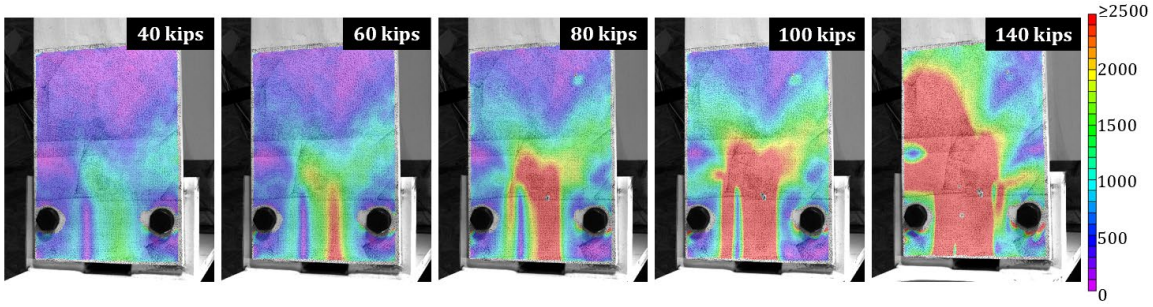

b.

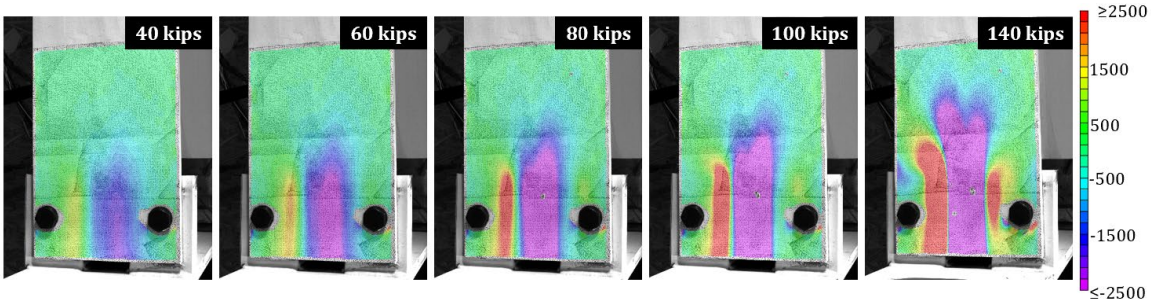

c.

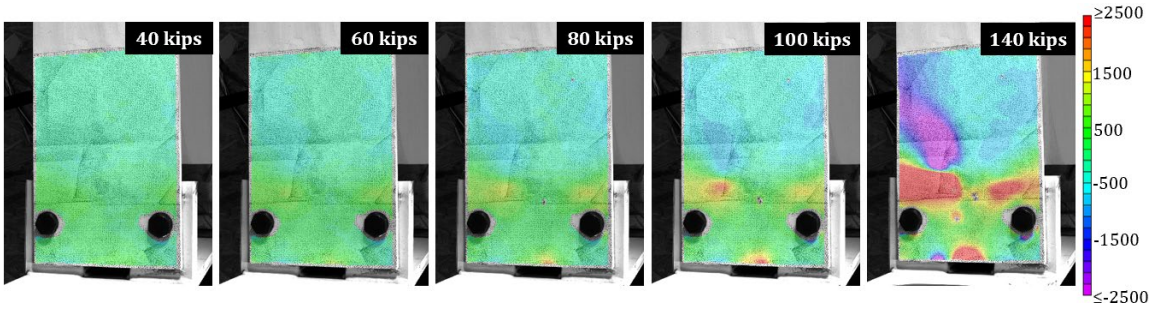

Figure 28: Connection B (Test-1.1) 2D DIC Flange Deformation Progression (a) Von Mises Strain (ε_v), (b) Transverse Strain (ε_{xx}) – Engineering, and (c) Longitudinal Strain (ε_{yy}) – Engineering

Figure 28 is oriented in such a way that the midspan of the girder is in the upper direction of each progression photo, and the stub column/connection angles are in the lower portion of each image. In parts (a) and (b), at a shear of 40 kips, a prominent strain field approaching yield and indicating a region of compression is seen having formed on the longitudinal centerline of the flange closest to the face of the column, between the regions supported by the angles. Through the progression, it gradually moves towards the midspan of the beam, eventually spreading out at an angle once passing the transverse edge of the connection angles. These yield lines continued for an approximate distance of five inches beyond the edges of the angles. According to Figure 28 (b), the region encased between these initial yield lines is in compression. As well, at a shear of 40 kips, a strain line approaching yield and

encasing an area of tension appears along the interior longitudinal left-hand angle edge and progresses towards midspan, branching out at an angle similar to, but shallower, than that of the initial yield lines. Eventually, a latent yield line like the previously described has fully formed along the right-hand angle's longitudinal interior edge at the maximum shear of 140 kips.

Starting to be revealed at a shear of 80 kips, longitudinal strains are seen encroaching the yield limit along the transverse edges of the angles. As shown in Figure 28(c), this area is in tension as the flange begins to deform about the transverse edge of the angles, increasing in-plane rotation; again, a rotation of 0.016 radians was achieved in this first round of testing. While the strains shown are not equivalent to the longitudinal centerline of the flange, these strains could likely be concluded as such had LTB not occurred in testing. Overall, the strain fields presented for Connection B are comparable to Connection A in their magnitude and formation; both flange surfaces were plastically deformed by the end of testing.

To further describe the deformations and strains that occurred in Connection B, Table 4 (noted in units of microstrain) visualizes the flange in a 3D space in which the displacement in the z-direction is amplified by 25% compared to the X and Y axes. The Z-axis is relative to the initial position of the flange immediately before testing (in which z equaled zero) and becomes negative as the specimen deformed away from the camera and towards the ground. The X-axis ranges from -4.75 in. to 4.75 in., in which 0 in. is located at the longitudinal centerline of the flange; a positive X-value reflects part of the flange that is to the right of the centerline and over the right-hand angle (in reference to the plan view seen in Figure 28) and vice-versa. The Y-axis ranges from -6.5 in. to 6.5 in., the largest value of 6.5 in. represents the part of the flange closest to midspan, while the smallest value of -6.5 in. represents the part of the flange closest to the stub column. Figure 29 shows a reference to orient the viewer for the 3D figures shown in Table 4.

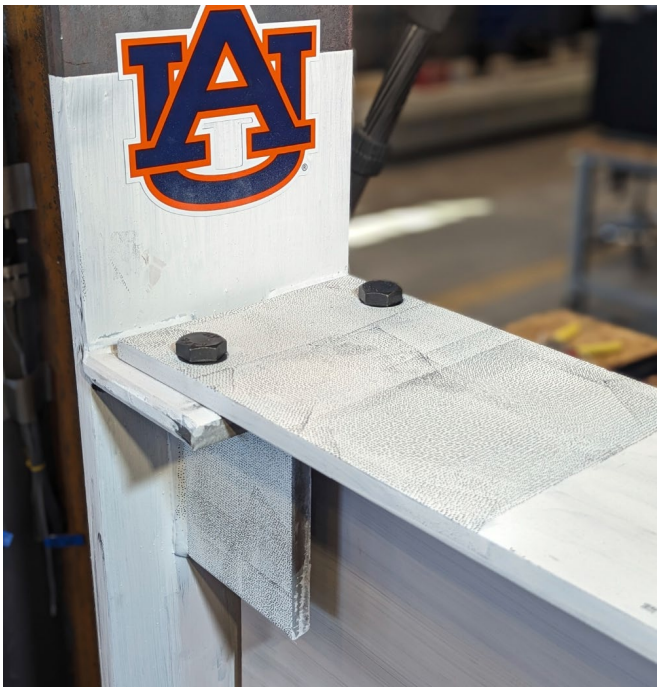

Figure 29: Connection B 3D Reference

In addition to the results discussed for the 2D strain progression; at a maximum shear of 140 kips, the flange is shown with a shallow deformation along the longitudinal centerline between the two connection angles. In the region in which the flange is no longer bearing on the angles (Y-coordinates of -1.5 in. and greater), the flange is seen deforming in the negative Z-direction with a maximum deformation of approximately 0.4 inches located at the far left-hand side of the flange.

Table 4: Connection B (Test-1.1) 3D DIC Flange Deformation Progression

	Von Mises Strain (ε_v)	Transverse Strain (ε_{xx}) - Engineering	Longitudinal Strain (ε_{yy}) - Engineering
Load (kips)	≥2500 2000 1500 1000 500 0	≥2500 1500 500 -500 -1500 ≤-2500	
40	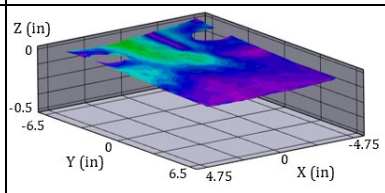	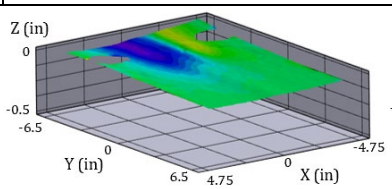	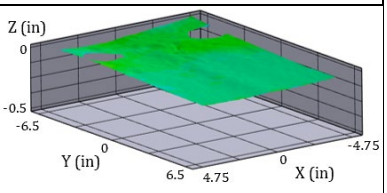
60	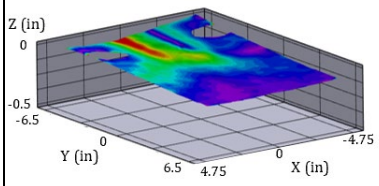	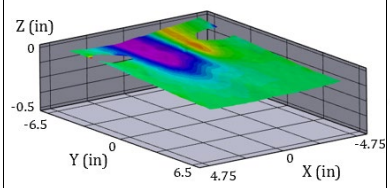	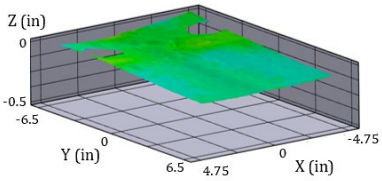
80	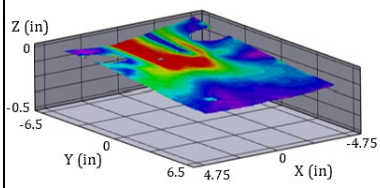	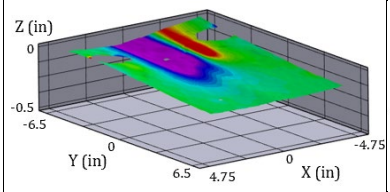	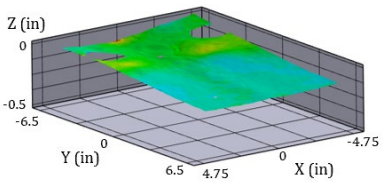
100	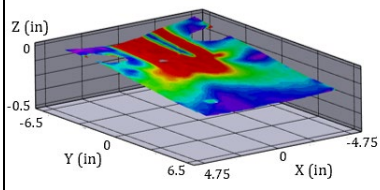	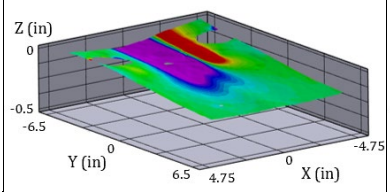	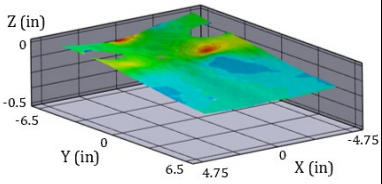
140	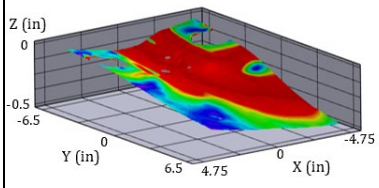	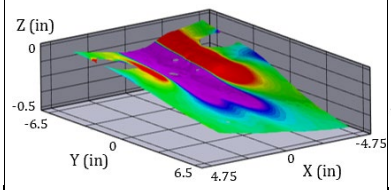	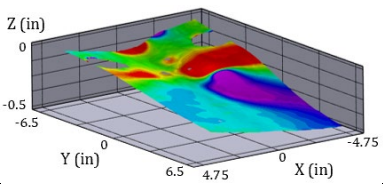

In further investigation of the initial failure mode, a transverse cross-sectional cut, like that of Connection A, was made approximately halfway between the transverse edge of the angles and the bolt centerline at the same shear reactions as previously listed. This is shown in Figure 30**.**

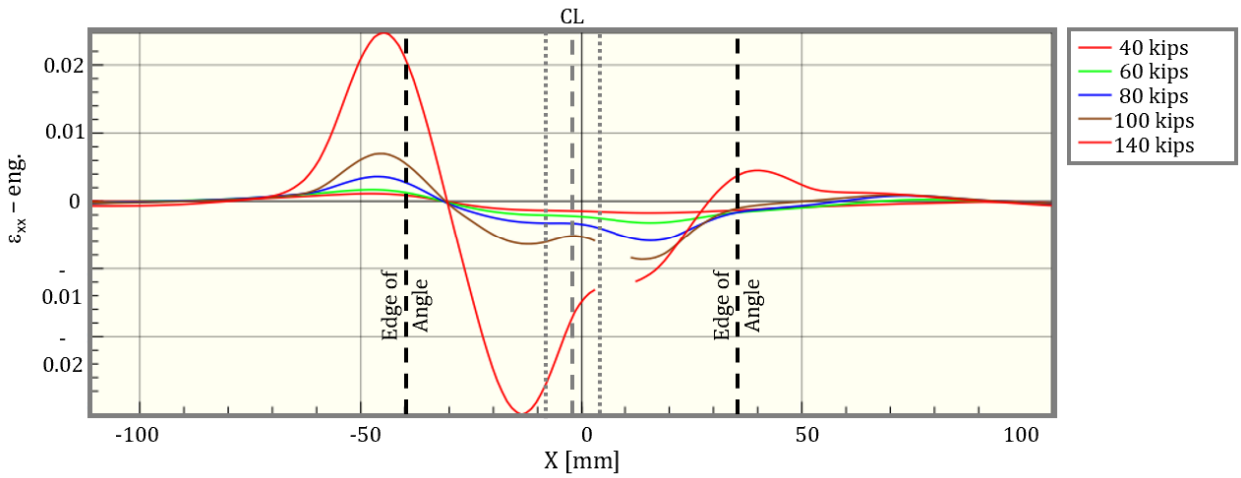

Figure 30: Connection B (Test-1.1) DIC Flange Section Cut Transverse Strain (ε_{xx}) Profile

The theoretical centerline (CL) of the flange (with the edges of the flange web noted on each side) and the edge of the right-hand and left-hand angles (as seen from plan view with the midspan of the girder into the plane) are noted for reference in Figure 30. Two plastic hinges developed in this flange, one of which occurred near or at the longitudinal edge of the left-hand angle and another that occurred near the left edge of the web in the fillet zone. Specifically, an absolute maximum tensile strain of 0.025 and maximum compressive strain of 0.03 developed approximately 0.2 in. (5.0 mm) left of the left-hand angle and 0.22 in. (5.7 mm) left of the left web edge, respectively. Again, these results are not symmetrical due to LTB of the girder.

Figure 31 shows the Connection B vertical angle leg strain formation, in microstrain units, in (a) Von Mises strain (ε_v) and (b) shear strain (ε_{xy}) for a connection shear of 40, 60, 80, 100, and 140 kips. The upper right-hand area (free end) of the angle begins to yield and extends across the angle to the left lower corner (attached to the column), displaying a complex strain field and areas of plastic deformation. It is noted that a small region in both (a) and (b) at 140 kips does not display data due to lighting variances encountered during testing.

a.

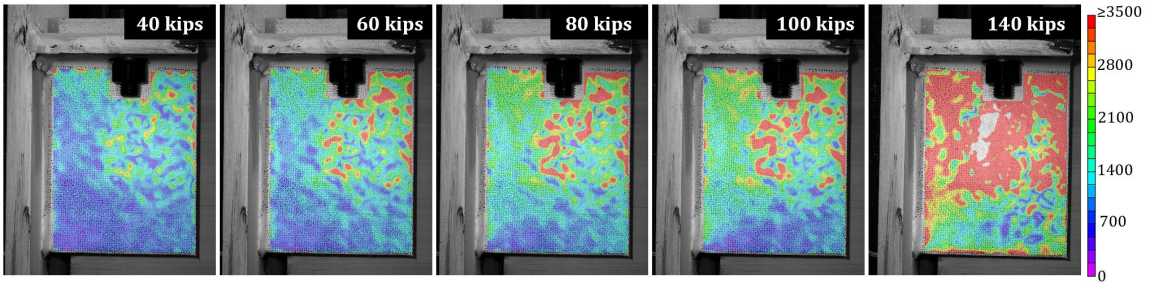

b.

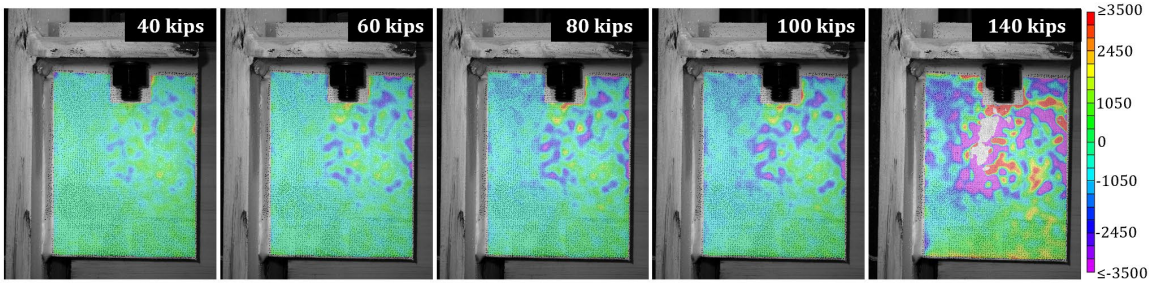

Figure 31: Connection B (Test 1) DIC Angle Deformation Progression (a) Von Mises Strain (ε_v) and (b) Shear Strain (ε_{xy}) – Engineering

The Drop-In Connections A and B satisfied the strength, stiffness, ductility, and torsional requirements. Overall, these are relatively conservative connections.

Test Two

In Test Two, Connections C and D, summarized in Table 1, were tested in the same test set-up as Test One. Connection C had the same angle size as Connections A and B (L8x4x3/4), but the bearing length was reduced from five to three inches. On the other hand, Connection D had a five-inch bearing length combined with a smaller (in terms of depth) and thinner angle (L6x4x5/16). Images of Connections C and D before the start of Test Two are shown in Figure 32.

a. **b.**

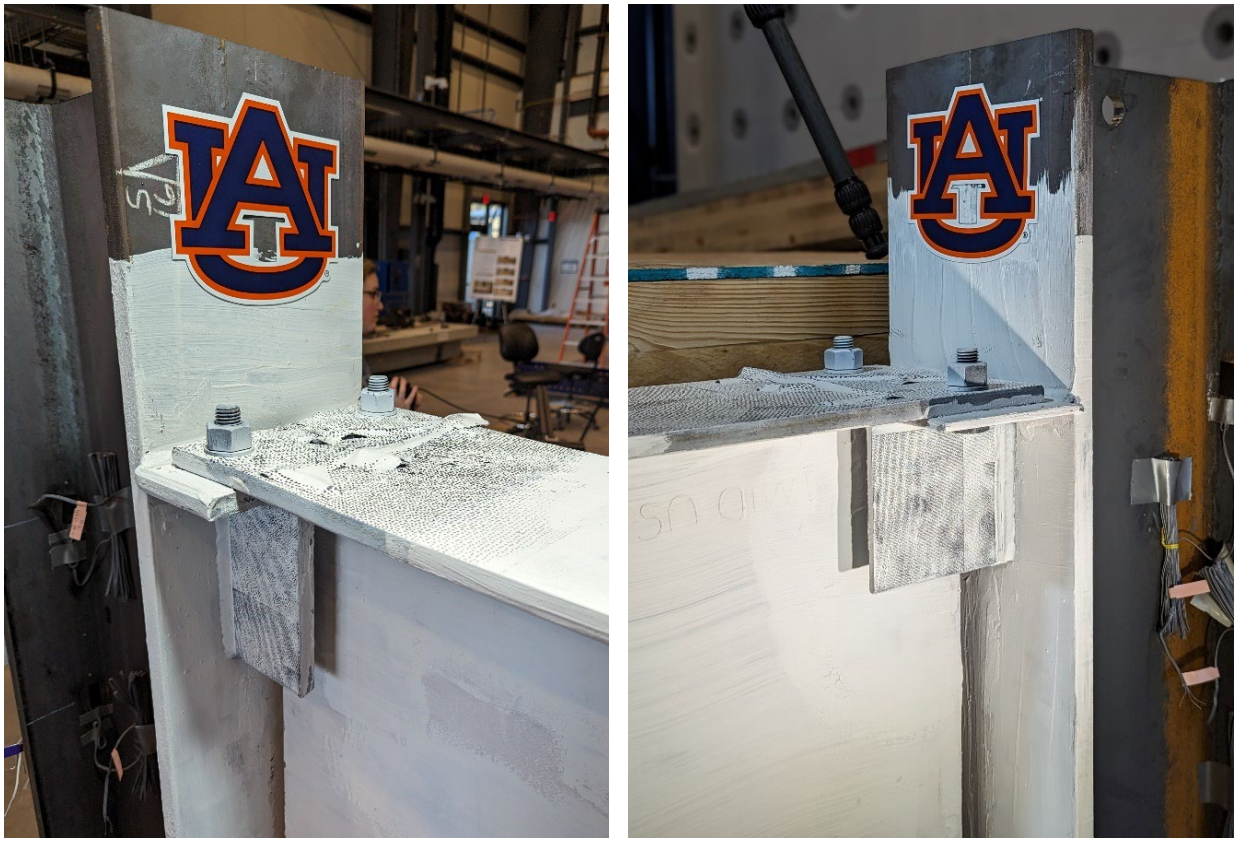

Figure 32: Connections Before Testing (a) Connection C and (b) Connection D

Similar to Test One, Test Two was conducted in two rounds. In the first round of loading (Test-2.1), the girder was subjected to four-point loading, with the loading points dividing the girder span into three equal segments of 66.75 inches. The resulting mid-span moment – mid-span displacement is shown in Figure 33. Test-2.1 was concluded due to a sudden weld failure on Connection D[1]. Figure 34 (b) shows the weld failure and the angle buckling that resulted from the weld failure. At the time of the weld failure, the connection shear was above the design shear (V_u), as shown in the connection shear strain-shear force plot of Figure 35. The engineering shear strain was calculated from strain gauge rosettes attached to both connection's North angles. The thicker and deeper angle on Connection C experienced a small shear strain within the elastic range. In comparison, Connection D's shallower and thinner angle underwent a large plastic shear strain before the weld failure. As shown in Figure 34 (a), Connection C had no noticeable damage at the end of Test-2.1; thus, Connection D was retrofitted to test Connection C to failure in Test-2.2.

[1] *Note that this was expected since the calculations prior to testing indicated the weld controlled. The failure load was above the calculated value.*

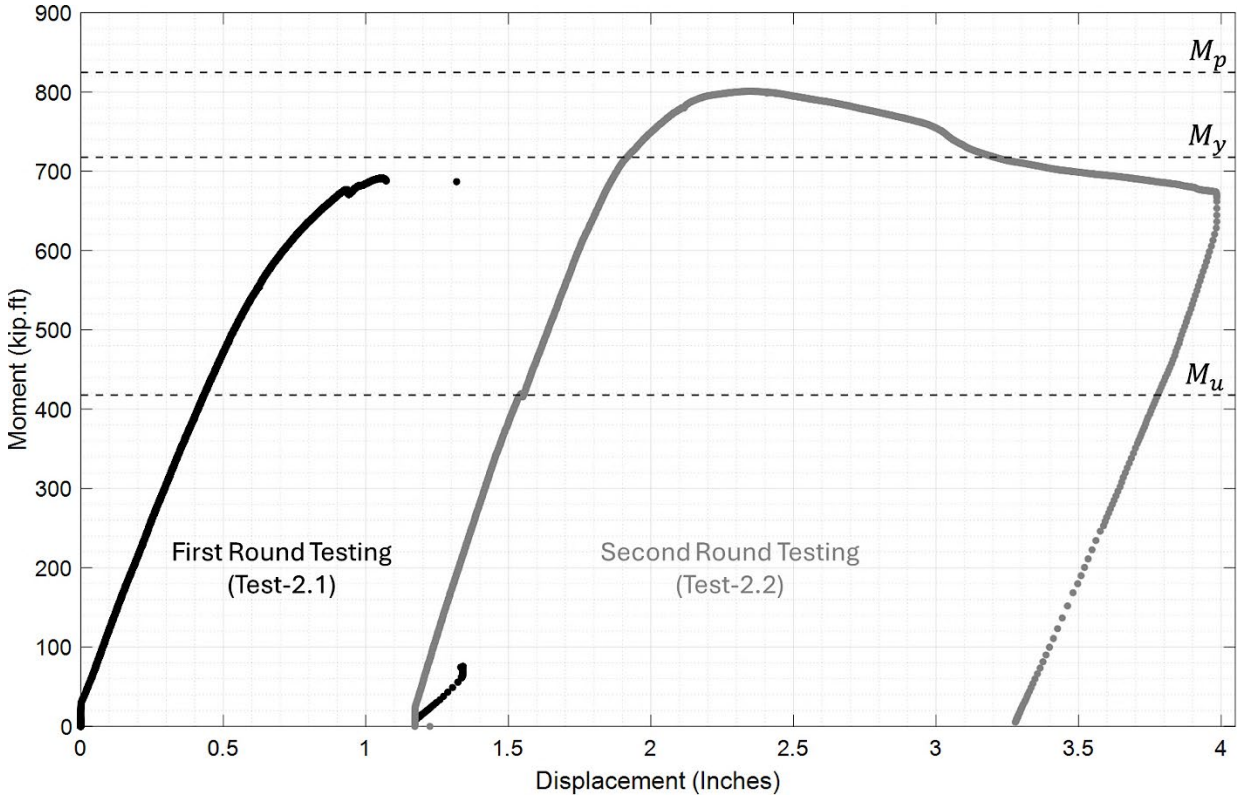

Figure 33: Mid-Span Moment – Mid-Span Displacement Curve

a. **b.**

Figure 34: Connections After First Round Testing (Test-2.1) (a) Connection C and (b) Connection D

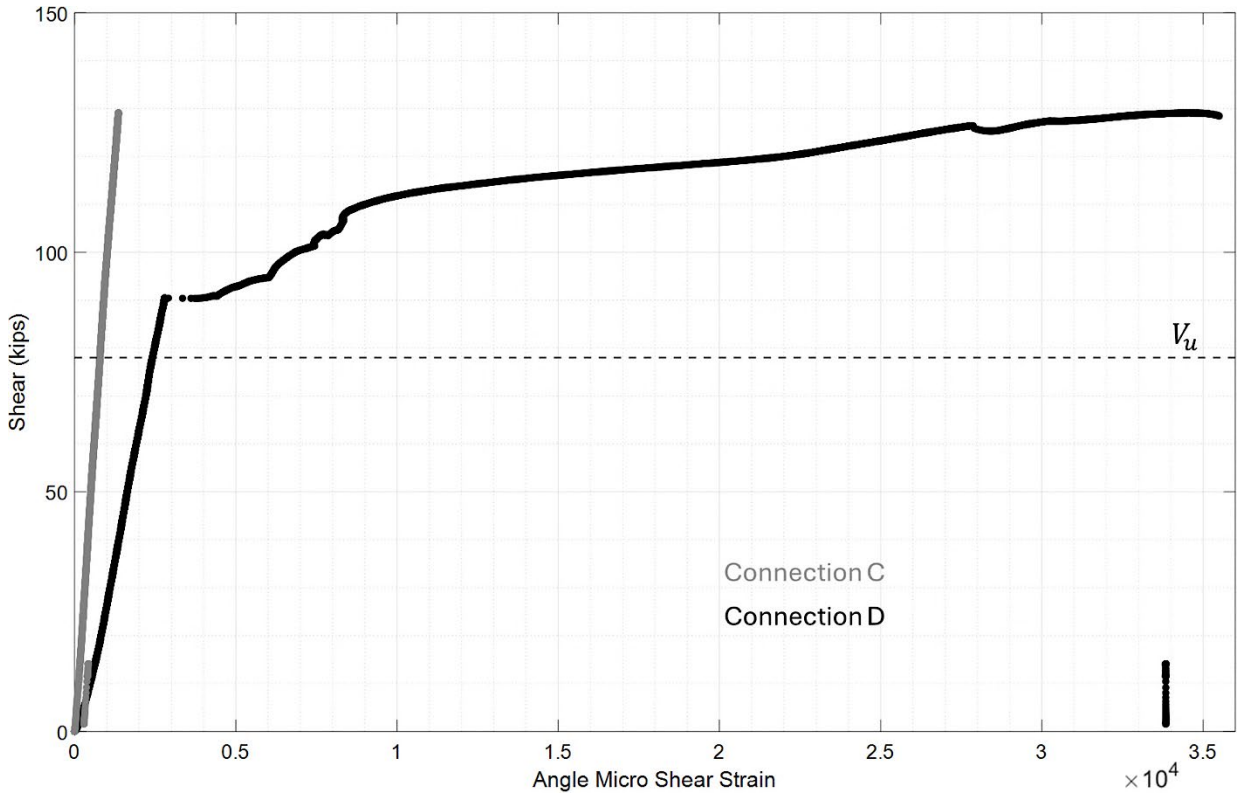

Figure 35: Angle Maximum Engineering Shear Strain - Connection Shear Force for Test-2.1

The shear-rotation plots from the two rounds of testing (Tests 2.1 and 2.2) are shown in Figure 36[2]. In Test-2.2, the loading points were moved closer to mid-span, two feet apart, and symmetric about mid-span to increase the rotational demand on the connections. Test-2.2 was concluded at an approximate Connection C rotation of 0.04-radian. The rotation was calculated as the difference between the measured girder end and column rotations. The connection shear at the maximum measured rotation was 28% higher than the design shear force V_u. The decrease in connection shear force observed after around 0.025-radian rotation resulted from girder flange and web buckling near the loading points and was not associated with connection failure. Connection C near the maximum measured rotation and the retrofit double angle connection on the opposite end are shown in Figure 37.

[2] *Note that Connection D data is not provided for Test-2.2 because this was a retrofitted connection.*

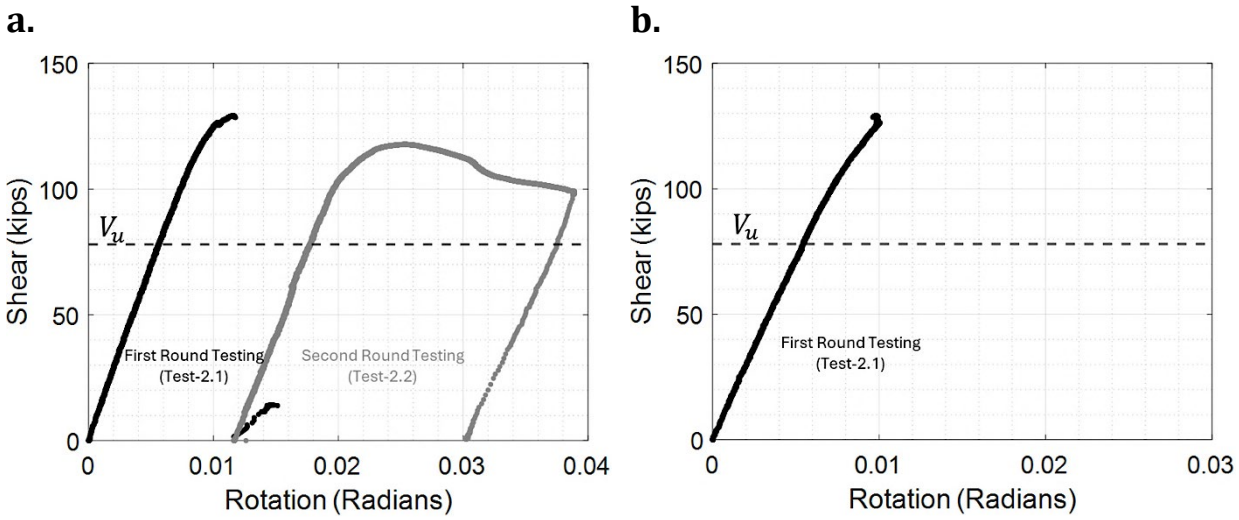

Figure 36: Shear-Rotation Plots (a) Connection C and (b) Connection D

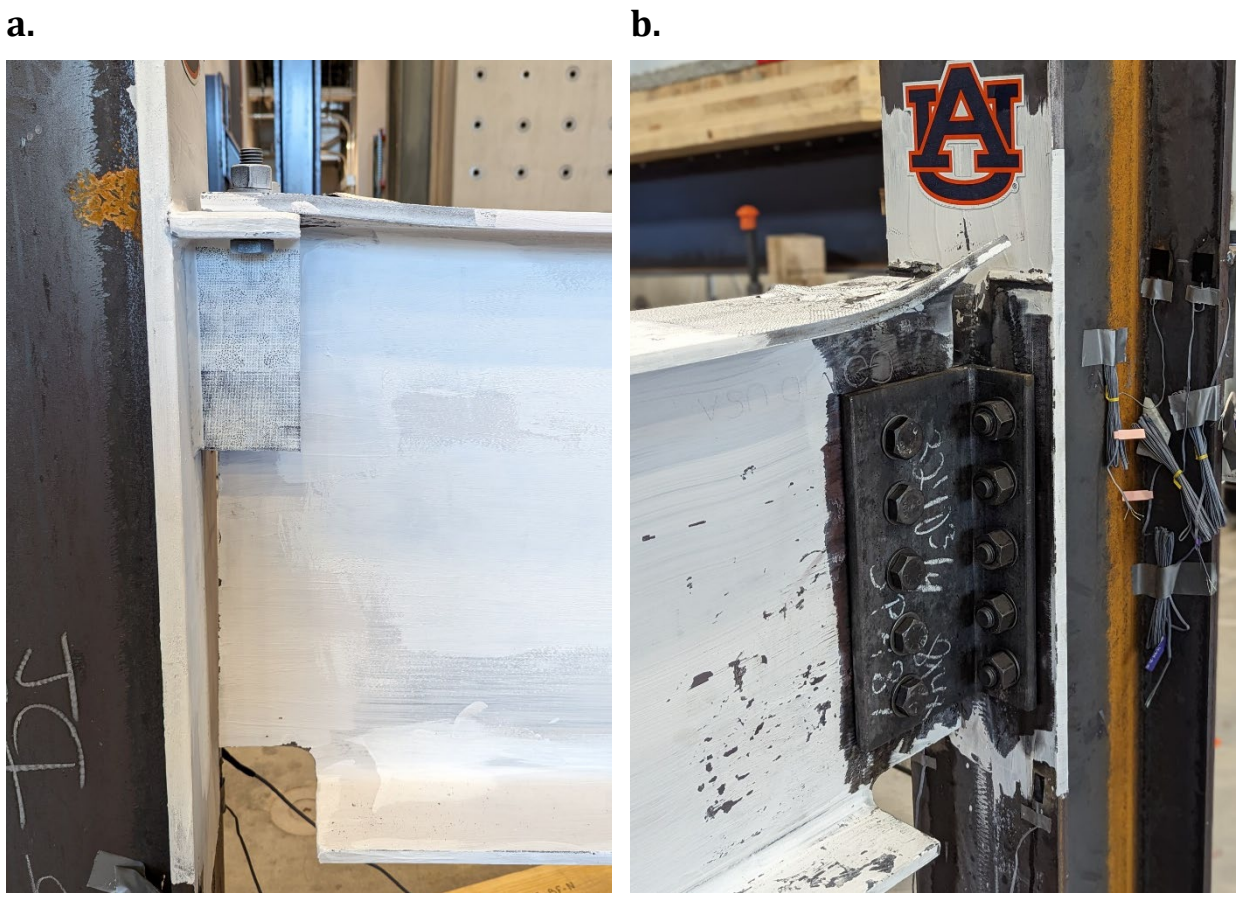

Figure 37: Connections During Test-2.2 (a) Connection C near 0.04-radian Rotation and (b) Retrofit Double Angle Connection

The girder's bending moment diagram was constructed using moments calculated from strain gage data at five different sections. The measured mid-span moment was assumed to

be constant between the loading points, and a linear line was fitted into the data to obtain the bending moment diagram. The resulting bending moment diagram is shown at the design load and over a range of load levels in Figure 38 (a) and (b), respectively. The bending moment diagram was then used to estimate the support moment, which was taken as the moment at the face of the column flange.

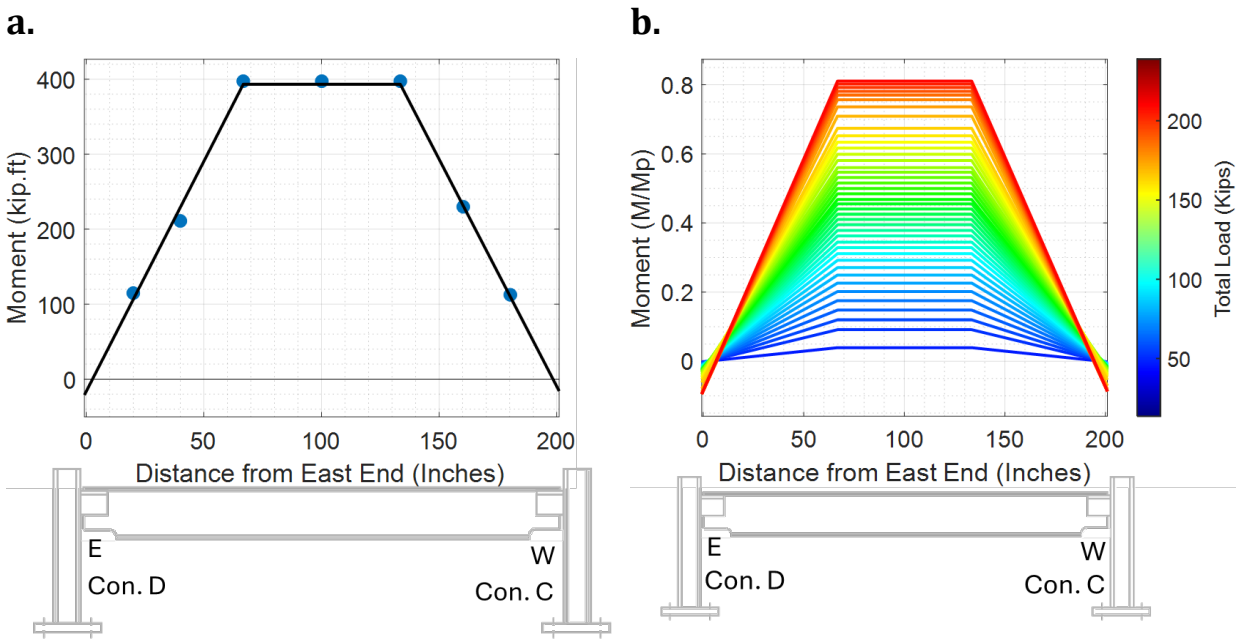

Figure 38: Girder Bending Moment Diagram (a) At the Design Load and (b) Over a Range of Loads

A plot of the resulting support moment normalized by the plastic moment of the girder (M_p) in relation to the connection rotation is shown in Figure 39. The plots show that the connections' rotational stiffness was less than the 2EI/L limit, and the rotation of Connection D was above the 0.03-radian limit. The support moment of Connection D peaked at $0.2M_p$ at approximately 0.02-radian rotation before dropping down and gradually increasing. At 0.02-radian rotation, the support moment is roughly at the $0.2M_p$ limit and considered sufficient.

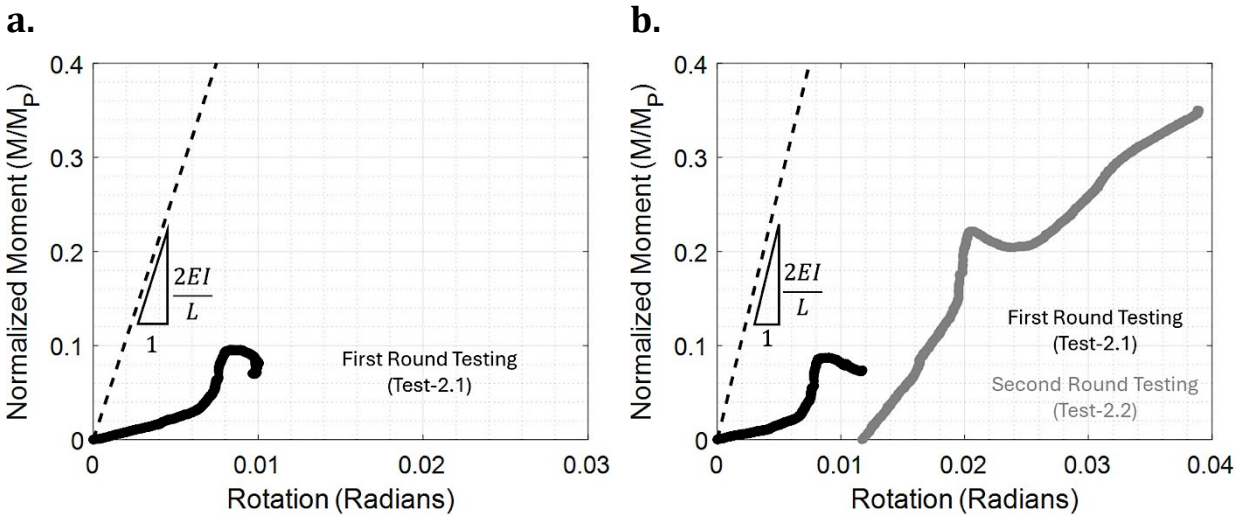

Figure 39: Normalized Support Moment – Rotation Curve (a) Connection C and (b) Connection D

Pertaining to the DIC investigation of Connections C and D, all four available cameras were utilized in Test-2.1. Connection C girder top flange, Connection C angle, Connection D girder top flange, and Connection D angle were captured in 2D with one camera allocated to each.

An approximate area of 81 square inches (9.0 inches longitudinally by the width of the girder top flange) was prepared closest to the column face to investigate Connection C's girder top flange. A rough area of 30 square inches (entire visible vertical angle face) was prepared for the angle. Once Test-2.1 was concluded, both sets of images were analyzed in VIC-2D. Figure 40 exhibits the girder's yield line formation, in units of microstrain, with (a) Von Mises strains (ε_v) and (b) transverse strains (ε_{xx}) for a connection shear (or reaction) of 25, 30, 35, 40, and 125 kips. Figure 40 is oriented in such a way that the midspan of the girder is in the upper direction of the progression photo and the stub column/connection angles are in the lower portion of the photo.

a.

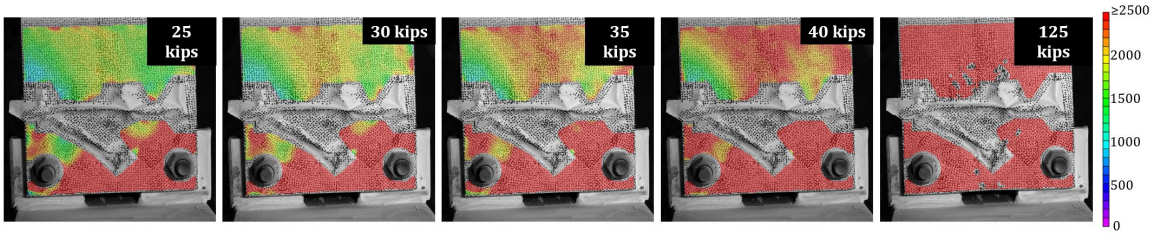

b.

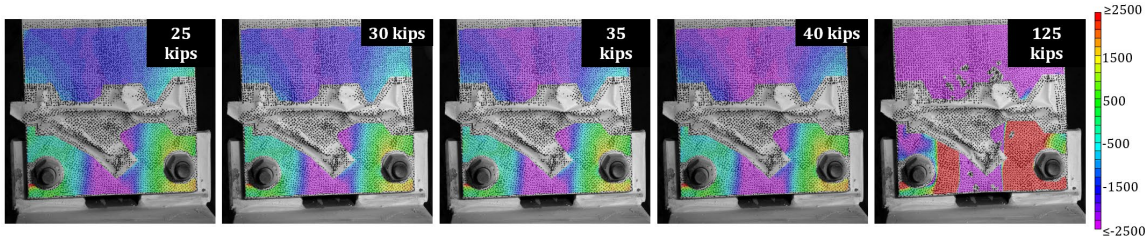

Figure 40: Connection C (Test-2.1) DIC Flange Deformation Progression (a) Von Mises Strain (ε_v) and (b) Transverse Strain (ε_{xx}) – Engineering

In both strain tensors at a shear of 25 kips, large areas of yielding (in compression) are seen beginning to form on the longitudinal centerline of the flange closest to the face of the column and gradually move towards the midspan of the beam, like that of previously discussed girders. Also, at the maximum shear of 125 kips, tensile yield lines are prominent along the interior longitudinal edges of the angles, corresponding to the observations shown in previous connections. After this test, the flange surface had completely yielded, as shown in the Von Mises strain progression.

Longitudinal strains (ε_{yy}) were not included in this figure due to insignificant data observed, likely due to the placement of the strain gauges in areas where large magnitudes of longitudinal strain would likely have occurred. These areas where the strain gauges were located were covered with tape and excluded from the defined area of interest in the VIC-2D analysis. This area is seen in the middle and lower portions of the flange and remains white with black speckling in all progression images.

Like that of Connection A, the area of the flange beyond the bearing length (towards midspan) cannot be referenced to provide any reliable data because of the girder's movement away from the visual sensor; a singular camera cannot interpret this out-of-plane movement properly and perceives it as compression, creating a compression bias in this region. Though this area towards midspan is not suitable for conclusive evidence pertaining to strain magnitudes and exact yield line progression distance, the flaking of paint shown (at the maximum shear) beyond the bearing length provides insight into the probable length of the yield lines. As the underlying steel surface deformed, the spray paint began to flake off, revealing the extent of the yield lines. This inference shows that the yield lines extended approximately three to four inches beyond the bearing length of three inches.

To further investigate the transverse strain observed in Connection C's girder top flange, a transverse cross-sectional cut was made approximately midway between the transverse edge of the angles and the bolt centerline at various shear forces, as shown in Figure 41.

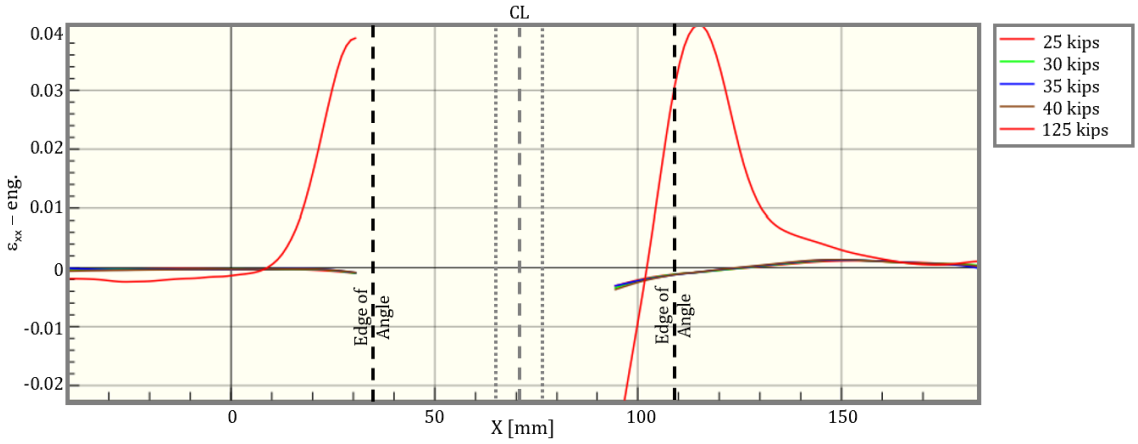

Figure 41: Connection C (Test-2.1) DIC Flange Section Cut Transverse Strain (ε_{xx}) Profile

The theoretical centerline (CL) of the flange (with the edges of the flange web shown on each side) and the edge of the right-hand and left-hand angles (as seen from plan view with the midspan of the girder into the plane) are noted for reference in Figure 41. While large portions of strain data are not visible due to the strain gauges, two plastic hinges are apparent near the longitudinal edges of the angles; another plastic hinge is found near the web edge, likely in the fillet zone. Precisely, two tensile strains of 0.04 and 0.038, at a connection shear of 125 kips, are located approximately 0.47 in. (12 mm) and 0.18 in. (4.6 mm) to the right and left of their respective angles edge. A maximum compressive strain of 0.02 is located approximately 0.79 in. (20 mm) left of the right-hand web edge.

In Figure 42 the strain field formation of Connection C's vertical angle leg, in microstrain units, is shown in (a) Von Mises strain (ε_v) and (b) shear strain (ε_{xy}) for a connection shear of 25, 30, 35, 40, and maximum of 125 kips.

a.

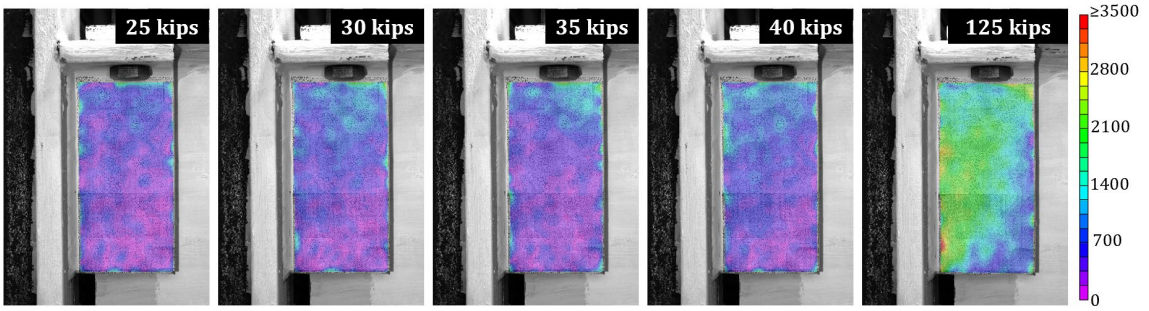

b.

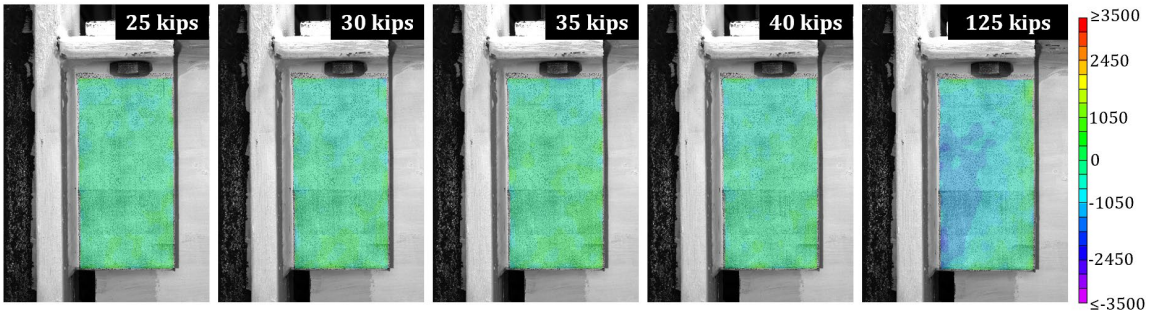

Figure 42: Connection C (Test 2) DIC Angle Deformation Progression (a) Von Mises Strain (ε_v) and (b) Shear Strain (ε_{xy}) – Engineering

As the angle is stocky compared to its bearing length, the angle's lower left-hand area (fixed to the column) does not show signs of surface yielding until a connection shear of 125 kips is reached. This area extends diagonally across the angle to the upper right-hand corner (free end), resulting in small amounts of plastic deformation. As displayed in Figure 42(b) and ignoring stress concentrations near the weld, most of the angle remains approximately equal to the yield prediction. However, complete angle failure of this connection was not observed.

Identical to the analysis of Connection C, Connection D's behavior was investigated via 2D-DIC of both the girder's top flange and the vertical angle leg. For the girder, an approximate area of 126 square inches (14 inches longitudinally by the width of the girder top flange) was prepared closest to the column face; a rough area of 34 square inches (entire visible vertical angle) was prepared for the angle. Figure 43 displays the girder's strain formation in units of microstrain with (a) Von Mises strain (ε_v) and (b) transverse strains (ε_{xx}) for a connection shear of 25, 30, 35, 40, and 125 kips. Progression photos are oriented in such a way that the midspan of the girder is in the upper direction of each photo, and the stub column/connection angles are in the lower portion of the photo.

a.

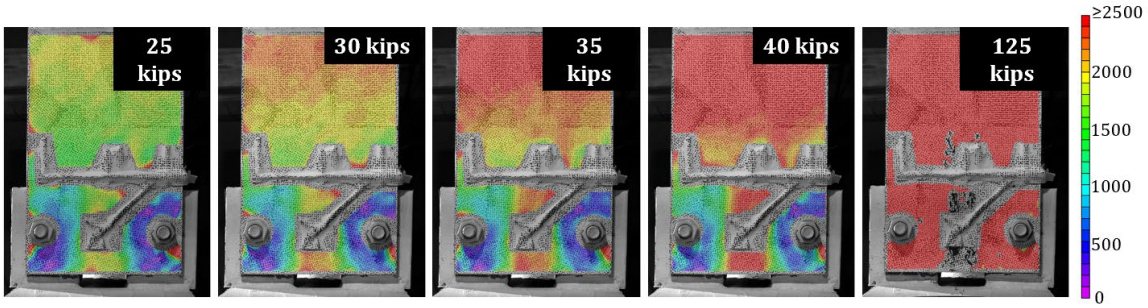

b.

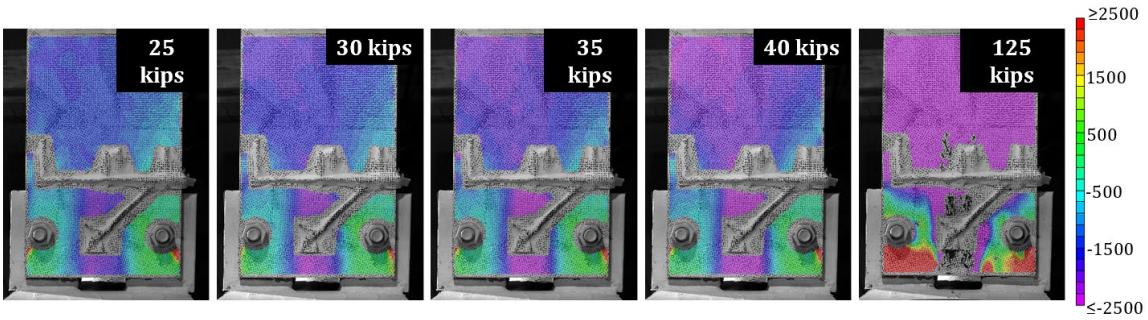

Figure 43: Connection D (Test-2.1) DIC Flange Deformation Progression (a) Von Mises Strain (ε_v) and (b) Transverse Strain (ε_{xx}) – Engineering

Prominently shown at a shear of 30 kips is a wide strain field along the longitudinal centerline of the flange, showing plastic deformation. According to Figure 43(b), this unsupported region between the angles has yielded in compression. While this initial yield line is akin to previously discussed connections, excluding yield lines along the interior longitudinal edges of the angles proves contrary to those seen in previous connections that utilized stiffer angles. Longitudinal strain (ε_{yy}) formation was not included in this figure due to little beneficial data regarding connection behavior due to the location of the strain gauges.

Similar to connections A and C, conclusive strain magnitudes beyond the edges of the angles cannot be determined due to out-of-plane movement of the area beyond the bearing length. The monocular vision of the 2D-DIC system cannot capture this movement so a clear compression bias was formed and is evident throughout progression images. While this area towards midspan is not suitable for conclusive evidence pertaining to strain magnitude, the flaking of the speckle pattern, shown at the maximum shear, can provide insight into the length and progression of the yield lines. Due to yielding at the steel's surface, the paint flakes off, revealing deformation areas. With this deduction, it can be assumed that the yield lines extend approximately three to four inches beyond the bearing length of five inches.

In further investigation of the discussed primary failure mode, a transverse cross-sectional cut of Connection D's girder top flange is presented in Figure 44. The cut was made approximately halfway between the transverse edge of the angles and the bolt centerline at various shear forces. The theoretical centerline (CL) of the flange (with the edges of the flange web noted on each side) and the edge of the right-hand and left-hand angles (as seen from the plan view with the midspan of the girder into the plane) are shown. Unlike previously seen in stiffer deeper connections, very little tensile strain is observed. The maximum compressive strain provided is 0.01, located 19 mm (0.75 in.) left of the web edge. If flaking had not occurred at the centerline late in testing, perhaps a compressive strain of greater magnitude would have been revealed closer to the web, similar to that seen in previous connections.

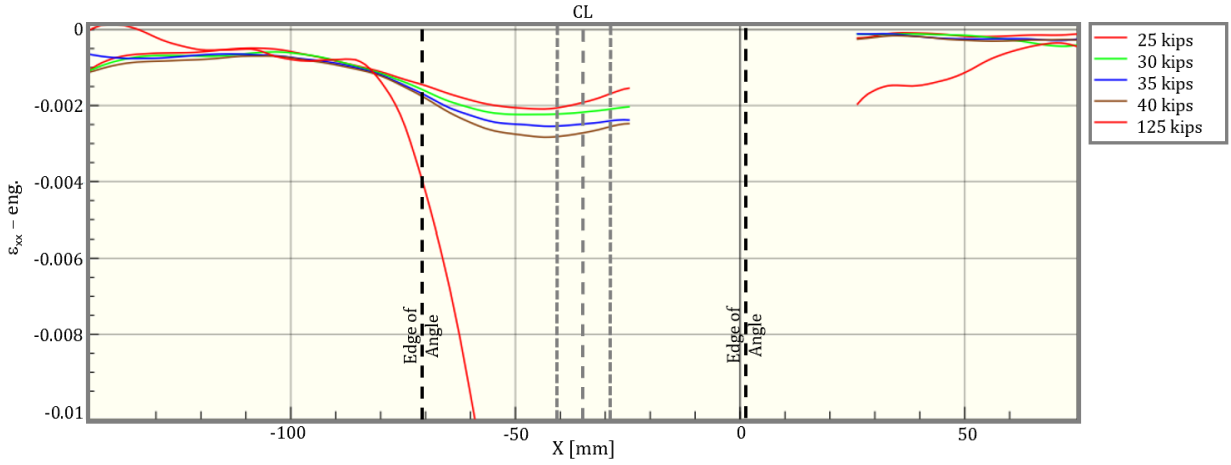

Figure 44: Connection D (Test-2.1) DIC Flange Section Cut Transverse Strain (exx) Profile

The strain field formation of Connection D's vertical angle leg is shown, in microstrain units, in Figure 45 (a) Von Mises strain (ε_v) and (b) shear strain (ε_{xy}) for a connection shear of 25, 30, 35, 40, and maximum of 125 kips. The upper right-hand area (attached to the column) of the angle begins to yield and extends along and down the angle to the lower right-hand corner (fixed end). As would be expected, the highest shear strain occurred closest to the column face and actual connection interface. At the highest shear, a majority of the angle has yielded according to the Von Mises strain. It is noted that this angle's weld did not fail but experienced buckling at the time of its counterpart's weld failure.

a.

b.

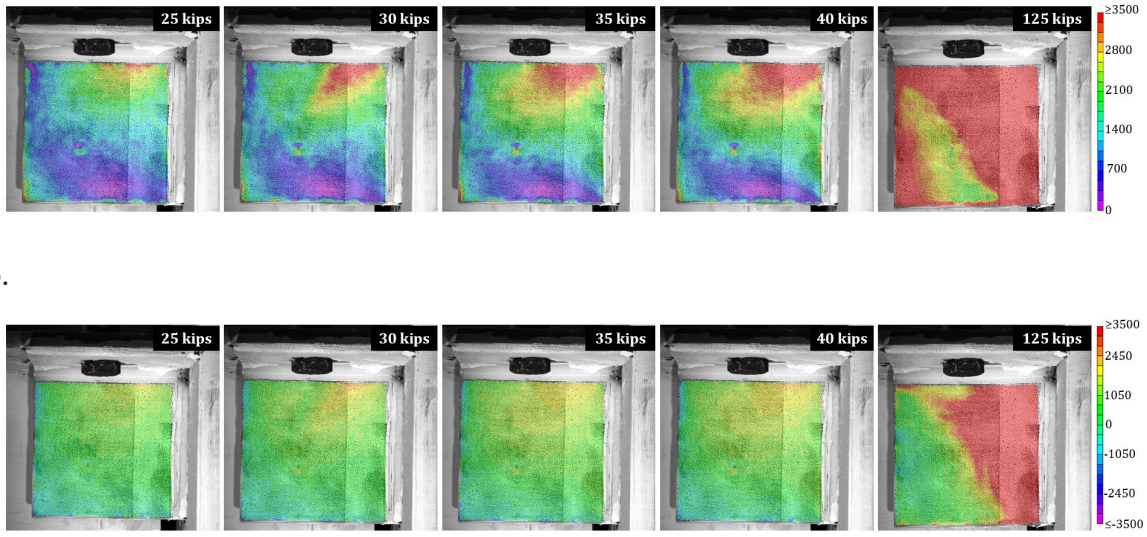

Figure 45: Connection D (Test-2.1) DIC Angle Deformation Progression (a) Von Mises Strain (ε_v) and (b) Shear Strain (ε_{xy}) - Engineering

The Drop-In Connection C satisfied the strength, stiffness, and ductility requirements. The torsional stiffness was not evaluated as part of Test Two. The Drop-In Connection D satisfied the strength and stiffness requirements but did not meet the necessary ductility due to the weld geometry provided.

Test Three

Test Three was conducted in the test setup shown in Figure 14, like the previous two tests. The lateral supports in Test Three were shimmed to be in contact with the girder or keep the clearance below a quarter of an inch. To avoid friction build-up, all the lateral supports were adequately lubricated. A drop-in connection with a five-inch bearing length and L8x4x1/2 angles was utilized on the East end (Connection E), and a 3/8-inch thick shear tab with four one-inch diameter bolts was utilized on the West end (Connection F). Connections E and F were designed to achieve the same magnitude of shear force and are shown in Figure 46 before testing. The test was conducted in two rounds. In the first round (Test-3.1), the girder was loaded in four-point bending, with the loading points dividing it into three equal 66.75-inch long segments. The maximum connection shear in Test-3.1 was 1.9 times the design shear strength of the connections; the maximum connection rotation was 0.028 and 0.03 radians in Connections E and F, respectively. Test-3.1 was concluded due to instability in the load spreader beam after the girder mid-span moment reached 81% of its plastic moment capacity. The shear-rotation graph of the connections and the mid-span moment-displacement plots are shown in Figure 47 and Figure 48, respectively.

At the end of Test-3.1, no damage or strength loss was observed in either connection, as illustrated in Figure 49 and Figure 50. Figure 49 and Figure 50 also depict the connections' in-plane and out-of-plane residual rotations. While the residual rotation of the drop-in and

shear tab connection were relatively similar in the in-plane direction, it was observed that the out-of-plane residual rotation of the shear tab connection was significantly higher.

a. **b.**

Figure 46: Connections Before Testing (a) Connection E and (b) Connection F

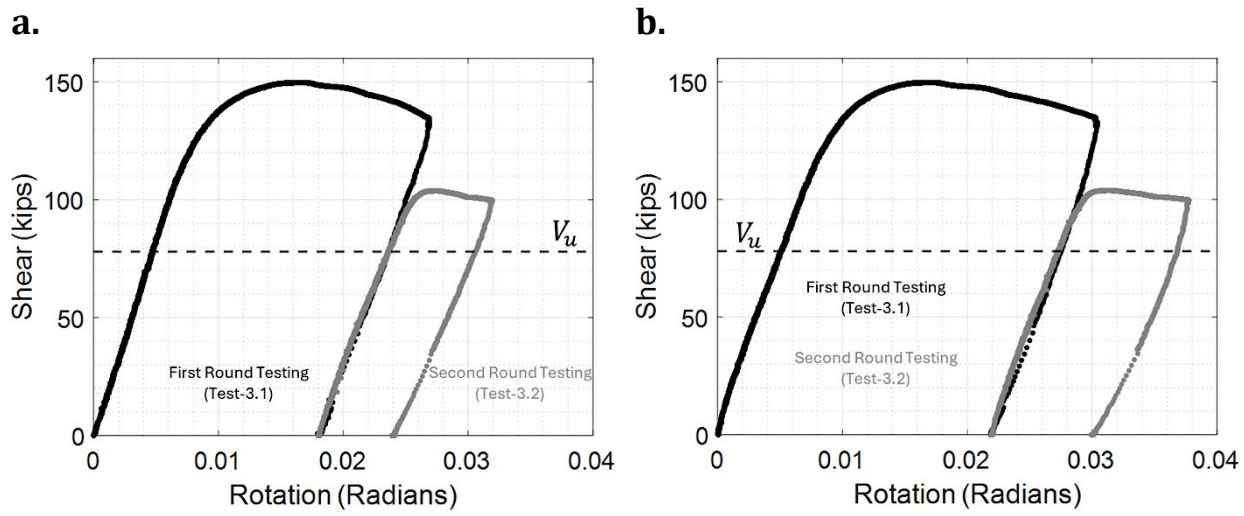

Figure 47: Shear-Rotation Plots (a) Connection E and (b) Connection F

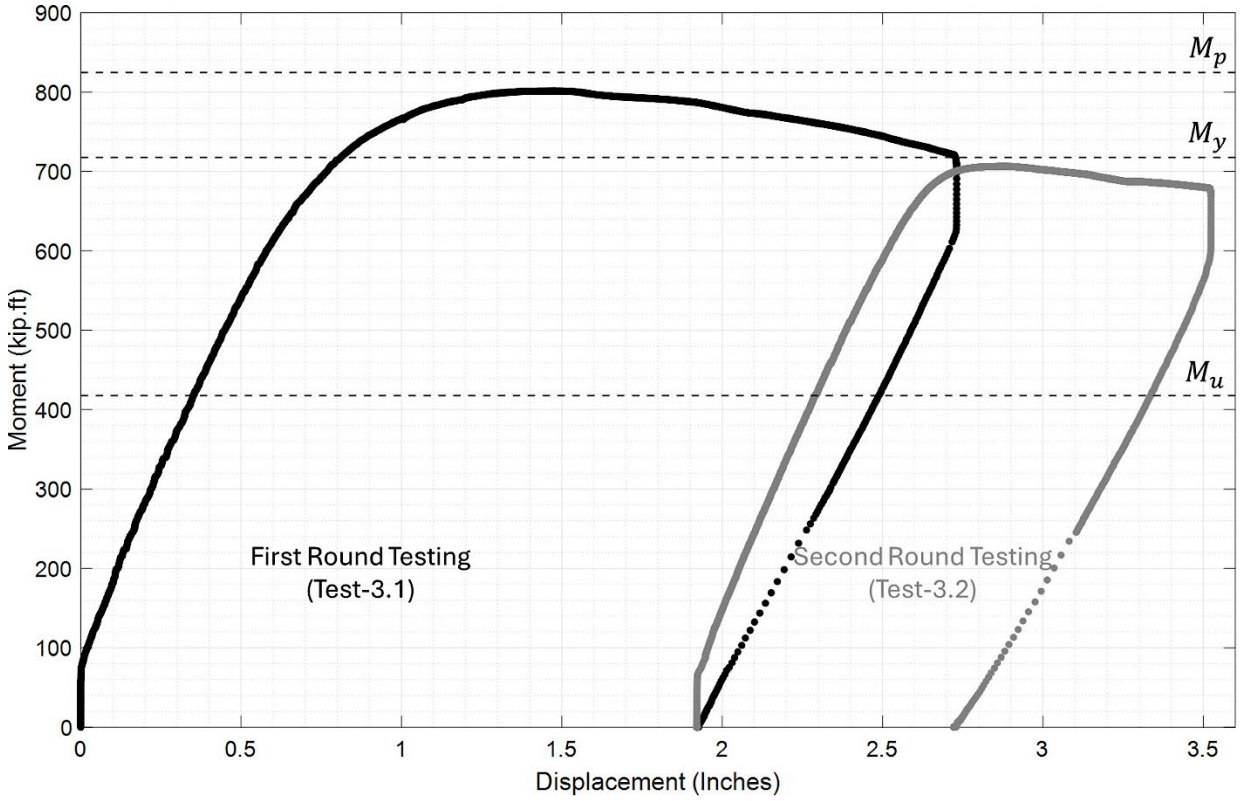

Figure 48: Mid-Span Moment – Mid-Span Displacement Curve

a. **b.**

Figure 49: Residual In-Plane Rotation After Round One Testing (Test-3.1)
(a) Connection E and (b) Connection F

Following the initial round of loading, the loading points were shifted one foot away from the mid-span in both directions to expose the connections to a greater degree of rotation. In the subsequent test (Test-3.2), both connections showed a rotation exceeding the 0.03-radian limit. The shear-rotation plot of Figure 47 shows that the maximum rotation in the shear tab was slightly higher than that in the drop-in connection. Specifically, the shear tab (Connection F) and drop-in (Connection E) reached rotations of 0.038 and 0.32 radians, respectively. Figure 51 shows the connections near their respective maximum rotation.

.a. **b.**

Figure 50: Residual Out-of-Plane Rotation After Round One Testing (Test-3.1)
(a) Connection E and (b) Connection F

a. **b.**

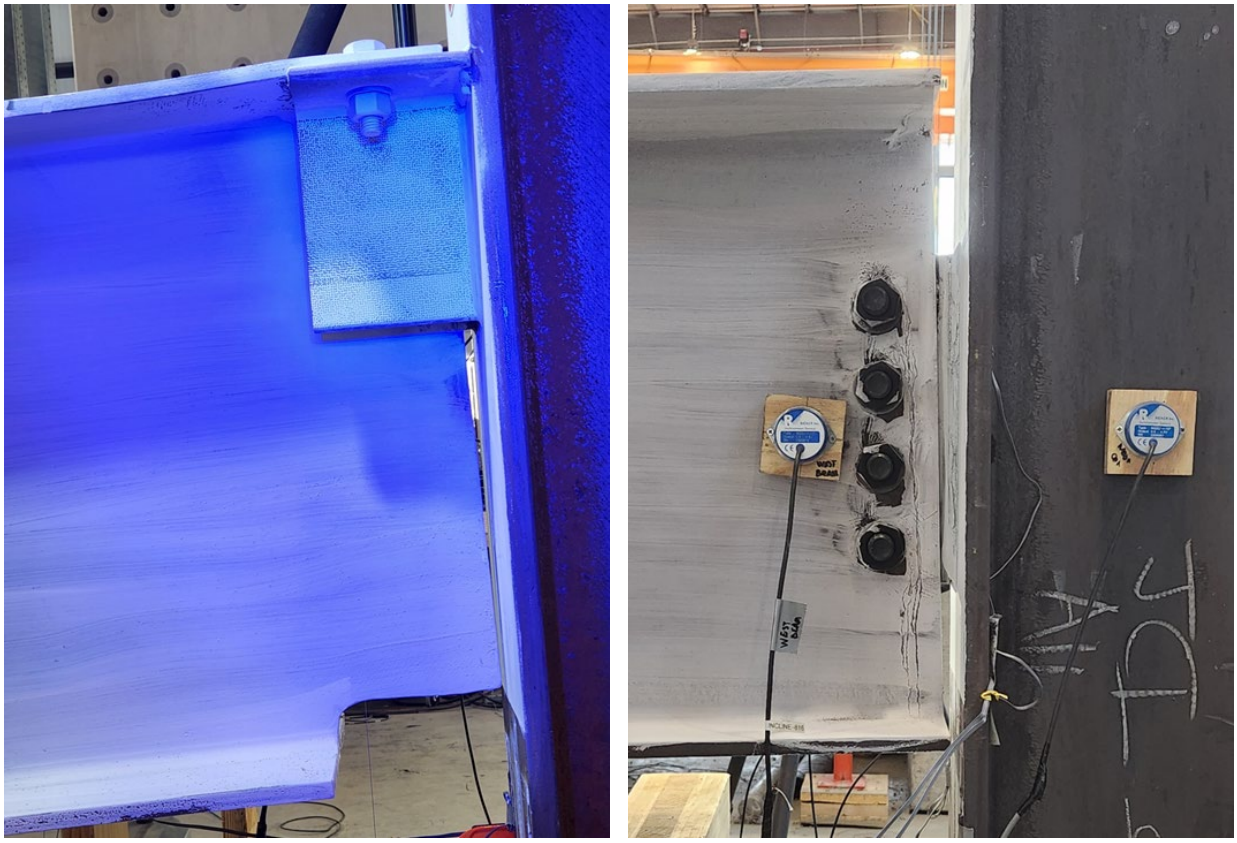

Figure 51: Connections During Test-2.2 (a) Connection E Near 0.032-radian Rotation and (b) Connection F Near 0.038-radian Rotation

The strain values measured at the centerline of the top and bottom flanges of the girder at distances of 20, 40, 100.125, 160.25, and 180.25 inches from the East end were used to calculate the moment at those sections and create the bending moment diagrams depicted in Figure 52. The constant portion of the bending moment was assumed to be equal to the measured mid-span moment, and the sloped portions of the bending moment diagram were determined by fitting lines to the data. These best-fit lines were then used to calculate the support moment (moment at the column face). A plot of the normalized support moment in relation to the connection shear is shown in Figure 53. As evident from Figure 53, the initial rotational stiffness of both connections was below the 2EI/L limit, and the support moment at 0.02-radian rotation was below the $0.2M_p$ limit.

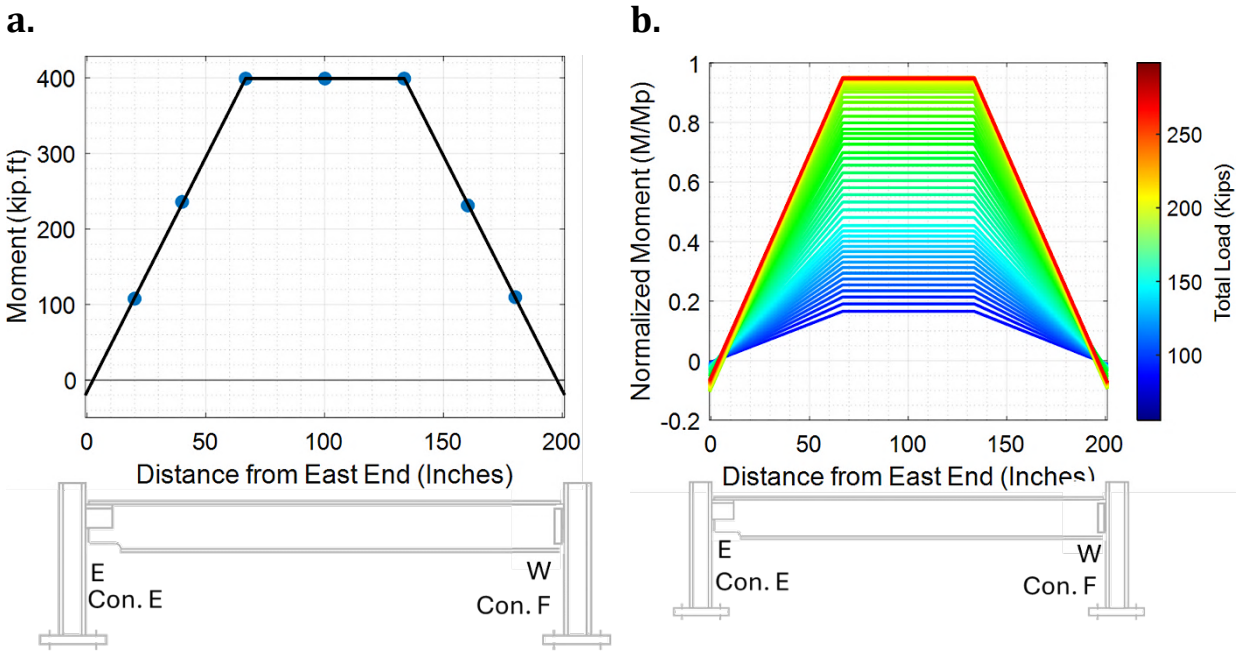

Figure 52: Girder Bending Moment Diagram (a) At the Design Load and (b) Over a Range of Loads

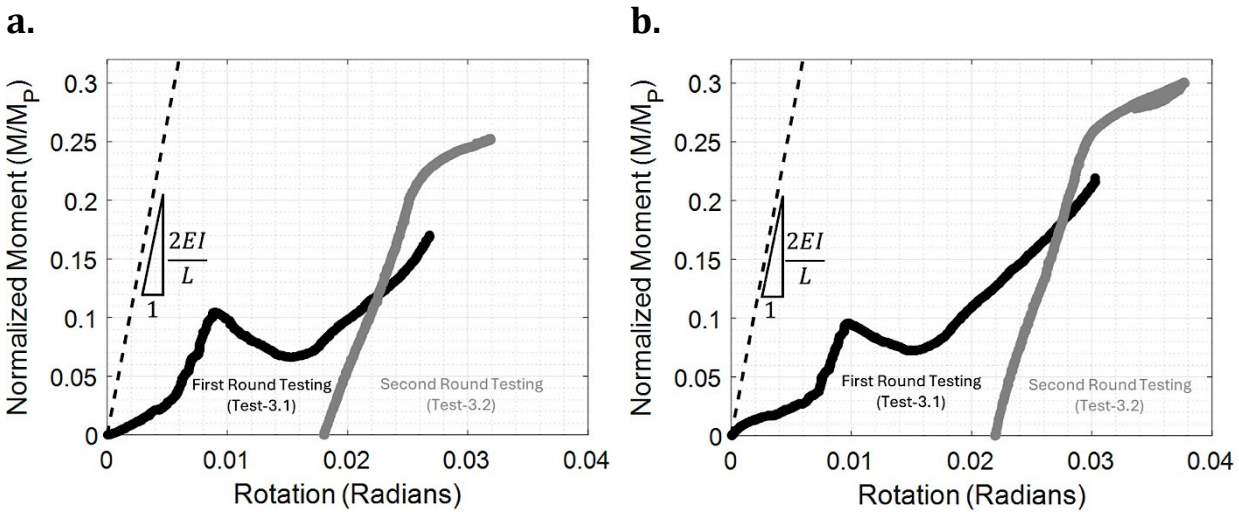

Figure 53: Normalized Support Moment – Rotation Curve (a) Connection E and (b) Connection F

To further investigate Connection E and F's behavior, DIC was utilized in Test-3.1. All four available cameras were used to capture the Connection E vertical leg angle and girder top flange, as well as the Connection F shear tab. Both the angle and shear tab were captured in 2D with one camera allocated to each; the girder top flange was captured in 3D with the two remaining cameras.

To capture Connection E's behavior, an approximate area of 126 square inches (14 inches longitudinally by width of the girder top flange) of the girder top flange was prepared closest

to the column face. As well, a rough area of 46 square inches (entire visible vertical angle face) was prepared for the angle.

Figure 54 shows the progression of the girder's strain field, in microstrain units, with (a) Von Mises strains (ε_v), (b) transverse strains (ε_{xx}), and (c) longitudinal strains (ε_{yy}) for a connection shear of 40, 60, 80, 100, and 145 kips. The photos below are oriented in such a way that the midspan of the girder is in the upper direction and the stub column/connection angles are in the lower portion of the photo. It is noted that due to a glare created by excessive lighting, Connection E's top flange DIC results display a small area of incomplete data. This area is seen in the upper left-hand portion of the flange in all progression images and should be noted when viewing the following figures.

a.

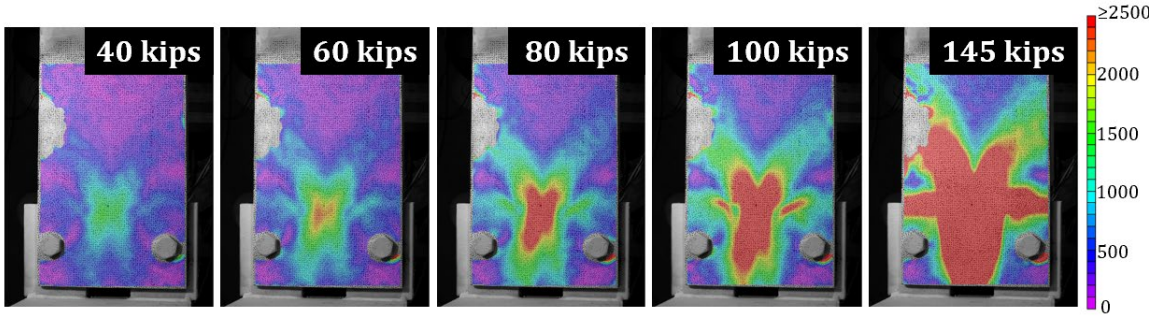

b.

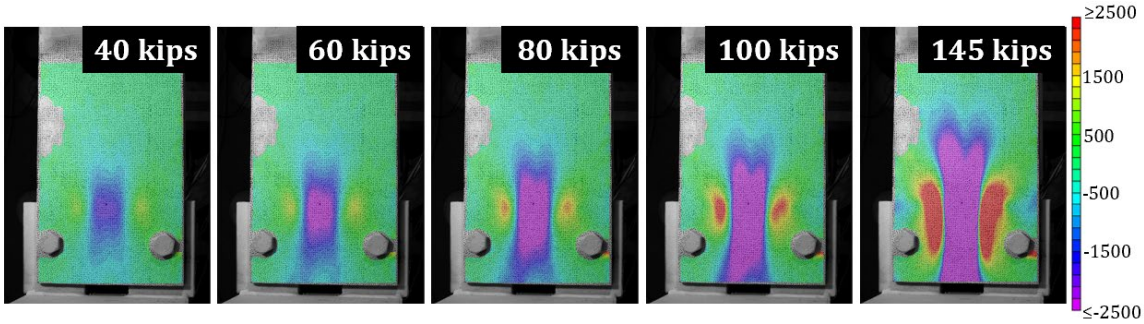

c.

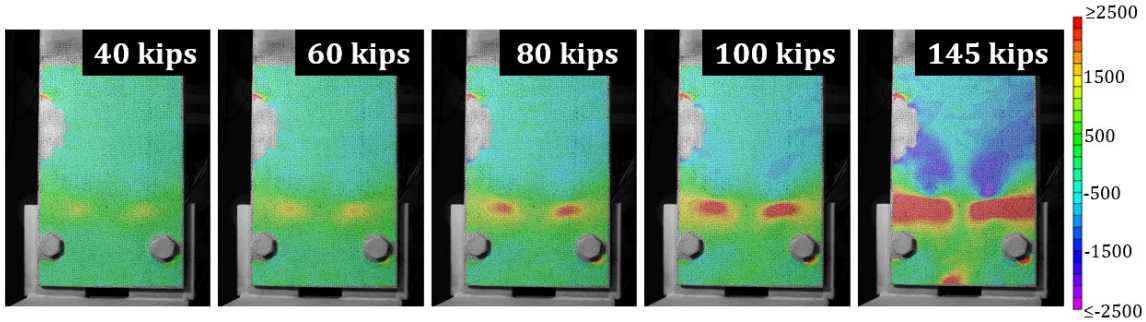

Figure 54: Connection E (Test-3.1) 2D DIC Flange Deformation Progression (a) Von Mises Strain (ε_v), (b) Transverse Strain (ε_{xx}) – Engineering, and (c) Longitudinal Strain (ε_{yy}) – Engineering

Referring to parts (a) and (b), initial yield lines are observed forming at the intersection between the longitudinal centerline of the flange and the transverse edge of the angles, spreading towards the column face and midspan of the beam. The starting location of transverse yielding is contrary to previous connection flanges in which the transverse yield lines began closest to the column face, nevertheless, the yield line eventually progresses towards the face of the column and midspan in a manner most like Connection B. Also, this distance beyond the bearing length is approximately four to five inches, comparable to that confirmed by DIC for Connection B which utilized an identical bearing length of five inches. Most clearly seen in Figure 54(b), secondary yield lines begin to form on the interior corners

of the connection angles at a shear of 80 kips, continuing along the longitudinal interior edge of the angle towards the column and past the angle's transverse edge towards midspan. Once again, the starting point of these secondary yield lines is akin to those observed in Connection A, but variant to connections B and C. However, the final formation along the interior longitudinal edge of the angles is rather identical for all those (besides Connection D that did not experience tensile yielding) previously discussed. The region between the initial yield lines is in compression and the secondary yield lines encase an area in tension.

While visible in all progressive shear forces, the longitudinal strains are seen approaching the yield limit at 80 kips along the transverse edge of the angles. Referencing Figure 54(c), this area is in tension; these yield lines continue along the transverse angle edge creating a plastic hinge in which the flange rotates about. Again, a rotation of 0.027 radians was achieved during this first round of testing, likely which occurred due to the yielding and subsequent loss of stiffness at the end of the bearing length. A secondary set of yield lines past the bearing length and away from the connection are also seen forming at a shear of 145 kips and encasing an area of compression. In total, four transverse and two longitudinal plastic hinges appeared to have formed during this test.

To adequately capture Connection E's behavior, Table 5, noted in units of microstrain, reveals the flange's strains and deformations in a 3D space in which the displacement in the z-direction is exaggerated by 25% compared to the X and Y axes. The Z-axis is relative to the initial position of the flange immediately before testing (z equal to 0) and becomes negative as the specimen moves further from the camera. The X-axis ranges from -4.75 in. to 4.75 in., in which 0 in. is located at the longitudinal centerline of the flange; a positive X-value reflects part of the flange that is to the right of the centerline and over the right-hand angle (in reference to the plan view seen in Figure 54) and vice-versa. The Y-axis ranges from -7 in. to 7 in., the largest value of 7 in. represents the part of the flange closest to midspan, while the smallest value of -7 in. represents the part of the flange closest to the stub column/connection angles. A reference image is shown in Figure 55 to orient the viewer properly.

Figure 55: Connection E 3D Reference

Supplementary to the results discussed for the previously shown strain progression; at a maximum shear of 140 kips, the flange is seen as significantly deformed in the Z-direction with the greatest deformation located at the end closest to midspan. This maximum deformation of approximately 0.25 inches is likely exaggerated due to the hinging of the flange about the transverse angle edges. Also, the small deformation in the area between the longitudinal angle edges is seen due to the multiple hinges formed about the interior longitudinal edge of each angle.

Table 5: Connection E (Test-3.1) 3D DIC Flange Deformation Progression

	Von Mises Strain (ε_v)	Transverse Strain (ε_{xx}) - Engineering	Longitudinal Strain (ε_{yy}) - Engineering
Load (kips)	≥2500 2000 1500 1000 500 0	≥2500 1500 500 -500 -1500 ≤-2500	
40	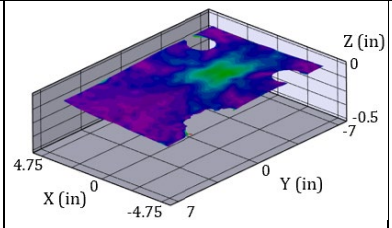	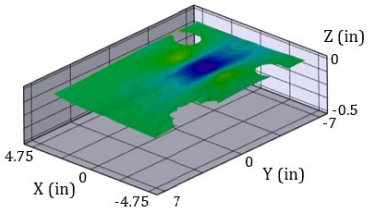	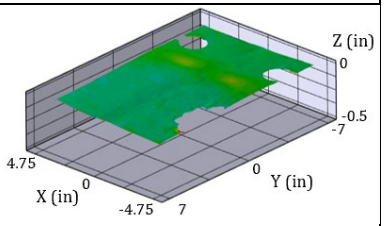
60	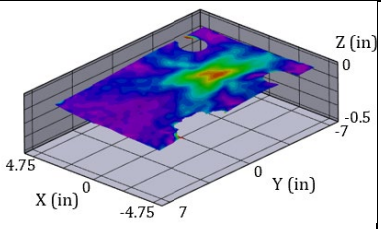	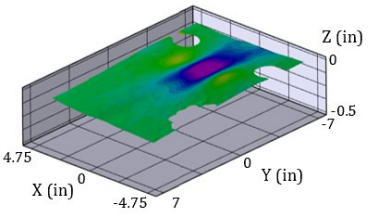	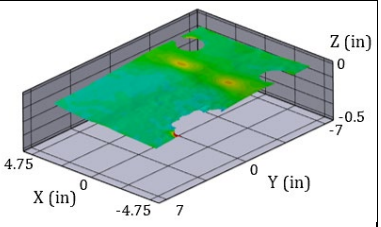
80	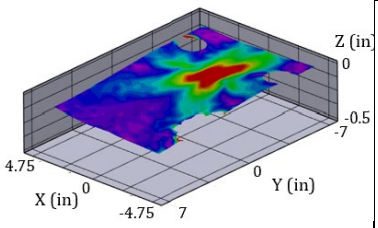	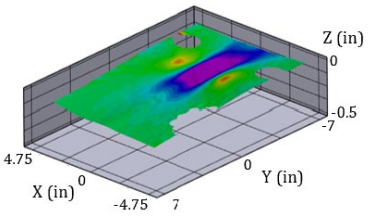	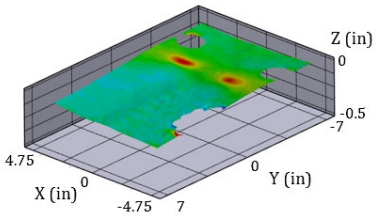
100	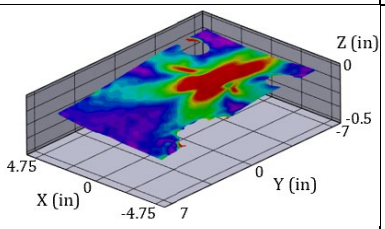	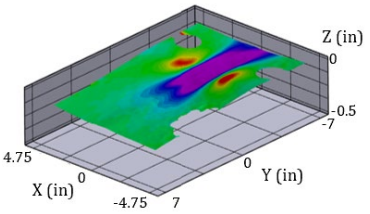	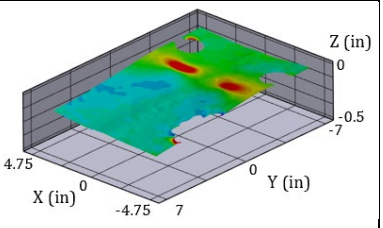
140	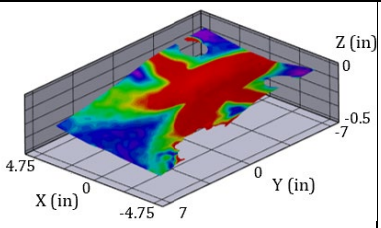	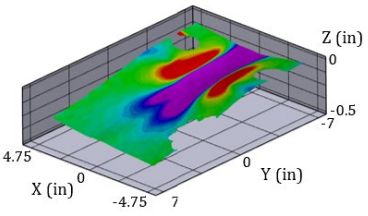	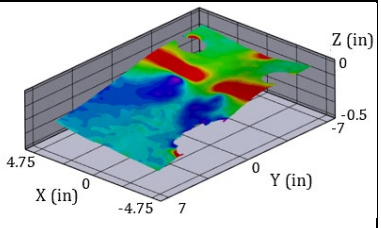

For further analysis of the initial failure mode of transverse bending, a transverse cross-sectional cut of Connection E's girder top flange made approximately midway between the transverse edge of the connection angles and the bolt centerline at various shear forces is shown in Figure 56.

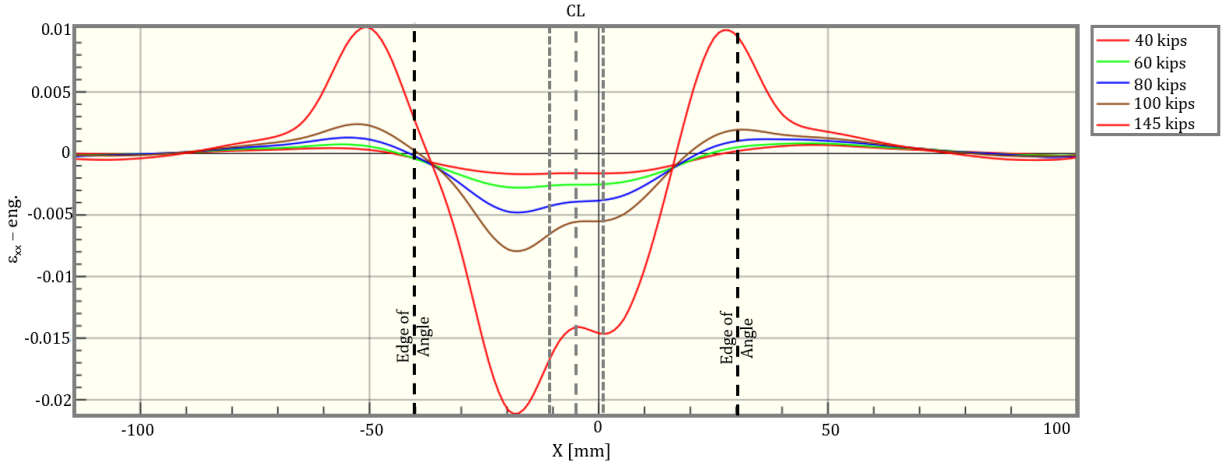

Figure 56: Connection E (Test-3.1) DIC Flange Section Cut Transverse Strain (ε_{xx}) Profile

The theoretical centerline (CL) of the flange (with the edges of the flange web noted on each side) and the edge of the right-hand and left-hand angles (as seen from plan view with the midspan of the girder into the plane) are noted for reference in Figure 56. Analogous to previously discussed cross-sectional plots, two maximum tensile strains are located near the longitudinal interior edges of each angle and two compressive strains are found close to the beam's web, likely in the fillet zone. Specifically occurring at a connection shear of 145 kips, two tensile strains of 0.01 formed approximately 0.38 in. (9.7 mm) left of the left-hand angle edge and 0.14 in. (3.5 mm) left of the right-hand angle edge. As well, compressive strains of a greater magnitude, 0.02 and 0.015, are located approximately 0.31 in. (8 mm) left of the web edge and 0.05 in. (1.5 mm) right of the web edge, respectively. The shift to the left for the right-hand side is likely due to the instability of the spreader beam.

Figure 57 shows the Connection E vertical angle leg strain formation in (a) Von Mises strain (ε_v) and (b) shear strain (ε_{xy}) for a connection shear of 40, 60, 80, 100, and 145 kips.

a.

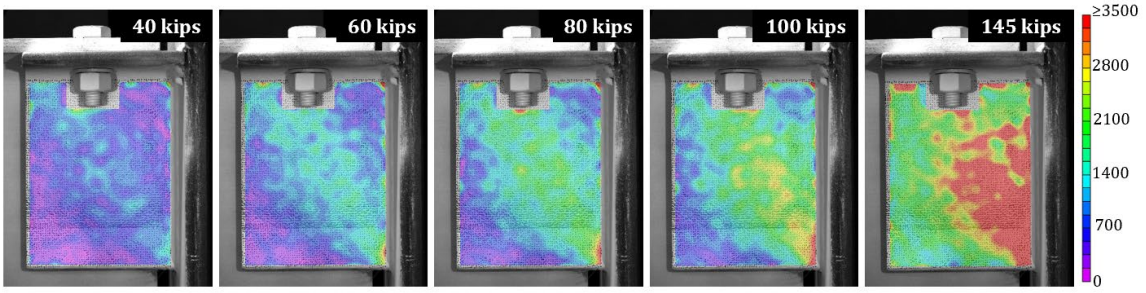

b.

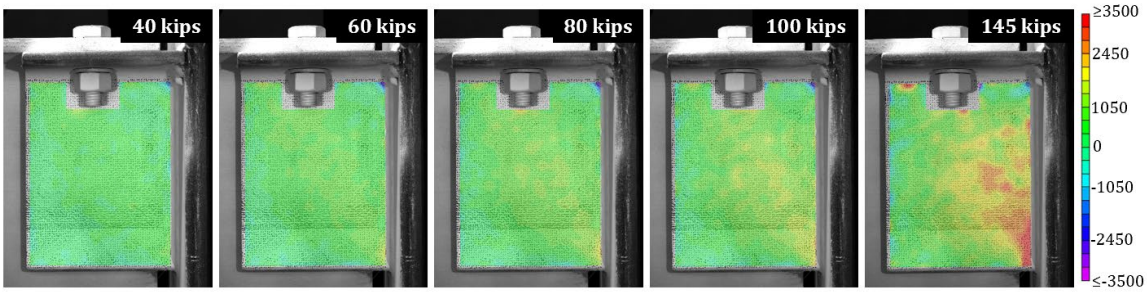

Figure 57: Connection E (Test 3) DIC Angle Deformation Progression (a) Von Mises Strain (ε_v) and (b) Shear Strain (ε_{xy}) – Engineering

Most prominently seen starting at a shear of 80 kips in Figure 57(a), the lower right-hand area (fixed to the column) of the angle begins to yield and extends diagonally across to the upper left-hand corner (free end) of the angle. This pattern is similar to the strain field progression seen in Connection C where yielding begins closest to the fixed end and propagates out at an angle towards the free end. As shown in Figure 57 (a) and (b), a large majority of the angle has reached or exceeded the predicted yield shear strain.

The entire visible steel plate face (approximately 58 square inches) of Connection F was prepared for 2D-DIC analysis. Figure 58 displays the Connection F shear tab strain development in (a) Von Mises strain (ε_v) and (b) shear strain (ε_{xy}) for a connection shear of 40, 60, 80, 100, and a maximum of 145 kips.

a.

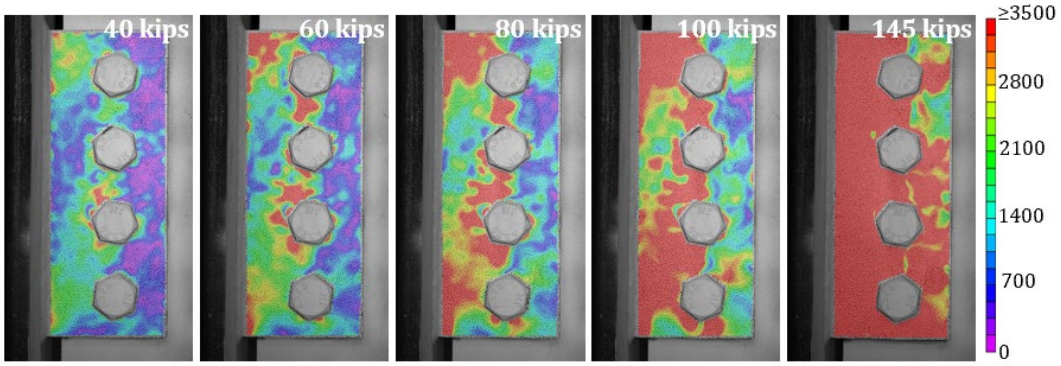

b.

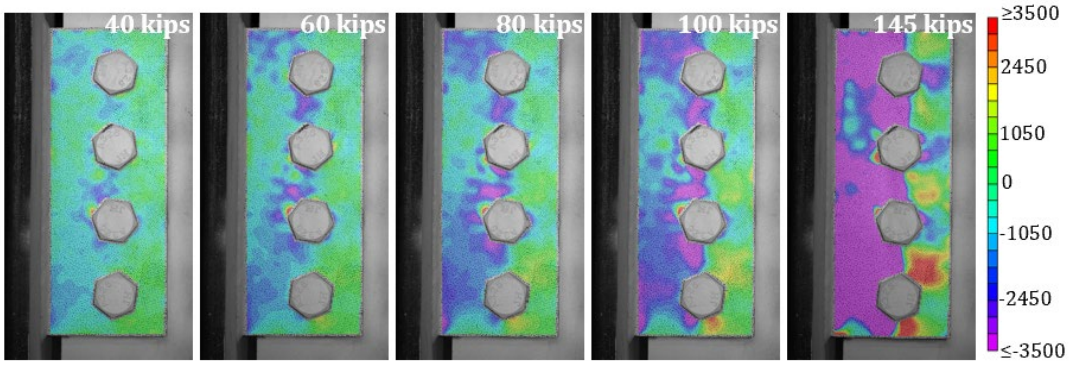

Figure 58: Connection F (Test-3.1) DIC Shear Tab Deformation Progression (a) Von Mises Strain (ε_v) and (b) Shear Strain (ε_{xy}) – Engineering

It is observed that the area between the bolt and weld line (left-hand side) uniformly yielded in shear through the progression of the test. It can be assumed that the yielding shown greatly contributed to the achieved rotation of 0.03 radians during this test cycle.

The Drop-In Connection E and the Shear Tab Connection F satisfied the strength, stiffness, and ductility requirements. The torsional stiffness was not directly evaluated as part of Test Three. However, the drop-in connection exhibited much lower out-of-plane rotation compared to the shear tab connection.

Test Four

Test Four consisted of a smaller girder (W16x36) with a shorter idealized span of 14 feet to evaluate the benchmark design shown in Figure 5. The stub columns shown in the test setup of Figure 14 were pushed inwards by two feet on either side to obtain a shorter span while keeping the lateral supports in the same position. The loading points were adjusted to divide the girder into three equal segments of 50.75 inches.

a. **b.**

Figure 59: Connections Before Testing (a) Connection G and (b) Connection H

The connections tested in Test Four consisted of L6x4x5/16 on the east side (Connection G) and L4x3x1/2 on the west side (Connection H). The bearing length in both cases was three inches, and the angle orientation in Connection H was flipped to investigate its effect. Connections G and H before testing are shown in Figure 59.

a. **b.**

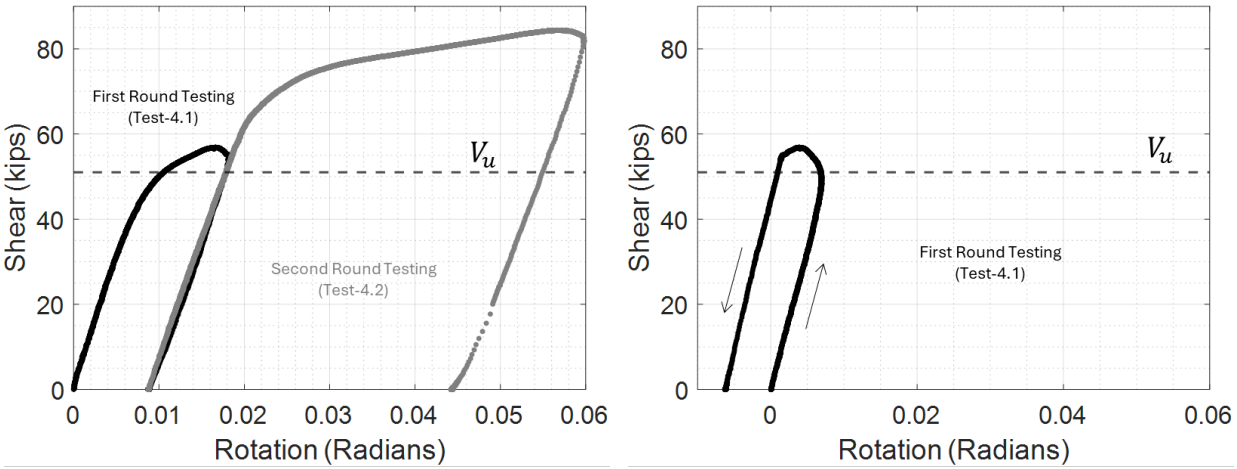

Figure 60: Shear-Rotation Plots (a) Connection G and (b) Connection H

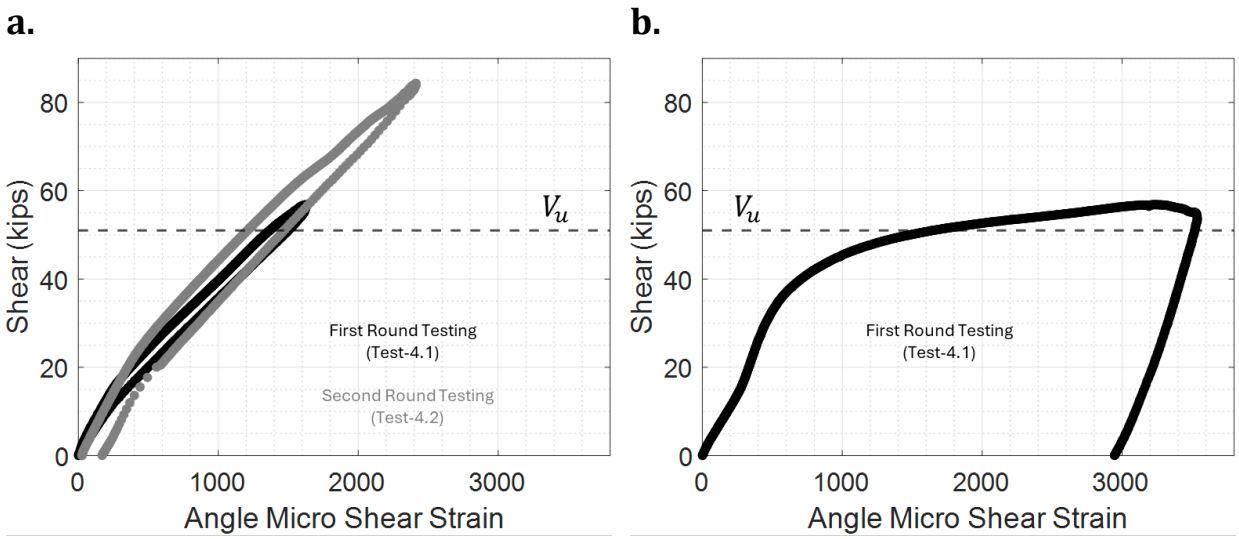

Figure 61: Angle Maximum Engineering Shear Strain (a) Connection G and (b) Connection H

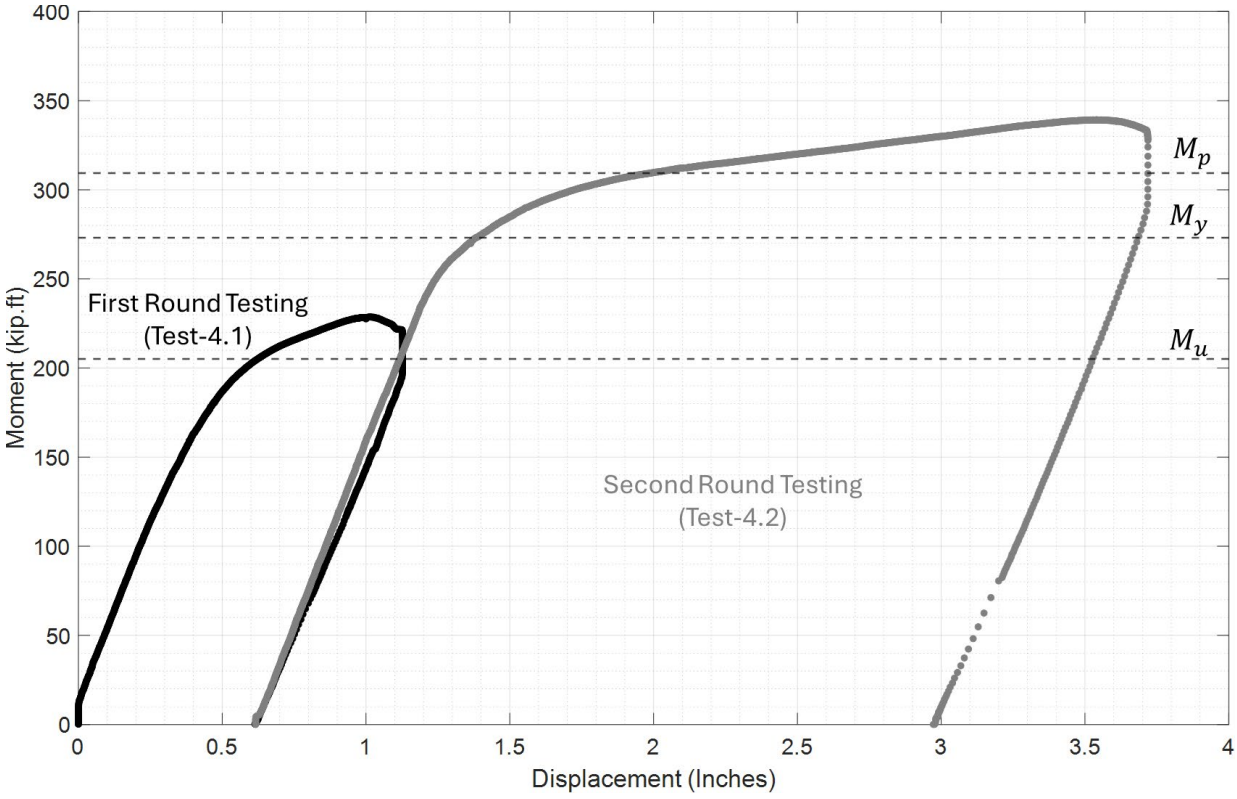

Figure 62: Mid-Span Moment – Mid-Span Displacement Curve

Test Four started by gradually loading the W16x36 girder and concluded when the connection shear was 12% higher than the design shear force V_u. The first round of testing (Test-4.1) was stopped due to excessive angle horizontal leg and girder flange bending for

Connection H, as shown in Figure 63 (b). The maximum rotation achieved by Connection H was 0.018 radians, and the beam end began displacing vertically following the flange and angle bending. During this time, a reversal in the rotation direction was observed and is reflected in the shear-rotation plot of Figure 60 (b). Figure 61 shows a plot of the engineering shear strain measured on the vertical leg of the angles. While the shear strain in Connection G returned to zero upon unloading, residual shear strain was seen in Connection H.

a. **b.**

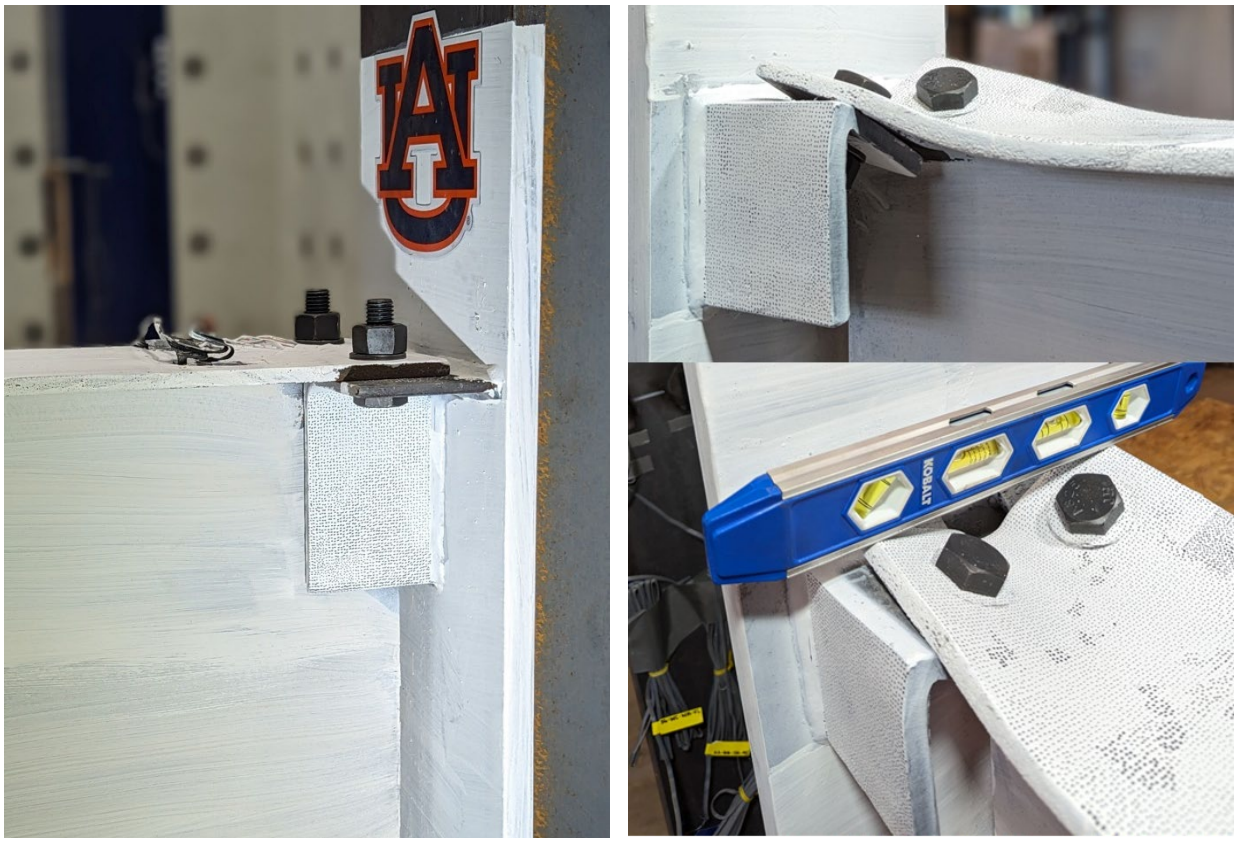

Figure 63: Connections After First Round Testing (Test-4.1) (a) Connection G and (b) Connection H

At the end of Test-4.1, there were no noticeable damages or deformations to Connection G, as shown in Figure 63. As a result, Connection H was retrofitted, and Connection G was further tested in Test-4.2. Figure 64 shows the retrofitted connection and Connection G near the maximum rotation during Test-4.2. During Test-4.2, the girder was loaded beyond its plastic moment capacity, as shown in Figure 62, and the girder underwent a significant plastic deformation, resulting in a great connection rotation demand. The position of the loading points in Test-4.1 and 4.2 were identical.

a. **b.**

Figure 64: Connections During Test-4.2 (a) Connection G Near 0.06-radian Rotation and (b) Retrofitted Connection

Like previous tests, the bending moment diagram was constructed by fitting three lines into the moments calculated using strain readings at five sections of the girder. The resulting moment diagram at the design load and over a range of loads is shown in Figure 65. The bending moment diagram was used to estimate the moment at the column face and was later used to plot the support rotation curve of Figure 66. As seen in Figure 66 (a), Connection G's rotational stiffness was below the 2EI/L limit. The moment-rotation plot of Connection H initially displayed a near-flat slope but quickly became nearly vertical as the girder flange and angle started to bend, resulting in vertical displacement of the girder end instead of rotation. The moment rotation plot of Connection G from Test-4.2 is not included in Figure 66 (a) due to the failure of some strain gages after Test-4.1.

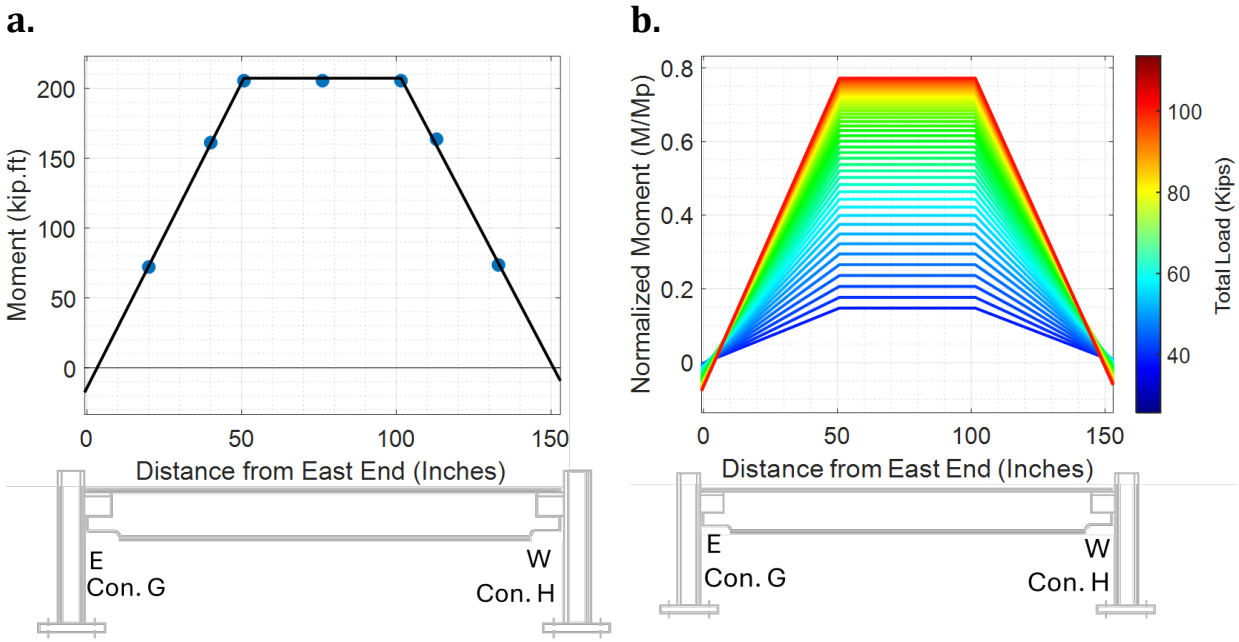

Figure 65: Girder Bending Moment Diagram (a) At the Design Load and (b) Over a Range of Loads

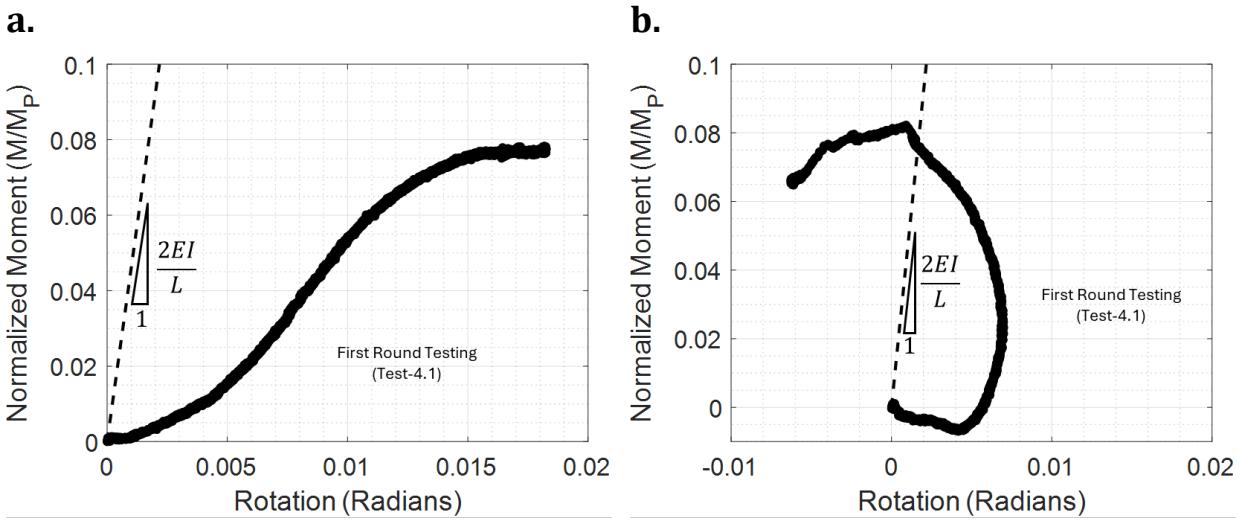

Figure 66: Normalized Support Moment – Rotation Curve (a) Connection G and (b) Connection H

To investigate the individual connection behavior via DIC, all available cameras were utilized in Test-4.1 for analysis of the angles and Connection H girder top flange. Connection G and H angles were captured in 2D with one camera allocated to each, and the Connection H girder top flange was captured in 3D utilizing the two remaining cameras.

An approximate area of 22 square inches (entire visible vertical angle face) was prepared to evaluate the Connection G angle. Figure 67 visualizes the Connection G vertical angle leg strain formation in (a) Von Mises strain (ε_v) and (b) shear strain (ε_{xy}) for a connection shear

of 25, 30, 35, 40, and 55 kips. Akin to connections C and E, strain fields begin to appear at the lower right-hand area (attached to the column) and upper left-hand area (free end) of the angle. This test sequence shows areas of plastic deformation at the surface, but further strength was achievable.

a.

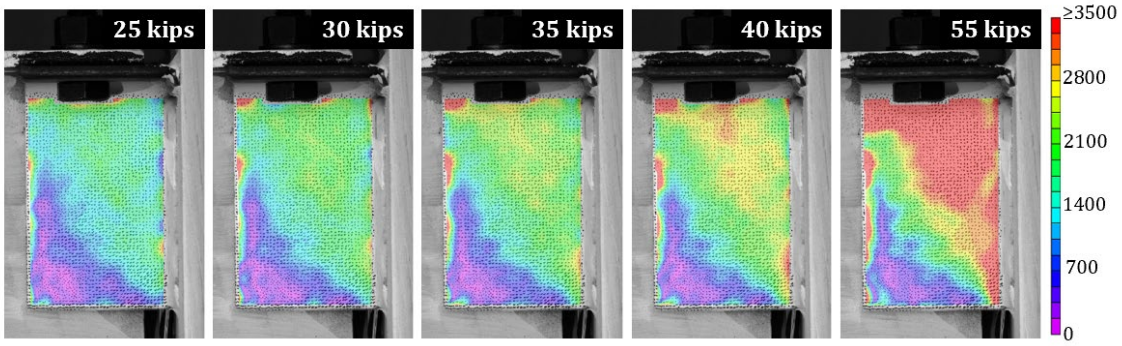

b.

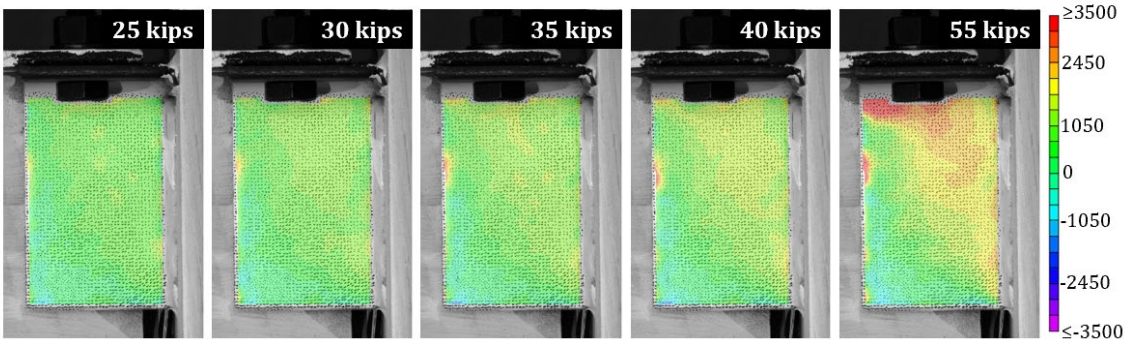

Figure 67: Connection G (Test-4.1) DIC Angle Deformation Progression (a) Von Mises Strain (ε_v) and (b) Shear Strain (ε_{xy}) – Engineering

Like that seen in connections C and E, the strain field is most prominently seen in the top right-hand portion nearest to the column face (fixed-end). According to Figure 67 (b), this portion has exceeded the predicted yield shear strain. This angle did not fail during the first round of testing and therefore the ultimate capacity of the angle alone cannot be determined.

For Connection H, an approximate area of 63 square inches (9 inches longitudinally by the width of the girder top flange) was prepared closest to the column face for the girder top flange and a rough area of 15 square inches (entire visible vertical angle face) was prepared for the angle. Figure 68 shows the girder's strain formation, in microstrain units, with (a) Von Mises strain (ε_v), (b) transverse strains (ε_{xx}), and (c) longitudinal strains (ε_{yy}) for a connection shear of 25, 30, 35, 40, and 55 kips.

a.

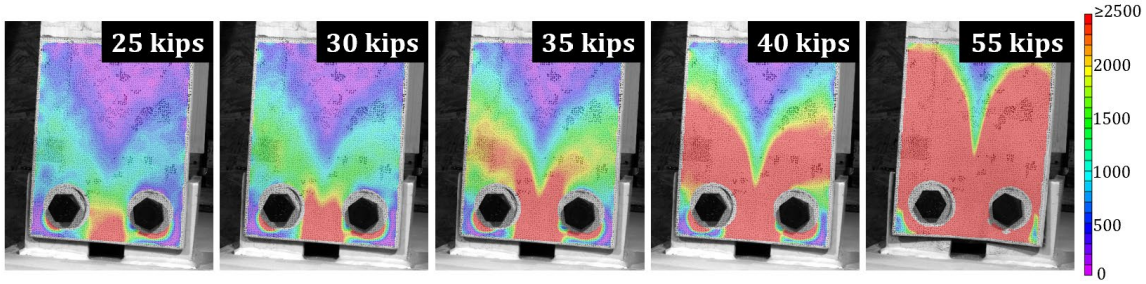

b.

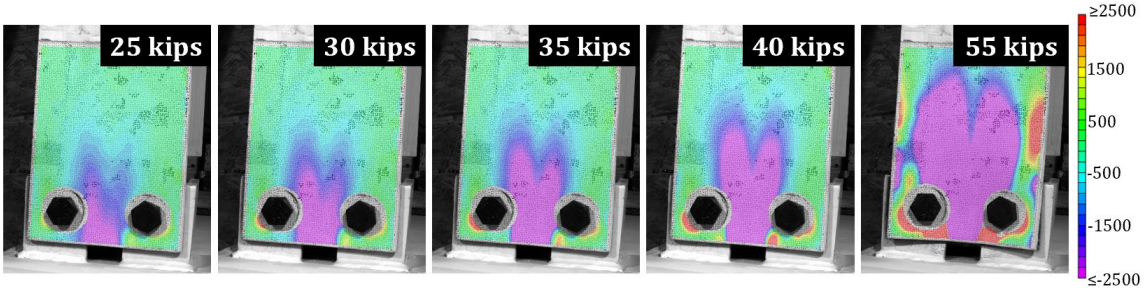

c.

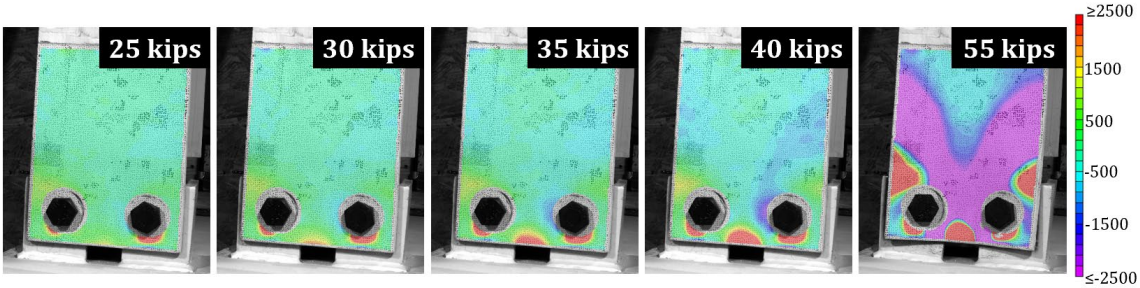

Figure 68: Connection H (Test-4.1) 2D-DIC Flange Deformation Progression (a) Von Mises Strain (ε_v), (b) Transverse Strain (ε_{xx}) – Engineering, and (c) Longitudinal Strain (ε_{yy}) – Engineering

In Figure 68 (a) and (b) at a low shear of 25 kips, the area closest to the column face and unsupported by the angles begins to show a significant compressive strain field indicating plastic deformation, similar to the starting location of yielding shown in connections B and C. Akin to the previous connections, these yield lines progress towards midspan as shear increases, however, in a dissimilar pattern, due to the horizontal angle leg deformation, the yield lines begin to spread out into two distinct separate paths, eventually encasing a larger area in compression.

At a shear of 55 kips, the longitudinal yield line pattern has suddenly formed. The yield lines closest to the exterior edges of the connection angles (nearest the stiffer vertical angle leg) encase an area of tension in which a plastic hinge has formed, allowing for the flange to partially rotate about the transverse edge of the angles. Instead of rotating about a stiff

transverse angle edge, the flexible horizontal angle leg deformed along with the flange and vice versa, causing less of a rotation (0.01 radians) and more of a "sinking" vertical translation compared to connections featured with angles that were regularly oriented.

To aid in the visualization of Connection H's behavior and vertical movement, Table 6, reported in units of microstrain, reveals the flange's strains and deformations in a 3D space. The Z-axis is relative to the initial position of the flange immediately before testing and becomes negative as the specimen moves further from the camera. The displacement in the Z-direction is exaggerated by 25% compared to the X and Y axes, to better identify the deformations. The X-axis ranges from -3.75 in. to 3.75 in., in which 0 in. is located at the longitudinal centerline of the flange; a positive X-value reflects part of the flange that is to the right of the centerline and over the right-hand angle (in reference to the plan view seen in Figure 68) and vice-versa. The Y-axis ranges from -4.5 in. to 4.5 in., the largest value of 4.5 in. represents the part of the flange closest to midspan, while the smallest value of -4.5 in. represents the part of the flange closest to the stub column/connection angles. A reference image is shown in Figure 69 to orient the viewer properly.

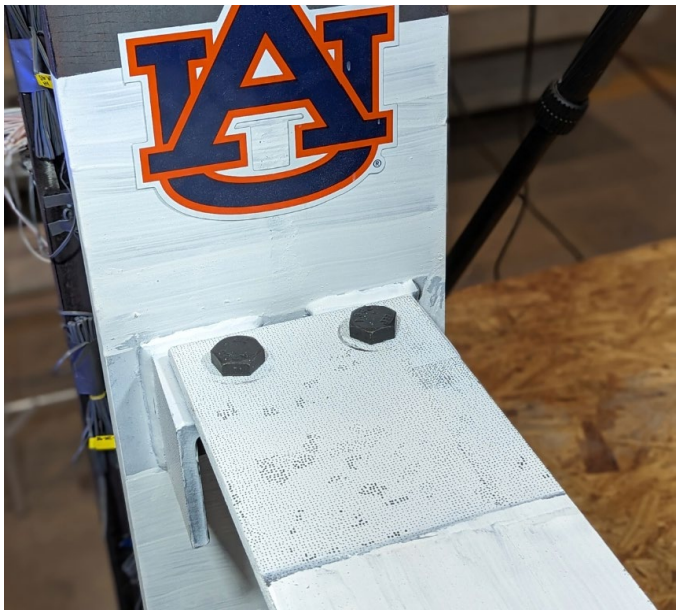

Figure 69: Connection H 3D Reference

In addition to the results discussed for the strain progression of Connection H; at a maximum shear of 55 kips, the flange is seen greatly deformed in the negative Z-direction with an approximate deformation of 0.7 inches located in the region closest to midspan. This maximum deformation is due to the sandwiching of the flange about its longitudinal centerline and vertical movement following the bending of the horizontal legs. Also, the area closest to the stub column has a 0.2 in. deformation in the positive Z-direction as the flange edges hinged upwards towards the stiff vertical angle legs.

Table 6: Connection H (Test-4.1) 3D DIC Flange Deformation Progression

	Von Mises Strain (ε_v)	Transverse Strain (ε_{xx}) - Engineering	Longitudinal Strain (ε_{yy}) - Engineering
Load (kips)			
25	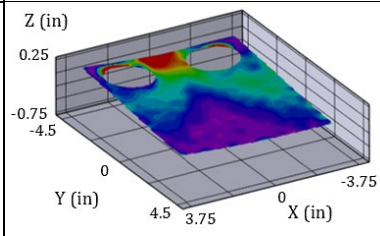	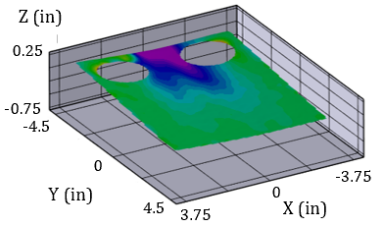	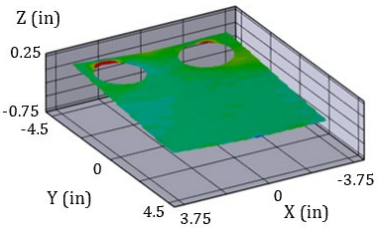
30	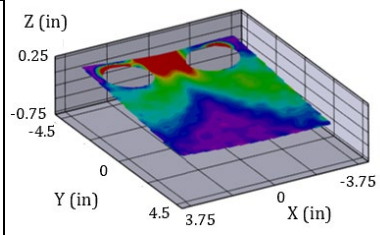	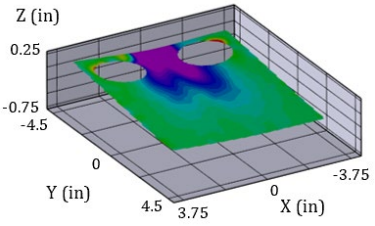	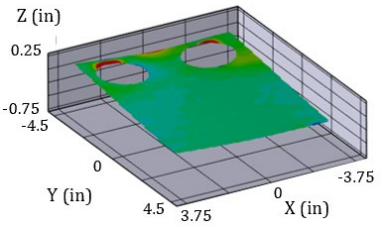
35	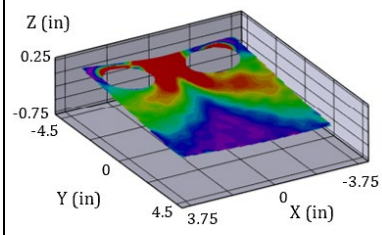	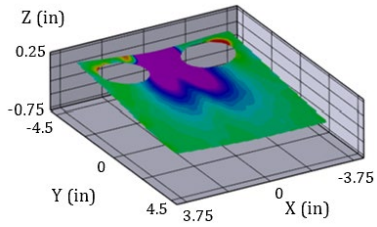	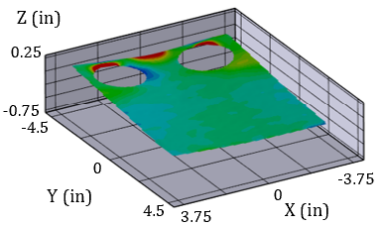
40	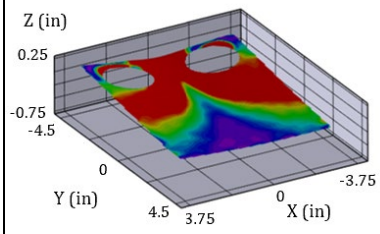	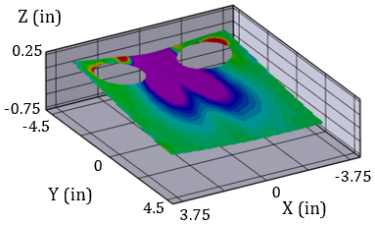	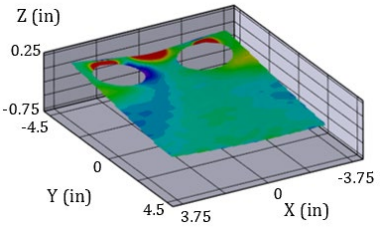
55	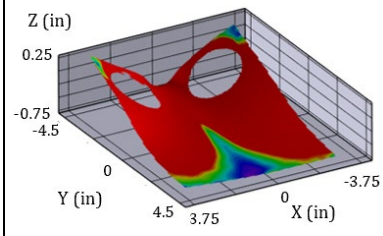	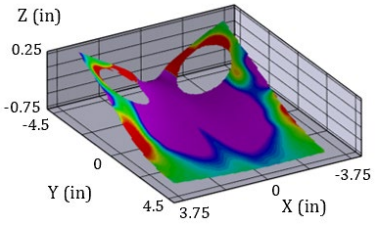	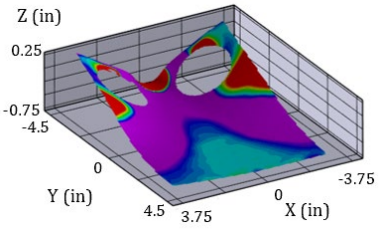

In further investigation of the failure mode of transverse yielding, a transverse cross-sectional cut of Connection H's girder top flange was made approximately at the transverse edge of the angle and is shown in Figure 70.

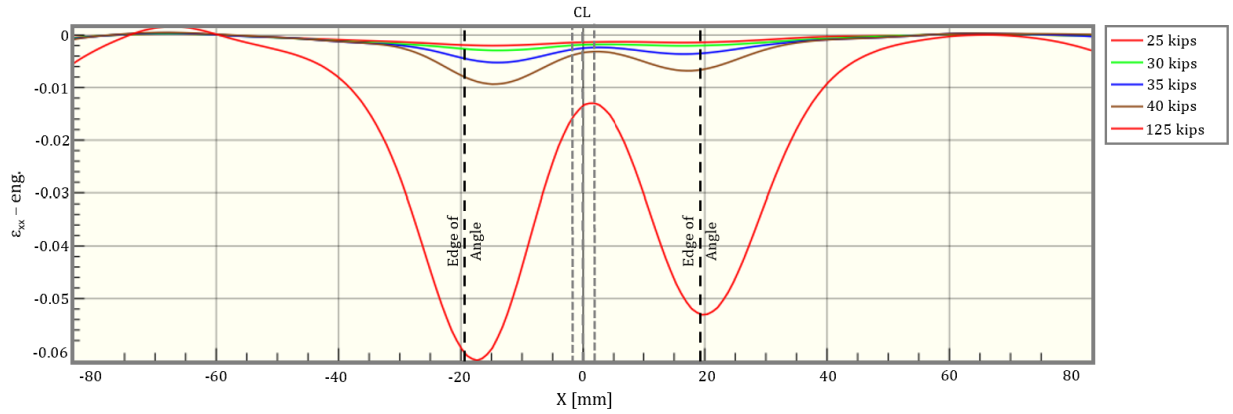

Figure 70: Connection H (Test-4.1) DIC Flange Section Cut Transverse Strain (ε_{xx}) Profile

It is noted that the transverse cut was not made midway between the transverse edge of the angle and the bolt line, like in previous plots, due to large areas of unprocessed data located around the bolts, as seen in Figure 68. The theoretical centerline of the flange (with the edges of the flange web noted on each side) and interior edge of the right-hand and left-hand angles (as seen from plan view with the midspan of the girder into the plane) are noted on the figure for reference. As shown in the strain progression profile, no transverse tensile strains are noted along the flange cross-section; this is a noticeable contrast against other angles that are oriented differently. Specifically, large compressive strains of 0.06 and 0.05 are located approximately 1.5 mm (0.06 in.) right of the left-hand angle's edge and 0.6 mm (0.02 in.) right of the right-hand angle's edge.

In Figure 71, the Connection H vertical angle leg strain formation in (a) Von Mises strain (ε_v) and (b) shear strain (ε_{xy}) for a connection shear of 25, 30, 35, 40, and maximum of 55 kips is shown. The upper portion of the angle begins to yield before a shear of 25 kips and throughout Test-4.1, it extends towards the lower portion of the angle, eventually resulting in a majority of the angle leg's surface yielding at the maximum shear. This angle's shear strain progression is in stark contrast to all other connections, likely due to their orientation.

a.

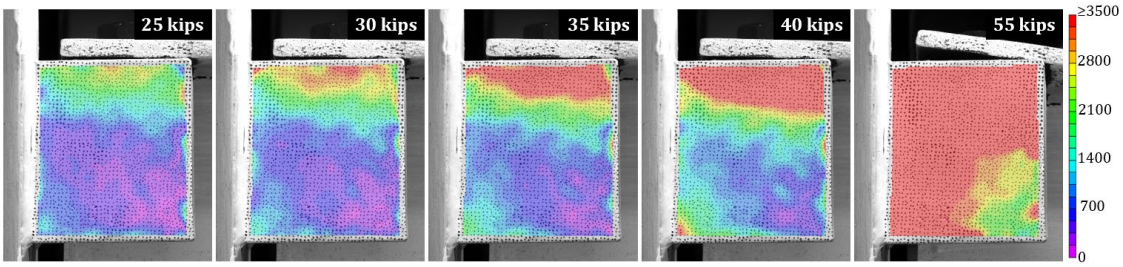

b.

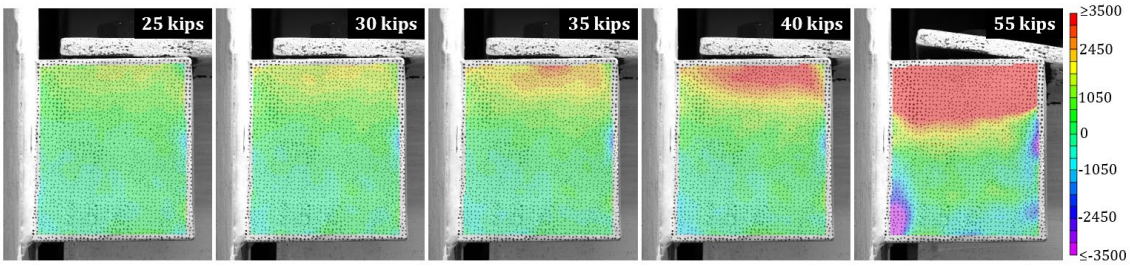

Figure 71: Connection H (Test-4.1) DIC Angle Deformation Progression (a) Von Mises Strain (ε_v) and (b) Shear Strain (ε_{xy}) – Engineering

The Drop-In Connection G satisfied the strength, stiffness, and ductility requirements. The torsional stiffness was not evaluated as part of Test Four. The Drop-In Connection H slightly exceeded the strength required but did not satisfy the stiffness or ductility needed. The mirrored angle orientation is not recommended.

Test Five

For Test Five, relatively small, undersized angles were utilized to better evaluate the angle failure modes. In addition to testing the in-plane response of the drop-in connections, Test 5 was used to assess the lateral torsional buckling (LTB) restraint provided by the connections. To achieve this, the lateral supports were removed before the first loading cycle (Test-5.1). Moreover, to minimize friction build-up and artificial lateral restraint at the loading points, the loading points were substantially lubricated, as shown in Figure 73. The test setup of Test-5.1 is depicted in Figure 72 and Figure 73. The loading points divide the girder into three equal segments of 66.75 inches.

a. **b.**

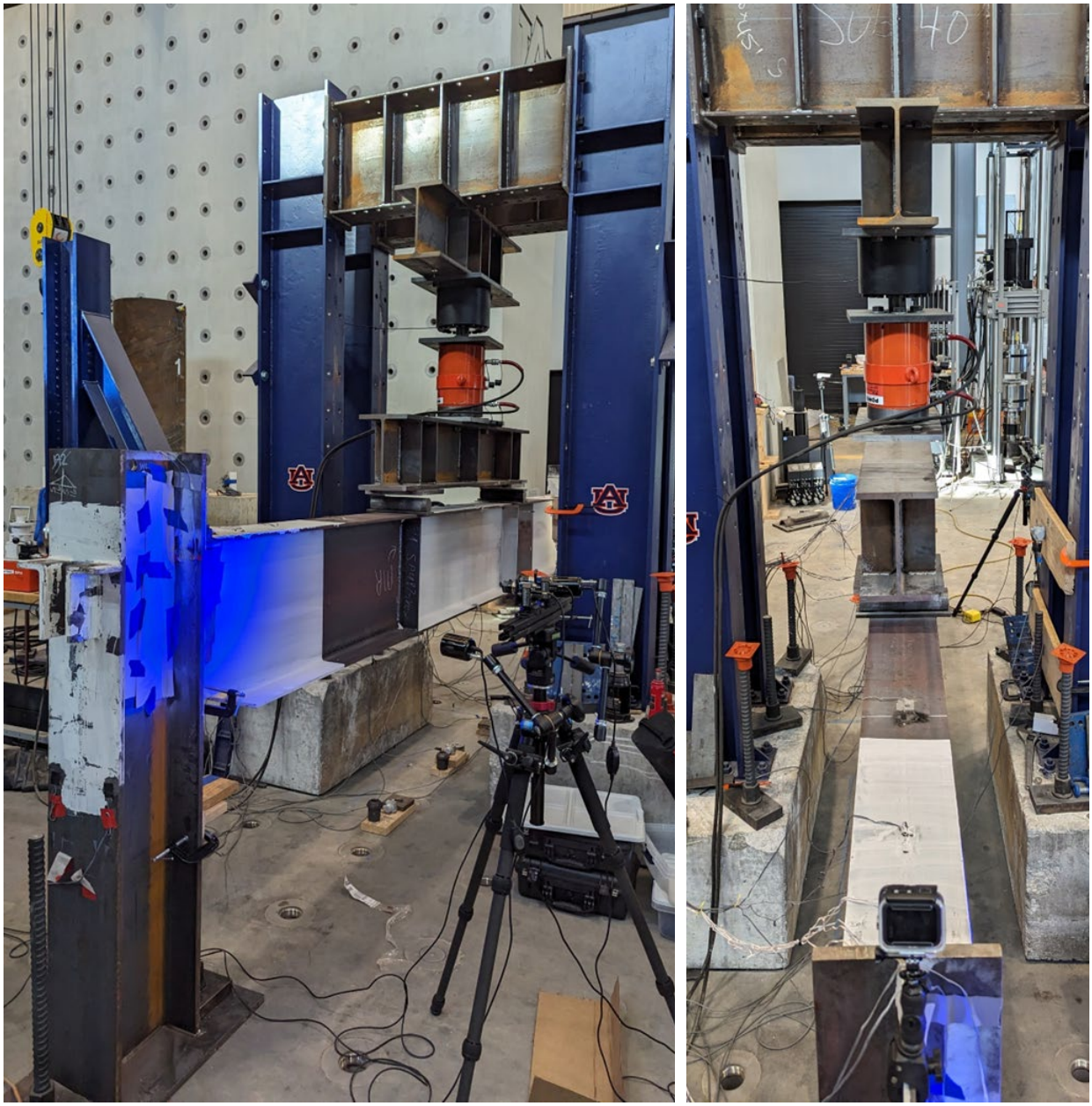

Figure 72: Connections Before Testing (a) Connection E and (b) Connection F with No Lateral Supports

a. **b.**

Figure 73: Lubricated Spreader Beam Supports

The connections tested in Test Five (Connection I and Connection J) utilized L6x4x5/16 and L4x3x1/2 angles with five inches and three inches bearing length, respectively. The connections before Test-5.1 are shown in Figure 74.

a. **b.**

Figure 74: Connections Before Testing (a) Connection I and (b) Connection J

In Test-5.1, the W24x68 girder was loaded to its nominal moment capacity (M_n), which was limited by LTB. Cb=1.14 was used to calculate M_n, which corresponds to four-point bending with no lateral support between the ends. The unbraced length of the girder, conservatively taken as the girder length, was 16.7 feet, putting it in the inelastic LTB range. L_r and L_p for the tested girder size are 18.9 feet and 6.61 feet, respectively.

Figure 75 shows that the girder was loaded until theoretical M_n was reached, and the corresponding lateral displacements of the top and bottom flange at mid-span were -0.25 inches and 0.01 inches, respectively. The load was maintained at M_n, and the test specimen was inspected before unloading occurred. Figure 76 shows pictures taken of the specimen at this stage of the test. There was almost no lateral displacement in the compression flange, while the tension flange displaced laterally by a quarter of an inch. The maximum connection shear during Test-5.1 was above the connection design shear force V_u, as shown in Figure 75 (b).

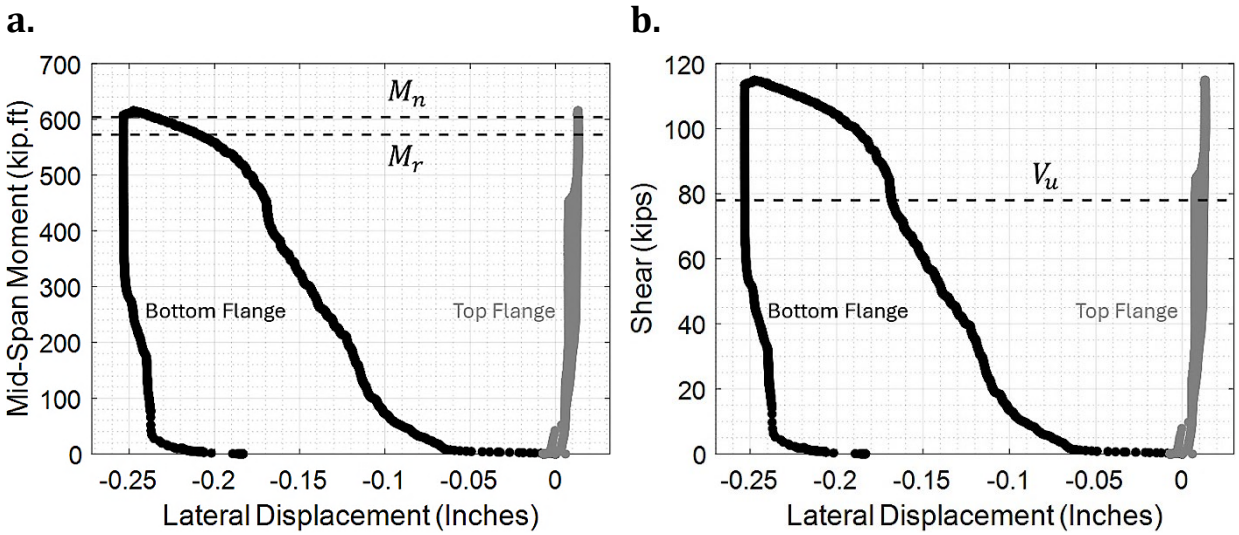

Figure 75: Mid-Span Lateral Displacement (Test-5.1) (a) Moment-Displacement and (b) Shear-Displacement

Figure 77 depicts the mid-span moment in relation to the out-of-plane rotation at the supports (measured with inclinometers). The rotations were calculated by measuring the difference between the out-of-plane rotations of the girder end and the column. The girder end out-of-plane rotation was measured at the mid-height of the girder, with the compression flanges clamped to the drop-in angles. The out-of-plane rotation of Connections I and J was similar. The out-of-plane rotation at Connection I, which had a longer bearing length and deeper angle, was relatively smaller. Moreover, as shown by the whitewash flaking in Figure 78, Connection J had more flange strain compared to Connection I.

a. **b.**

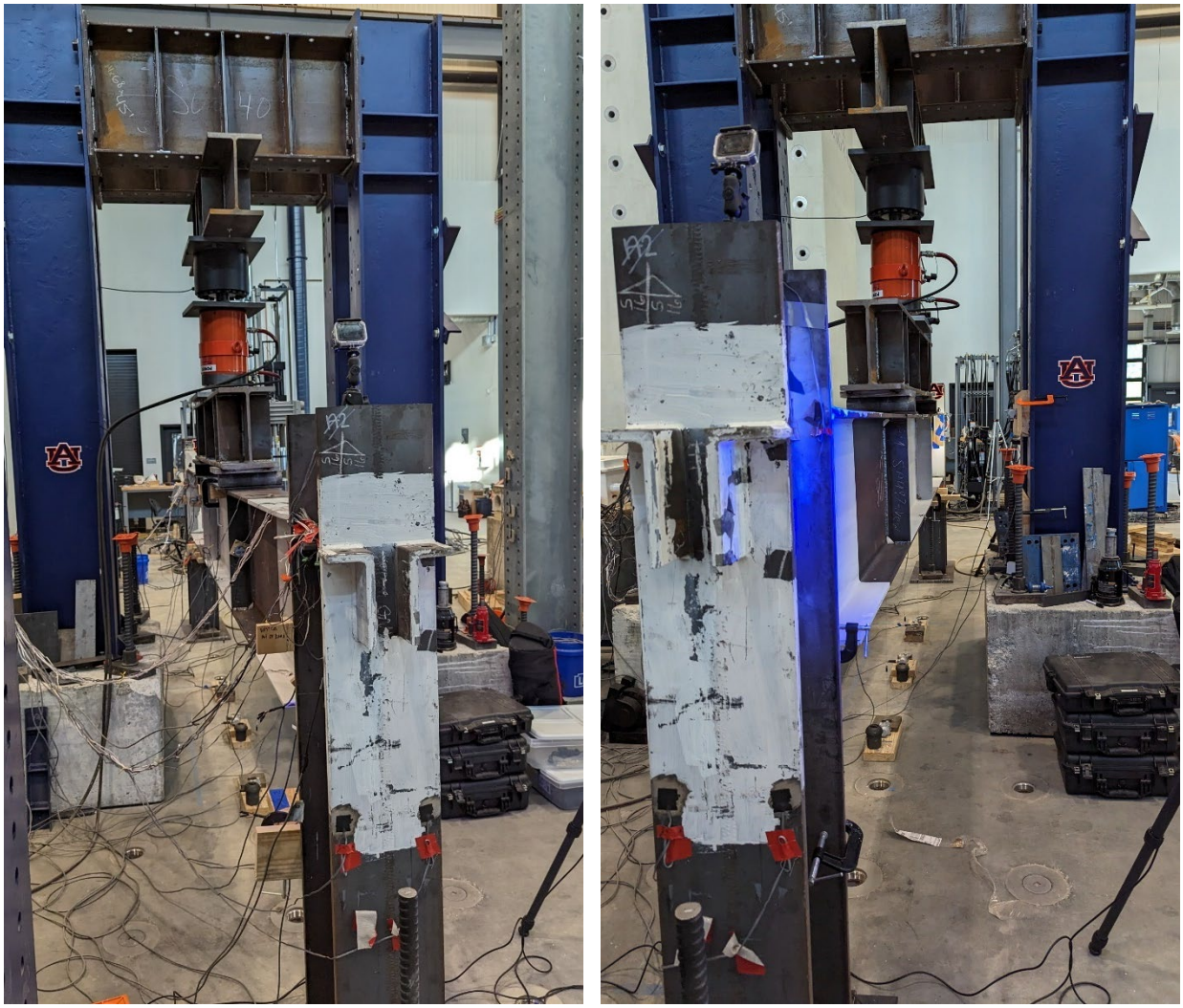

Figure 76: Girder at Theoretical Lateral Torsional Buckling Load (a) View from North-West and (b) View from South-West

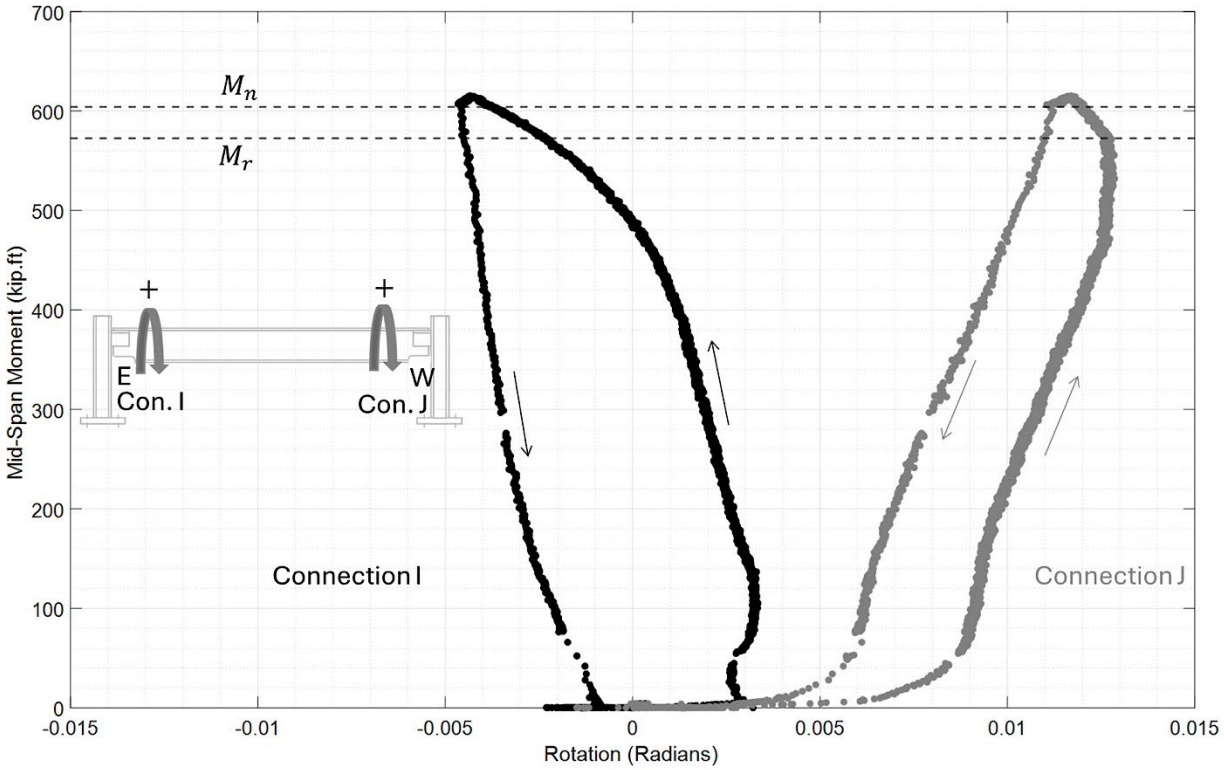

Figure 77: Mid-Span Moment – Support Out of Plane Rotation Curve (Test-5.1)

a. **b.**

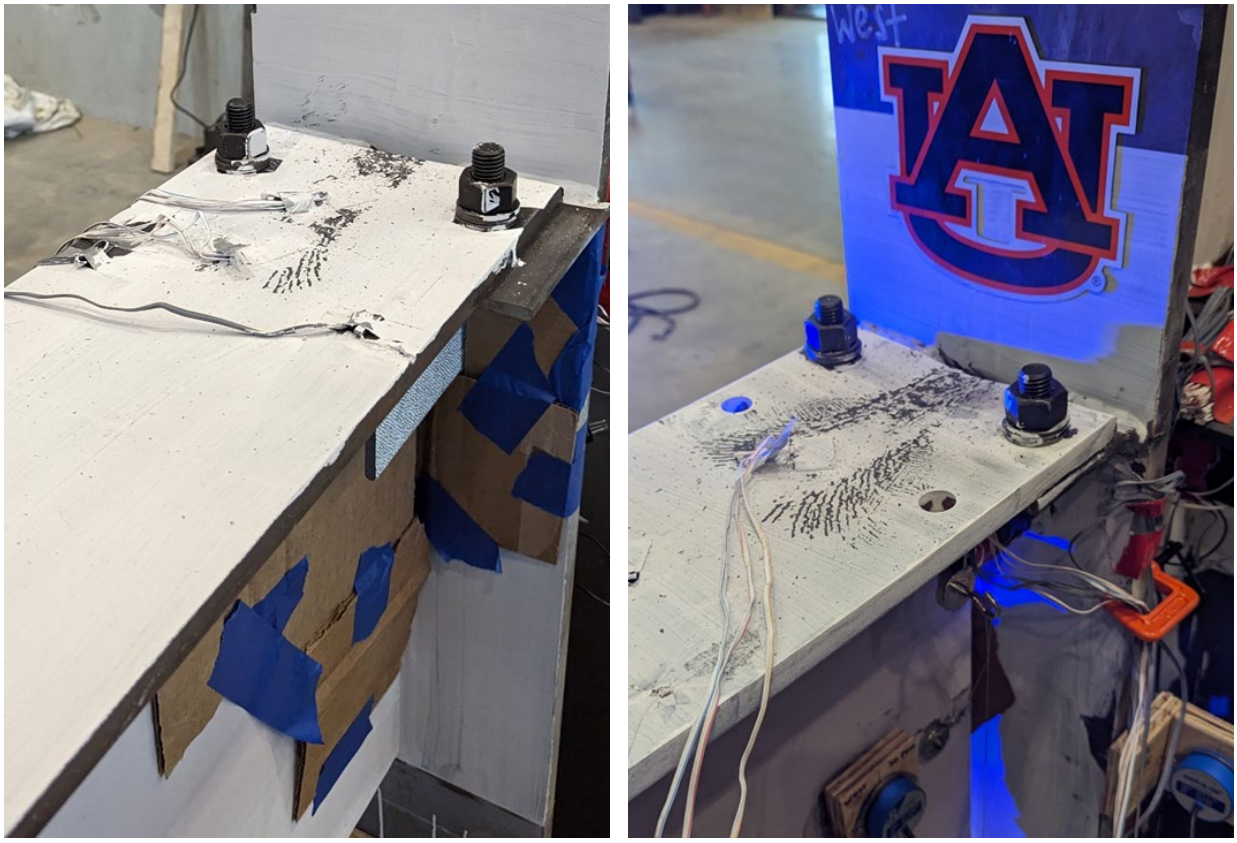

Figure 78: Connections After First Round Testing (Test-5.1) (a) Connection I and (b) Connection J

Following Test-5.1, the lateral supports were placed back for further testing of the connections. The loading points in the subsequent tests were not changed. During Test-5.2, the maximum connection shear reached was 72% higher than the design shear force ($1.72V_u$), Figure 80. Under this load, the girder flange at Connection J went under significant plastic deformation. It should be noted that the bearing length of Connection J was three inches, and the clear distance between the angles was 1/8 inch wider than the previously tested connections. The relatively shorter bearing length and increased flange bending span resulted in a more pronounced flange yielding. In contrast, a smaller flange deformation and minor initiation of angle buckling were observed in Connection I. Connections I and J at the end of Test-5.2 are shown in Figure 79.

As seen in the shear-rotation plots of Figure 80. Connection J exhibited less rotation compared to Connection I due to girder end deformation transitioning from rotation to vertical displacement following the flange bending. In addition, high engineering shear strain was recorded in the vertical legs of both connections, as shown in Figure 82. Test-5.2 was concluded due to weld failure in Connection J.

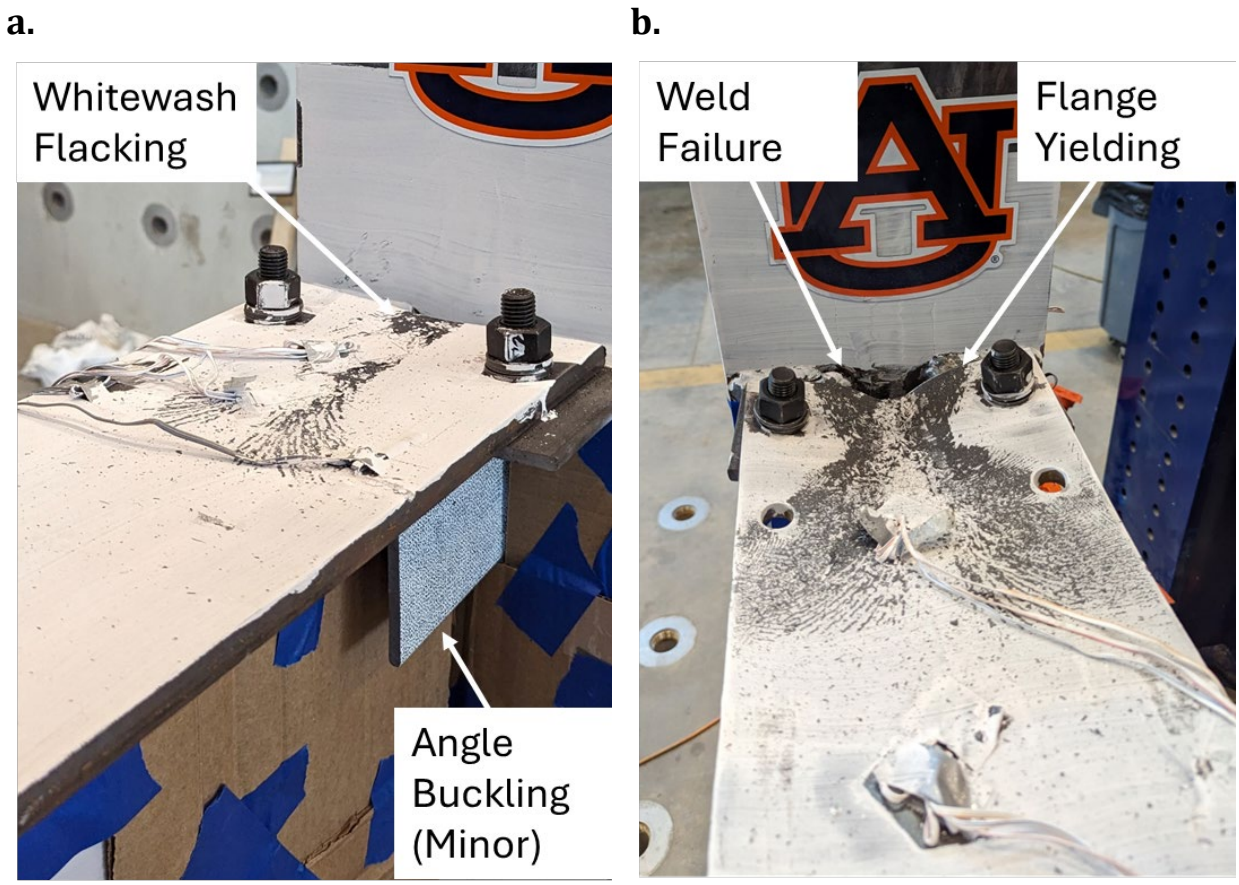

Figure 79: Connections After Second Round Testing (Test-5.2) (a) Connection I and (b) Connection J

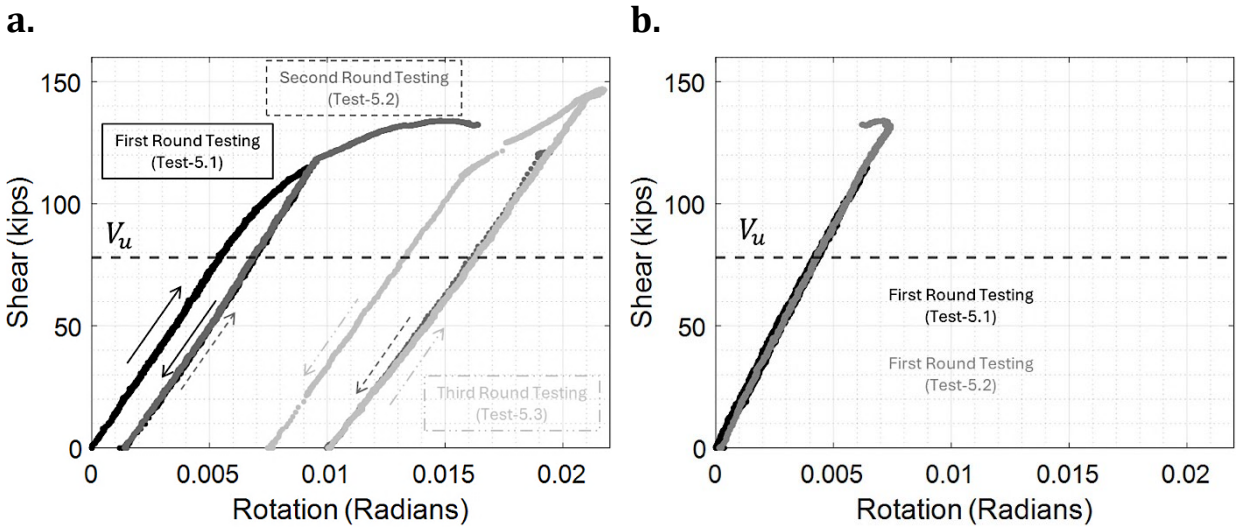

Figure 80: Shear-Rotation Plots (a) Connection I and (b) Connection J

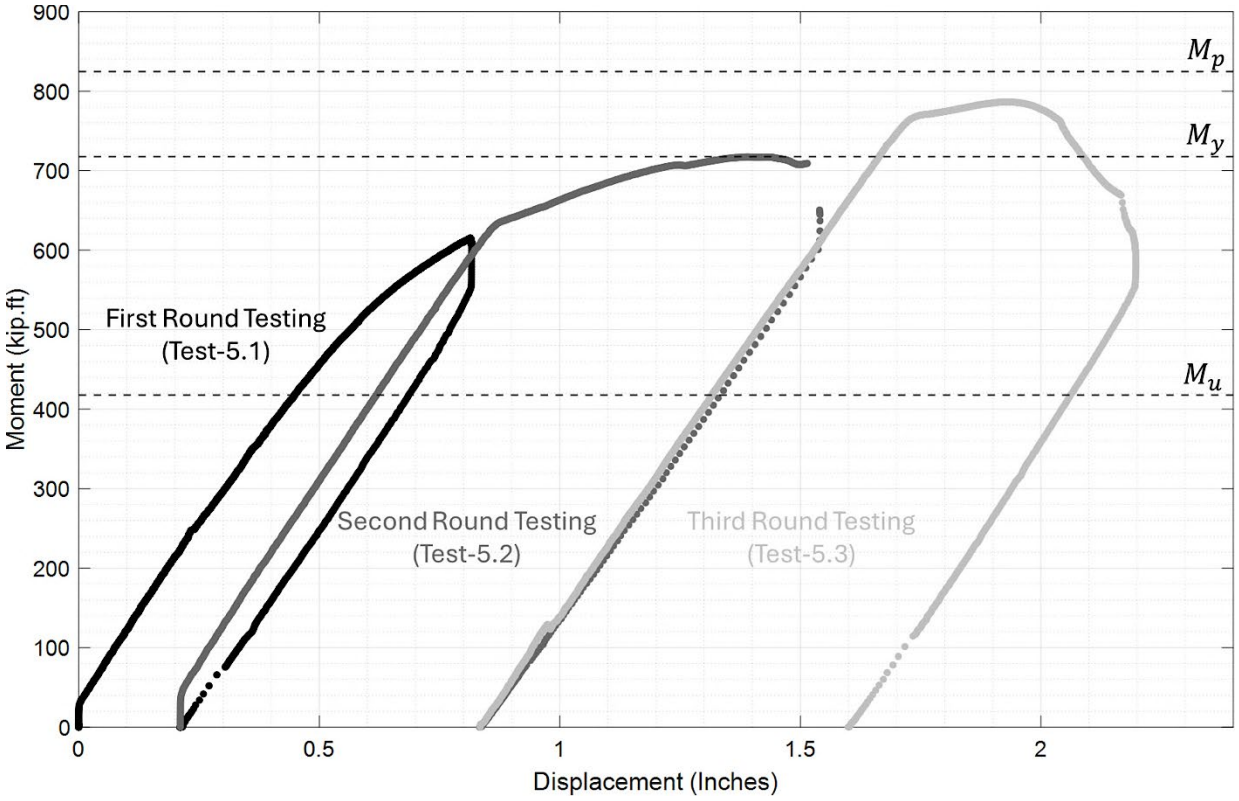

Figure 81: Mid-Span Moment – Mid-Span Displacement Curve

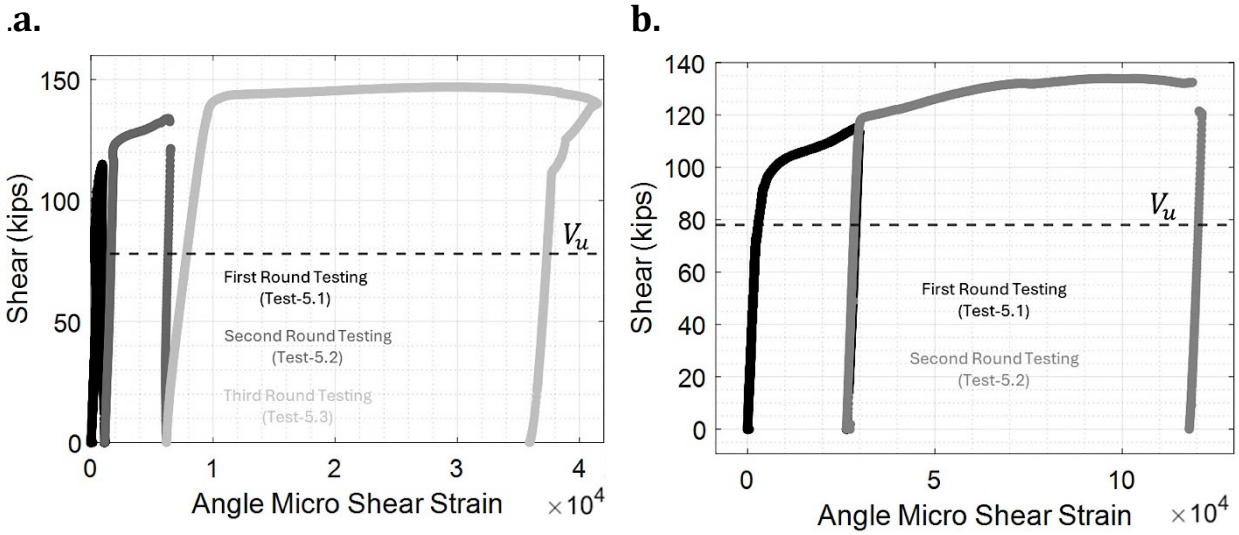

Figure 82: Angle Maximum Engineering Shear Strain (a) Connection I and (b) Connection J

a. **b.**

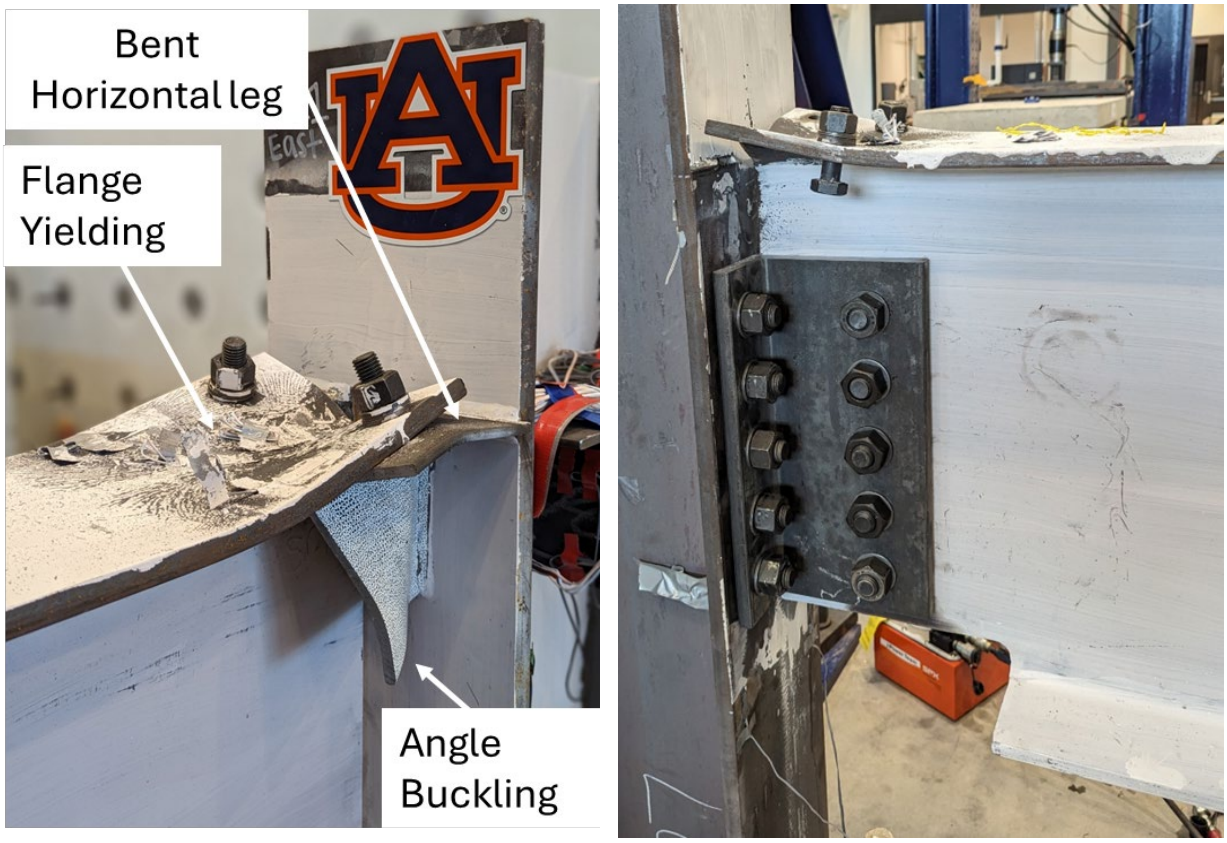

Figure 83: Connections After Third Round Testing (Test-5.3) (a) Connection I and (b) Retrofitted Connection

In Test-5.3, Connection J was retrofitted, and Connection I was tested to failure. The retrofitted connection and Connection I at the end of Test-5.3 are shown in Figure 83. The maximum shear force in this loading cycle was 88% higher than the design shear force ($1.88V_u$). The corresponding mid-span moment was between M_y and M_p, as shown in Figure 81. During Test-5.3, girder flange yield and angle vertical leg buckling were observed. Test-5.3 was concluded due to Connection strength degradation following the angle buckling. Figure 84 shows the angle buckling in Connection I and the angle yielding in Connection J after the girder was removed.

Similar to Connection J, the rotation of Connection I transitioned to vertical displacement after the angle buckling and the flange transverse bending. This phenomenon is reflected in the shear-rotation plot of Figure 80.

a. **b.**

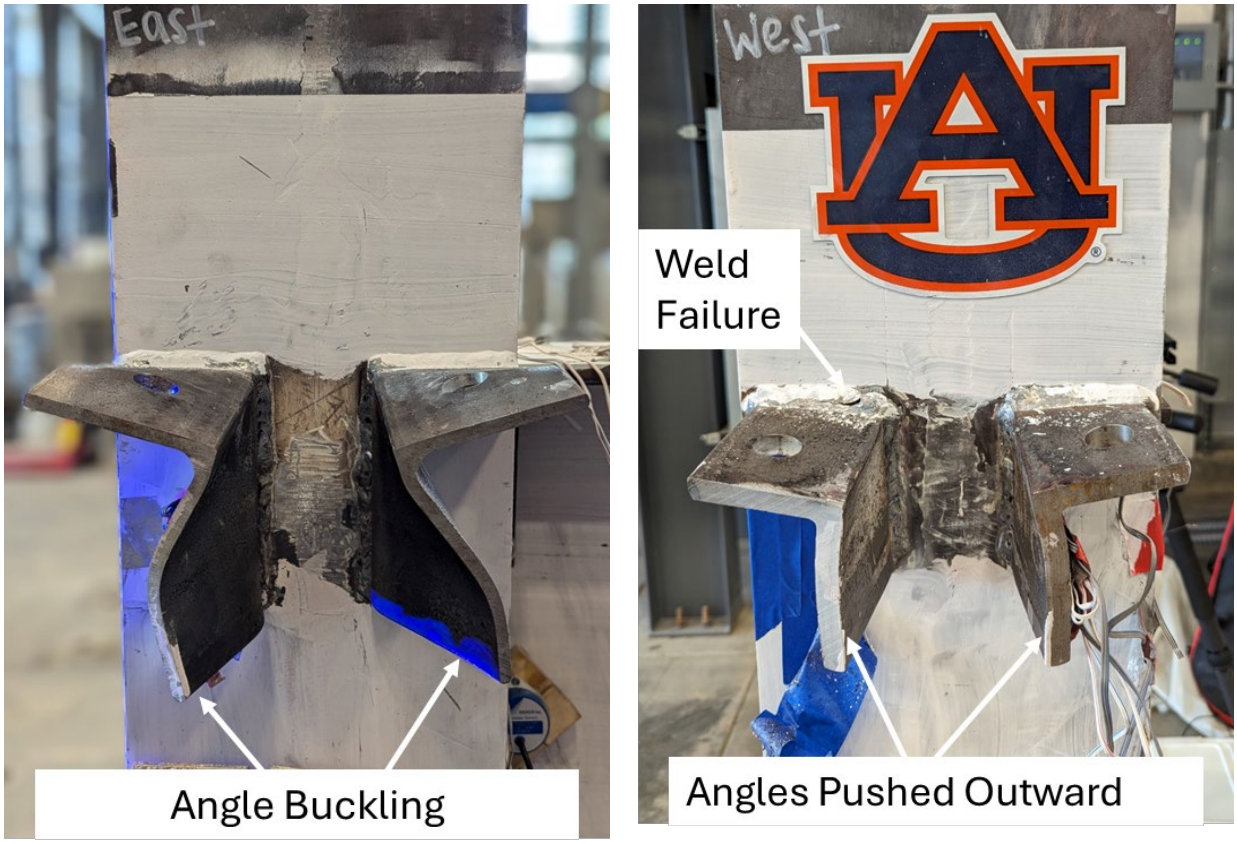

Figure 84: Drop-In Angles After Testing (a) Connection I After Test-5.3 and (b) Connection J After Test-5.2

The connection moment was estimated by fitting best-fit lines into moments calculated at five sections using strain gauge data. The constructed bending moment diagram at the design load and over a range of loads is shown in Figure 85. The bending moment diagram was then used to estimate the support moment and construct the support moment vs rotation plots of Figure 86. As seen in Figure 86, the connections' initial rotational stiffness was lower than the 2EI/L limit and appeared rigid when the beam end rotation transitioned from rotation to vertical displacement. Moreover, the support moment of Connection I at 0.02 radian rotation was less than the $0.2M_p$ limit.

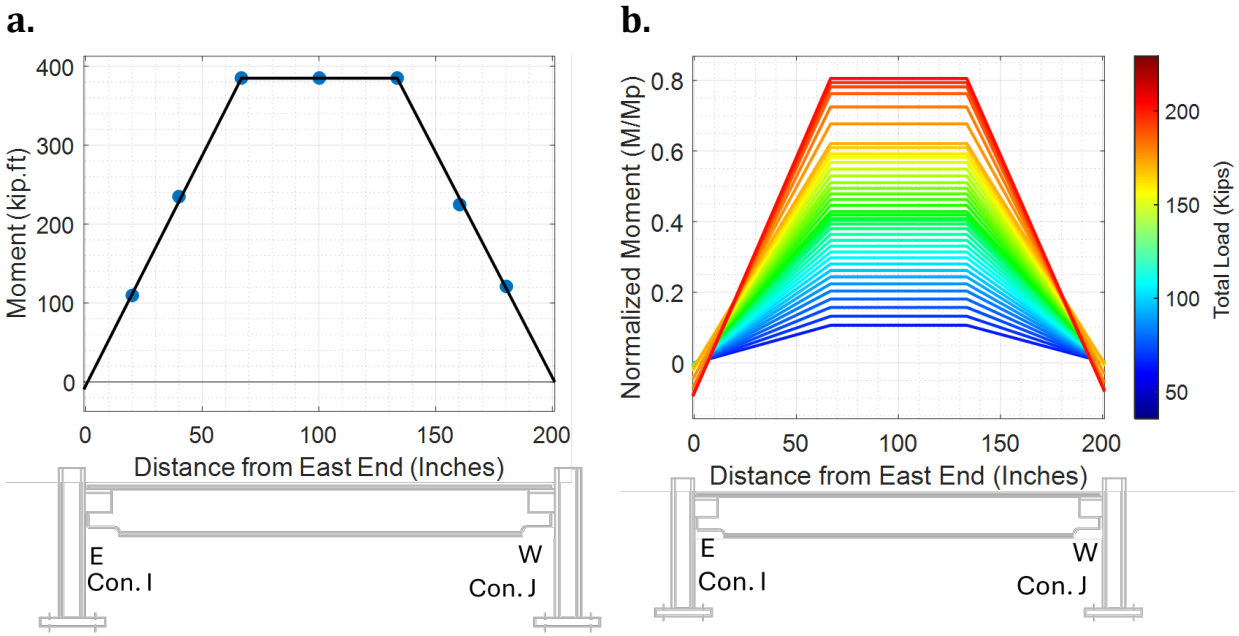

Figure 85: Girder Bending Moment Diagram (Test-5.1) (a) At the Design Load (b) Over a Range of Loads

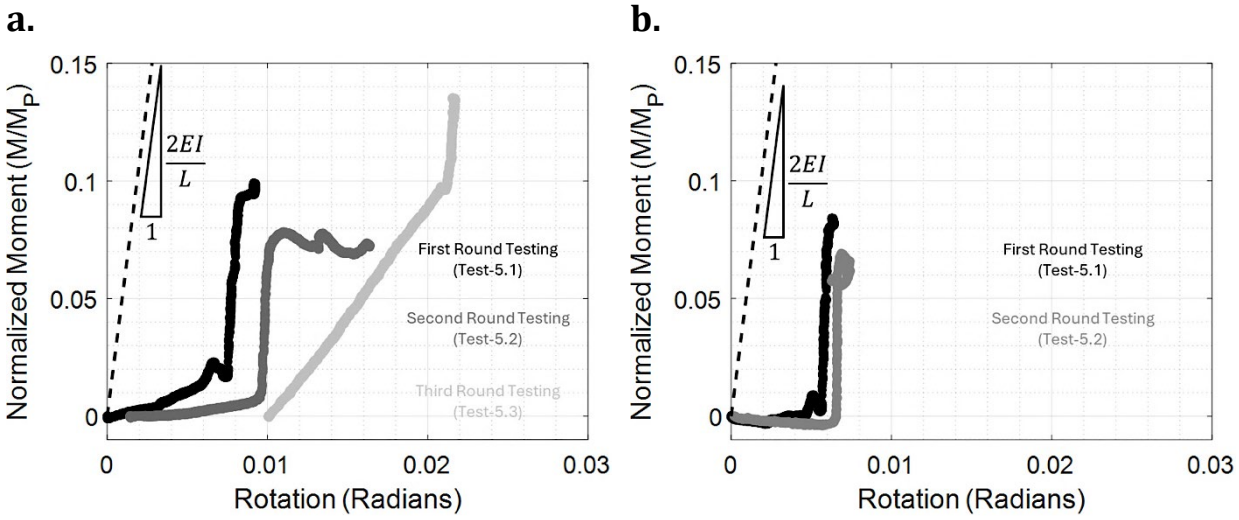

Figure 86: Normalized Support Moment – Rotation Curve (a) Connection I and (b) Connection J

DIC was utilized in Test-5.1 to investigate both Connection I and J vertical angle legs. The focus was on the angles and not the flanges because the angle behavior was the main focus of this test. Each connection was processed in VIC-3D and utilized two cameras each.

For Connection I, an approximate area of 30 square inches (entire visible vertical angle face) was prepared to evaluate the vertical angle leg. Figure 87 shows the Connection I vertical angle leg strain formation, in microstrain units, in (a) Von Mises strain (ε_v) and (b) shear strain (ε_{xy}) for a connection shear of 40, 60, 80, 100, and 110 kips. Yielding is seen starting

before a shear of 40 kips, in which the upper right-hand corner (attached to the column), lower right-hand corner (attached to the column), and upper left-hand (free end) of the angle begin to yield. At a shear of 60 kips, these yield lines connect, resulting in complete yielding of the upper right-hand area at the maximum shear. As connections C and I utilize the same bearing length and angle section, their final strain field patterns are relatively the same.

a.

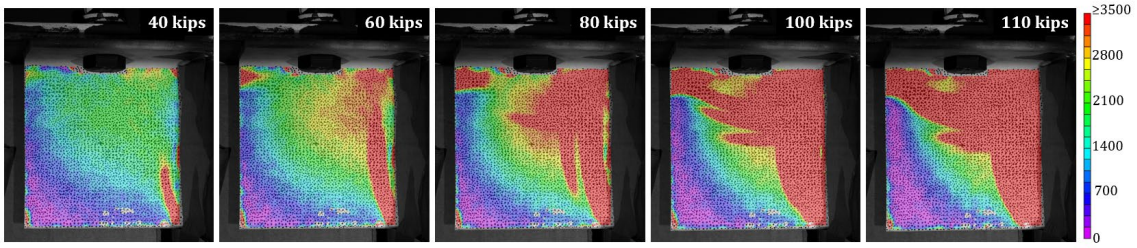

b.

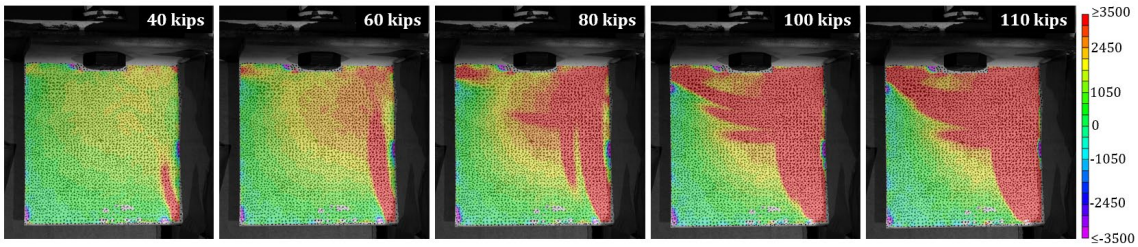

Figure 87: Connection I (Test-5.1) DIC Angle Deformation Progression (a) Von Mises Strain (ε_v) and (b) Shear Strain (ε_{xy}) – Engineering

An approximate area of 15 square inches (entire visible vertical angle face) was investigated via DIC for Connection J. Shown in Figure 88, the strain field formation of the vertical angle leg, in units of microstrain, is visualized in (a) Von Mises strain (ε_v) and (b) shear strain (ε_{xy}) for a connection shear of 40, 60, 80, 100, and 110 kips. Similar to connections C and I, the upper and lower left-hand area (attached to the column) and upper-right-hand area (free end) of the angle begin to yield before a shear of 40 kips. Eventually, at maximum shear, the upper left-hand diagonal of the angle is completely yielded.

a.

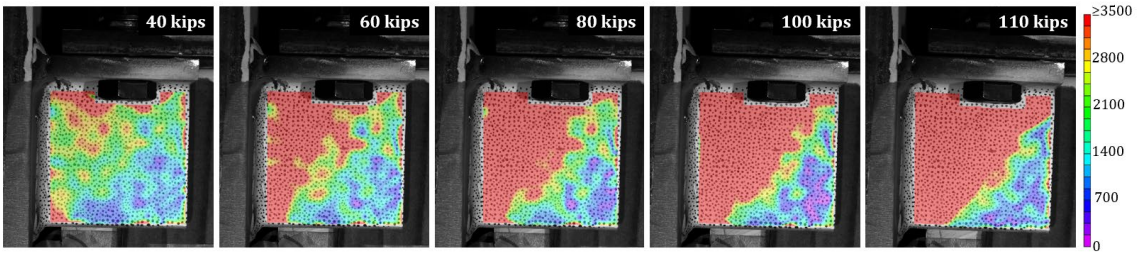

b.

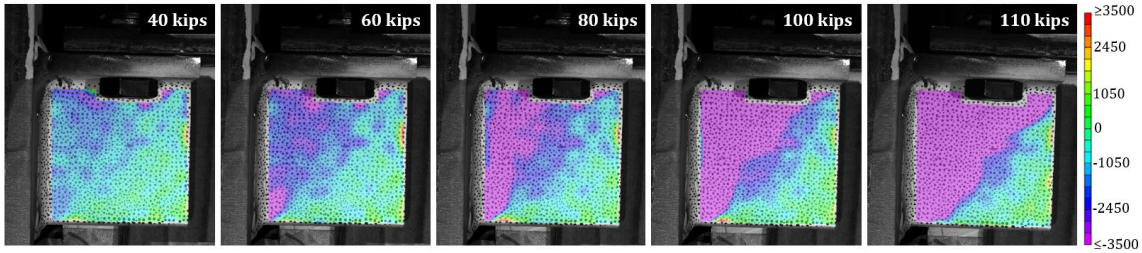

Figure 88: Connection J (Test-5.1) DIC Angle Deformation Progression (a) Von Mises Strain (ε_v) and (b) Shear Strain (ε_{xy}) – Engineering

The Drop-In Connections I and J confirmed adequate torsional support stiffness to meet the torsionally pinned connection assumption for standard LTB girder analysis. The ***drop-in connections met the requirements for strength and stiffness***. The girder was relatively large for the connection sizing, which limited the amount of rotation applied to the connections. Therefore, the rotational ductility could not be evaluated.

Test Six

The performance of two beam-column drop-in connections was evaluated in Test Six. Similar to Test Five, relatively small angle sizes were utilized. Connections K and L were used to connect the W24x68 beam to the weak axis of the W14x82 column, as shown in Figure 89. While oversized, a W24x68 beam was used due to immediate availability for testing. The benchmark building shows W21x44 beams, which would have yielded earlier in the testing. This would have applied more rotation. Therefore, Test Six was a high shear but minimal rotation test.

Both connections had a five-inch bearing length, and Connections K and L utilized L6x4x5/16 and L4x3x1/2 angles, respectively. The spacing between the angles was 2-7/8 inches in Connection K and three inches in Connection L.

The beam of Test Six was loaded in the test setup shown in Figure 14. The loading points were situated at third points, dividing the beam into three equal 66.75-inch-long segments. The loading was gradually increased to the design shear level and the limit of the

connections. The resulting connection shear-rotation plot and mid-span moment displacement curves are shown in Figure 90 and Figure 91, respectively.

a. **b.**

Figure 89: Connections Before Testing (a) Connection K and (b) Connection L

a. **b.**

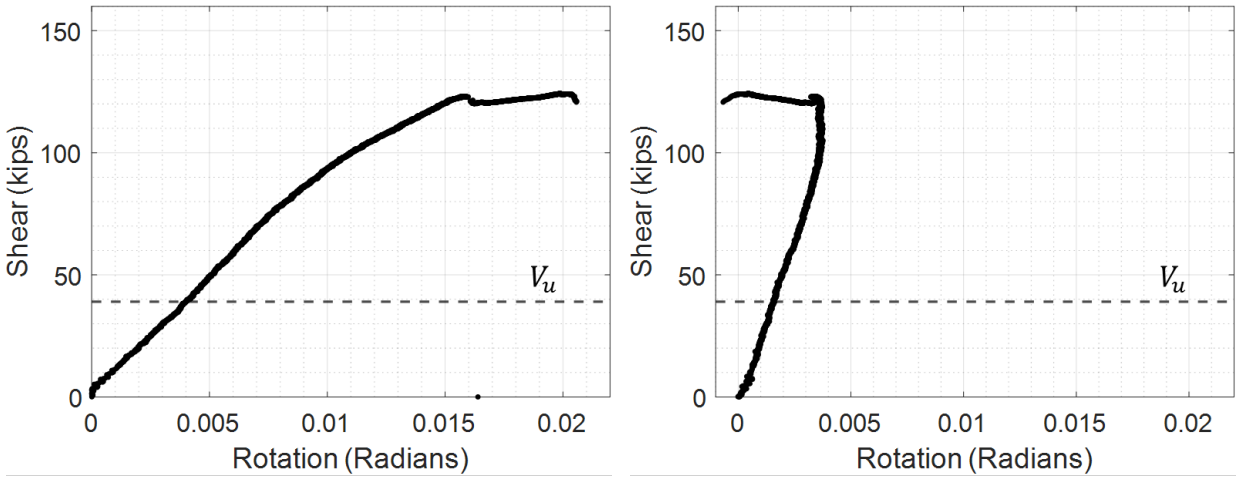

Figure 90: Shear-Rotation Plots (a) Connection K and (b) Connection L

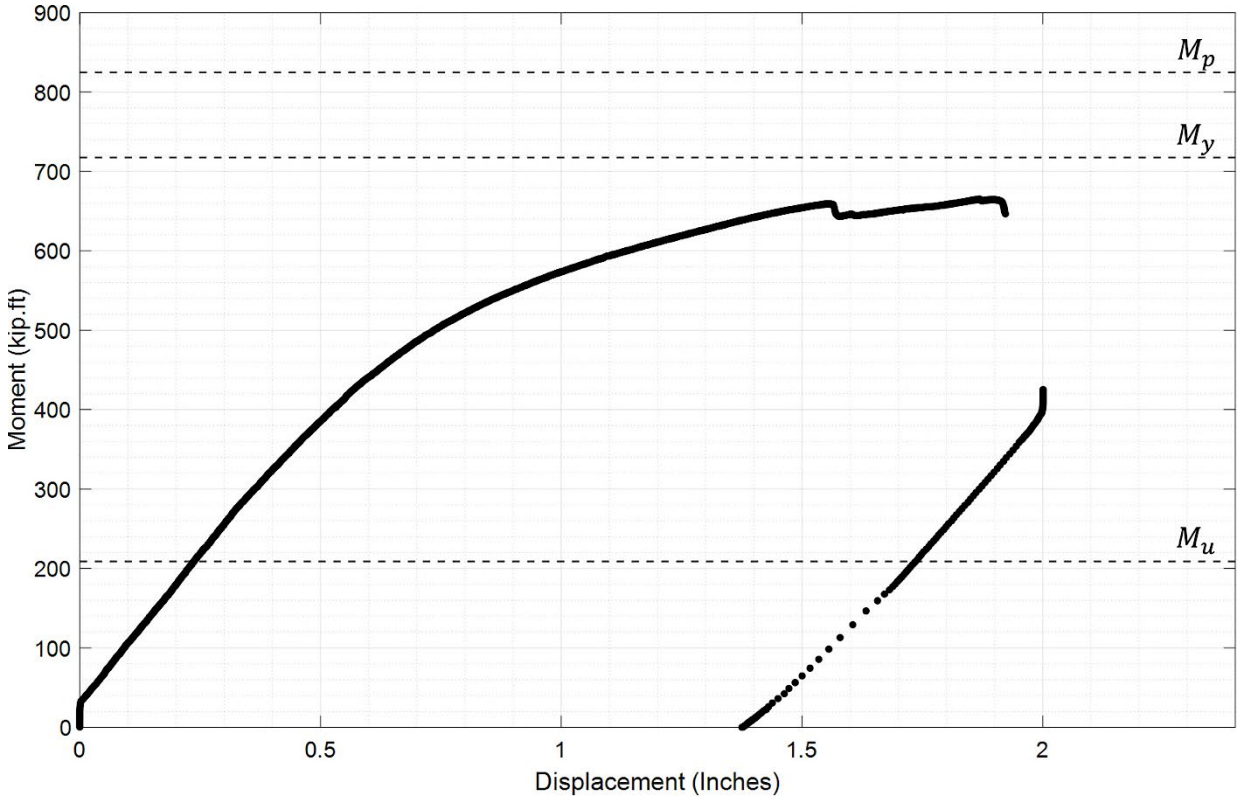

Figure 91: Mid-Span Moment – Mid-Span Displacement Curve

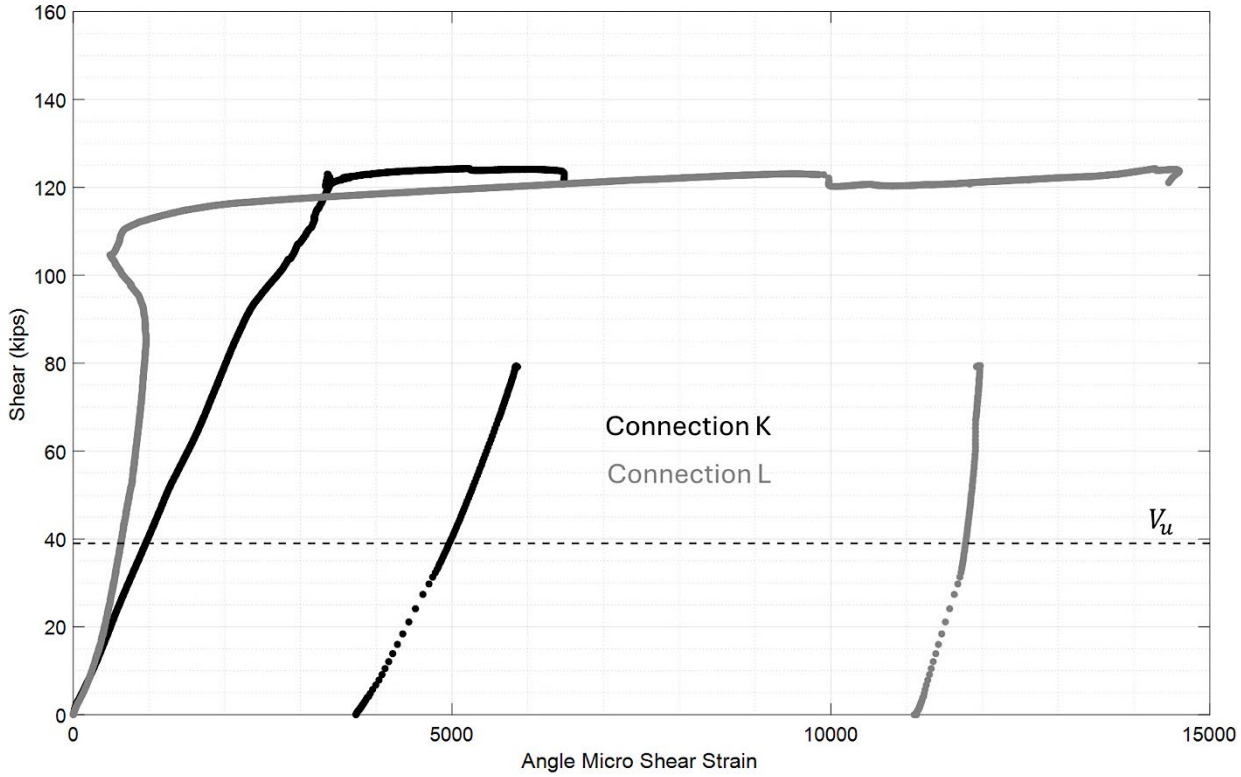

Figure 92: Angle Maximum Engineering Shear Strain-Connection Shear Plot

Three sources of plastic deformation were observed near the connections. The first and the most dominant was flange yielding, as shown in Figure 93 and Figure 94, followed by large angle shear strain, as shown in Figure 92. Both were more pronounced in Connection L as the angle size was smaller and the angle spacing was larger than the same parameters in Connection K. The second source of inelastic deformation occurred in the column web, as shown in Figure 95. Bowing out of the column web was observed as the applied load was increased. Test Six was concluded due to flange rupture in Connection L. The flange rapture occurred after a considerable amount of plastic deformation. The influence of the large flange deformation is reflected in the shear rotation plot of Figure 90 (b).

a. **b.**

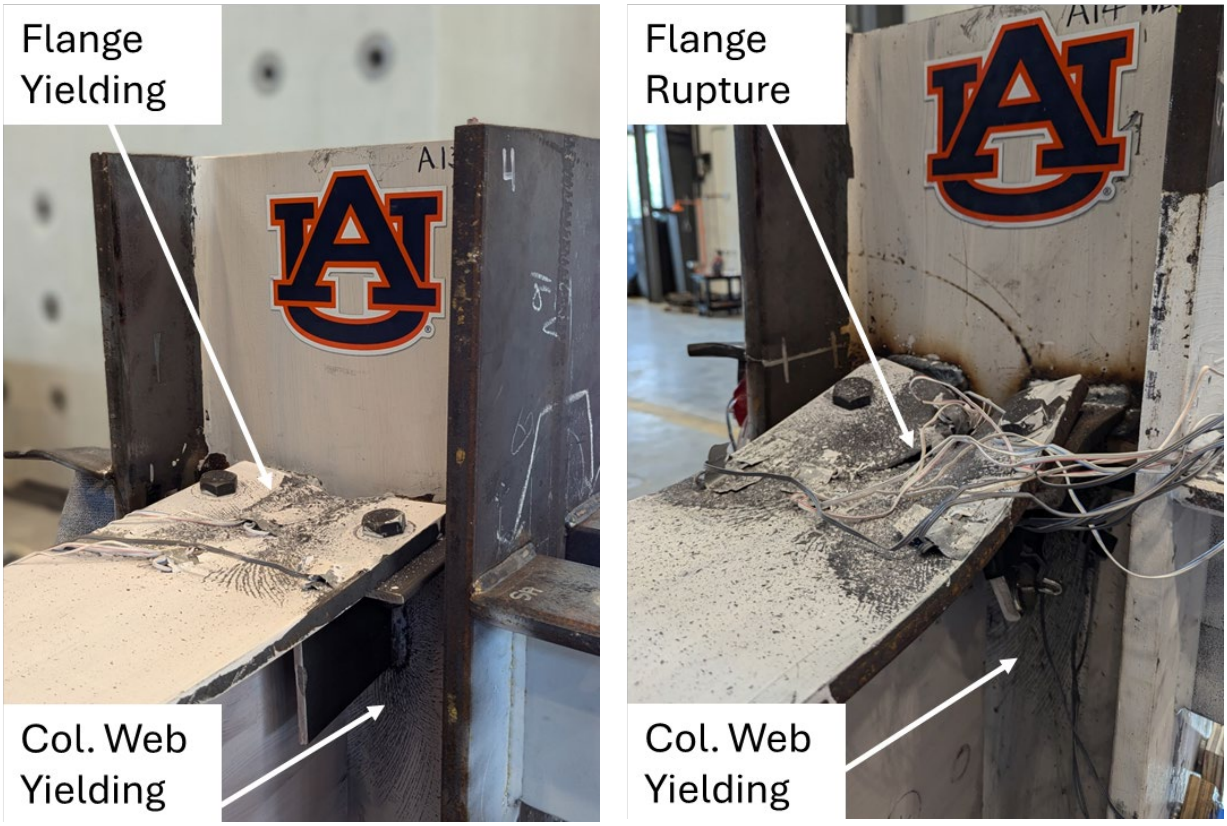

Figure 93: Connections After Testing (a) Connection K and (b) Connection L

a. **b.**

Figure 94: Drop-In Beam Flanges After Testing (a) Connection K and (b) Connection L

a. **b.**

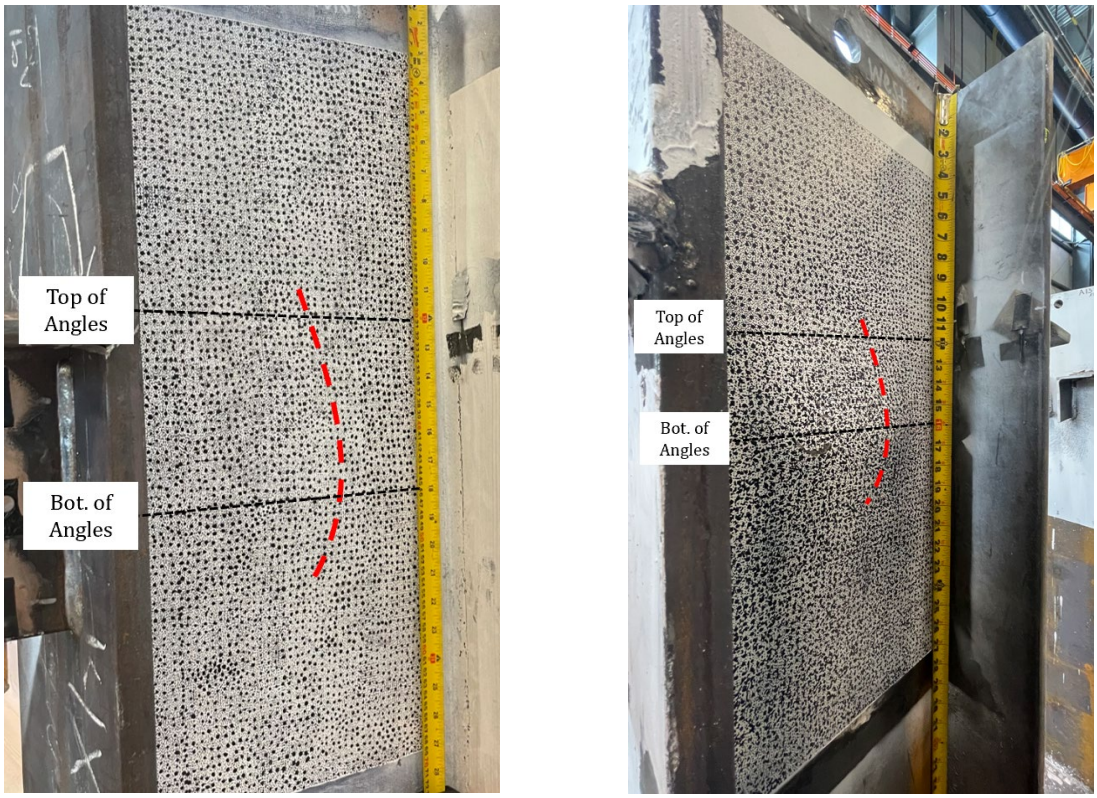

Figure 95: Column Web Deformation After Testing (a) Connection K and (b) Connection L

The support moment was estimated using the same approach that was followed in previous tests using the bending moment diagram. The bending moment diagrams at the design load and over a range of loads are shown in Figure 96. A plot of the support moment plotted against the connection rotation is shown in Figure 97. The support moment was taken as the moment at the face of the column web. The rotational stiffness of Connections K and L was smaller than the 2EI/L limit, and the moment in Connection K at 0.02-radian rotation was less than the $0.2M_p$ limit.

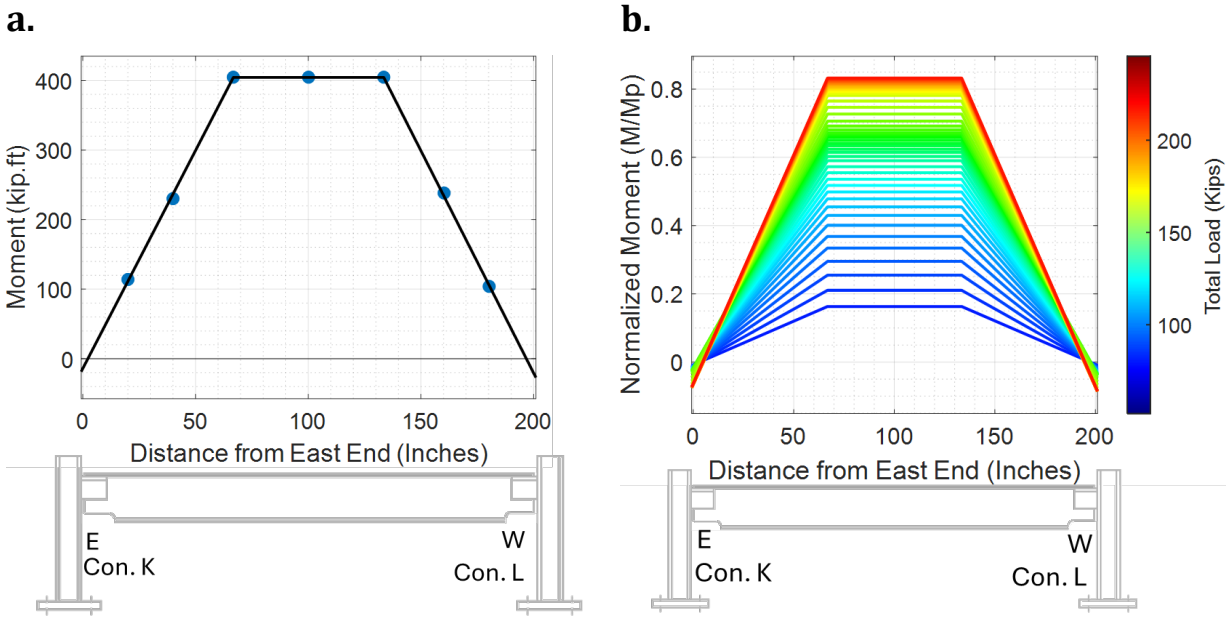

Figure 96: Girder Bending Moment Diagram (a) At the Design Load and (b) Over a Range of Loads

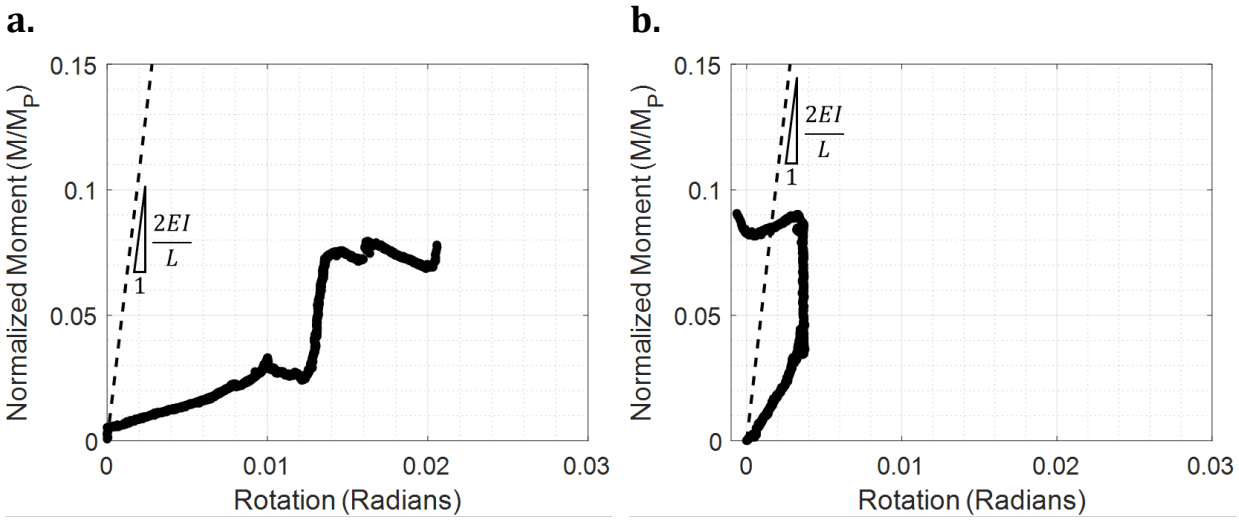

Figure 97: Normalized Support Moment – Rotation Curve (a) Connection K and (b) Connection L

In the investigation of Connection K and L's impact on the column web, DIC was utilized in Test-6.1. The opposing column web of both connections was imaged for DIC analysis, utilizing all DIC cameras. It is to be noted that Connection K was analyzed via 3D DIC utilizing two cameras. However, while Connection L was observed in testing with two cameras, it was unable to be analyzed via the VIC-3D software due to variations in the angle of the cameras. Connection L was instead processed via 2D DIC utilizing one camera's deformed images.

To analyze Connection K's column web behavior, an approximate area of 260 square inches (24 inches longitudinally by the width of the column web) of the column web was prepared directly behind the connection angles. Figure 98 shows the strain field formation for Connection K's column web, in units of microstrain, in (a) Von Mises strain(ε_v), (b) transverse strain (ε_{xx}), and (c) longitudinal strain (ε_{yy}) for a connection shear of 40, 60, 80, 100, and 120 kips. It is noted that areas of unprocessed data in the following figure are due to lighting discrepancies during the test and steel strain in these locations cannot be concluded via DIC. These areas are seen in the form of black and white speckled patches along the longitudinal centerline of the column web.

In reference to Figure 98 (a), yielding starts at a shear of 60 kips at the approximate location of the bottom of the connection angle. These yield lines then spread in a butterfly shape, eventually encasing the entire surrounding area of the connection angle at the maximum shear, denoting plastic deformation. As the shear increases and, therefore, rotation of the connection, the tops of the angles begin to move towards the midspan of the beam, while the bottom of the angles push into the column web. It is observed in both Figure 98(b) and (c), that the location corresponding to the bottom of the angle is greatly increasing in the tensile strain as connection shear increases, creating a bulging area out of the plane of the web (towards the camera/viewer). Also, the strains at the location corresponding to the top of the connection angles yield in compression, resulting in a collapsed area into the plane of the web (away from the camera/viewer).

a.

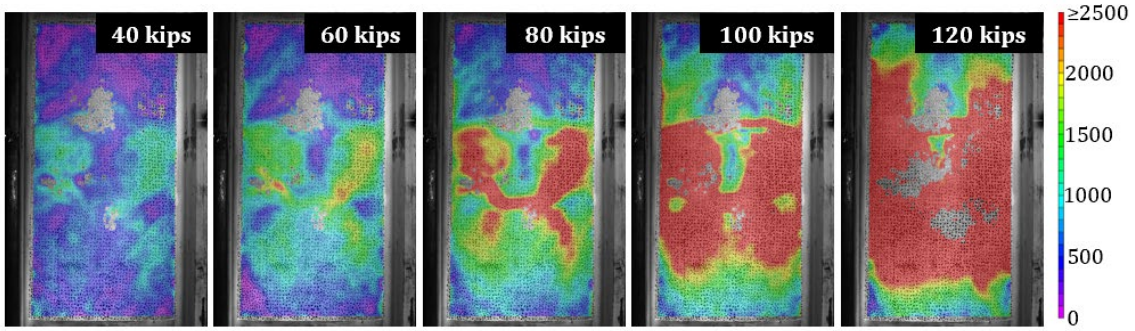

b.

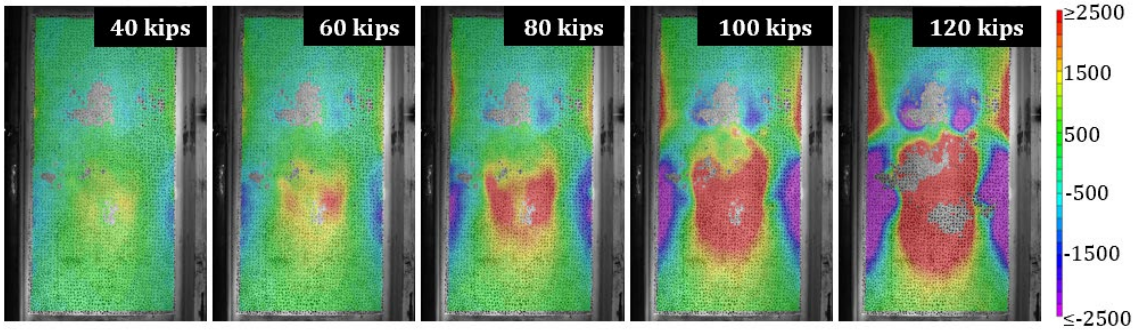

c.

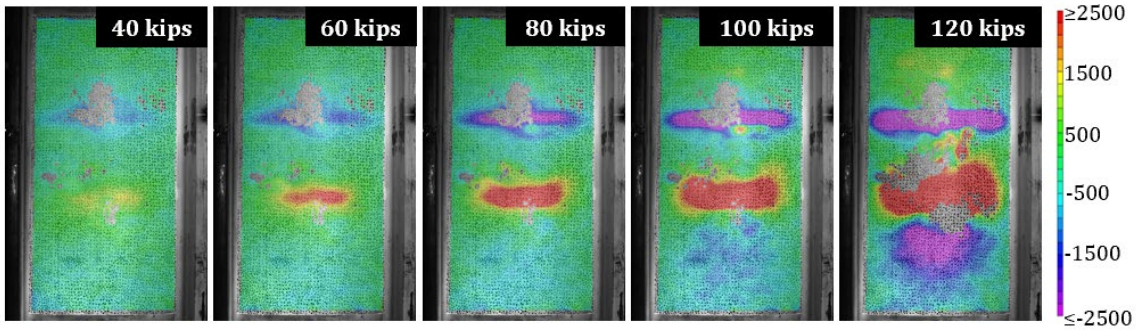

Figure 98: Connection K (Test-6.1) 2D DIC Column Web Deformation Progression (a) Von Mises Strain (ε_v), (b) Transverse Strain (ε_{xx}) – Engineering, and (c) Longitudinal Strain (ε_{yy}) – Engineering

An approximate area of 245 square inches (22.5 inches longitudinally by width of the column web) of the column web was prepared directly behind the connection angles. As noted above, due to the monocular vision of the 2D-DIC analysis, the large deformations in the column web created compression and tension biases leading to unreliable magnitudes of strain. However, the formation of the strain fields shown may be considered reliable due to small amounts of deformation at lower connection shears. Figure 98 visualizes the strain field progression for Connection L's column web, in units of microstrain, in (a) Von Mises strain

(ε_v), (b) transverse strain (ε_{xx}), and (c) longitudinal strain (ε_{yy}) for a connection shear of 40, 60, 80, 100, and 120 kips. Referring to Figure 99(a), yielding begins before a shear of 40 kips at the approximate location of where the column web and top of the angle are connected. This onset of yielding occurs at a lower shear than that of Connection K. These yield lines then begin to spread around the angle until the entire web surface has yielded at the maximum shear. Figure 99(b) and (c) show large portions of the column web being in compression, leading to a collapse of the web into the plane (away from the camera/viewer). However, the location corresponding to the bottom of the angle is in tension, creating an out-of-plane bulging (towards the camera/viewer) area. It is to be noted that this region is much smaller in area than that of Connection L but is significantly more pronounced.

a.

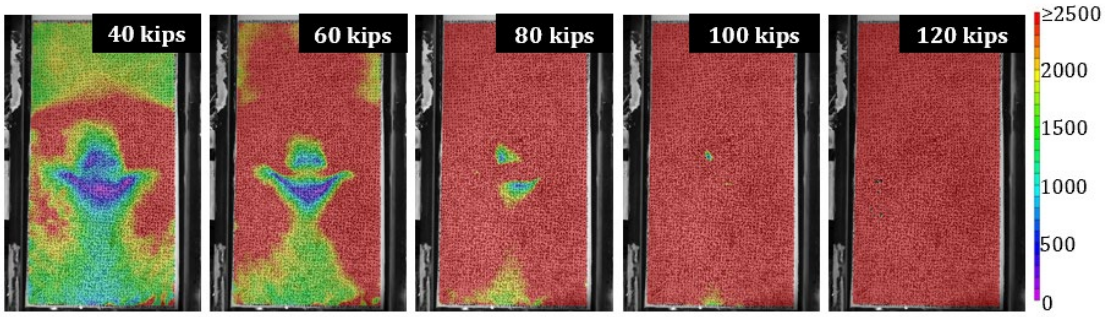

b.

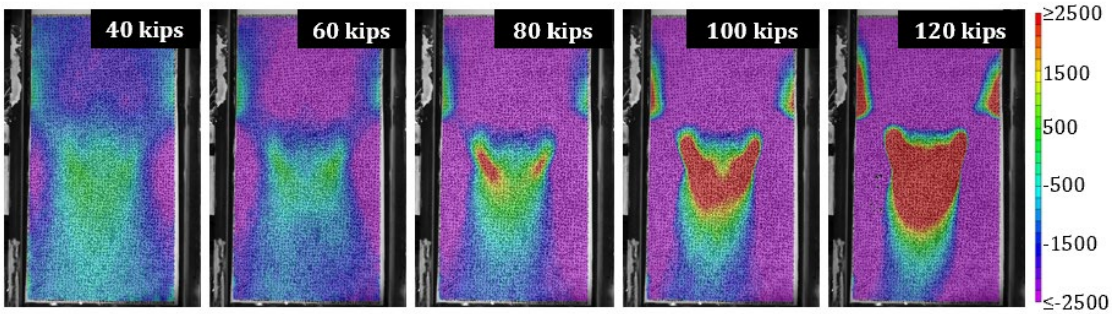

c.

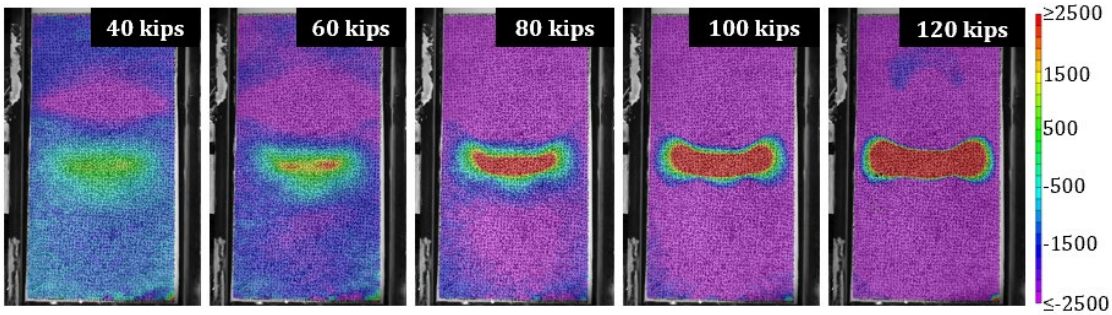

Figure 99: Connection L (Test 6) 2D DIC Column Web Deformation Progression (a) Von Mises Strain (ε_v), (b) Transverse Strain (ε_{xx}) – Engineering, and (c) Longitudinal Strain (ε_{yy}) – Engineering

The Drop-In Connections K and L met the requirements for strength and stiffness. The beam was oversized due to availability. This produced a high shear and low rotational demand test. Therefore, the rotational ductility was not fully evaluated. The performance of the column web was sufficient to adequately develop the strength of the connection.

Testing Summary

Ten girder-to-column (strong axis) and two beam-to-column (weak axis) connections were tested via the previously described methods. The test variables included angle size, bearing

length, girder size and span, angle orientation and spacing, and lateral restraint. For comparison, one industry standard shear tab connection was tested. The tested connections, along with key parameters from the tests, are summarized in Table 7.

All tested connections met and exceeded the strength requirements. The measured maximum shears ranged from $1.2V_u$ to $1.9V_u$. The lower value was observed when the angle orientation was flipped (Connection H).

The connections tested in Tests One to Three were subjected to high shear in the first round of testing and then, by adjusting the loading points, subjected to a relatively lower shear and higher rotation. All the connections tested in this manner, except for Connection D, met the 0.03 radian rotational ductility requirement. Connection D experienced weld failure at 0.01-radian rotation, which was the controlling design limit state.

The loading points in Tests Four to Six were not adjusted, and the connections were subjected to relatively higher shear and lower rotation demand. Unlike the connections in the previous group, which showed girder flange yielding and greater connection rotation, the connections in Tests Four to Six exhibited plastic deformation concentrated in the connection regions, apart from Connection G, which showed a remarkable 0.06-radian rotation.

Table 7: Test Summary

Test (1)	Conn.	Angle Size (2)	Brg. Lgth. (in.)	Max. Shear (Kips)	Max. Rotation Applied (Radian)	Rot. Stiffness (%) (3)	Achieved Connection Limit States (6)	Ultimate Connection Failure
Girder to Column								
1	A	L8×4×3/4	5	141	0.03	4.7	FB	None
	B	L8×4×3/4	5	141	0.03	11.4	FB	None
2	C	L8×4×3/4	3	129	0.04	6.2	FB	None
	D	L6×4×5/16	5	129	0.01	9.2	FB / AY	Weld and angle buckling
3	E	L8×4×1/2	5	150	0.03	11.0	FB	None
	F	3/8×5×12.5 (Shear tab)	-	150	0.04	9.1	STY	None
4	G	L6×4×5/16	3	84	0.06	11.8(4)	FB / AY	None
	H	L4×3×1/2 (Flipped)	3	57	0.01	0.0	AY	Flange and angle horizontal leg yielding
5 (5)	I	L6×4×5/16	5	147	0.02	2.4	FB / AY	Angle buckling and flange yielding
	J	L4×3×1/2	3	134	0.01	3.1	FB / AY	Flange yielding and weld
Beam to Column								
6	K	L6×4×5/16	5	124	0.02	4.4	FB / AY / CWY	Flange yielding
	L	L4×3×1/2	5	124	0.00	18.8	FB / AY / CWY	Flange rupture

(1) W16×36 girder for Test 5 and W24×68 girder/beam for the remaining tests.

(2) The shorter legs were horizontal. The clear distance between the Drop-in angles was 2-7/8", except for Connections G, H, J, and L, which was 1.5" for the first two and 3" for the latter two.

(3) As a percentage of girder/beam 2EI/L. L was taken as 30 feet (Composite span).

(4) At 0.018 rad. (Maximum rotation before a strain gauge failure).

(5) Test Five validated the connection torsional stiffness with an unbraced test.

(6) FB = flange bending, AY = angle yielding, STY = shear tab yielding, CWY = column web yielding

The rotational stiffness of all tested connections was well below the *2EI/L* limit, classifying it as a simple connection. When calculating the limiting stiffness, *L* was conservatively taken as the composite length of the tested girder/beam. Moreover, the support moment at 0.02-radian rotation was below $0.2M_p$ for all connections that were able to achieve that level of rotation (not shown in Table 7 due to space limitations). If 0.02-radian rotation was in multiple loading cycles, the moment from the first loading cycle is reported.

It was observed that flange bending was one of the limit states controlling the strength of the drop-in connections. For this failure mode, four parallel yield lines were developed, as illustrated in Figure 100. The maximum transverse tension and compressive strains were recorded near the edge of the angles and the fillet of the girder. Since the k_1 values provided in Table 1-1 of the AISC manual are upper bound values, the distance between the inner two yield lines is less than $2k_1$, resulting in a wider gap between the tension yield line and the compression yield lines on one side of the center line.

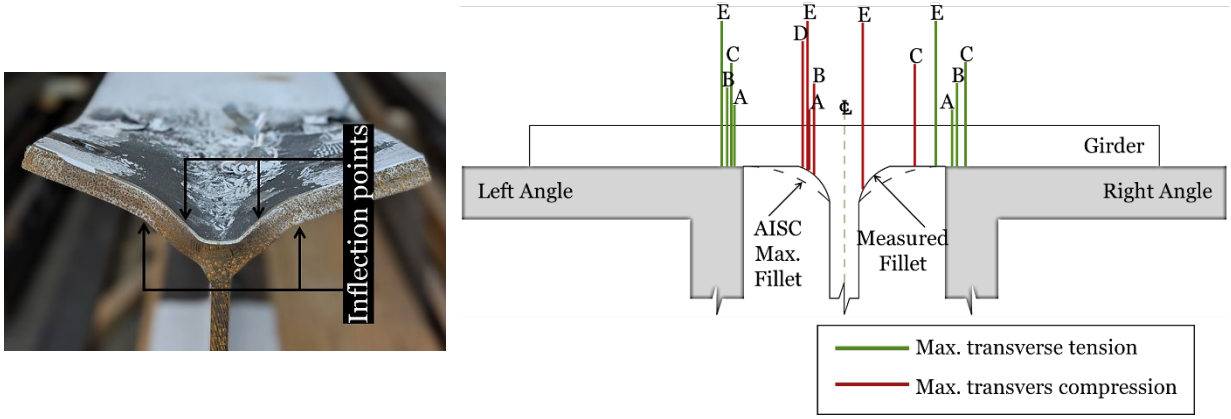

(a) Typical drop-in flange after testing

(b) Position of yield lines using DIC strain data in connections A to E

Figure 100: Visualization of Flange Yield Lines

The distance between the maximum tension and compress strain for connections A through E is listed in Table 8. The results varied between $0.5k_1$ and $0.86k_1$ with an average of $0.73k_1$. For design purposes, $0.75k_1$ is recommended (see Phase 4).

Table 8: Distance Between Maximum Tension and Compression Strain in the Top Flange

Connection	Distance Between Max. Tension and Max. Compression (inches)	Percentage of k_1 value listed in AISC Manual (%)
A	1.05	73
B	1.24	86
D	0.72	50
E	1.22	85
	1.04	72
Average		**73**

All the information gathered during the extensive full-scale testing (Phase 2) was utilized in conjunction with the refined analysis (Phase 3) to develop clear design guidance for drop-in connections (Phase 4).

Phase 3 - Refined Analysis

Purpose and Approach

The purpose of this phase was to ***comprehensively evaluate the drop-in top flange connection critical parameters*** listed earlier in Phase 1. The experimental program can only test a selection of these parameters. Therefore, a common technique utilized herein was to validate a numerical modeling approach with experimental data. After this process was complete, extensive parametric studies were performed to explore the behavior of the connection.

FEA Model Validation

Refined finite element modeling was performed for Tests One and Five and validated against the experimental results. All modeling was performed in ABAQUS software with full material and geometric nonlinearity. Material nonlinearity was modeled using the von Mises yield criterion and strain hardening behavior was incorporated using the isotropic hardening model governed by the power law stress-strain relationship defined by Eq. 3-1. Here σ and ε represent the stress and corresponding strain; σ_y, σ_u, ε_{sh}, ε_u, and n represent the yield stress, ultimate stress, strain at the onset of strain hardening, ultimate strain, and power law coefficient, respectively. The values of these constants used to model the grade 50 steel and A325 bolts are tabulated in Table 9. The yield and ultimate strengths represent the expected values rather than the specified minimum. The ε_{sh} defines the length of the yield plateau and corresponds to a yield plateau length eight times the yield strain for the grade 50 steel and no yield plateau for the A325-bolt. The resulting stress-strain was applied to the finite element model after converting it to true stress-true strain. The modulus of elasticity used for both materials was 29,000 ksi.

$$\sigma = \sigma_u - \left(\sigma_u - \sigma_y\right) \times \left(\frac{\varepsilon_u - \varepsilon}{\varepsilon_u - \varepsilon_{sh}}\right)^n \qquad (3\text{-}1)$$

Table 9: Material Properties Used for FEA

Material	σ_y (ksi)	σ_u (ksi)	$\varepsilon_{sh}/\varepsilon_y$[1]	$\varepsilon_u/\varepsilon_y$	n
Grade 50	55	71.5	9	85	3
A325-Bolt	94.5	126	1	50	3

1 ε_y - yield strain ($\varepsilon_y=\sigma_y/E$)

A model of Test One is shown in Figure 101. The model combines solid, shell, and line elements to balance accuracy and computational efficiency. Quadratic solid elements with 20 nodes per element were used for the angles and parts of the girder and column near the connections. The remaining portions of the girder and column were modeled using a quadratic shell and quadratic line elements having eight and three nodes per element, respectively. The bolts were modeled with linear solid elements having eight nodes per element.

The interaction between steel components, such as angles, girder, and bolts, was modeled as hard contact with no penetration in the normal direction. Separation after contact was

allowed to permit possible separation during loading. The tangential behavior of the contact was modeled through a penalty friction formulation with a friction coefficient of 0.1 to simulate the dry steel-to-steel interface. Before the application of loads, a bolt pretension with a magnitude of 5.6 ksi was applied to all bolts. The 5.6 ksi is 20% of the bolt pretension for a slip critical condition on a ¾" A325 bolt. The weld between the angles and the columns was modeled using a tie constraint, and parts of the girder modeled with shell and solid elements were joined using shell-to-solid coupling. Similarly, the column's line and solid elements were joined using a coupling constraint.

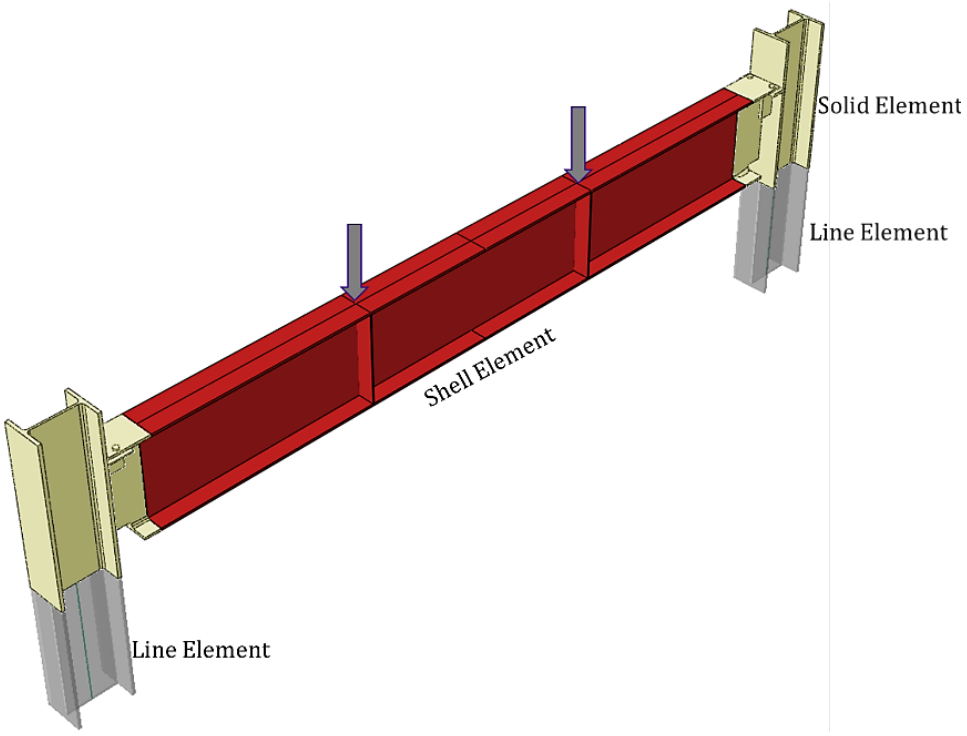

Figure 101: Finite Element Model for FEA Validation

All translational and rotational degrees of freedom at the column base were restrained. Moreover, the loading and lateral restraints provided replicate the testing conditions. The resulting nonlinear static analysis was solved using the full Newton method as a solution technique.

Figure 102 compares the mid-span moment vs. displacement and connection shear vs. rotation results from Test One and the finite element model. The connection rotation was calculated as the difference between the beam end rotation and the column rotation. As seen from the graphs, the finite element result agrees with the test result both globally and locally. In addition, the girder and connection deformation observed in the test (Figure 17 and Figure 19) are well reflected in the FEA results. The global and connection angles deformed shape and von Mises stress contours are shown in Figure 103.

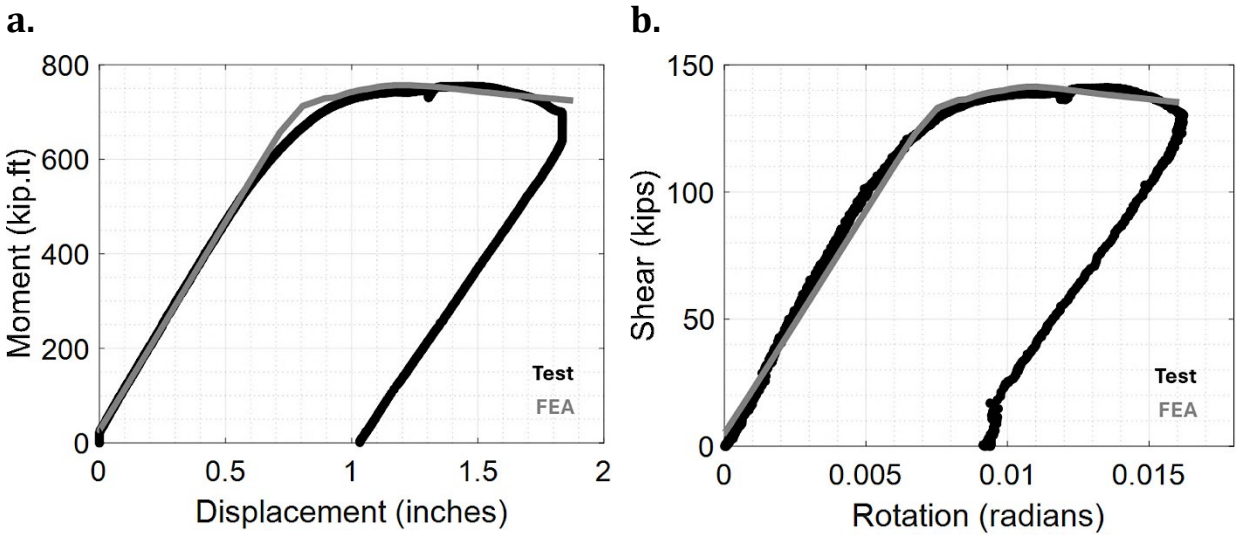

Figure 102: Comparison of Test and Finite Element Results (a) Mid-Span Moment-Displacement and (b) Connection Shear-Rotation

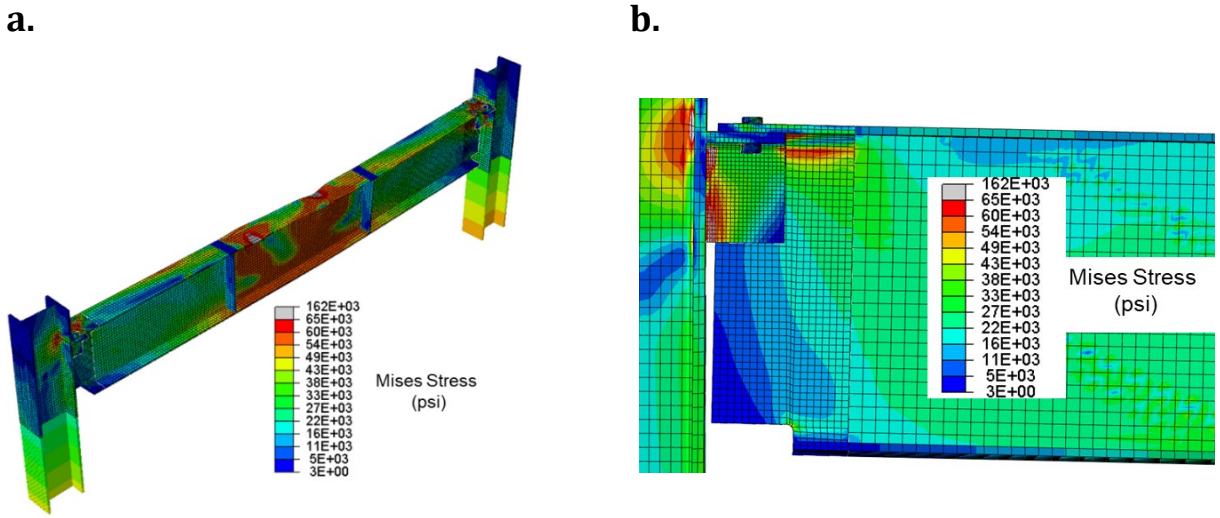

Figure 103: Von Mises Stress and Deformed Shape (a) Global and (b) Connection A

Furthermore, Figure 104 compares the failure mode and maximum shear from FEA and Test Five. As can be seen from the figure, the angle buckling and girder flange yielding are well reflected in the FEA, and the maximum connection shears are in good agreement with the test results. In modeling these two connections, half of the test assembly was constructed employing symmetric conditions about mid-span.

a.

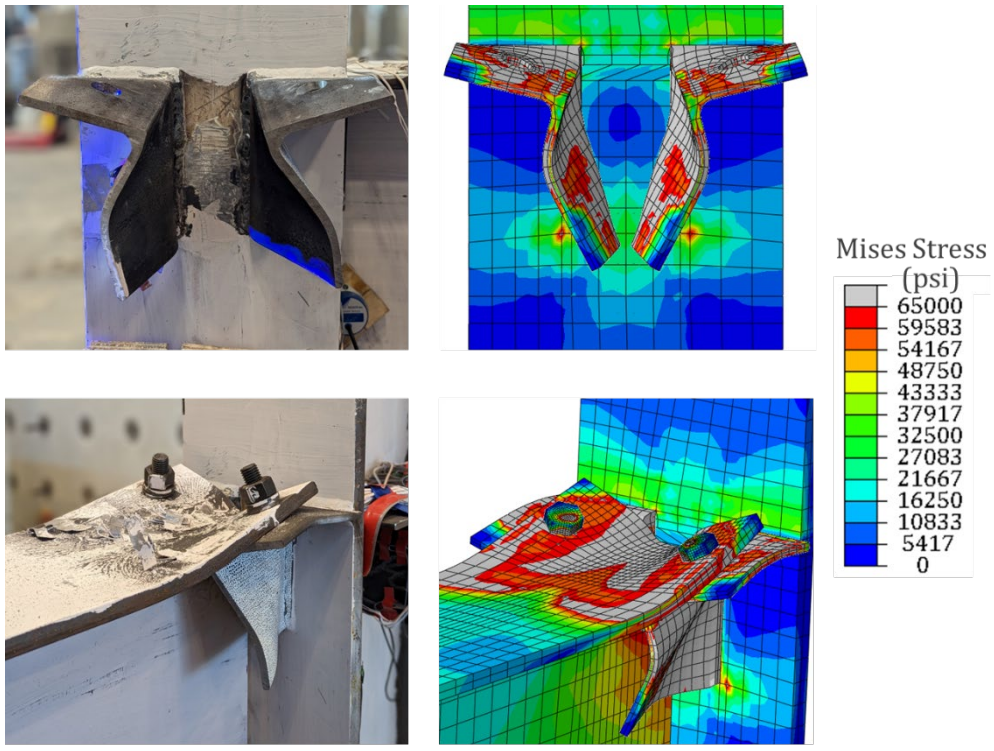

$V_{max} = 147\ kip$ $V_{max} = 149\ kip$

b.

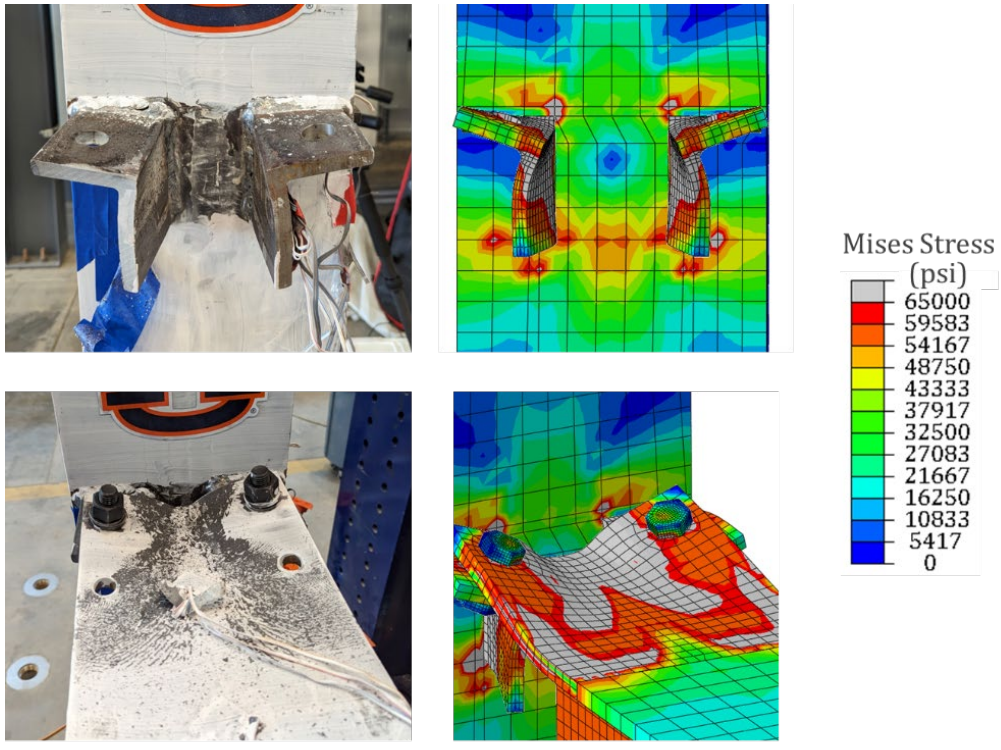

$V_{max} = 134\ kip$ $V_{max} = 133\ kip$

Figure 104: Comparison of Test and FEA results (a) Angle Buckling and Maximum Shear in Connection I and (b) Flange Yielding and Maximum Shear in Connection J

Parametric Study

A parametric study was conducted using the validated finite element model. This study included 192 models by varying the angle thickness (t_A), angle depth (d_A), girder flange thickness (t_f), bearing length (l_b), girder fillet size (k_1), and angle encroachment into the girder fillet (E_n). The variables of the parametric study and their values are schematically illustrated in Figure 105. The W24×68 section was adopted for the parametric study, and the flange thickness was varied as indicated in Figure 105. A flange thickness of 0.585 corresponds to a standard W24×68. The horizontal leg of the angles was maintained at four inches in all instances. The k_1 values indicated in Figure 105 represent the percentage relative to the AISC Manual (AISC 2017) specified value for a W24×68 section. The encroachment is also measured in relation to this k_1 value. The length of the bottom flange cope was set at one inch longer than the bearing length.

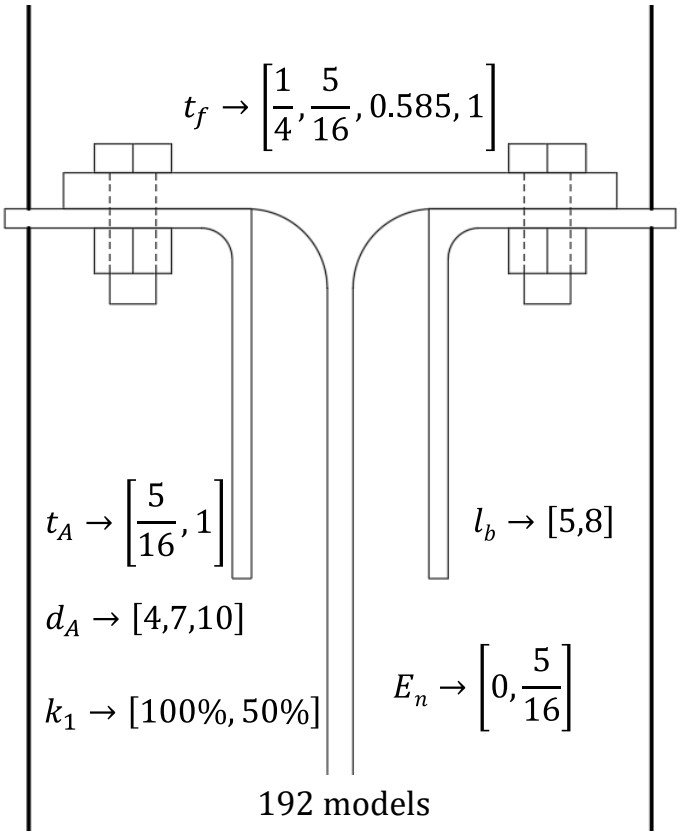

Figure 105: Parametric Study Variables and their Assigned Values (Units: Inches)

The parametric study included drop-in connections with varying shear strengths that must fulfill dual strength and ductility criteria. To subject the connections to a realistic combination of shear and rotation, a loading protocol established by (Astaneh-Asl, Call et al. 1989, Astaneh 1989) illustrated in Figure 106, was adopted. The vertical axis shows the beam end shear (V) normalized by the beam end shear corresponding to the initial yielding of the beam at mid-span (V_y). The initial segment of the loading path (segment a-b) represents the elastic end-rotation versus end-shear response of a simply supported beam. Point b indicates the initial yield of the beam at mid-span, marking the onset of increased

end rotation demand until the mid-span moment reaches M_p at point c. Within the proposed loading path, point c coincides with the shear yield strength of the connection (R_y), and the beam end reaction at point b can be computed by dividing R_y by the shape factor. A shape factor of 1.12 is recommended, with points b and c corresponding to 0.02 and 0.03-radian rotations, respectively (Astaneh-Asl, Call et al. 1989). If loading is continued beyond point c, segment cd represents strain hardening of the beam, and point d is a practical value for infinite rotation.

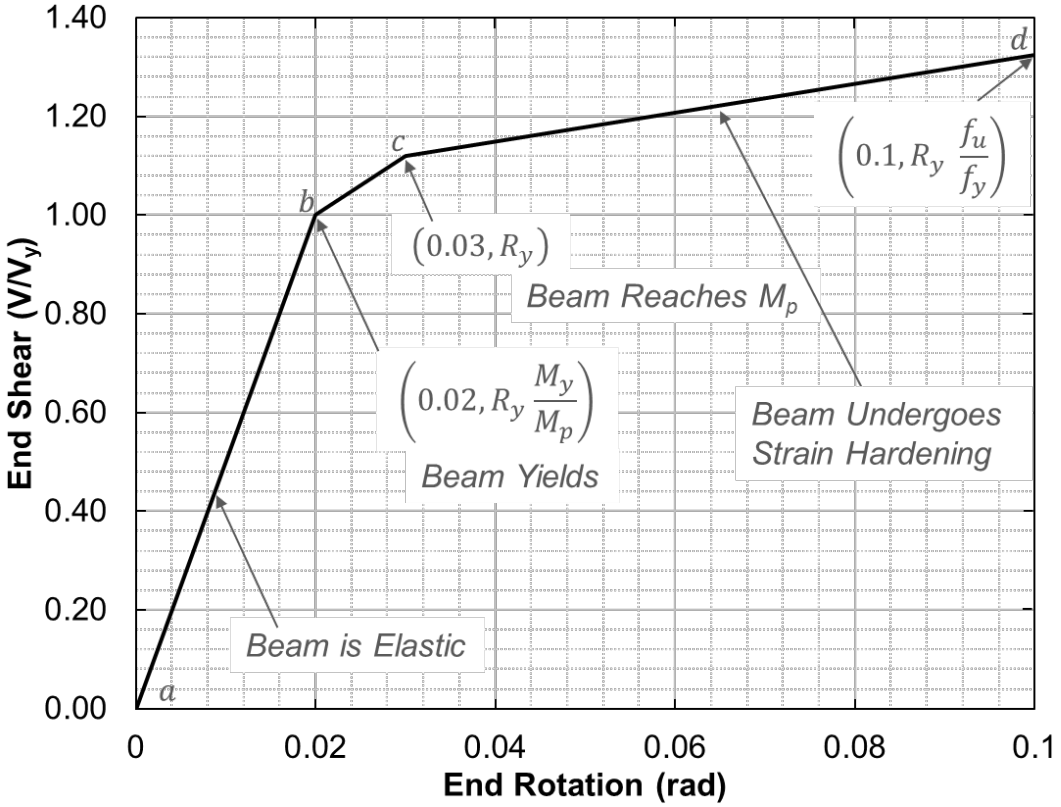

Figure 106: Shear-rotation relationship for simple beams (Astaneh-Asl, Call et al. 1989)

Therefore, estimating the shear strength of connections (R_y) is necessary to implement the loading protocol. As a result, the parametric study analysis was done in two steps. First, the shear strength of the connections was determined by conducting an analysis identical to the validation model and employing symmetry about the mid-span. The shear-to-rotation ratio from this analysis (Analysis I) is unrealistic, particularly for the small and large connections, as the girder span and section size are not reasonably proportional to the connection size. Therefore, the result from Analysis I was used to estimate R_y and establish the loading path illustrated in Figure 106. R_y was taken as the maximum connection shear from Analysis I. To rule out reduced connection shear due to yielding and/or buckling in the girder, part of the girder 36 inches from the connection was modeled as a linearly elastic beam using quadratic shell elements. The 36-inch length was adopted after a sensitivity study.

After establishing the loading path using the results of Analysis I, Analysis II was used to subject the connections of the parametric study to a realistic combination of shear and

rotation. In Analysis II, a 36-inch-long girder drop-in top flange connected to a stub column was modeled. The model assembly was subjected to the prescribed shear from the loading path, and the rotation of the free end of the girder was controlled to ensure the target shear and beam end rotation were applied. In Analysis II, the column top displacement in the longitudinal direction was restrained to prevent column rotation. In addition, the lateral displacement of the beam end and the top of the column were restrained. Figure 107 summarizes the steps followed to run the parametric study analysis.

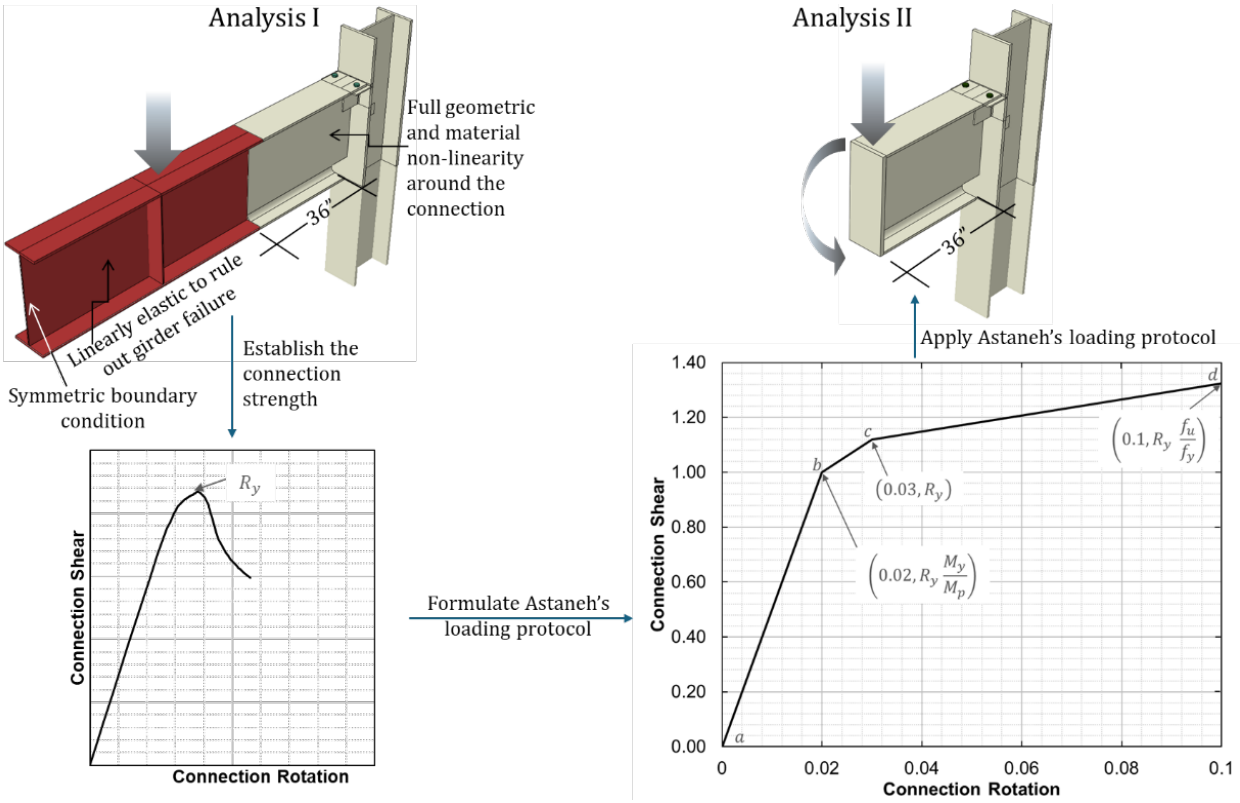

Figure 107: Steps Followed to Run Parametric Study Analysis

Parametric Study Results

A summary of the maximum shear for the first 36 models obtained from Analysis I is provided in Figure 108 through to Figure 111. The maximum reactions are provided as V_{max}. Note that the model did not converge in all cases. These are denoted with red text in the figures. The corresponding results from Analysis II, along with the maximum connection rotation (θ_{max}) are provided in Figure 112 through to Figure 115. These figures show how the connection strength and applicable limit states vary with different geometric parameters of the connection. Moreover, all the connections were able to accommodate the rotational demand. The connections that exhibited rotation that is less than 0.03 radian were due to the analysis not converging to the end. Three limit states were identified that control the strength and behavior of the drop-in connection. These include shear yielding and/or buckling of the angle vertical leg, transverse bending and yielding of the flange, and the strength of the coped beam. Since the angle-to-column weld was modeled with a tie constraint, strength limitation due to weld failure was not reflected.

Flange yielding was the primary limit state for connections with 5/16" and 1/4" flange thickness. Increasing the bearing length in these connections led to enhanced strength and, in certain instances, shifted failure to the angles. The observed angle failure was characterized by the shear yielding of the vertical leg, with or without buckling. Flange transverse bending also became dominant when a 0.585" flange thickness was paired with stout angles. In line with the tests, the observed flange-yielding pattern began between the angles and extended beyond the end of the angle. The total length of the flange plastic zone (yield line) was recorded for selected cases that fully converged and is included in Table 10. The yield line length was measured as the distance between the beam and the section where the Von Mises stress is below the yield stress. Figure 116 illustrates how the yield line length was measured. These values and the test data are later utilized in Phase 4 to develop a design equation for flange bending. In cases where the flange and angle limit states were not the controlling factors, the connection strength was ultimately limited by the coped beam strength. Phase 4 offers comprehensive design guidance for the drop-in connection.

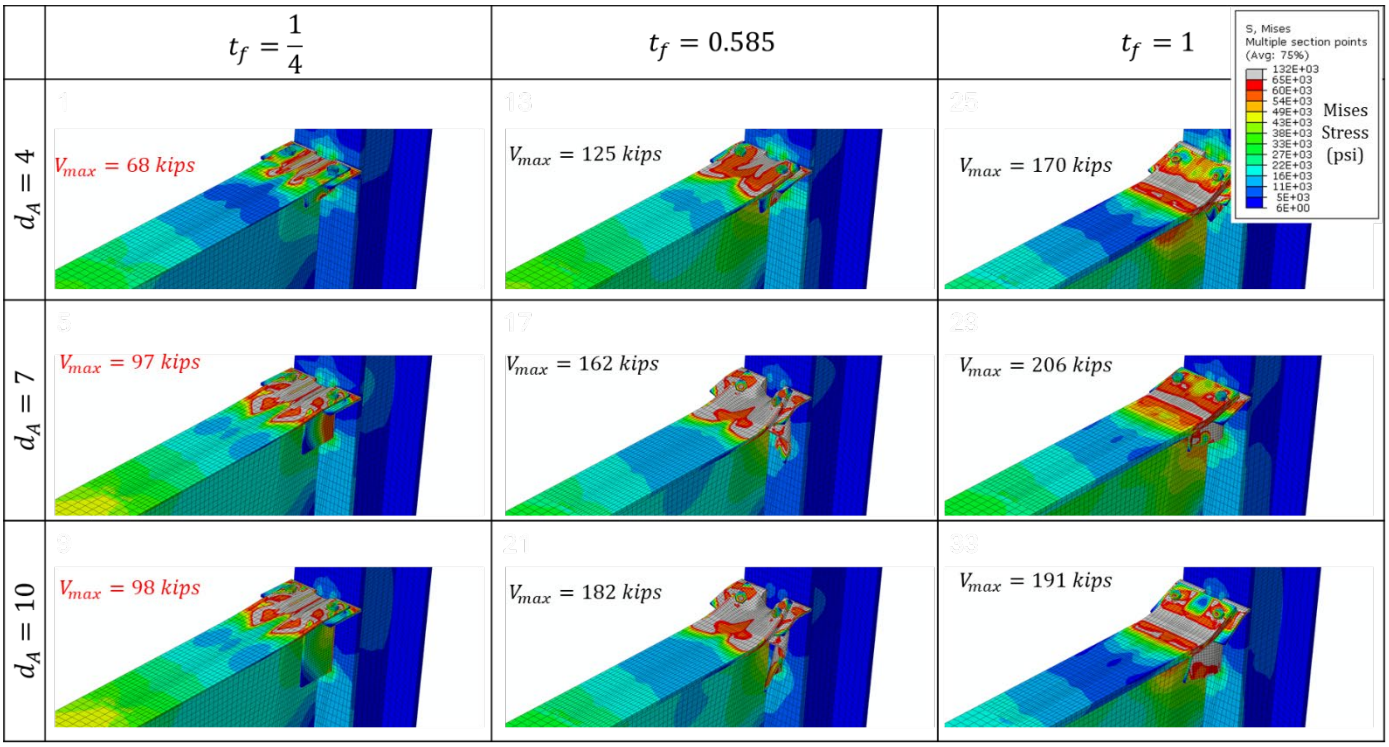

Figure 108: Maximum Shear and Von Mises Stress from Analysis I (t_A=5/16, l_b=5, k_1=100%, E_n=0)

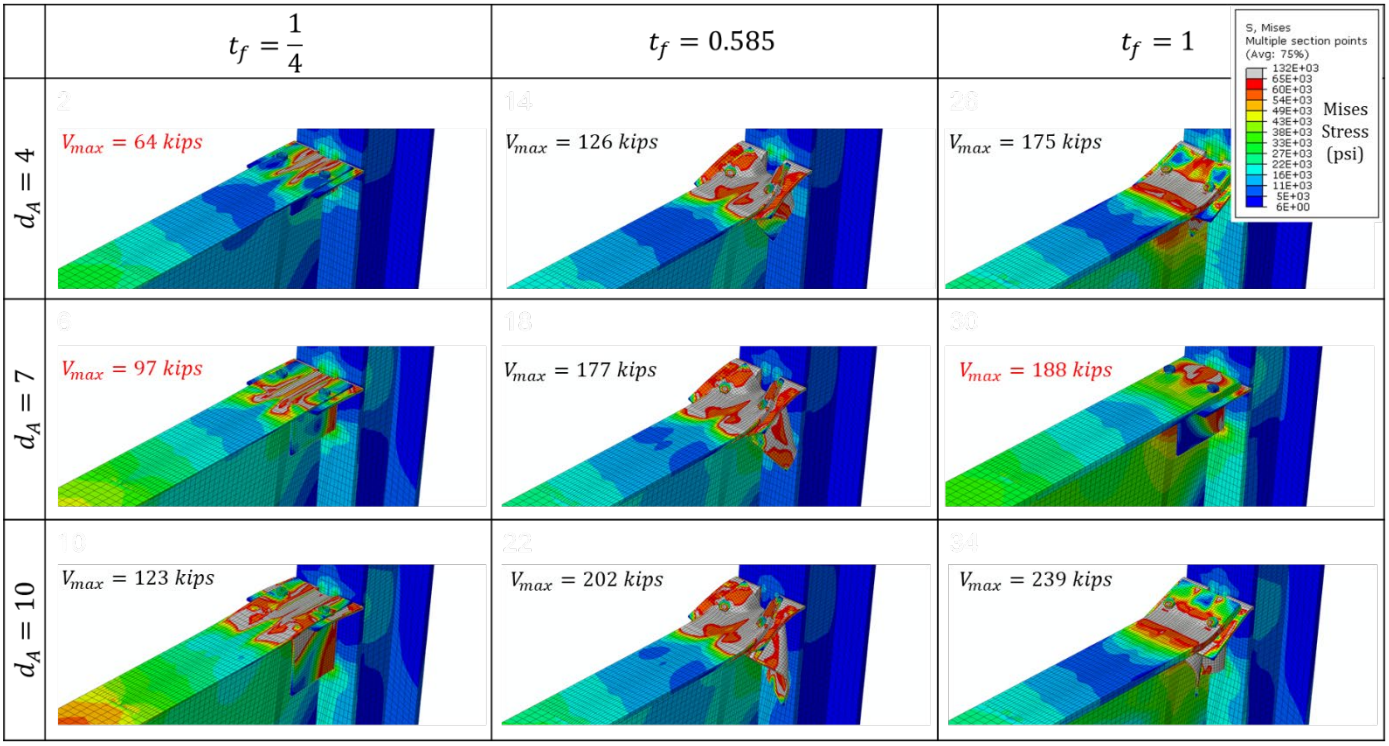

Figure 109: Maximum Shear and Von Mises Stress from Analysis I (t_A=5/16, l_b=8, k_1=100%, E_n=0)

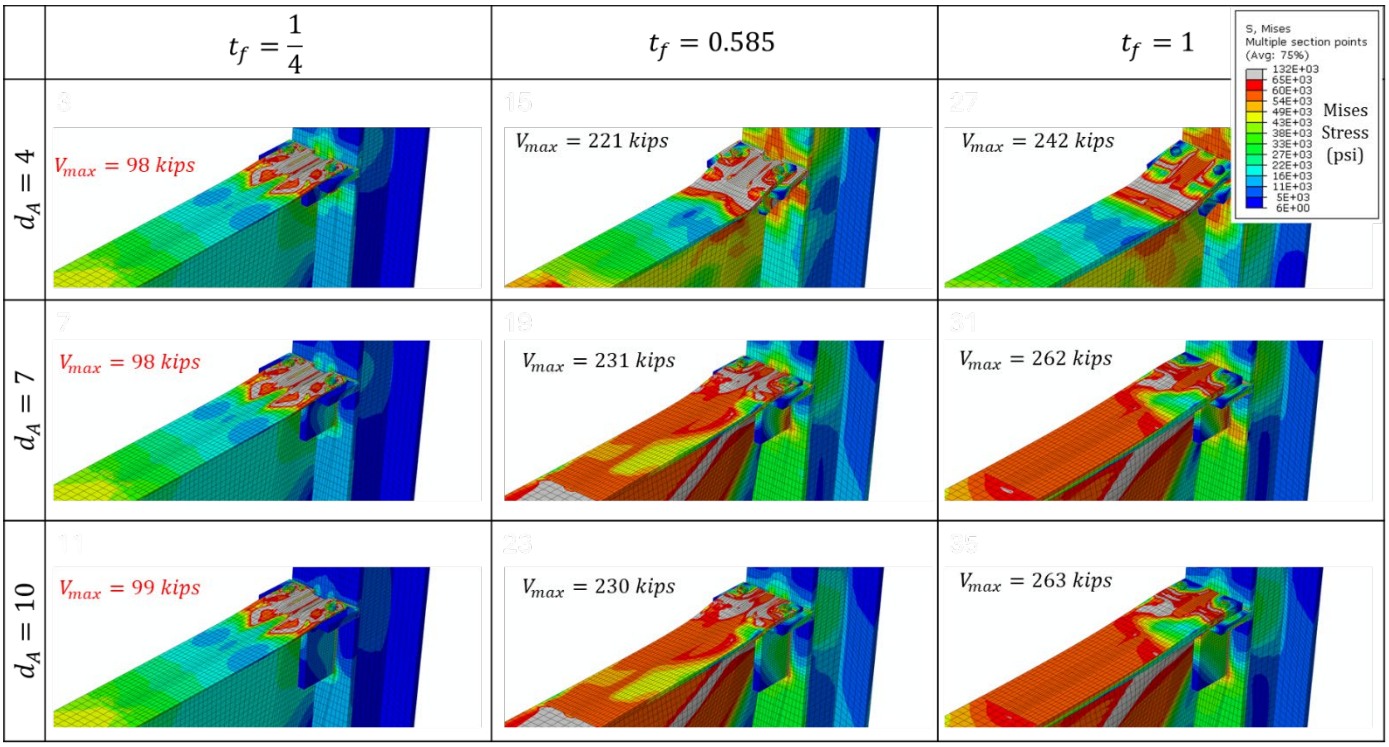

Figure 110: Maximum Shear and Von Mises Stress from Analysis I (t_A=1, l_b=5, k_1=100%, E_n=0)

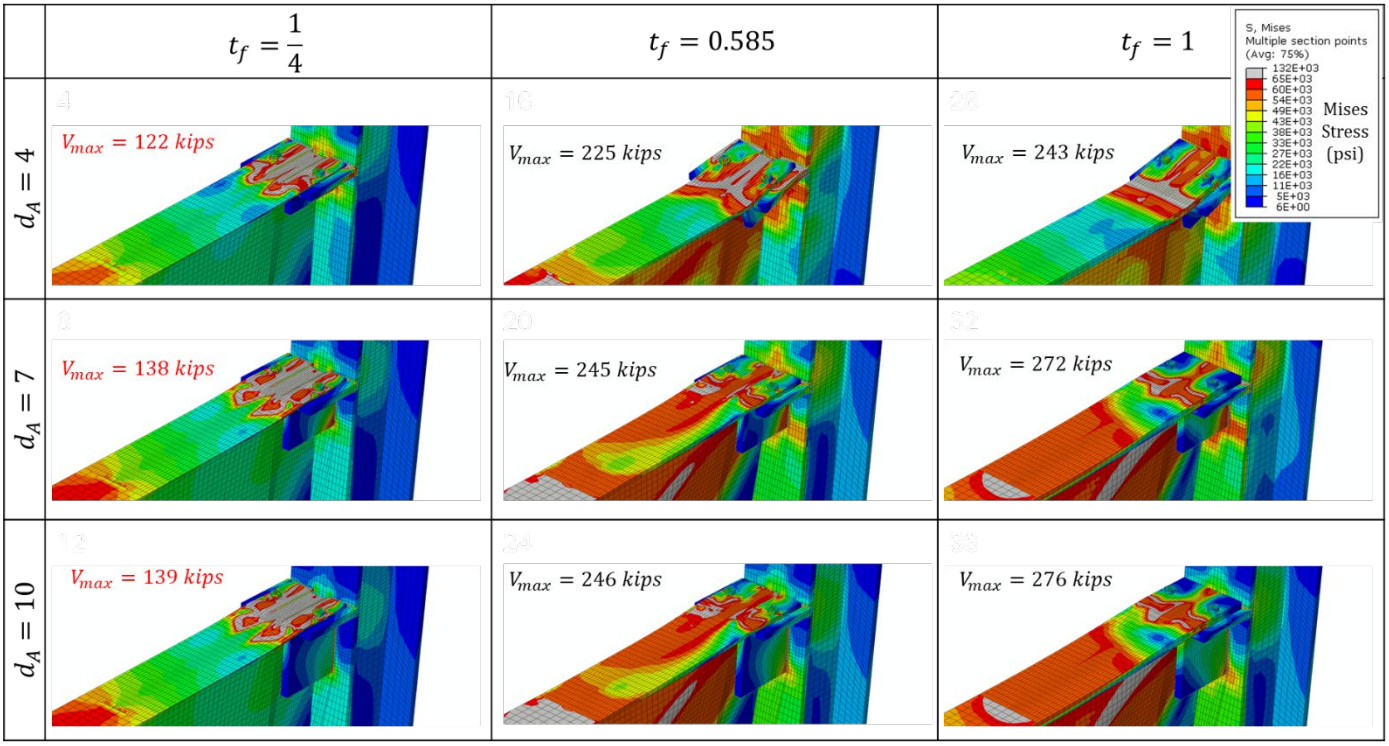

Figure 111: Maximum Shear and Von Mises Stress from Analysis I (t_A=1, l_b=8, k_1=100%, E_n=0)

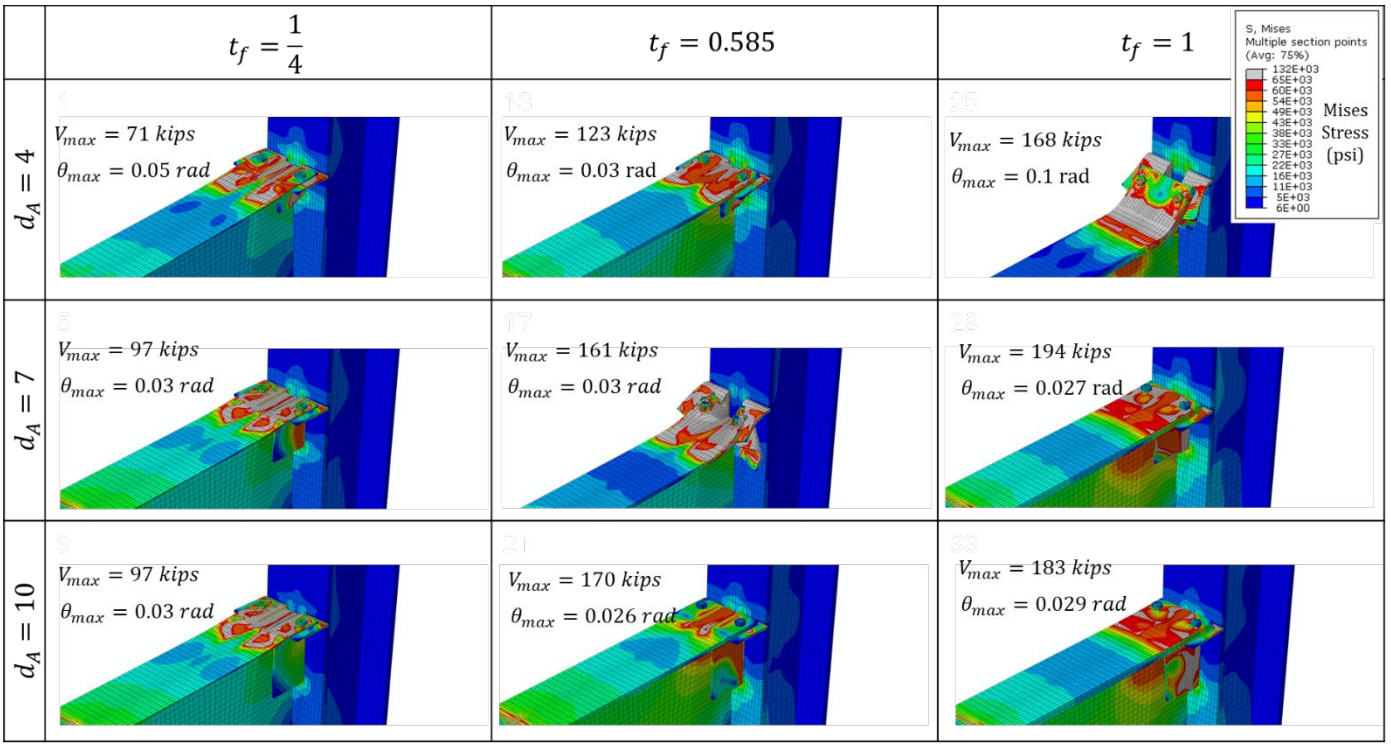

Figure 112: Maximum Shear and Von Mises Stress from Analysis II (t_A=5/16, l_b=5, k_1=100%, E_n=0)

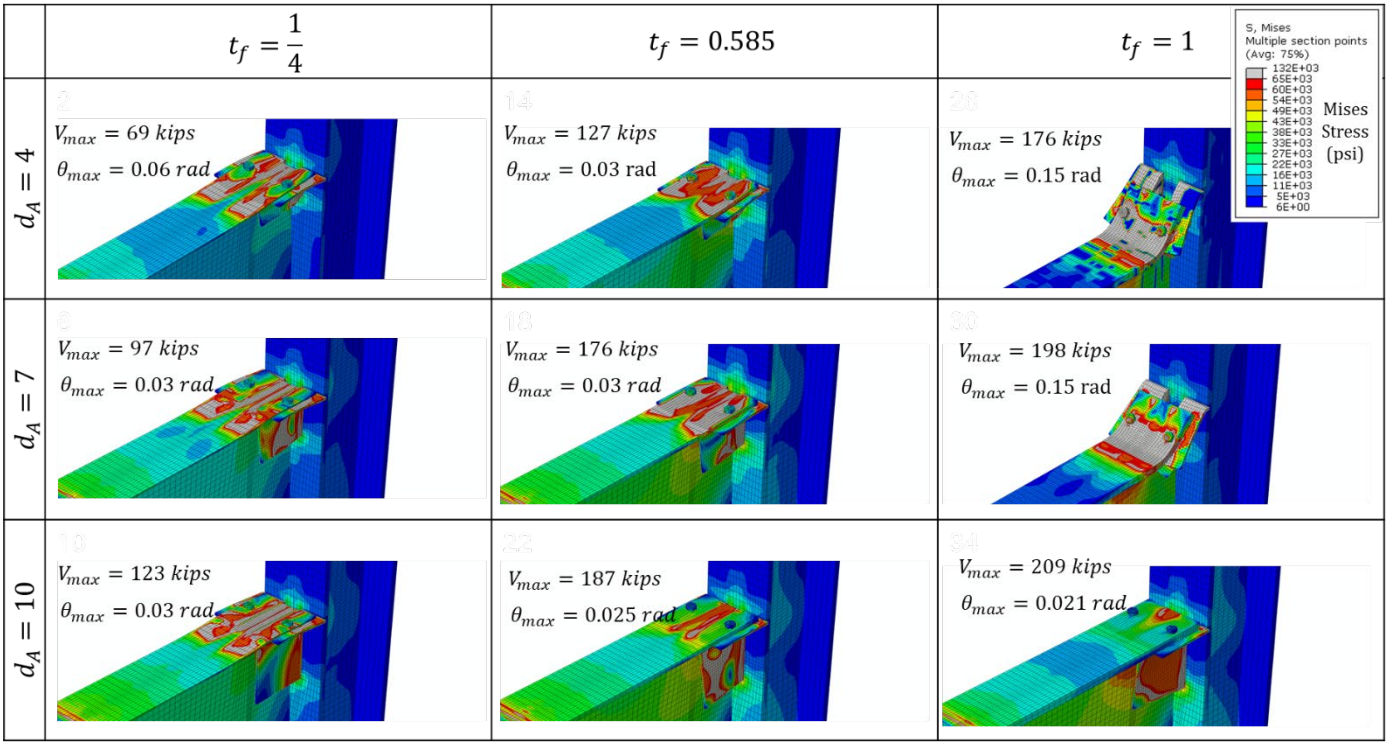

Figure 113: Maximum Shear and Von Mises Stress from Analysis II (t_A=5/16, l_b=8, k_1=100%, E_n=0)

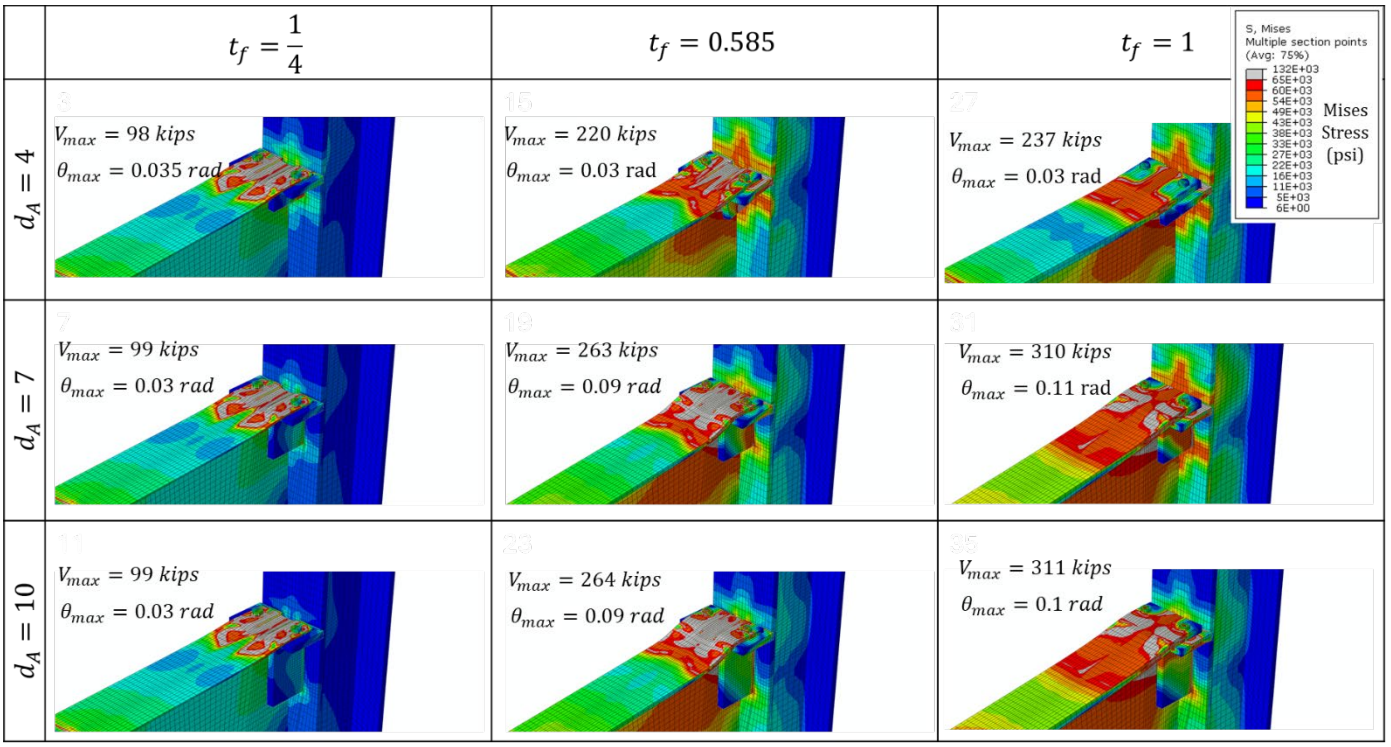

Figure 114: Maximum Shear and Von Mises Stress from Analysis II (t_A=1, l_b=5, k_1=100%, E_n=0)

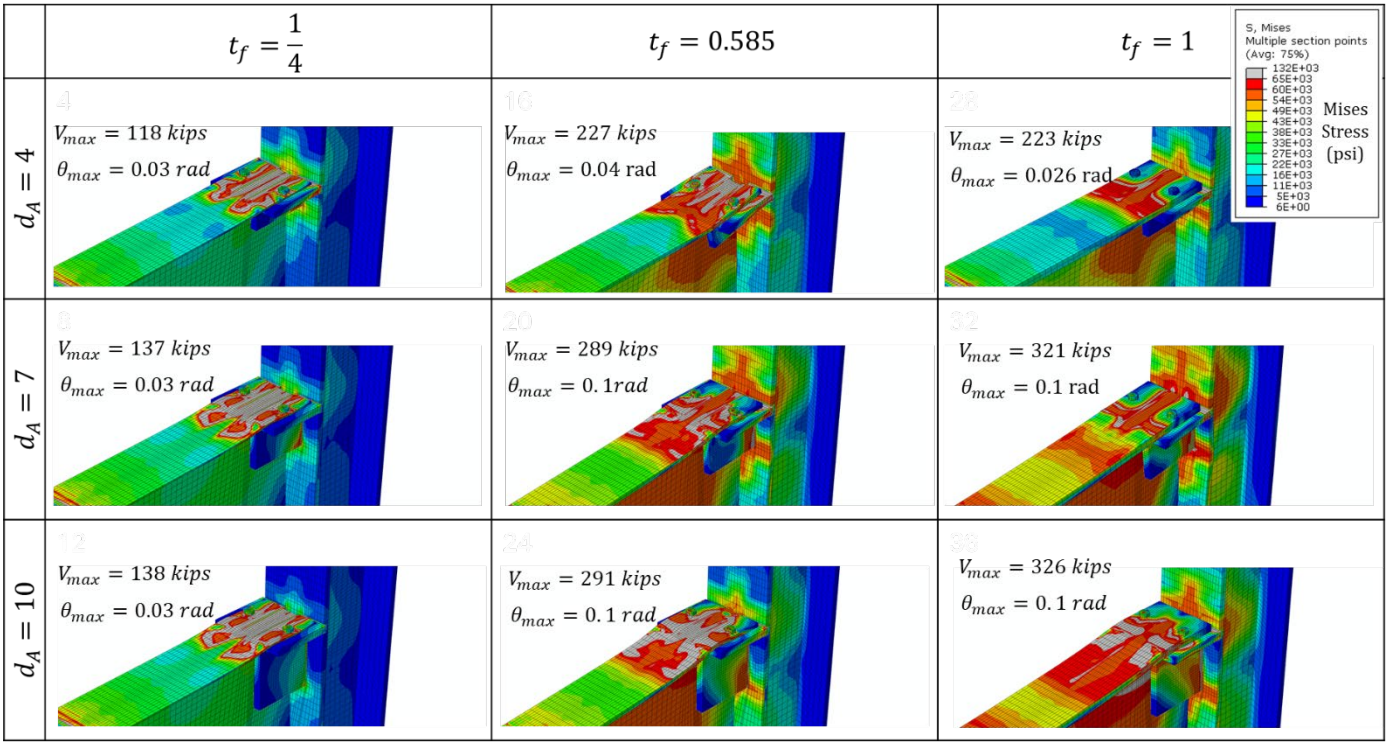

Figure 115: Maximum Shear and Von Mises Stress from Analysis II (tA=1, l_b=8, k1=100%, E_n=0)

Table 10 Total Length of Top Flange Plastic Zone (Yield Lines)

Flange Thickness (Inches)	Bearing Length (Inches)	Angle Size	Total Length of Top Flange Plastic Zone (Inches)
E_n = 0, k_1=100%			
0.585	5	L10×4×5/16	7.7
0.585	8	L10×4×5/16	10.4
0.585	5	L10×4×1	8.9
0.585	8	L10×4×1	14.1
5/16	8	L10×4×5/16	13.7
E_n = 5/16, k_1=100%			
5/16	8	L10×4×5/16	13.8
5/16	8	L10×4×1	13.8
E_n = 0, k_1=50%			
5/16	8	L10×4×5/16	15.0
0.585	5	L10×4×5/16	11.5
0.585	8	L10×4×5/16	13.8
0.585	5	L10×4×1	13.1
0.585	8	L10×4×1	14.6
E_n = 5/16, k_1=50%			
5/16	8	L10×4×5/16	14.6
5/16	8	L10×4×1	14.0
0.585	5	L10×4×5/16	8.4
0.585	8	L10×4×5/16	11.4
0.585	5	L10×4×1	12.7
0.585	8	L10×4×1	14.6

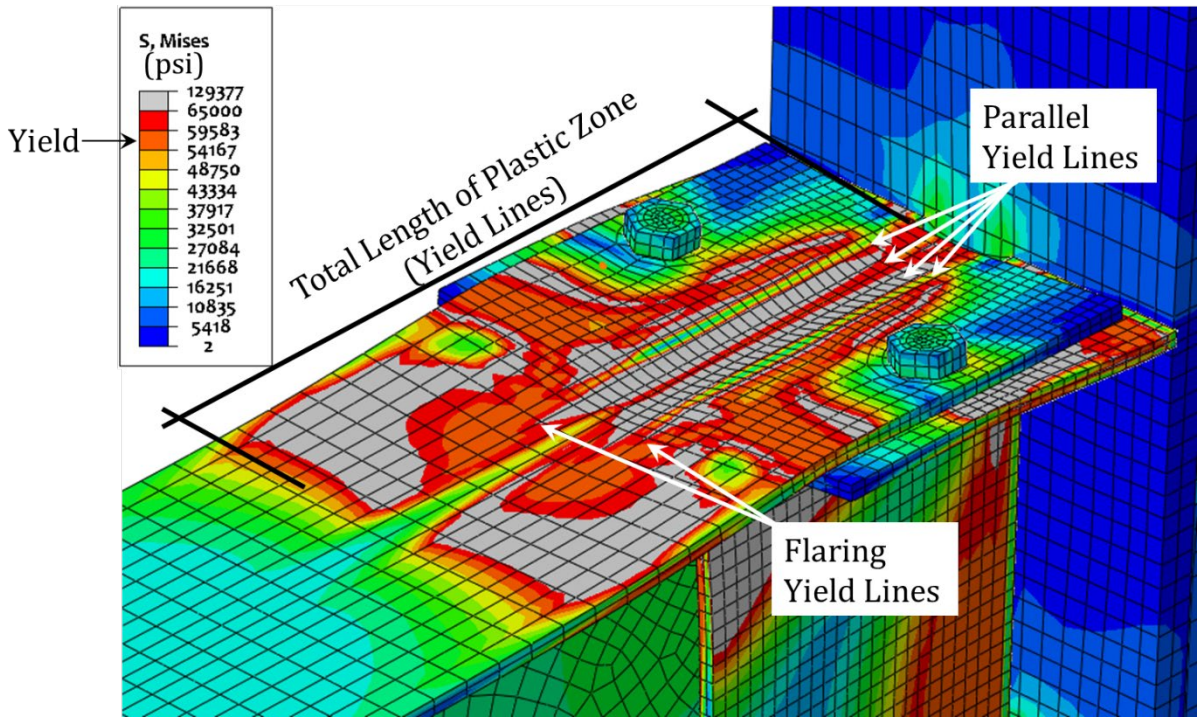

Figure 116 Yield Line Pattern and Measured Length of Plastic Zone (Yield Lines) (L10×4×5/16, l_b=8", and t_f=5/16")

Parametric Study Summary

In this subsection, a finite element modeling technique was validated against the results of Tests One and Five and used to conduct a parametric finite element analysis. The validation models reproduced the test results reasonably well in global and local connection behavior. The parametric study included 192 models that utilized various combinations of flange thickness, bearing length, angle depth, angle thickness, girder filet size, and angle encroachment into the girder filet. A loading protocol proposed by (Astaneh-Asl, Call et al. 1989, Astaneh 1989) was adopted to subject the connections of the parametric study to a realistic combination of shear and rotation.

The parametric study results indicate that flange bending, yielding or buckling of the vertical leg of the angles, and strength of the coped beam determine the connection's load-carrying capacity. The flange yield line pattern and dimensions were analyzed to aid in developing design guidelines later in Phase 4 – Design Guidance. Additionally, the connection strength corresponding to the above three limit states was quantified to aid in formulating design guidelines. The parametric study did not consider the weld limit state, as the weld was modeled with a tie constraint. Furthermore, most of the connection combinations were able to accommodate the rotational ductility demand set by the adopted loading protocol.

Stability Study

In addition to supporting vertical reactions, connections must also provide adequate lateral and torsional restraint to ensure the stability of the supported beam/girder. One form of instability is lateral torsional buckling (LTB). When designing for LTB, the connections are

expected to provide torsional restraint. AISC Spec F1 indicates that "*the points of support for beams and girders are restrained against rotation about their longitudinal axis*" (ANSI/AISC 2022). The support torsional stiffness can directly influence the LTB capacity (Bose 1982). To supplement Tests One and Five, which tested the stability of drop-in supported girders, linear elastic eigenvalue analysis was conducted and presented in this section. As LTB is particularly important when the minor axis moment of inertia (I_y) is significantly smaller than the major axis moment of inertia (I_x), a W30×90 section with a low I_y to I_x ratio was adopted for the eigenvalue analysis. Note that nonlinear large displacement analysis is typically performed with initial imperfections and residual stresses to capture the conservative critical buckling load. However, only eigenvalue buckling was utilized herein since the focus was on the relative comparison of support conditions.

When a beam is subjected to a concentrated load and the top flange is laterally restrained, sideway movement of the bottom flange has been experimentally observed in scenarios where the bottom flange is free (Summers and Yura 1982, Grondin and Cheng 1999). This mode of instability is termed as sidesway buckling. The AISC Specification (ANSI/AISC 2022)design approach for sidesway buckling, is based on the work from (Summers and Yura 1982). They attribute sidesway buckling to the presence of a critical compressive stress field in the web below the loading point and treat a portion of the web under the concentrated load as a column supported between the flanges. The braced top flange restrains lateral movement, while the unbraced bottom flange provides lateral resistance with some finite stiffness derived from out-of-plane bending of the bottom flange between the end supports. Summers and Yura's column model, along with the assumed triangular stress distribution, is illustrated in Figure 117. The spring stiffness k_b is the lateral bending stiffness of the bottom flange between the end restraints. The drop-in connection, which supports the top flange only, could appear susceptible to sidesway buckling. Thus, linear elastic eigenvalue analysis was conducted, and the resulting buckling loads were compared to the AISC nominal resistance values. For the analysis, a W30×90 section was used as it is among the W-sections with the most slender web and is vulnerable to sidesway buckling. The beam span used for the LTB and sidesway eigenvalue analysis was 30 feet. This span results in an elastic buckling mode.

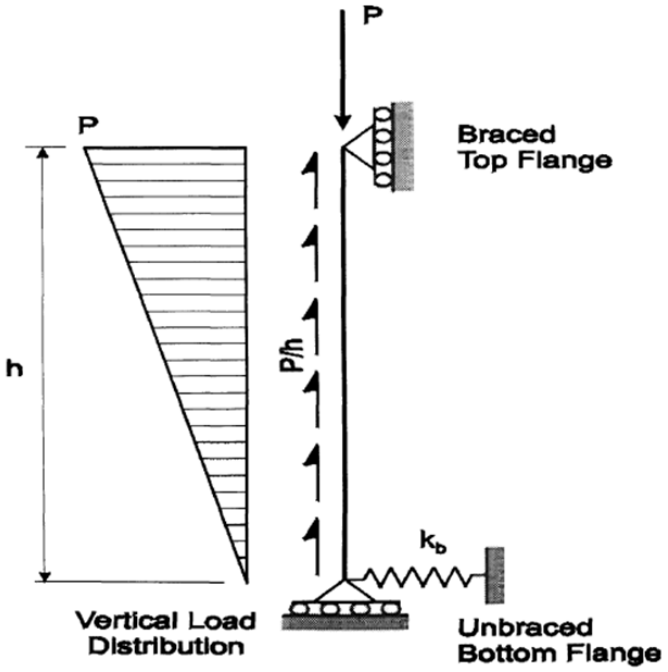

Figure 117: Column Model Used by Summers and Yura (Summers and Yura 1982)

Lateral Torsional Buckling Study

The linear eigenvalue analysis used the same modeling technique as the parametric study models. The stub columns were removed, and the full 30 feet W30×90 section was modeled using eight-node quadratic shell elements. A four-point bending load with no lateral restraints between the supports was applied. Before modeling the drop-in support, the eigenvalue results were validated by modeling an ideal torsionally pin end restraint under a constant moment and four-point bending. The end boundary condition was adopted from (Valeš and Stan 2017) and restricts translation in all three orthogonal directions and twisting about the longitudinal axis while permitting rotation in the other two orthogonal directions and warping. Movement in the longitudinal direction was permitted at one end to create a roller. The results of the validation models and the drop-in supported model are summarized in Table 11. The same section supported by a shear tab connection was also incorporated for comparison. The shear tab and drop-in connections were modeled by restraining the three translational degrees of freedom, as shown in Table 11. The drop-in had a three-inch bearing length, and the shear tab was 13" × 4.5". The shear tab was centered at the centroidal axis of the beam and covered more than half of the *T* dimension of the W30×90 beam, where *T* is as defined in Table 1-1 of the AISC Manual (AISC 2017).

Table 11: LTB Eigenvalue Analysis Results

Support Condition	Loading	First Buckling Mode Shape	Eigenvalue
Ideal-Pin-Roller	 Constant Moment	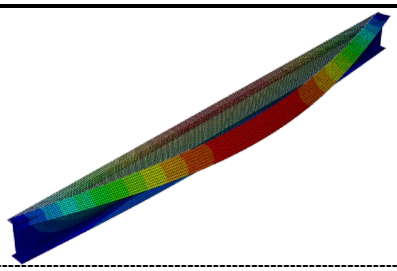	$0.99M_n$
Ideal-Pin-Roller	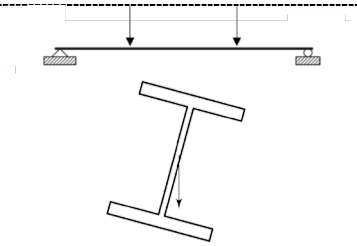 Four-Point Bending (Load at the Centroid)	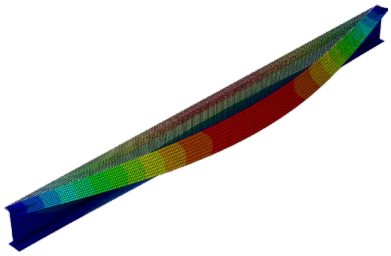	$1.04M_n$ (1)
Ideal-Pin-Roller	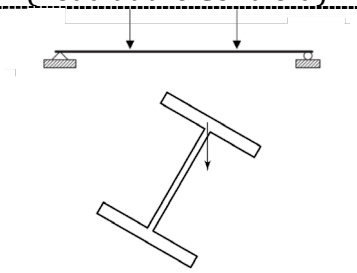 Four-Point Bending (Load at the Top)	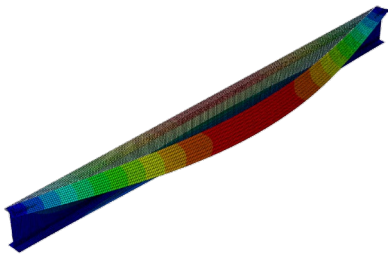	$0.73M_n$ (2)
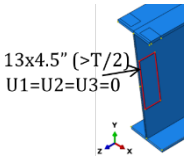 Shear Tab	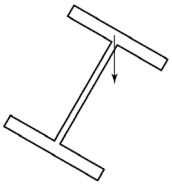 Four-Point Bending (Load at the Top)	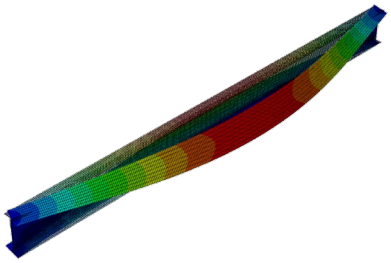	$0.96M_n$ (2)
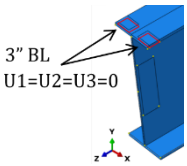 Drop-in	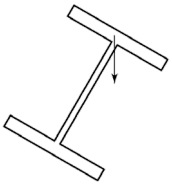 Four-Point Bending (Load at the Top)	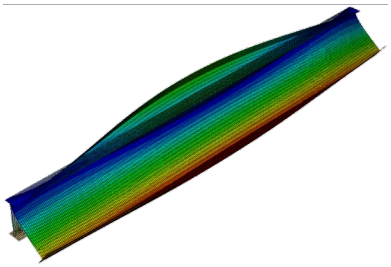	$1.66M_n$ (2)

(1) C_b=1.14

(2) C_b=1.14, no adjustment for load height effect.

Table 11 illustrates the first buckling mode shape and compares the nominal moment capacity of the beam (M_n) limited by LTB with the first mode eigenvalue. The first three cases compare ideal end conditions under constant moment and four-point bending. The four-point bending cases used a moment gradient modification factor C_b of 1.14. The theoretical LTB equation is based on loads applied at the centroid of the cross-section, and a smaller buckling load is expected for top loading due to a tipping effect. No adjustment factor for the load height effect was introduced in all cases with top loading. As shown in the table, the buckling moment from the eigenvalue analysis of the beam with ideal end condition is in good agreement with theoretical values. Moreover, the ***buckling moment of the drop-in supported beam was 73% higher than that of the shear tab-supported beam***. This is attributed to the added restraint by the drop-in connection on the compression flange. As can be seen from Table 11, the drop-in connection offers partial restraint against the out-of-plane rotation of the compression flange, unlike the other end conditions in the table. For compression flanges partially restrained against out-of-plane rotation (Way and Cosgrove , Gardner 2011) suggest an effective length factor of 0.85 when calculating the LTB critical moment.

Sidesway Buckling Study

The same finite element models were used to assess the performance of the drop-in connection under scenarios that lead to sidesway buckling. The compression flange of the 30-foot-long W30×90 was laterally restrained along the full length, and the tension flange was not restrained. The available strength of the web under a single concentrated load for the limit state of sidesway buckling was calculated per AISC Spec J10.4. The available strength R_n was calculated for cases where the compression flange is restrained against rotation, such as when connected to a slab, and when the compression flange is not restrained against rotation. The calculated strengths were compared with the eigenvalue analysis results under a three-point bending load. To rule out other limit states, such as web local crippling, the load was applied over a five-inch bearing length at mid-span. The results of the eigenvalue analysis are summarized in Table 12.

Table 12: Sidesway Eigenvalue Analysis Results

Support Condition	Compression Flange Restrained Against Rotation		Compression Flange Not Restrained Against Rotation	
	First Buckling Mode Shape	Eigenvalue	First Buckling Mode Shape	Eigenvalue
Ideal-Pin-Roller	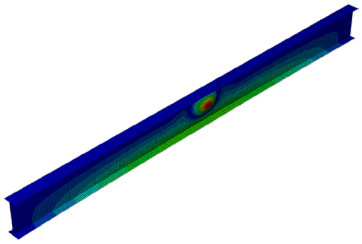	$2.34R_n$	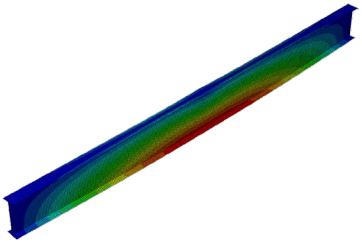	$0.69R_n$
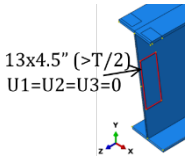 Shear Tab	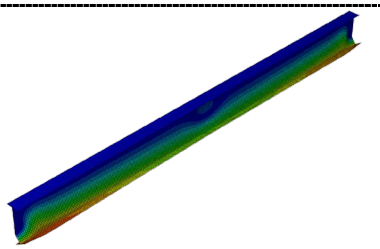	$1.93R_n$	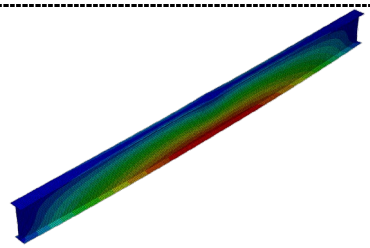	$1.10R_n$
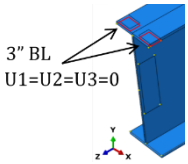 Drop-in	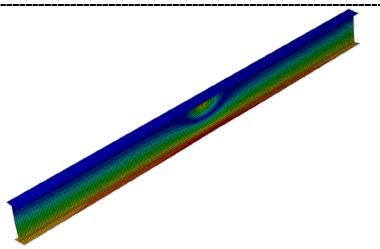	$3.06R_n$	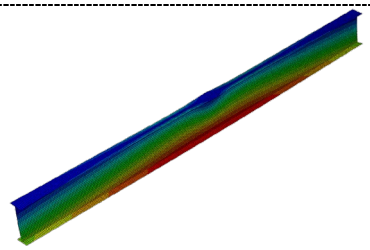	$2.58R_n$

The eigenvalue analysis results show that the ***sidesway buckling load of the drop-in supported beam is higher than that of the ideal pin-roller and shear tab supported beam***. Typical section views under the concentrated load and away from the load are shown in Figure 118 and are consistent with the test results by Summers and Yura (Summers and Yura 1982).

Note that a comprehensive study by Topkaya (Topkaya 2006) evaluated sidesway buckling for a larger variation in beam geometries with varying support conditions. He evaluated 200 cases where the bottom flange was not supported. In some cases, the sidesway buckling capacity was reduced when the bottom flange was not restrained. However, he stated, "*the excess capacity gained by restraining the bottom flange movement is not as high as expected*." He found that the maximum increase in sidesway buckling capacity was only 10% when the bottom flange was restrained at the support. As a result, the drop-in connection design guidance (provided in Phase 4) does not recommend a reduction in beam sidesway capacity. However, drop-in connections are not recommended when significant concentrated loads are near the connection until further research is performed.

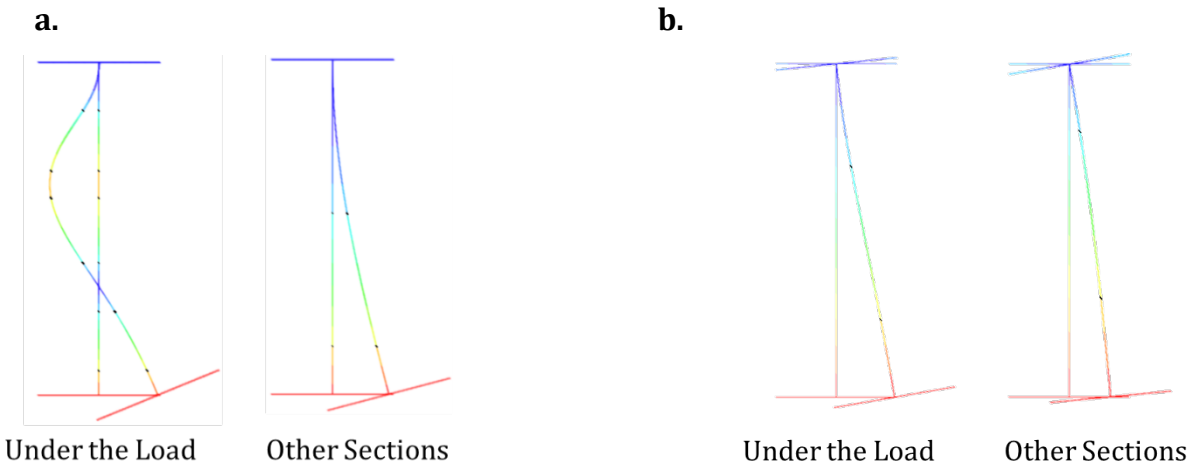

Figure 118: Typical Section View after Sidesway Buckling (a) Compression Flange Restrained Against Rotation (b) Compression Flange Not Restrained Against Rotation

Stability Study Summary

The performance of the drop-in connection under scenarios that can cause lateral torsional buckling and sidesway buckling was examined through linear elastic eigenvalue analysis of a 30-foot-long W30×90 under various end conditions. The 30-foot span was selected to achieve an elastic buckling load, and the section size was chosen for its high web depth-to-thickness ratio.

The LTB eigenvalue analysis was initially validated by examining the beam under constant moments and a four-point bending load with ideal pin-roller support conditions. The analysis results closely matched the theoretical buckling load. After validating the models, the ideal supports were substituted with a shear tab deeper than half the beam's T zone and a drop-in with a three-inch bearing length. The finite element results indicate that the drop-in supported beam had a 73% higher LTB load. This increased LTB capacity is attributed to the out-of-plane restraint the drop-in connection provides to the compression flange.

In the second set of eigenvalue analyses, the compression flange was laterally restrained to prevent lateral-torsional buckling, while the beam was subjected to a three-point bending load. Scenarios in which the compression flange is restrained against rotation, such as when a slab is present and those where the compression flange is free, were analyzed. In both scenarios, the drop-in supported beam exhibited a higher sidesway buckling load.

Phase 4 – Design Guidance

Purpose and Approach

The final phase was to coalesce all the experimental and numerical FEA data to determine final design guidance regarding drop-in top flange connections (not extended). This design guidance was created in three main ways, which include:

1. Design methodology (see below)
2. Design tables (Appendix D and E)
3. Design examples (Appendix F)

Design Methodology

The design methodology below applies to drop-in top flange connections for girder-column, beam-column, and steel-concrete wall connections. For the design of these connections, there are two main areas of focus. The first is the dimensional limitations for adequate erection. Limits are also provided due to the scope of the research. The second area of focus is the design checks for sufficient strength and ductility of the connection.

Dimensional Limitations

There are two categories of dimensional limits provided herein. The first is geometric compatibility, which facilitates the erection of the drop-in top flange connection. The second set of limits is due to the scope of dimensions studied.

Compatibility

Four main geometric constraint locations must be considered to erect drop-in top flange connections. This includes:

1. Minimum flange edge distance for the bolt (see AISC Spec. J3.4 and J3.5)
2. Minimum angle horizontal edge distance for the bolt (see AISC Spec. J3.4 and J3.5)
3. Entering and tightening (E&T) clearance for bolt installation adjacent to the vertical leg of the angle (see AISC Manual Table 7-15).
4. Horizontal proximity of the angle to the beam. The recommended horizontal position of the angle is to have the back corner at the toe of the beam fillet. However, encroachment can be applied (see AISC Manual Figure 10-3).

Figure 119 graphically illustrates the geometric constraints. ***Appendix D*** provides detailed equations for the calculation of the geometric constraints, along with providing AISC criteria references. In addition, ***Appendix D*** provides tables for compatible angles with common wide flange sections.

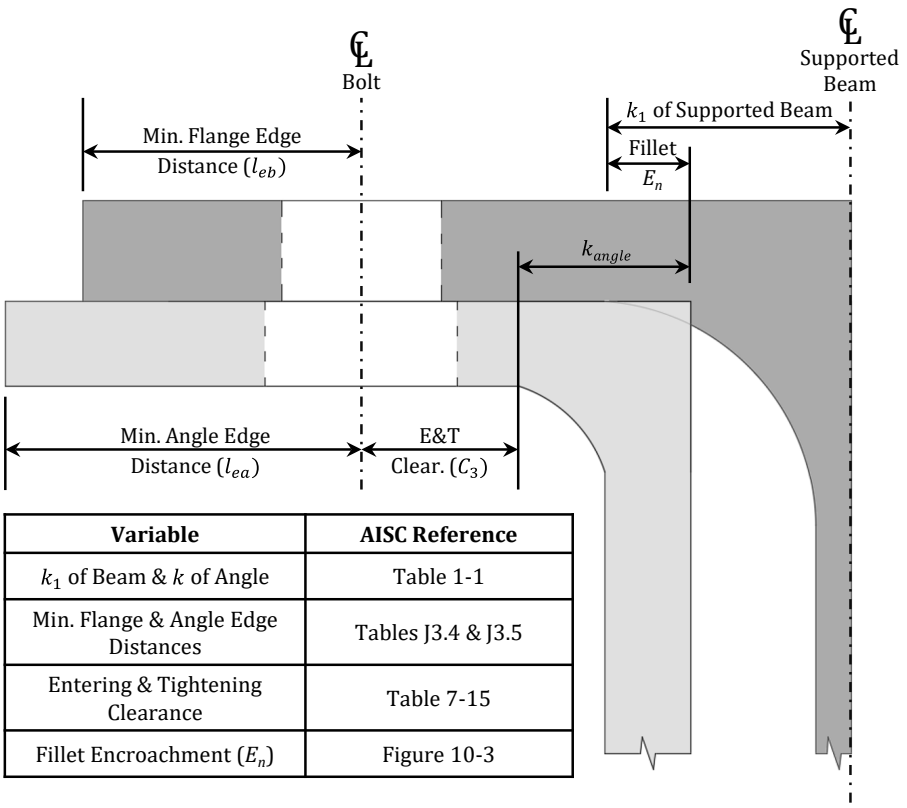

Variable	AISC Reference
k_1 of Beam & k of Angle	Table 1-1
Min. Flange & Angle Edge Distances	Tables J3.4 & J3.5
Entering & Tightening Clearance	Table 7-15
Fillet Encroachment (E_n)	Figure 10-3

Figure 119: Drop-In Connection Geometric Constraints

Scope Limits

The following dimensional limits are provided due to the scope of this study.

- Maximum flange thickness of 1.0 inches
- Maximum girder depth of 30 inches
- Minimum bearing length of 3.0 inches
- Maximum bearing length of 8.0 inches
- One row of bolts (two total)

Design Checks

This section provides the design checks for drop-in top flange connections. Four primary limit states must be evaluated. This includes the capacity of the (1) weld group, (2) flange bending, (3) angle shear, and (4) girder/beam shear. There are additional limit states/provisions that should be considered for the design. These are discussed at the end of this sub-section. Finally, a comparison of the design equations with the experiments and FEA results is provided.

(1) Weld Limit State

The design of the welds for attachment of the angles to the column (or an embed plate) should be in accordance with AISC Spec J2 and AISC Manual Part 8. The weld group is eccentrically loaded, which must be considered. It is recommended to utilize the instantaneous center of rotation method (as outlined in AISC Manual Part 8).

Providing fillet welds along the top and bottom edges of the angle's horizontal legs is recommended. In addition, a single-sided fillet weld is to be provided along the outside edge of the angle's vertical legs. Single-sided fillet welds are typically not recommended. However, extensive experimental testing verified the use of symmetric single-sided fillet welds in this application. Figure 120 illustrates the recommended fillet weld group for drop-in top flange connections.

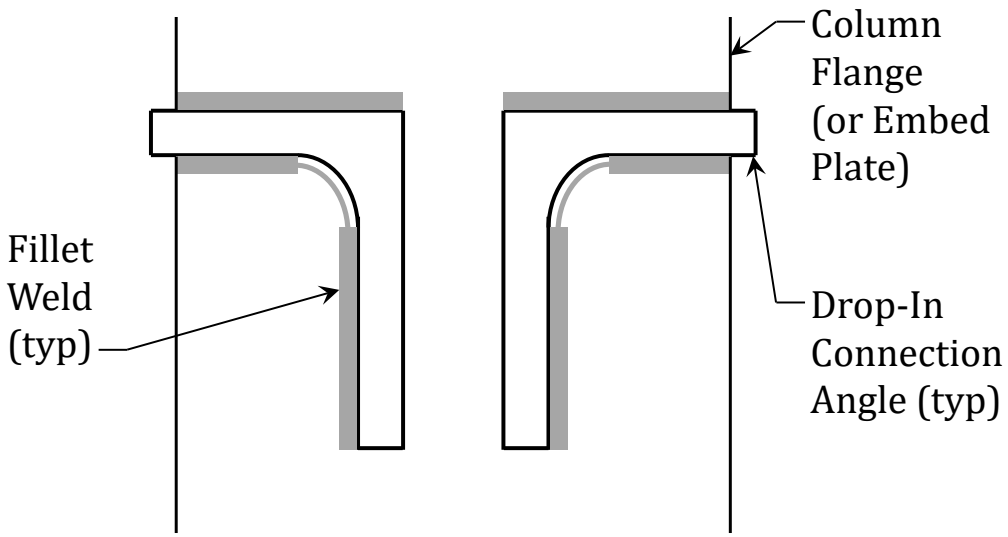

Figure 120: Recommended Fillet Weld Group

Additional design recommendations include:

- The girder/beam reaction eccentricity (e_x in AISC Manual Figure 8-5b) for designing the weld group should be placed at the center of the bolts. This is illustrated in Figure 121.
- The fillet welds should be limited to 5/16" in size where possible to minimize the number of weld passes. A deeper angle may be provided for adequate weld lengths.
- Fillet welds could be provided on the inside of the angle's vertical legs. However, access is only sufficient for short angles (in the direction of the girder/beam) with adequate angle-to-angle spacing.

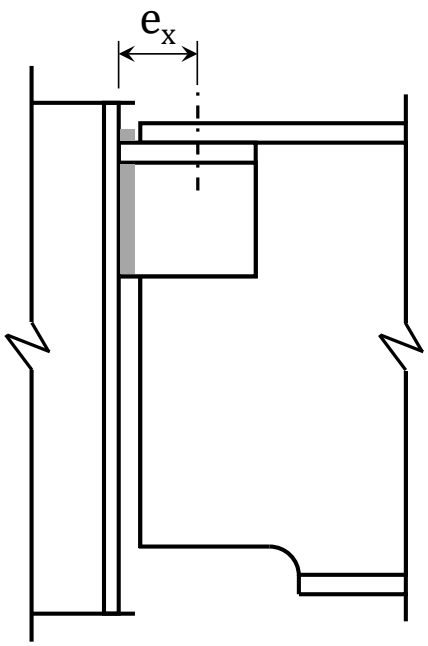

Figure 121: Recommended Fillet Weld Group Eccentricity (e_x)

(2) Flange Bending Limit State

The bending of the girder/beam top flange is the primary limit state for drop-in top flange connections. Figure 122 illustrates the flange bending failure mode.

Figure 122: Flange Bending Illustration

A new design approach for flange bending was developed as part of this study due to the unique nature of this limit state. Yield line analysis was the methodology utilized to simplify a complex failure mode into expressions appropriate for routine design. This approach has been utilized in the design of many steel connections (Kapp 1974, Stockwell Jr 1974, Dranger 1977).

Energy methods applied to yield line analysis develop a solution by equating the work required to achieve plastic deformation (internal work) to the work performed by moving the load through the distance compatible with the deformation (external work). The deformation of the connected material is assumed to occur by bending on idealized yield line patterns, which permits movement of the load in a collapse mechanism. The result is an upper bound magnitude of the load. Therefore, a critical aspect of yield line analysis is the assumed yield line pattern. For this drop-in top flange connection study, a significant effort was placed on the top flange yield lines through experimental testing (using DIC) and FEA.

The drop-in connection top flange yield lines typically occur as those illustrated in Figure 123. Two longitudinal yield lines develop on each side of the web. These yield lines stay parallel to the web until after the angle support. At this point, the yield lines "fan out" and terminate at the edge of the flange.

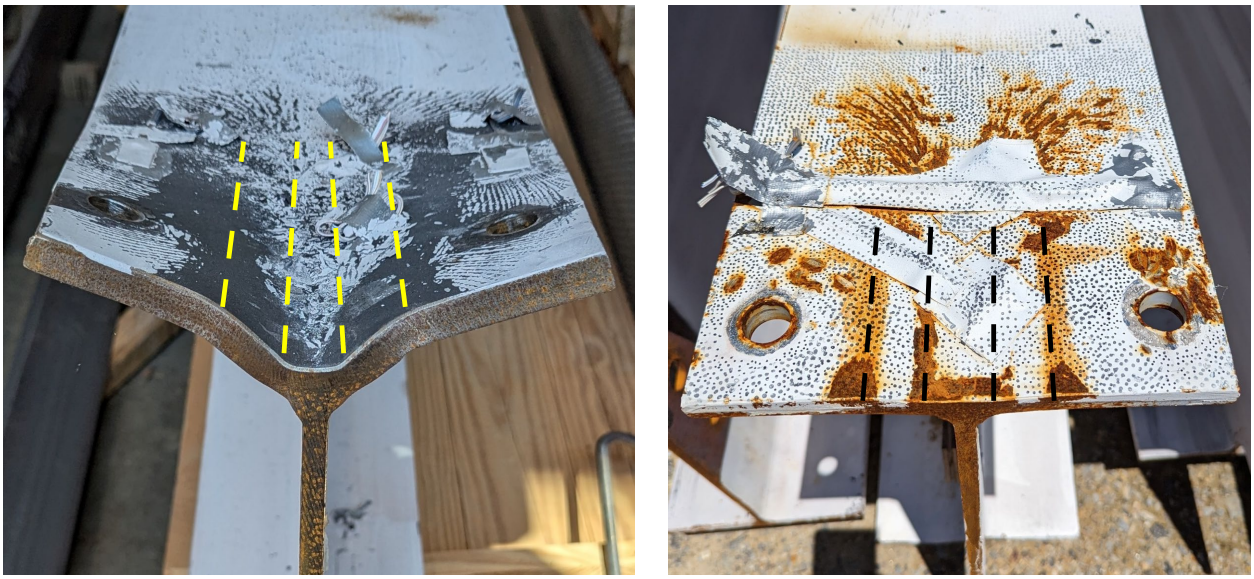

Figure 123: Flange Bending Examples from Experimental Testing with the Yield Lines Highlighted

The experimental and FEA yield lines were synthesized to develop a repetitive pattern. The lateral position of these yield lines occurs near the edge of the angle and slightly inside the fillet. Figure 124 illustrates these locations. An important parameter is the distance between the pairs of yield lines (a). As concluded earlier in the Phase 2 summary (Figure 100) this distance can be estimated as 75% of k_1 for the girder/beam. The FEA work supports this as a reasonable estimate. This is also conservative to account for fillets manufactured below the upper bound dimensions of k_1 provided in the AISC Manual (as was the case for the beams used in the testing phase). Note that if encroachment (E_n) is utilized for detailing the

connection, the distance between yield lines can be reduced (increasing the flange bending capacity)[3]. The resulting expression for a is provided in Eq. 4-1.

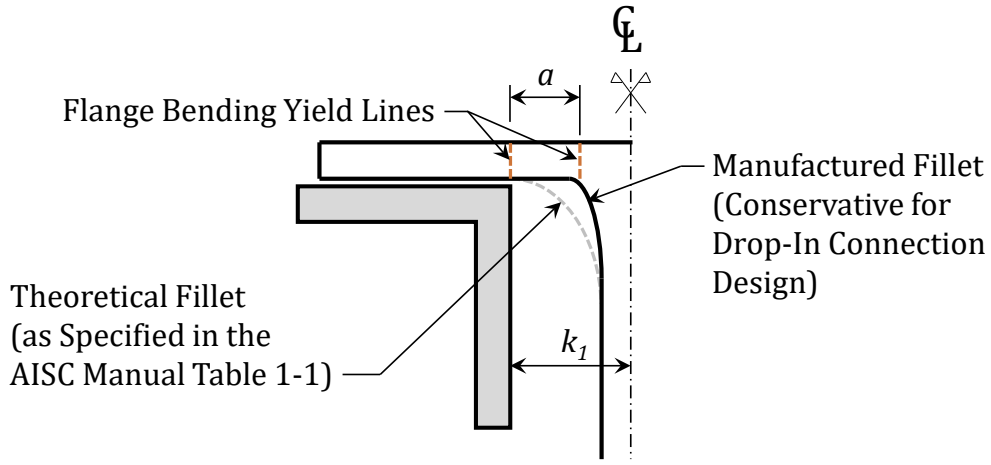

Figure 124: Flange Bending Yield Lines Transverse Spacing (no Encroachment)

$$a = 0.75k_1 - E_n \tag{4-1}$$

To simplify the yield line analysis and the resulting design equations, the top flange was analyzed as a plate with a finite length (b) and constant flange thickness (t_f). This is considered conservative since it neglects the increased thickness at the fillet (for the yield lines near the web) and mostly neglects the continuity of one side of the flange. The critical decision for this analysis was the longitudinal dimension (b) of this flange "plate" region. Figure 125 graphically illustrates this dimension and the yield line pattern.

[3] *Encroachment (E_n) is positive when the angle is encroaching (or riding) on the theoretical fillet. Figure 119 illustrates positive encroachment.*

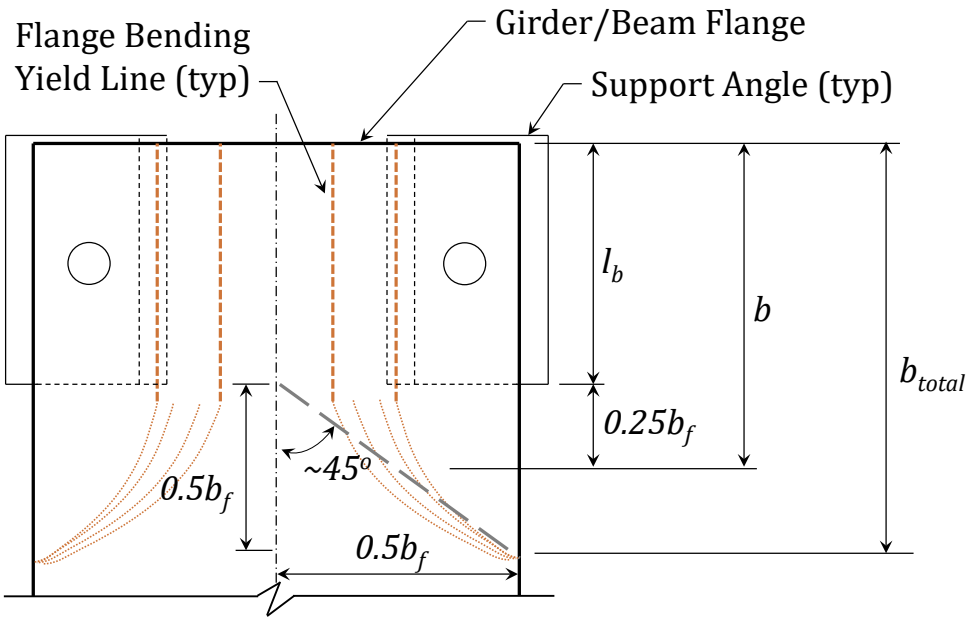

Figure 125: Flange Bending Yield Line Pattern (Top View)

To establish this dimension (b) the trend of yield lines was observed (experimental and FEA). In general, the yield lines follow an angle of 45 degrees from the centerline of the girder/beam (illustrated in Figure 125). The length from the end of the girder/beam to the extreme limit of the yield lines was defined as b_{total}. As a result, parameter b was estimated as the average between the bearing length (l_b) and b_{total}, which results in Eq. 4-2.

$$b = l_b + 0.25b_f \tag{4-2}$$

The yield line analysis was performed by treating the top flange as a simply supported plate with the yield lines as shown in Figure 126. To calculate the external work (W_E) a small virtual unit displacement is imposed (Δ=1). The work is equal to the product of the total load and distance through which the load moves, as shown in Eq. 4-3. In this case, a line load (w_u) is approximated for the load application, which comes from the web pulling down on the girder/beam at the support. Note that the resultant force is the connection reaction for flange bending (R_{nFB}), which is shown in Eq. 4-4. Therefore, in this case, W_E is equal to R_{nFB}.

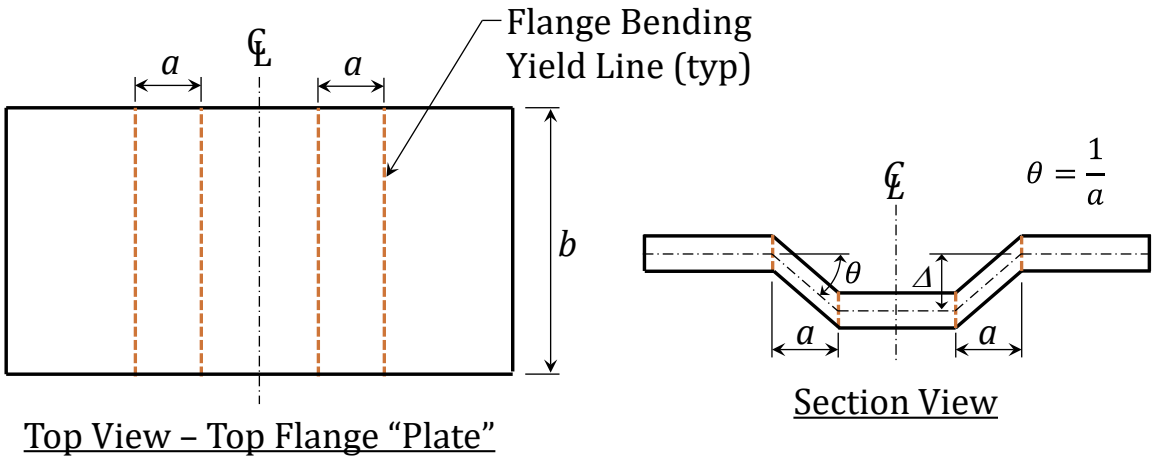

Figure 126: Yield Line Analysis Diagrams

$$W_E = (w_u b)\Delta \tag{4-3}$$

$$R_{nFB} = w_u b \tag{4-4}$$

The internal work done from the assigned virtual displacement is found by summing the products of the yield moments per unit length of hinge times the plastic rotation at the respective yield lines (consistent with the virtual displacement). The internal work (W_I) can then be calculated as shown in Eq. 4-5 where the 4 multiplier represents the number of yield lines and the plastic rotation (θ) is defined in Figure 126. In this expression, M_p represents the plastic moment capacity of the flange, per unit length. Eq. 4-6 provides this calculation where t_f is the flange thickness and F_{yf} is the yield strength of the steel flange.

$$W_I = 4[M_p \theta b] = 4M_p \frac{b}{a} \tag{4-5}$$

$$M_p = \frac{{t_f}^2}{4} F_{yf} \tag{4-6}$$

Substituting Eq. 4-6 into Eq. 4-5 and equating the internal and external work produces an expression that is shown in Eq. 4-7. This equation provides a relatively simple approach to quantify the flange bending capacity of drop-in top flange connection (R_{nFB}). A resistance factor (ϕ) value of 0.90 and a safety factor (Ω) value of 1.67 are recommended for design and consistency with related limit states.

$$R_{nFB} = \frac{{t_f}^2}{a} F_{yf} b \tag{4-7}$$

(3) Angle Shear Limit State

The shear capacity of the angles for drop-in top flange connections ($\phi_v R_{nAV}$ or R_{nAV}/Ω) should be designed in accordance with AISC Spec G3. The experimental testing and FEA support this criterion. The experimental testing found that angle shear failure was relatively ductile.

For the calculation of the angle's shear capacity, equal load sharing between the two angles can be assumed. The result is the connection angle shear capacity shown in Eq. 4-8, where the 2 multiplier represents the number of angles. The height (b) and thickness (t) are illustrated in Figure 127. The variable C_{v2} accounts for the shear buckling of relatively slender elements and is defined in AISC Spec G2.2. A resistance factor (ϕ_v) value of 0.90 and safety factor (Ω) value of 1.67 are recommended as per AISC Spec G1.

$$R_{nAV} = 2(0.6F_y btC_{v2}) \tag{4-8}$$

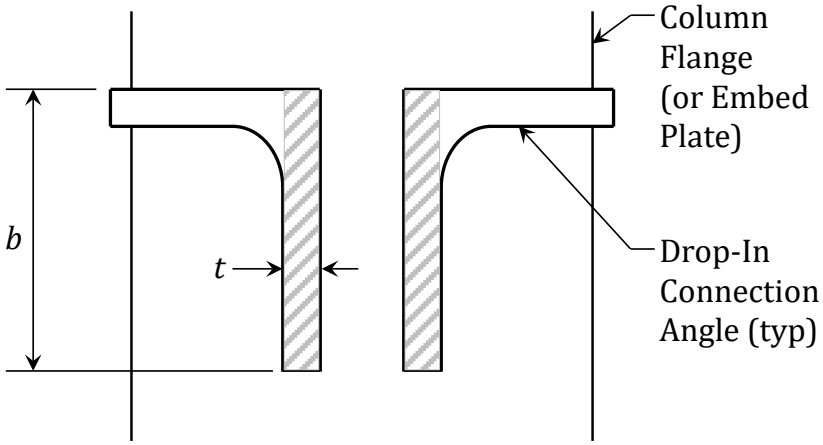

Figure 127: Angle Shear Areas and Dimensions

(4) Girder/Beam Shear Limit State

The shear capacity of the girder/beam ($\phi_v R_{nBV}$ or R_{nBV}/Ω)) should be evaluated according to AISC Spec G. The FEA found shear stresses still develop through the depth of the web despite the reaction from the connection being applied to the bottom surface of the top flange. However, the bottom flange is coped where a portion of the web is removed. The coped bottom region has shown to be a relatively low-stress region. Nevertheless, it is conservatively recommended that the area of the web should be reduced accordingly. Utilizing this assumption with AISC Spec G2 produces Eq. 4-8. A resistance factor (ϕ_v) value of 0.90 and safety factor (Ω) value of 1.67 are recommended as per AISC Spec G1. Figure 128 illustrates several of the geometric parameters. The variable C_{v1} accounts for the shear buckling of relatively slender webs and is defined in AISC Spec G2.

$$R_{nBV} = 0.6F_y h_c t_w C_{v1} \tag{4-8}$$

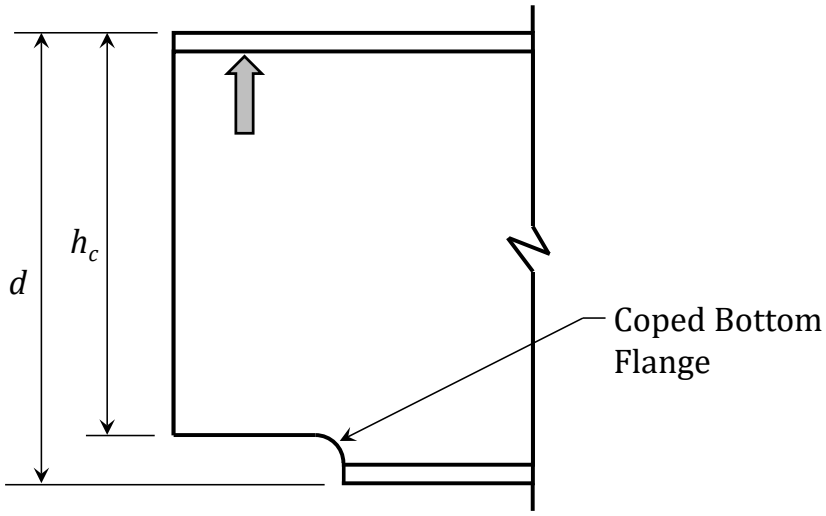

Figure 128: Angle Shear Areas and Dimensions

Note that AISC Manual Part 9 addresses cope beam strength. However, the configurations are different than those of drop-in top flange connections.

Additional Limit States/Provisions to Consider

The following may be considered when designing drop-in top flange connections.

- Sidesway Buckling: Web sidesway buckling should be considered for girders/beams subjected to significant concentrated forces. The literature (Topkaya 2006) and FEA for this study indicate a top flange connection has a relatively small reduction in the sideway buckling capacity compared to other common shear connections (e.g., shear tab). The literature also suggests the provisions in AISC Spec J10.4 (Summers and Yura 1982) are relatively conservative (Grondin and Cheng 1999). As a result, for drop-in top flange connections, AISC Spec J10.4 is recommended. However, for significant concentrated forces near the support (within a distance of twice the depth), drop-in top flange connections are not recommended since this has not yet been studied.

- Lateral-Torsional Buckling (LTB): The girder/beam LTB capacity is increased if sufficient restraint is provided to the top flange at the supports (Gardner 2011). Essentially the effective length of the top flange is reduced due to the out-of-plane flange restraint. The FEA for this study supports this behavior.

- Structural Integrity: When designing for structural integrity, the provisions in AISC Spec B3.9 should be applied. For these situations, bolt shear may control the design for drop-in top flange connections since the tensile demand on the connection is two-thirds the required shear strength. The shear capacity of the bolts should be in accordance with AISC Spec J3. Larger diameter bolts may be required or higher-grade bolts (if geometric compatibility is an issue). The tensile capacity of the angles should be in accordance with J4, but will likely not control. The design example provided in Appendix F includes the structural integrity calculations.

- Bolt Capacity: The tensile capacity of the bolts should be considered in the connection design, including prying action. The design example provided in Appendix F includes these calculations. Note that the bolt tensile capacity did not control for any of the connections tested in this study.

- Column Web Capacity: The capacity of the column web should typically not be an issue for drop-in top flange connections; however, it should be considered during design. This is particularly the case for relatively thin webs of edge columns (beam only on one side). Local stiffening may be required for these cases. The experimental beam-column showed deformation of the edge column web but at loads well above the connection design capacity. Interior columns with beams on both sides should not have column web capacity issues.

- Column Flange Capacity: The capacity of the column flange should typically not be an issue for drop-in top flange connections. Nevertheless, it should be considered during design. This is particularly the case for relatively thin column flanges. Note that no column flange bending was observed during the experimental or numerical studies conducted herein. However, the column flange thickness was not varied.

Design Methodology Comparison with Research Results

The design equation capacities presented in the prior section were compared with the ***experimental results***. Table 13 provides a quantitative summary. The connections and their primary failure modes are provided on the left side of the table. The maximum shear force (or reaction) from the experiment (Exp) is provided. Then all four of the primary limit states presented in the prior section are presented. The far-right column provides a ratio of the controlling design equation (DE) to the experiment. A ratio below 1.0 is conservative.

Table 13: Experimental Results Compared to the Design Equations

Conn.	Failure Mode from Testing	Max Shear: Exp	R_{nW}	R_{nFB}	R_{nAV}	R_{nBV}	$\frac{DE}{Exp}$
A&B	Girder/Flange	141	DNC	129	396	303	0.91 [1]
C	Flange	129	181	93	396	303	0.71 [1]
D	Weld	129	88	129	131	303	0.6
E	Girder/Flange	150	132	129	269	303	0.86 [1]
G	Girder	84	116	91	131	143	1.08 [1]
I	Angles	147	173	129	131	303	0.88
J	Angles/Flange	134	172	93	132	303	0.70
K	Angles/Web	124	173	129	131	303	1.04 [2]
L	Angles/Flange/Web	124	174	129	132	303	1.04 [2]

Notes:
- *DNC = did not control (more than sufficient capacity provided)*
- *Connection F not shown since it was a shear tab*
- *Connection H not shown since it was flipped angles*
- *Units are in kips*

[1] Tests where the connection did not fail first

[2] Beam-column one-sided connections (web yielding not accounted for in the calculations)

Overall, the design equations illustrate conservative, yet reasonable results. The main takeaways include the following:

- Connections A, B, C, and E had flange bending as the primary mode of failure from the testing. The DE/Exp ratios ranged from 0.71 to 0.91. This indicates the design equations are adequately predicting the capacity. In addition, flange bending provided adequate rotational ductility of the connection in all these cases.

- Connection D the weld controlled, but the DE/Exp ratio was only 0.68. This indicates there was more than sufficient shear capacity. However, the ductility was not sufficient.

- Connections I, J, K, and L had the angles shear capacity as the primary mode of failure from the testing. The DE/Exp ratios varied from 0.70 to 1.04. These results are reasonable and indicate the angle shear capacity equation is sufficient. The ratio of 1.04 for Connections K and L can be attributed to the fact that column web yielding was not accounted for in the calculations.

- Connection G did not get tested to the full capacity because the girder failed. As a result, the DE/Exp ratio is 1.08 which is not a true comparison of the connection capacity. Nevertheless, the ratio is only slightly above 1.0.

The design equations were also compared with the ***FEA results*** (from Phase 3). The FEA methodology was validated with experimental testing. Then a parametric study was performed, which varied the flange thickness, angle depth, angle thickness, bearing length, girder fillet (50% and 100% of k_1), and angle spacing. The weld was not explicitly modeled. However, only the nodes along the angle weld locations were rigidly connected to the column. In total 108 models converged and were utilized for the design equation comparison[4]. Refer to the Phase 3 section of the report for the full details.

Overall, the design equation predicted shear capacities were predominantly conservative in comparison to the FEA results. Figure 129 provides a histogram of the ratios of the predicted design equations to the FEA results. These ratios have a wide range from 0.23 to 1.17 with an average of 0.75. The range of ratios is partly due to the extreme geometric variations in the parametric study. For example, scenarios with slender flanges were included (to cover plate girders). For these cases, the flange bending equation is very conservative. Also, the design equations better align with a girder/beam with 50% of the k_1 value provided in the AISC Manual. This was intentional so the design equations were conservative since the k_1 value in the Manual is an upper bound for detailing. When the slender flange and 100% k1 girder/beams cases are removed the range of ratios reduces to 0.48 to 1.17 with an average of 0.82.

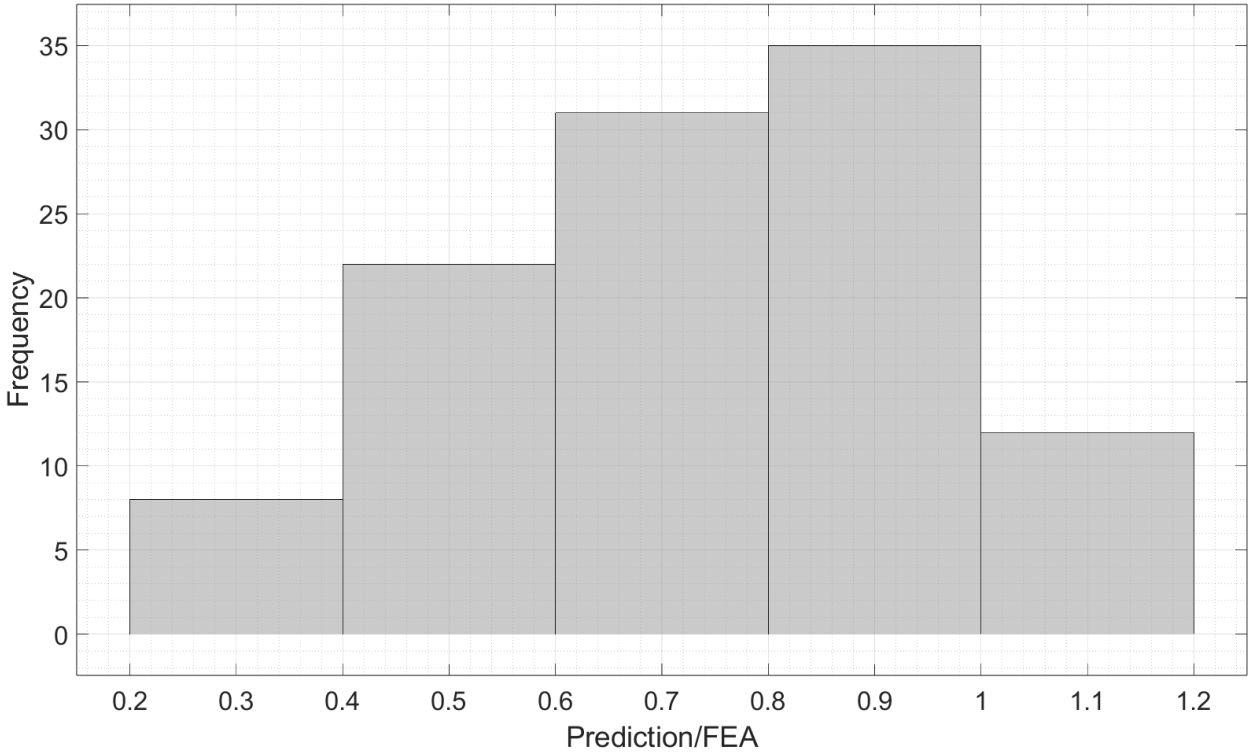

Figure 129: Histogram of the Predicted Shear Capacity from the Design Equations versus All the FEA Results

[4] *Some of the finite element models did not converge due to meshing and other modeling challenges. Since more than sufficient data was present those models were discarded instead of being revised.*

Figure 130 provides a graphical comparison of the predicted connection shear capacity from the design equations versus the FEA results. The main limit states are separated for better interpretation of the results. In addition, a dashed line is included with a slope of 1.0 to show where the design equations were conservative (lower right region) versus unconservative (upper left region). As mentioned above, the flange bending equations are conservative for slender flanges and when there is a large fillet (100% k_1). However, for typical flanges and fillets, the equations are conservative yet reasonable.

The cases where angle shear controls were mostly conservative, with a sub-set of cases having ratios above 1.0 (maximum of 1.17). Similar to flange bending, these were relatively extreme angle geometries (shallow depth and thick) for the girder size. The angles were 4 inches deep and 1.0 inch thick. No modification to the shear design equations (using AISC Spec G3) is recommended for this reason. Note that in a few cases, beam shear was controlled because the parametric study did not vary the web thickness. As a result, beam shear governed for cases with sizable flanges and angles.

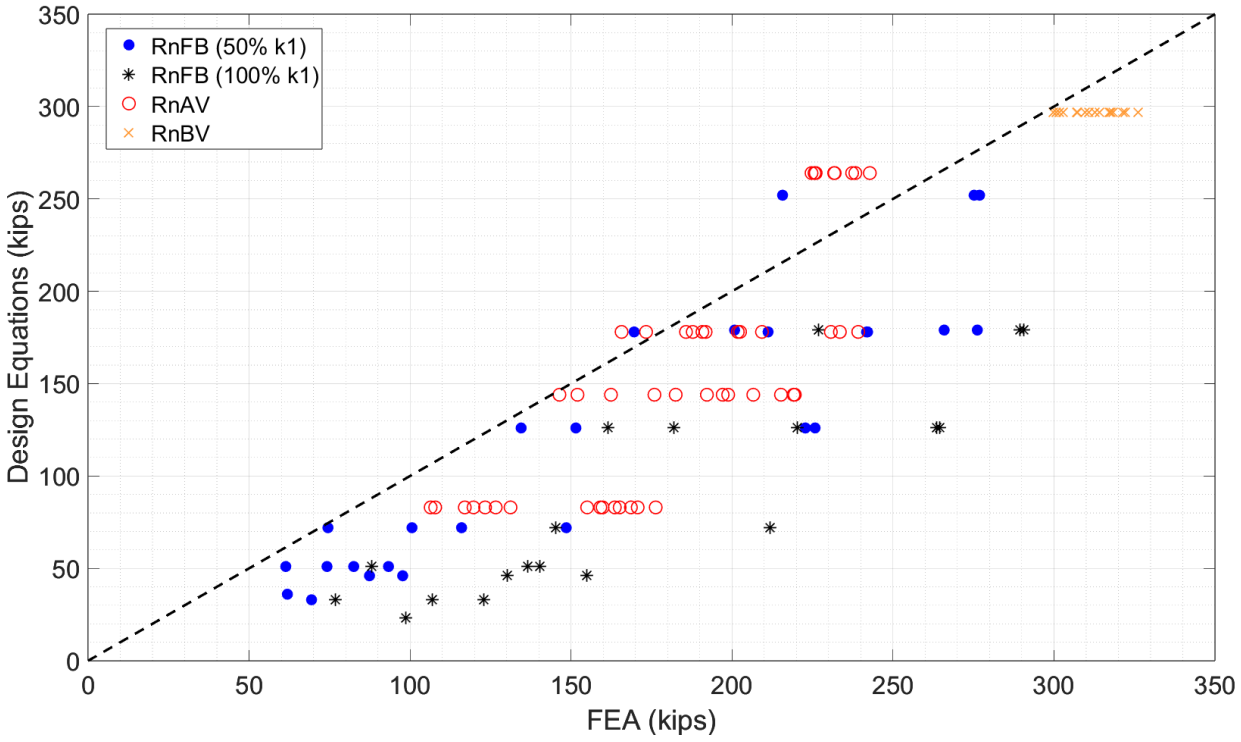

Figure 130: FEA Results Compared to the Design Equations

Design Summary and Tables

The design of drop-in top flange connections requires meeting the dimensional limits provided along with providing sufficient strength and ductility. The dimensional limits are summarized in Figure 119. ***Appendix D*** provides tables for compatible angles with common wide flange sections. Figure 131 illustrates an example compatibility table.

7/8-in. Bolts
W21x55
W21x48

Table 10-D
Drop-In Connection
Compatible Angles

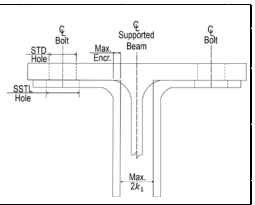

L8X8X7/8*	L7X4X3/4	L5X5X7/8*	L4X4X3/4
L8X8X3/4*	L7X4X5/8	L5X5X3/4	L4X4X5/8
L8X8X5/8	L7X4X1/2	L5X5X5/8	L4X4X1/2
L8X8X9/16	L7X4X7/16	L5X5X1/2	L4X4X7/16
L8X8X1/2	L7X4X3/8	L5X5X7/16	L4X4X3/8
L8X6X1*	L6X6X1*	L5X5X3/8	L4X4X5/16
L8X6X7/8*	L6X6X7/8*	L5X5X5/16	L4X4X1/4
L8X6X3/4	L6X6X3/4	L5X3-1/2X3/4	L4X3-1/2X1/2
L8X6X5/8	L6X6X5/8	L5X3-1/2X5/8	L4X3-1/2X3/8
L8X6X9/16	L6X6X9/16	L5X3-1/2X1/2	L4X3-1/2X5/16
L8X6X1/2	L6X6X1/2	L5X3-1/2X3/8	L4X3-1/2X1/4
L8X6X7/16	L6X6X7/16	L5X3-1/2X5/16	L4X3X1/2
L8X4X1*	L6X6X3/8	L5X3-1/2X1/4	L4X3X3/8
L8X4X7/8*	L6X6X5/16	L5X3X7/16	L4X3X5/16
L8X4X3/4	L6X4X7/8*	L5X3X3/8	L4X3X1/4
L8X4X5/8	L6X4X3/4	L5X3X5/16	L3-1/2X3-1/2X1/2
L8X4X9/16	L6X4X5/8	L5X3X1/4	L3-1/2X3-1/2X7/16
L8X4X1/2	L6X4X9/16		L3-1/2X3-1/2X3/8
L8X4X7/16	L6X4X1/2		L3-1/2X3-1/2X5/16
	L6X4X7/16		L3-1/2X3-1/2X1/4
	L6X4X3/8		L3-1/2X3X1/2
	L6X4X5/16		L3-1/2X3X7/16
	L6X3-1/2X1/2		L3-1/2X3X3/8
	L6X3-1/2X3/8		L3-1/2X3X5/16
	L6X3-1/2X5/16		L3-1/2X3X1/4
			L3X3X1/2
			L3X3X7/16
			L3X3X3/8
			L3X3X5/16
			L3X3X1/4
			L3X3X3/16

Notes:
STD = Standard holes
SSTL = Short-slotted holes transverse to longitudinal beam axis
* = angle must encroach on beam fillet

Figure 131: Example Drop-In Connection Compatible Angles Table from Appendix D

Adequate strength and ductility for typical drop-in connections (not extended or with substantial concentrated loads near the support) can be achieved through the following.

1. Weld group available strength should be checked in accordance with AISC Spec J2 and Manual Part 8.
2. Flange bending available strength should be checked in accordance with Eq. 4-7 above.
3. Angle shear available strength should be checked in accordance with AISC Spec G3.

4. Supported member shear capacity should be checked in accordance with AISC Spec G, accounting for the coped flange.
5. Bolt available strength must be in accordance with AISC Spec J3 and Manual Part 7.
6. Weld and angle shear must not control the design to ensure rotational ductility.
7. In all cases, the available strength, ϕR_n or R_n/Ω, must equal or exceed the required strength, R_r.

Appendix E provides a drop-in connection design table along with the front matter typically provided in the AISC Manual. Figure 132 provides the table as well.

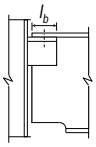

Table 10-E
Drop-In Connetions

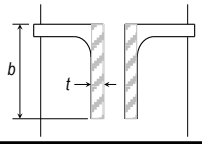

Flange Bending Available Strength, kips

Shape	l_b = 4 in		l_b = 8 in	
	ASD	LRFD	ASD	LRFD
W27X84	73.9	111.1	119.4	179.5
W24X84	103.0	154.8	168.9	253.8
W24X76	80.2	120.6	131.6	197.8
W24X68	59.3	89.2	97.3	146.3
W24X62	75.3	113.2	127.6	191.9
W24X55	58.6	88.0	99.3	149.2
W21X83	193.7	291.2	321.0	482.4
W21X73	151.8	228.1	251.7	378.3
W21X68	129.9	195.2	215.5	323.9
W21X62	112.6	169.3	186.9	281.0
W21X55	81.1	121.8	134.6	202.3
W21X48	54.8	82.4	91.2	137.0
W18X86	150.9	226.8	240.0	360.8
W18X76	117.3	176.3	186.8	280.7
W18X71	176.9	265.9	296.6	445.8
W18X65	151.3	227.5	254.0	381.8
W18X60	139.8	210.1	234.7	352.8
W18X55	114.7	172.4	192.7	289.7
W18X50	93.8	141.0	157.6	236.9
W16X89	189.9	285.4	304.9	458.3
W16X77	142.7	214.5	229.5	344.9
W16X67	115.6	173.8	186.2	279.9
W16X57	134.8	202.6	228.1	342.8
W16X50	112.5	169.0	190.5	286.3
W16X45	90.3	135.8	153.1	230.1
W16X40	72.0	108.3	122.2	183.6
W16X36	56.6	85.0	95.9	144.2
W14X82	179.2	269.4	289.1	434.5
W14X74	151.1	227.1	243.7	366.3
W14X68	126.6	190.3	204.5	307.4
W14X61	108.0	162.2	174.4	262.1
W14X53	104.6	157.2	174.2	261.8
W14X48	84.9	127.6	141.4	212.6
W14X43	67.3	101.1	112.1	168.5
W12X87	173.2	260.3	271.8	408.5
W12X79	142.6	214.3	223.8	336.3
W12X72	118.1	177.4	185.5	278.8
W12X65	102.3	153.7	160.7	241.6
W12X58	113.4	170.4	183.1	275.3
W12X53	91.5	137.5	147.8	222.2
W12X50	105.0	157.8	174.8	262.7
W12X45	84.6	127.2	141.0	211.9
W12X40	72.6	109.2	121.0	181.9
Beam			ASD	LRFD
F_y = 50 ksi			Ω = 1.67	ϕ = 0.90

Angles Available Strength, kips

Angle Vertical Leg		ASD	LRFD
b, in	*t*, in		
10	1	359.3	540.0
	7/8	314.4	472.5
	3/4	269.5	405.0
8	1 1/8	323.4	486.0
	1	287.4	432.0
	7/8	251.5	378.0
	3/4	215.6	324.0
	5/8	179.6	270.0
	9/16	161.7	243.0
	1/2	143.7	216.0
	7/16	125.7	189.0
7	3/4	188.6	283.5
	5/8	157.2	236.3
	1/2	125.7	189.0
	7/16	110.0	165.4
	3/8	94.3	141.8
6	1	215.6	324.0
	7/8	188.6	283.5
	3/4	161.7	243.0
	5/8	134.7	202.5
	9/16	121.3	182.3
	1/2	107.8	162.0
	7/16	94.3	141.8
	3/8	80.8	121.5
	5/16	67.4	101.3
5	7/8	157.2	236.3
	3/4	134.7	202.5
	5/8	112.3	168.8
	1/2	89.8	135.0
	7/16	78.6	118.1
	3/8	67.4	101.3
	5/16	56.1	84.4
4	3/4	107.8	162.0
	5/8	89.8	135.0
	1/2	71.9	108.0
	7/16	62.9	94.5
	3/8	53.9	81.0
3 1/2	1/2	62.9	94.5
	7/16	55.0	82.7
Angles		ASD	LRFD
F_y = 50 ksi		Ω = 1.67	ϕ = 0.90

Figure 132: Drop-In Top Flange Connection Design Table

The drop-in connection design table is essentially two tables combined into one (analogous to AISC Table 6-1). The left side of the table provides the flange bending available strength for common wide-flange sections (no greater than 90 pounds per foot having a flange width of at least 7.0 inches) with the back corner of the angles placed at the toe of the girder/beam fillets. The right side of the table provides the available shear strength of the angles.

This table should expedite common drop-in connection designs. An engineer can select a W-Shape, and corresponding bearing length (l_b), that exceeds their required strength[5]. Then the engineer can use the right side of the table to select the angle vertical leg size needed to ensure the angles have more shear capacity than flange bending. The depth of the angle vertical leg may also be dictated by the weld design.

Design Examples

Two comprehensive drop-in top flange connection design examples were developed and are provided in ***Appendix F***. The first example (F.1) provides detailed calculations for the dimensional limitation checks and the structural design checks. The second example (F.2) goes through the structural integrity calculations.

[5] *Note that bearing lengths between the values provided can be interpolated. Also, the flange bending available strength will increase if encroachment is utilized.*

Conclusions

It was concluded that drop-in top flange shear connections are a viable alternative for girder-column, beam-column, and steel-concrete wall connections (not extended). The basis for this finding is extensive full-scale testing and numerical modeling. This study performed 12 tests, which included 11 drop-in connections and a shear tab connection. The numerical study included 192 unique models where the experimental data validated the modeling approach. From this work, design guidance was developed that included a detailed design methodology, design tables (Appendix E), and design examples (Appendix F).

The specific drop-in top flange connection findings include:

- Shear strength: Relatively high shear capacity can be achieved. The testing reached up to 150 kips of shear capacity for the geometries investigated. In many of the experiments, the girder failed before achieving the full connection capacity. Higher capacities were found through finite element modeling.
- Rotational stiffness: Relatively low in-plane rotational stiffness is provided by drop-in connections, classifying them as simple connections.
- Rotational ductility: Adequate ductility can be achieved that meets AISC criteria. Many of the tests met or exceeded the rotation limit of 0.03 radians. Other connections that failed before this limit were subjected to high shear/low rotation loading. The modeling showed that a more realistic shear/rotation loading achieves the necessary ductility.
- Torsional stiffness: Adequate torsional stiffness is provided for these connections. In fact, the LTB and sidesway buckling capacities can be increased with a drop-in connection due to the top flange restraint. However, research was not performed for relatively large concentrated loading near the support. Therefore, large concentrated loads are not recommended within a distance of twice the member depth to the support.

A drop-in top flange connection has many advantages and disadvantages compared to a shear tab connection. The top five advantages include:

- Faster erection speed due to the drop-in nature of the girder/beam placement and reduced number of bolts to tighten.
- Stability during erection due to the compression flange being supported before bolting.
- Safety during erection due to the improved stability (and reduction in bolt installation).
- Column loading is less concentrated than a shear tab. This may not require column stiffening of an HSS column like shear tab connections.
- High shear capacity and torsional stiffness in the completed state.

The top five disadvantages of drop-in top flange connections compared to shear tab connections include:

- More welding may be required due to the double angles as compared to a single plate.
- Requires the coping of the girder/beam bottom flange for the drop-in erection process.
- Geometric clearance limitations may reduce the girder/beam selection options.
- Structural integrity must be satisfied with two bolts in shear.
- Requires vertical girder/beam placement.

Future Work

The research presented herein illustrated the high potential for drop-in top flange shear connections. One area of future research is to ***expand the capabilities to beam-girder extended connections***. Several challenges arise for this type of connection, which include the torsional demand on the girder and the potential elevation difference between the top of the beam and the girder.

Future research may also consider further testing in the following areas:

- Axial capacity for structural integrity
- Shear capacity of different geometries than those in the presented study
- Torsional capacity of the connection
- Flexural behavior of the connection for a composite girder and/or beam

Acknowledgments

The research team is incredibly grateful for the support from AISC and the Industry Panel. Individuals from each are recognized below. In addition, the research team acknowledges the donated fabrication work from the North Alabama Fabrication Company (NAFCO).

AISC Representatives

The authors are grateful to AISC for supporting this study. The research was guided by several AISC representatives. The most active individuals are provided below.

- Devin Huber - Director of Research
- Carlo Lini - Director of AISC Steel Solutions Center
- Erin Conaway -Senior Director of Market Development
- Larry Kruth - former Vice President of Engineering & Research

Industry Panel

The research team was also guided by many individuals with extensive industry experience. These individuals include:

- Bo Dowswell – ARC International
- W. Duff Zimmerman – Cooper Steel

- Matthew Trammell – Trammell Engineering Group, LLC
- Keith Palmer – Simpson Gumpertz & Heger
- Larry Muir – Consultant (former Cives Steel/AISC)
- Brian Volpe – Cives Steel
- Tom Kuznick – Herrick Steel (retired)
- Victor – Lejeune Steel (retired)
- Doug Abernathy - North Alabama Fabrication Company

References

AISC (2017). Steel construction manual, American Institute of Steel Construction.

AISC (2018). Office conventional steel framing study. https://www.nxtbook.com/nxtbooks/aisc/officestudy_2018/index.php?startid=1.

ANSI/AISC (2022). AISC 360-22, specification for structural steel buildings. Chicago AISC.

Astaneh-Asl, A., S. M. Call and K. M. Mcmullin (1989). "Design of single plate shear connections." Engineering Journal **26**(1): 21-32.

Astaneh, A. (1989). "Demand and supply of ductility in steel shear connections." Journal of Constructional Steel Research **14**(1): 1-19.

Bose, B. (1982). "The influence of torsional restraint stiffness at supports on the buckling strength of beams." Structural Engineer. Part B **60**(4).

Dranger, T. S. (1977). "Yield line analysis of bolted hanging connections." Engineering Journal **14**(3): 92-97.

Ellifritt, D. S. and T. Sputo (1999). "Design criteria for stiffened seated connections to column webs." Engineering Journal **36**(4): 160-168.

Gardner, L. (2011). STABILITY OF STEEL BEAMS AND COLUMNS.

Grondin, G. and J. Cheng (1999). "Sidesway web buckling of steel beams." Engineering Journal **36**(4): 169-180.

Huber, D. and C. Colsia (2025). Speed Studies. Modern Steel Magazine**:** 50-55.

Kapp, R. (1974). "Yield line analysis of a web connection in direct tension." Engineering Journal **11**(2): 38-41.

Richard, R. M., P. E. Gillett, J. D. Kriegh and B. A. Lewis (1980). "The analysis and design of single plate framing connections." Engineering Journal **17**(2): 38-52.

Stockwell Jr, F. W. (1974). "Yield line analysis of column webs with welded beam connections." Engineering Journal **11**(1): 12-17.

Summers, P. B. and J. A. Yura (1982). The behavior of beams subjected to concentrated loads, Citeseer.

Sutton, M. A., J. J. Orteu and H. Schreier (2009). Image correlation for shape, motion and deformation measurements: basic concepts, theory and applications, Springer Science & Business Media.

Topkaya, C. (2006). "A numerical study on linear bifurcation web buckling of steel I-beams in the sidesway mode." Engineering structures **28**(7): 1028-1037.

Valeš, J. and T.-C. Stan (2017). "FEM modelling of lateral-torsional buckling using shell and solid elements." Procedia engineering **190**: 464-471.

Way, A. and T. Cosgrove "STABILITY OF STEEL BEAMS AND COLUMNS."

White, R. N. (1965). "Framing connections for square and rectangular structural tubing." Engineering Journal **2**(3): 94-102.

Appendix A: Measured Weld Sizes and Positions

Connection	Weld Size/Position Measured (Inches)																							
	1			2			3			4			5			6			7			8		
	Left	Mid	Right	Left	Mid	Right	Bott	Mid	Top	Bott	Mid	Top	Left	Mid	Right	Left	Mid	Right	Bott	Mid	Top	Bott	Mid	Top
A	3/8	3/8	5/16	5/16	5/16	5/16	13/16	13/16	13/16	5/16	1/4	1/4	1/4	1/4	1/4	5/16	5/16	5/16	3/4	3/4	3/4	1/4	1/4 [1]	1/4
B	5/16	5/16	5/16	5/16	5/16	3/8	3/8	3/8	3/8	3/16	3/16	1/4	3/8	3/8	3/8	3/8	3/8	3/8	3/8	3/8	3/8	1/4	1/4	1/4
C	1/4	1/4	1/4	1/4	1/4	1/4	5/16	5/16	5/16	-	-	-	1/4	1/4	1/4	5/16	5/16	1/4	1/4	1/4	5/16	-	-	-
D	1/4	3/8	5/16	-	-	-	5/16	5/16	5/16	-	-	-	5/16	5/16	5/16	-	-	-	3/8	3/8	3/8	-	-	-
E	5/16	5/16	1/16	1/4	5/16	5/16	5/16	5/16	5/16	-	-	-	5/16	5/16	5/16	5/16	5/16	5/16	5/16	5/16	5/16	-	-	-
F	-	-	-	-	-	-	5/16	5/16	5/16	5/16	5/16	5/16	-	-	-	-	-	-	-	-	-	-	-	-
G	1/4	5/16	5/16	5/16	5/16	5/16	5/16	5/16	5/16	-	-	-	5/16	5/16	5/16	5/16	5/16	5/16	1/4	5/16	5/16	-	-	-
H	5/16	5/16	5/16	5/16	5/16	5/16	1/4	5/16	5/16	5/16	5/16	5/16	5/16	5/16	5/16	5/16	5/16	1/4	5/16	5/16	5/16	5/16	5/16	5/16
I	1/4	5/16	5/16	5/16	5/16	5/16	5/16	5/16	5/16	1/4	5/16	5/16	5/16	5/16	5/16	5/16	5/16	5/16	5/16	5/16	5/16	5/16	5/16	5/16
J	3/8	3/8	3/8	5/16	5/16	5/16	5/16	5/16	5/16	5/16	5/16	5/16	5/16	5/16	5/16	5/16	5/16	5/16	5/16	5/16	5/16	3/8	5/16	5/16
K	1/4	5/16	5/16	5/16	5/16	5/16	5/16	5/16	5/16	5/16	1/4	1/4	5/16	5/16	5/16	5/16	5/16	5/16	5/16	5/16	5/16	5/16	5/16	5/16
L	5/16 [2]	5/16 [2]	5/16 [2]	5/16 [2]	5/16 [2]	5/16 [2]	5/16 [2]	3/8 [2]	3/8 [2]	5/16 [2]	5/16 [2]	5/16 [2]	5/16 [2]	5/16 [2]	5/16 [2]	5/16 [2]	5/16 [2]	5/16 [2]	1/2	3/8 [2]	3/8 [2]	5/16 [2]	5/16 [2]	5/16 [2]

[1] Weld discontinuous at two points, between middle and top

[2] Increased to 1/2'' via in-house welding

As seen from the beam towards the column

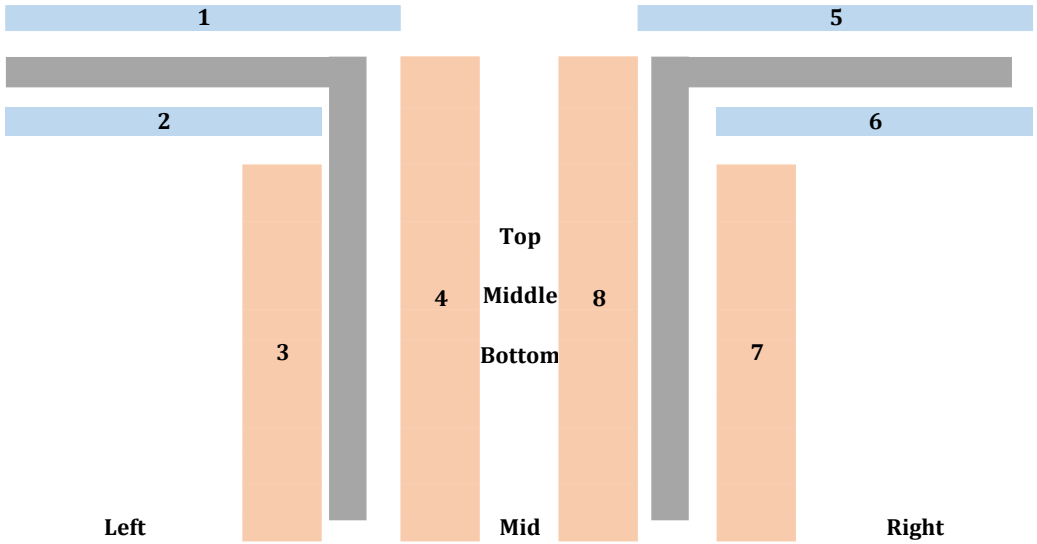

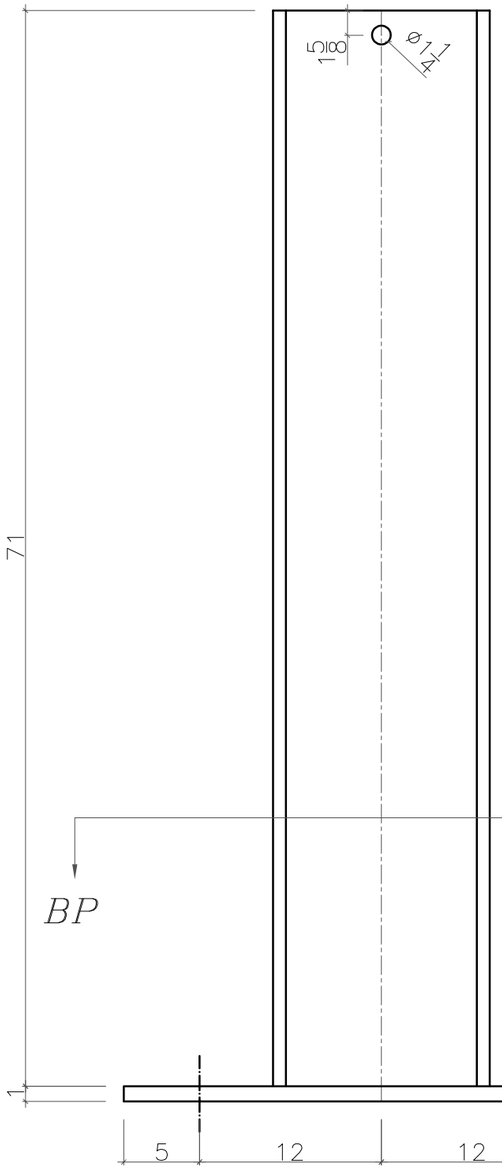

TYPICAL LATERAL SUPPORT COLUMN
(4 Pcs)
Scale 1:10

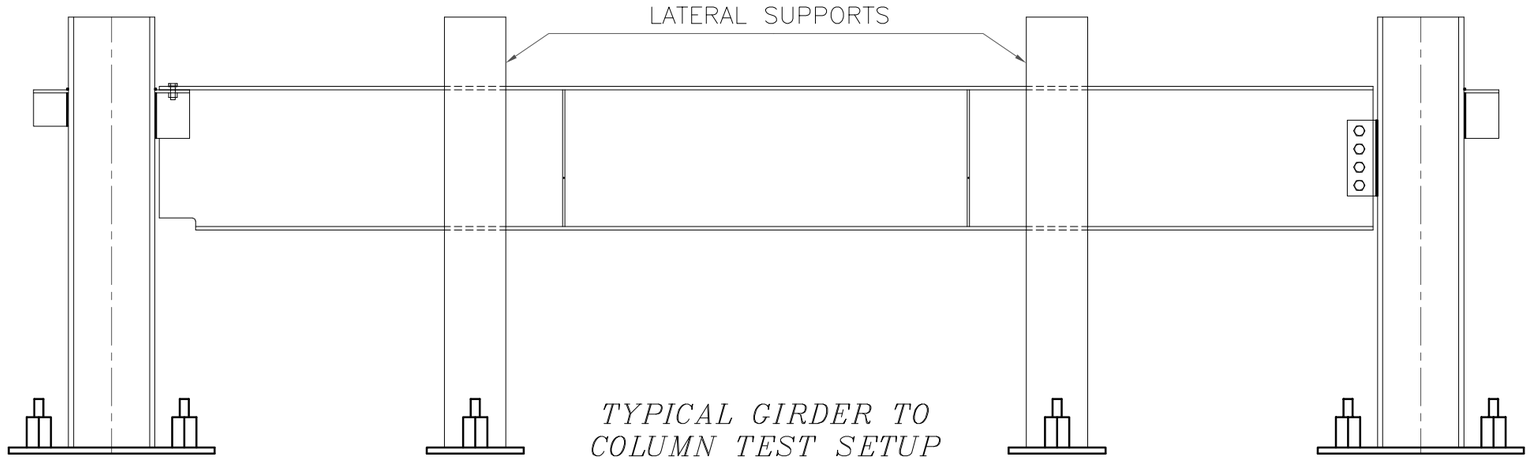

TYPICAL GIRDER TO
COLUMN TEST SETUP
ELEVATION
Scale 1:25

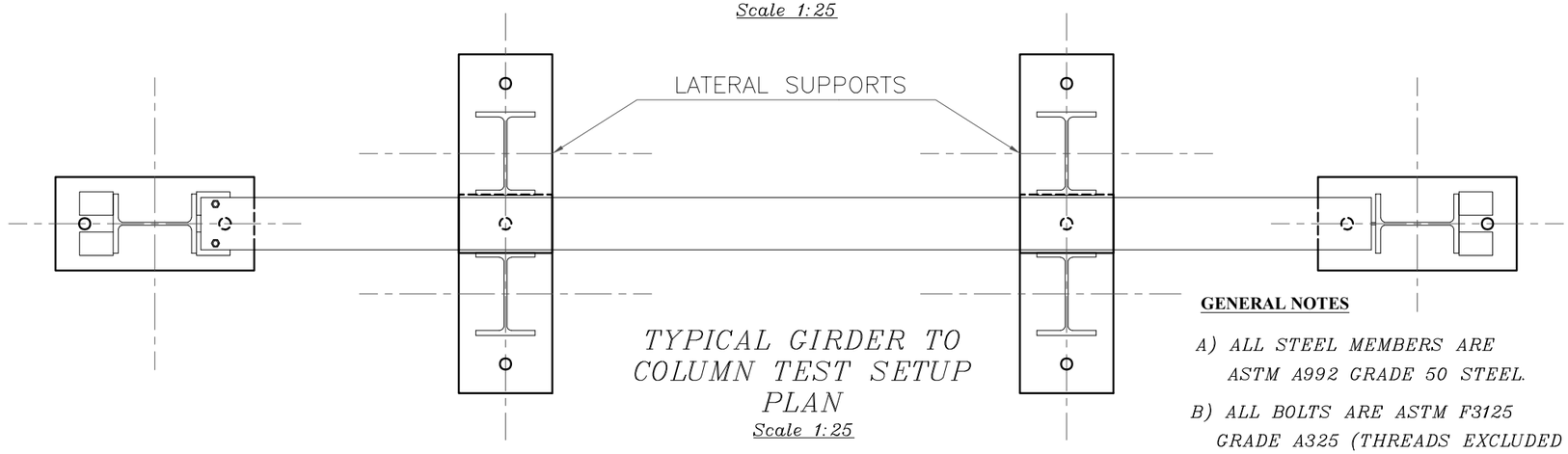

TYPICAL GIRDER TO
COLUMN TEST SETUP
PLAN
Scale 1:25

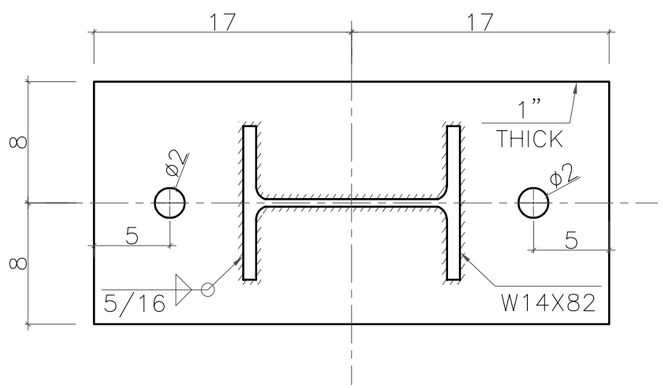

SECTION BP–BP
Scale 1:10

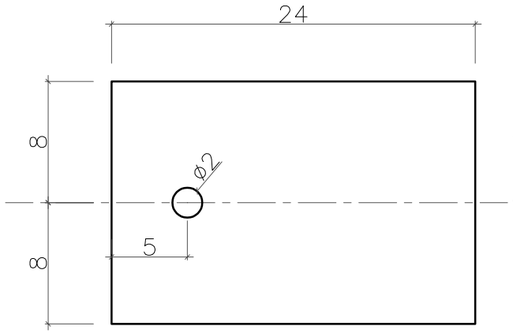

ONE INCH THICK PLATE
(2Pcs)
Scale 1:10

GENERAL NOTES

A) ALL STEEL MEMBERS ARE ASTM A992 GRADE 50 STEEL.

B) ALL BOLTS ARE ASTM F3125 GRADE A325 (THREADS EXCLUDED FROM THE SHEAR PLANE).

C) ELECTRODE TYPE IS E70.

D) ALL MEASUREMENTS ARE IN INCHES UNLESS SPECIFIED.

E) FOR ANGLES WITH UNEQUAL LEGS, THE LONGER LEG IS VERTICAL.

F) ALL STEEL TO BE UNCOATED BARE METAL

AUBURN UNIVERSITY
ADVANCED STRUCTURAL ENGINEERING LAB

PROJECT: AISC SPEED CONNECT: DROP–IN TOP FLANGE CONNECTION	
Drawing Title: TEST SETUP, LATERAL SUPPORT COLUMNS, AND BASE PLATES	
DATE: DECEMBER 2024	DRAWING No.
DESIGNED BY R.A & E.D	1 of 12
DRAWN BY R.A & E.D	
CHECKED BY M.Y & K.S	

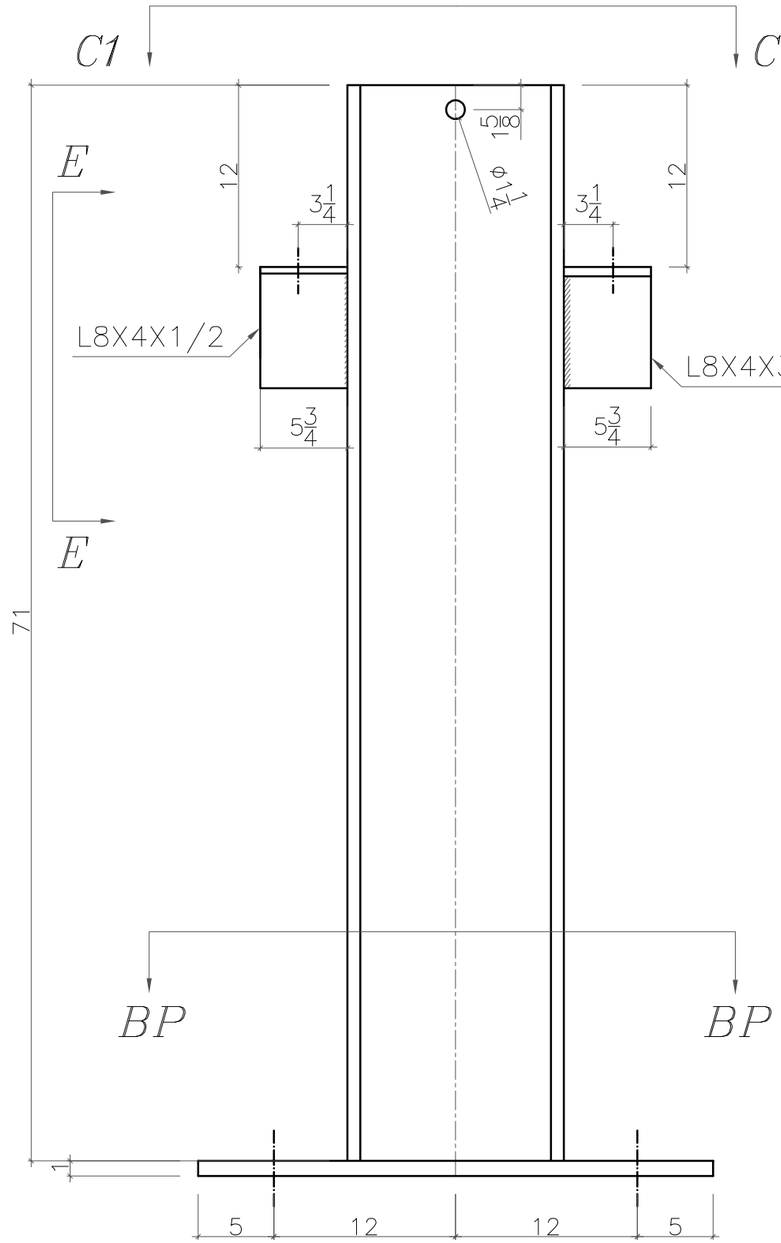

COLUMN 1 – W14X82

Scale 1:10

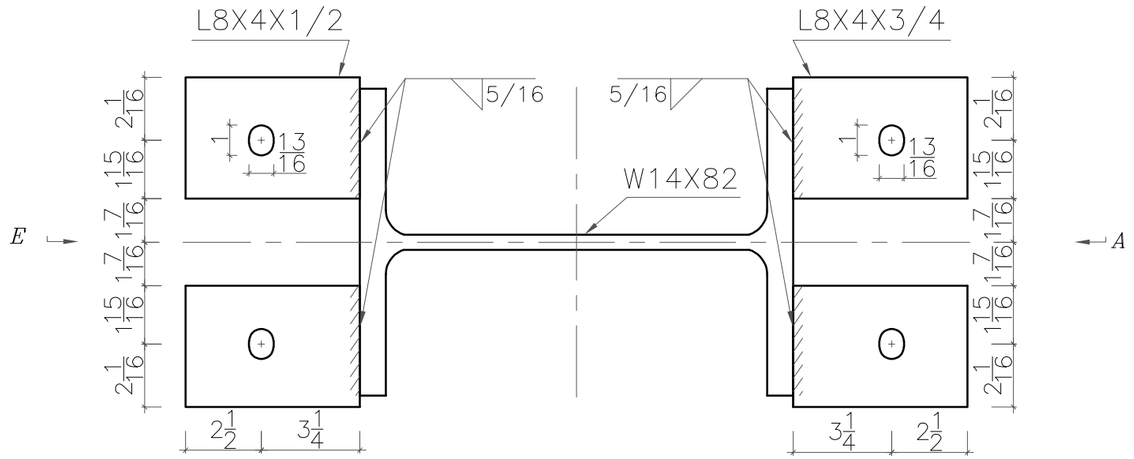

VIEW C1–C1

Scale 1:5

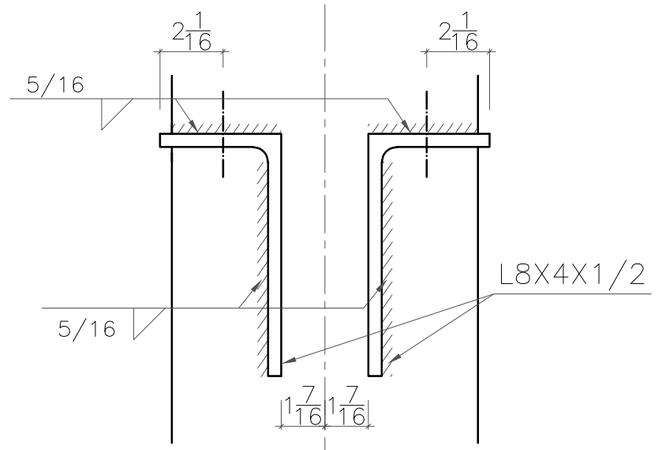

VIEW E–E

Scale 1:5

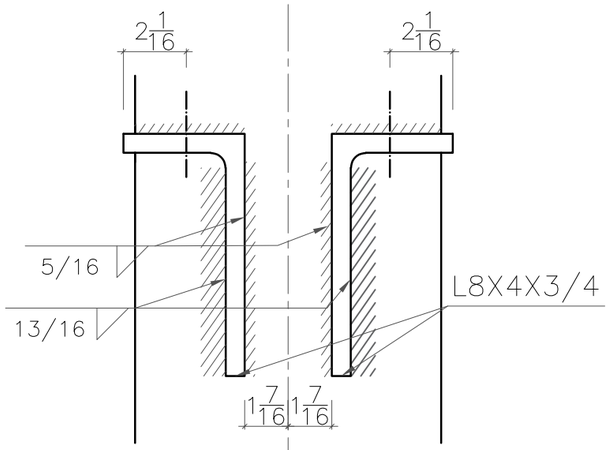

VIEW A–A

Scale 1:5

AUBURN UNIVERSITY ADVANCED STRUCTURAL ENGINEERING LAB	
PROJECT: *AISC SPEED CONNECT: DROP-IN TOP FLANGE CONNECTION*	
Drawing Title: COLUMN 1	
DATE: DECEMBER 2024	DRAWING No.
DESIGNED BY R.A & E.D	2 of 12
DRAWN BY R.A & E.D	
CHECKED BY M.Y & K.S	

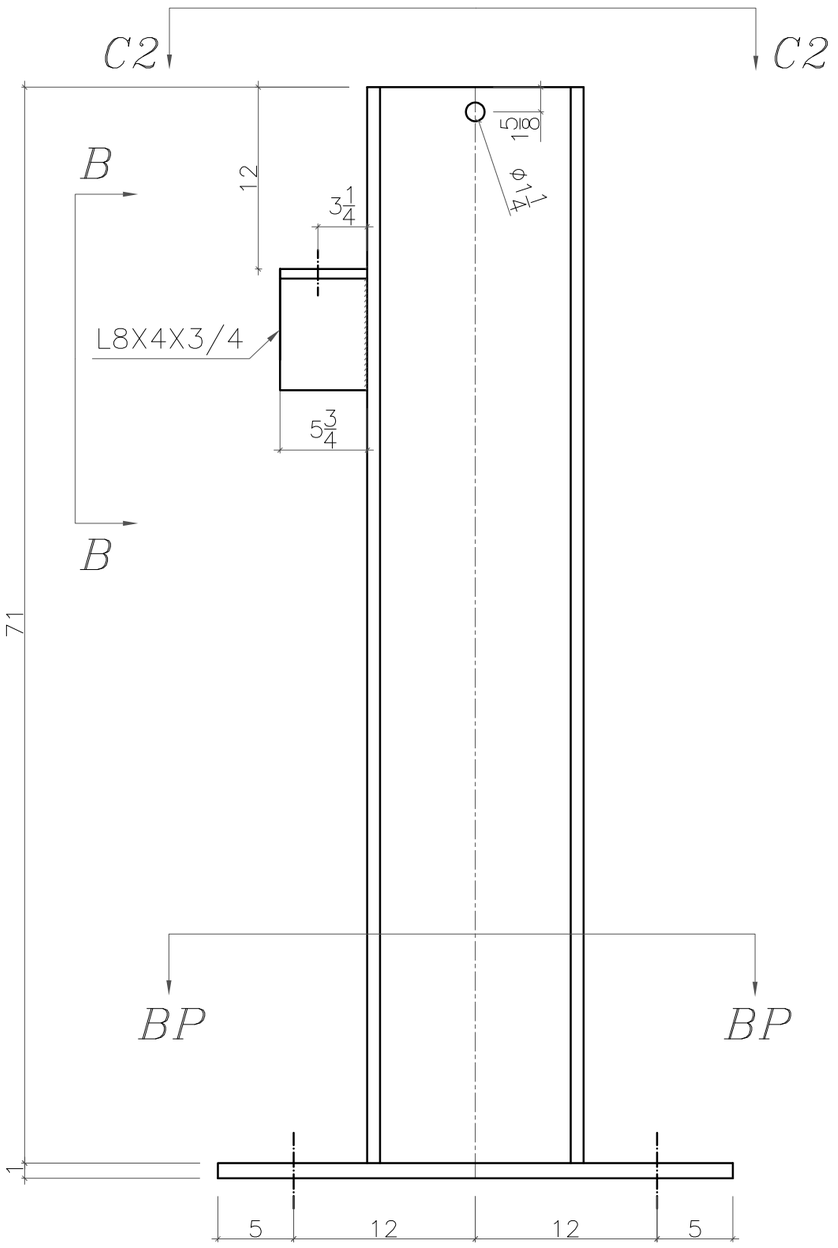

COLUMN 2 – W14X82

Scale 1:20

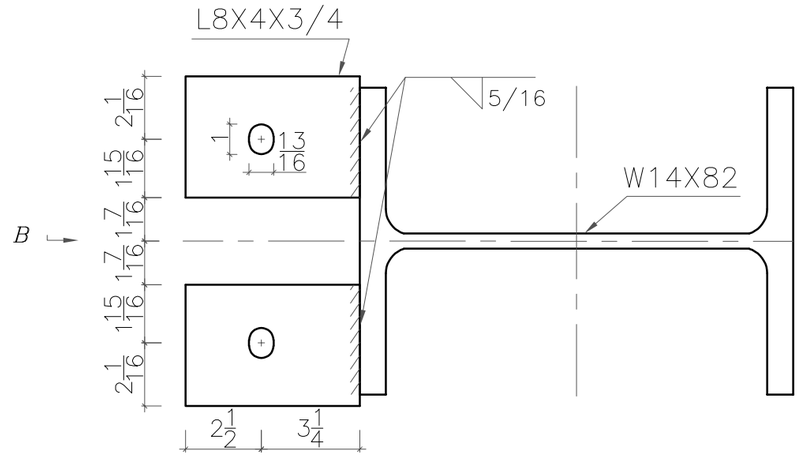

VIEW C2–C2

Scale 1:5

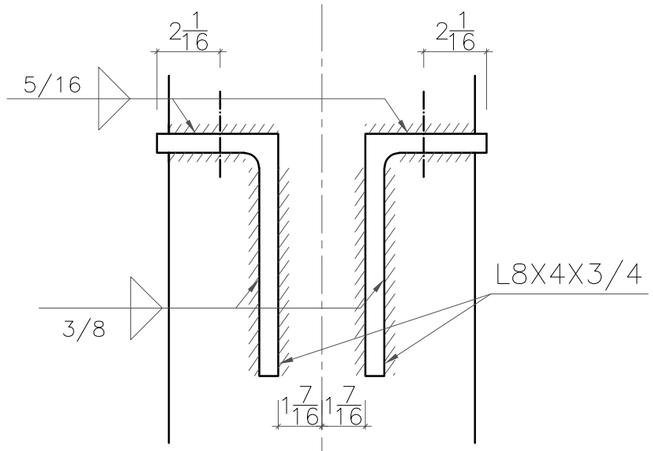

VIEW B–B

Scale 1:5

AUBURN UNIVERSITY ADVANCED STRUCTURAL ENGINEERING LAB	
PROJECT: *AISC SPEED CONNECT: DROP–IN TOP FLANGE CONNECTION*	
Drawing Title: COLUMN 2	
DATE: DECEMBER 2024	DRAWING No.
DESIGNED BY R.A & E.D	3 of 12
DRAWN BY R.A & E.D	
CHECKED BY M.Y & K.S	

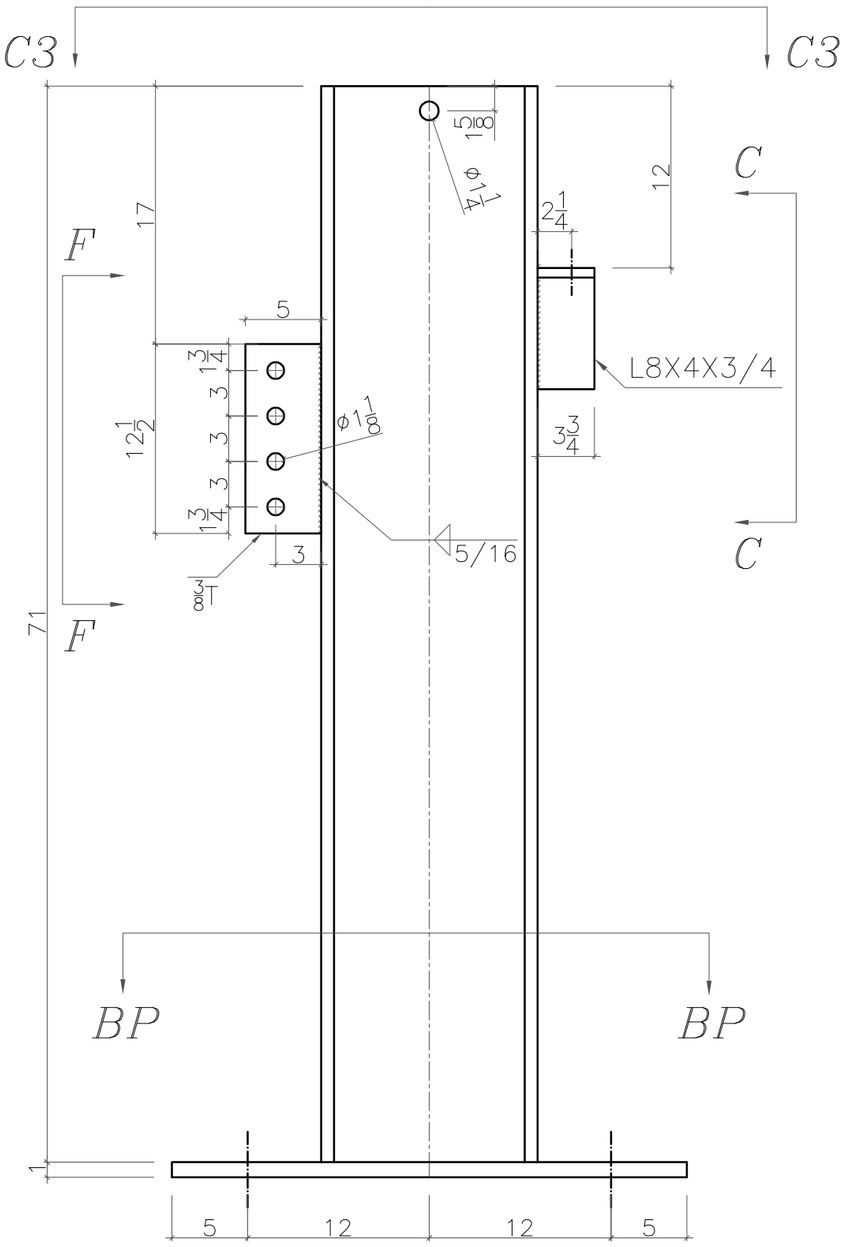

COLUMN 3 – W14X82

Scale 1:10

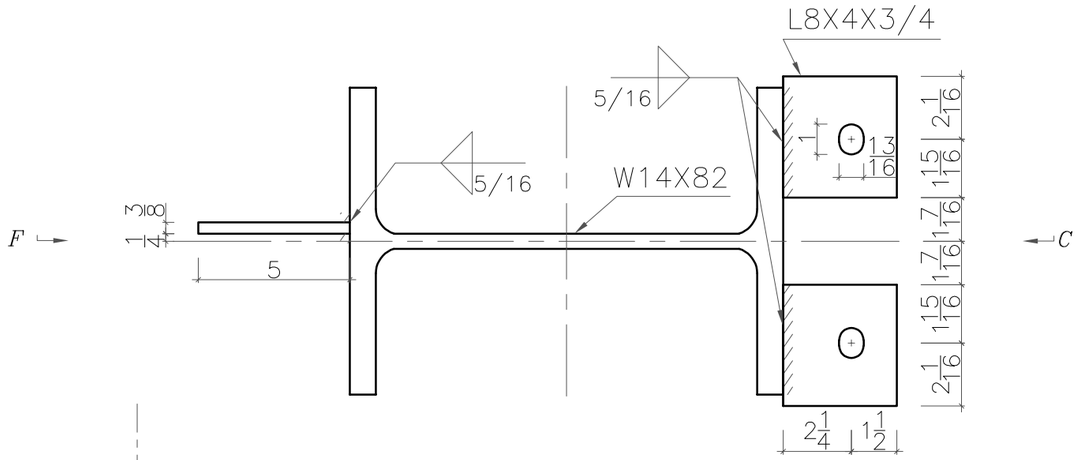

VIEW C3–C3

Scale 1:5

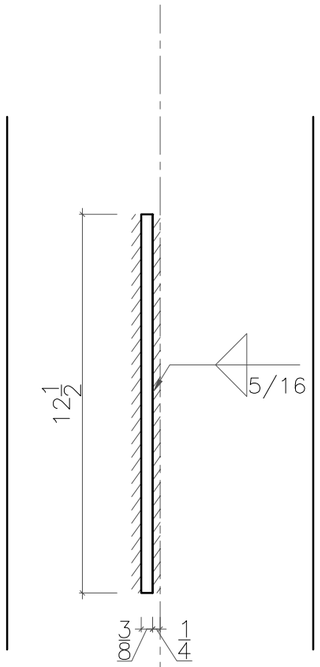

VIEW F–F

Scale 1:5

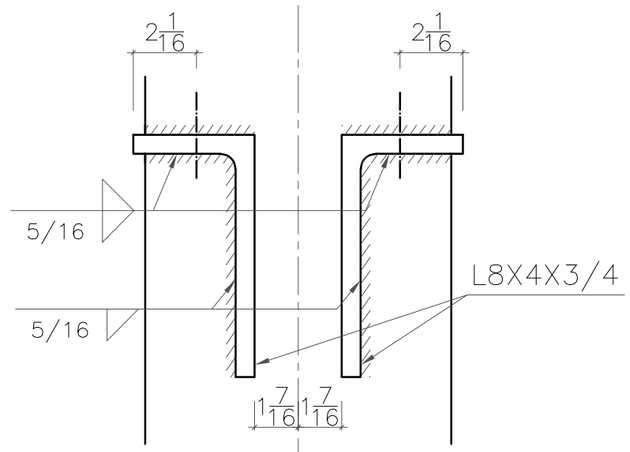

VIEW C–C

Scale 1:5

AUBURN UNIVERSITY ADVANCED STRUCTURAL ENGINEERING LAB	
PROJECT: *AISC SPEED CONNECT: DROP-IN TOP FLANGE CONNECTION*	
Drawing Title: COLUMN 3	
DATE: DECEMBER 2024	DRAWING No.
DESIGNED BY R.A & E.D	4 of 12
DRAWN BY R.A & E.D	
CHECKED BY M.Y & K.S	

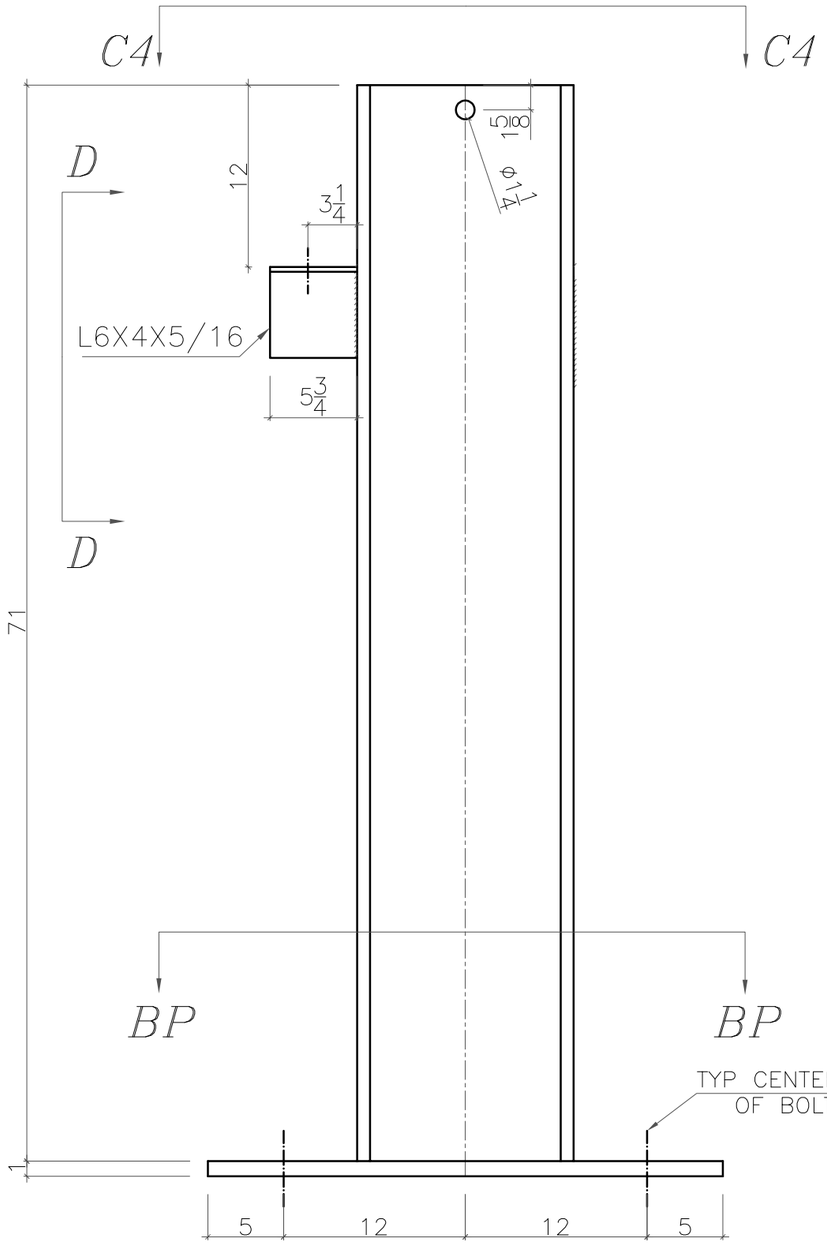

COLUMN 4 – W14X82

Scale 1:10

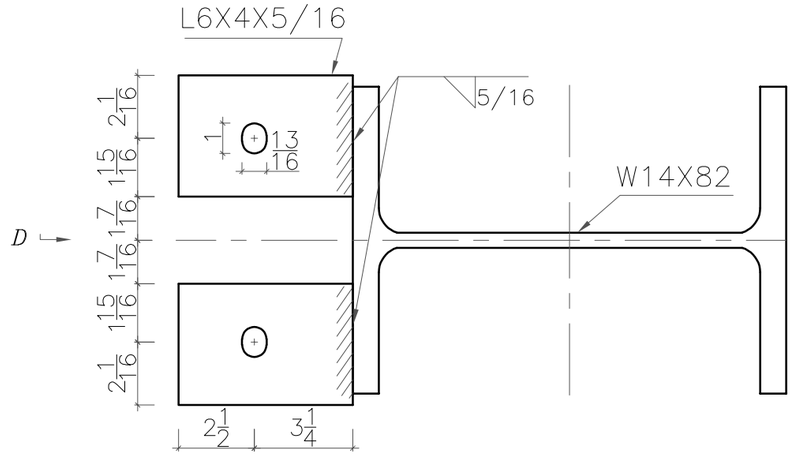

VIEW C4–C4

Scale 1:5

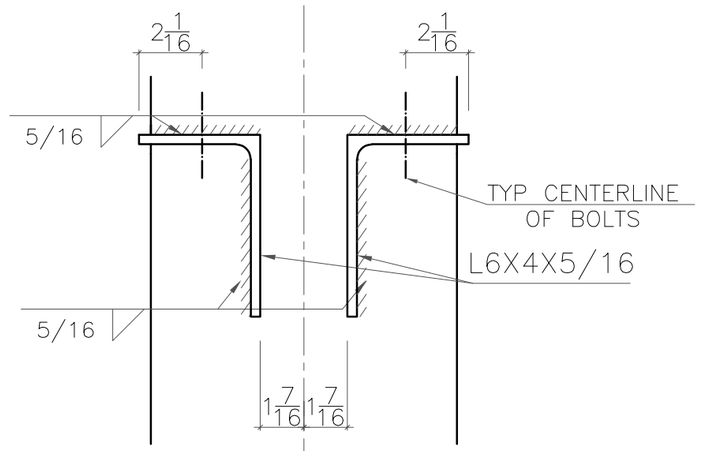

VIEW D–D

Scale 1:5

AUBURN UNIVERSITY ADVANCED STRUCTURAL ENGINEERING LAB	
PROJECT: *AISC SPEED CONNECT: DROP–IN TOP FLANGE CONNECTION*	
Drawing Title: COLUMN 4	
DATE: DECEMBER 2024	DRAWING No.
DESIGNED BY R.A & E.D	5 of 12
DRAWN BY R.A & E.D	
CHECKED BY M.Y & K.S	

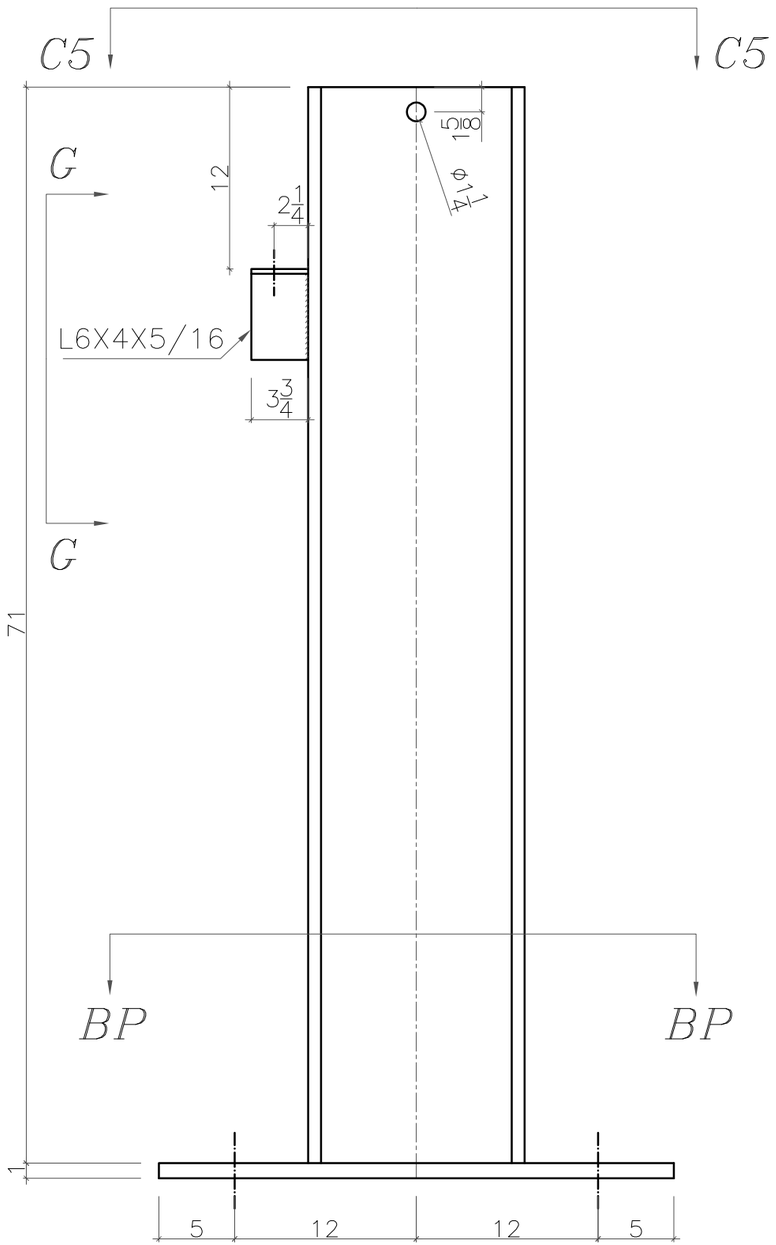

COLUMN 5 – W14X82

Scale 1:20

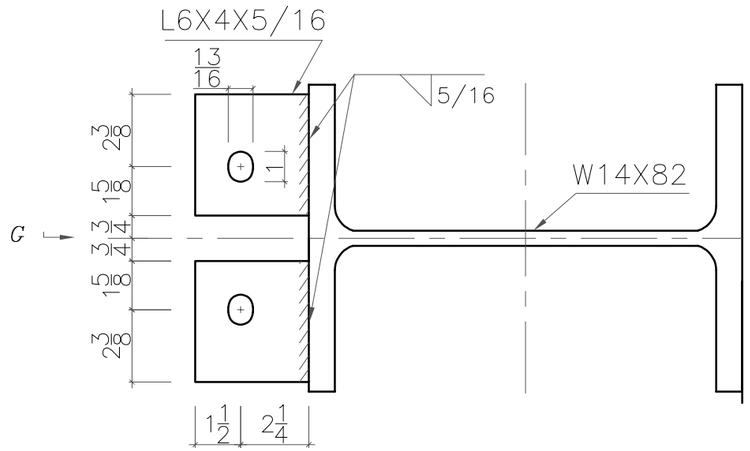

VIEW C5–C5

Scale 1:5

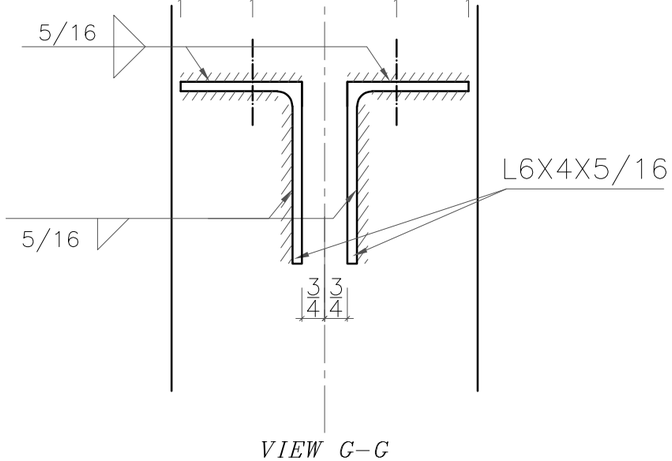

VIEW G–G

Scale 1:5

AUBURN UNIVERSITY ADVANCED STRUCTURAL ENGINEERING LAB	
PROJECT: *AISC SPEED CONNECT: DROP–IN TOP FLANGE CONNECTION*	
Drawing Title: COLUMN 5	
DATE: DECEMBER 2024	DRAWING No.
DESIGNED BY R.A & E.D	6 of 12
DRAWN BY R.A & E.D	
CHECKED BY M.Y & K.S	

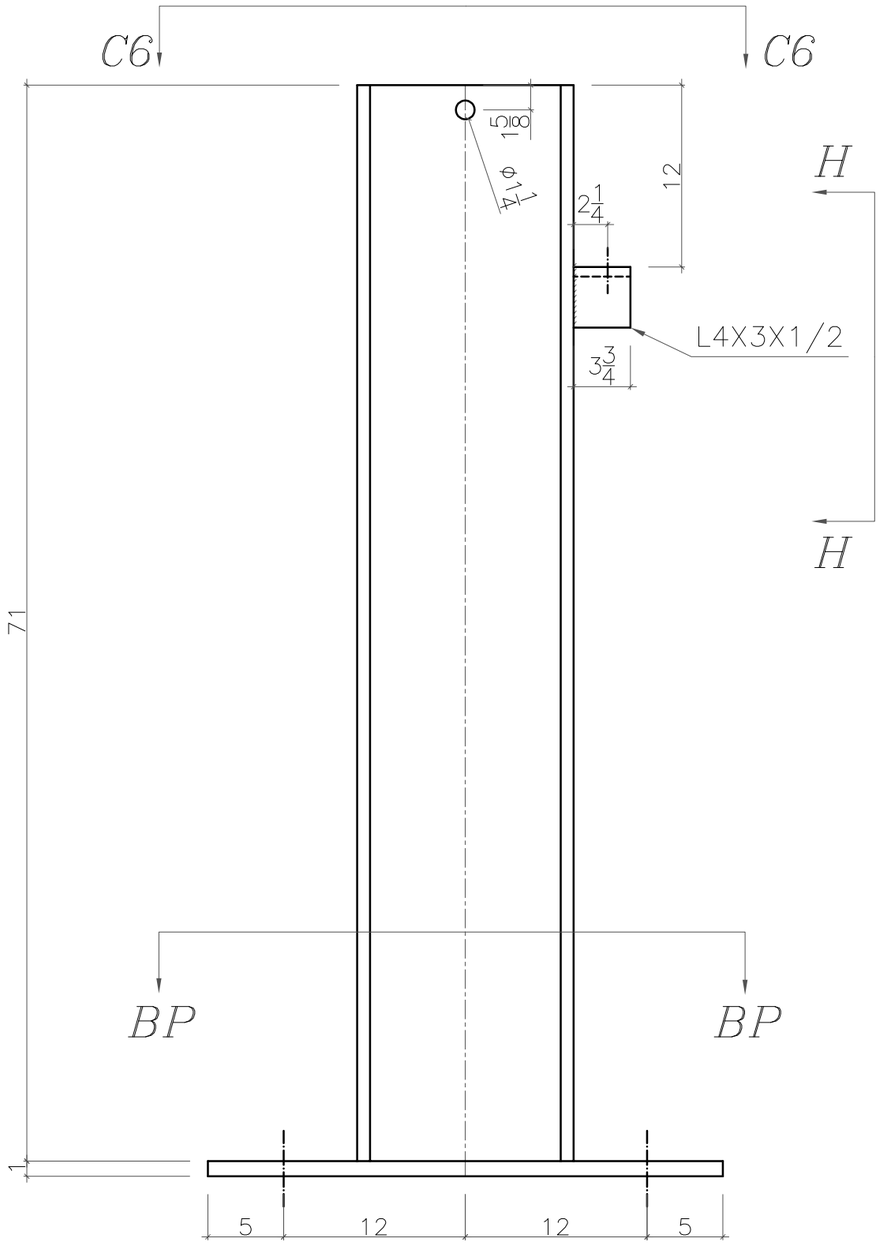

COLUMN 6 – W14X82

Scale 1:10

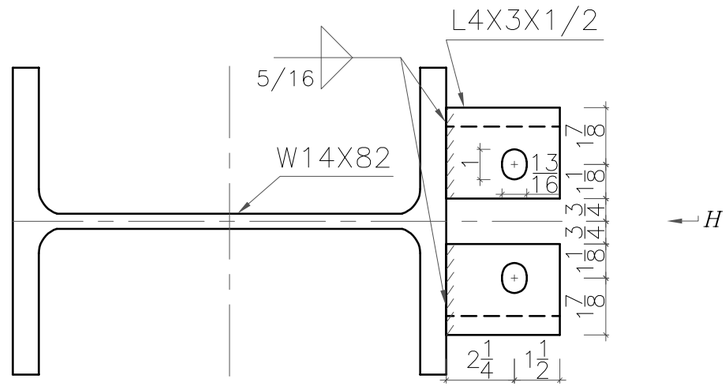

VIEW C6–C6

Scale 1:5

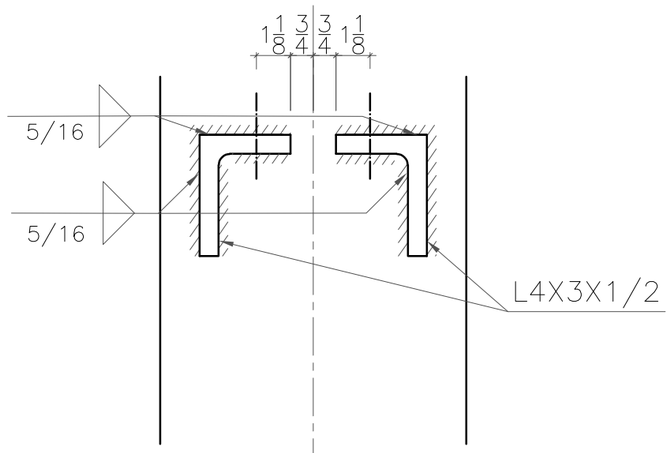

VIEW H–H

Scale 1:5

AUBURN UNIVERSITY
ADVANCED STRUCTURAL ENGINEERING LAB

PROJECT: *AISC SPEED CONNECT: DROP–IN TOP FLANGE CONNECTION*

Drawing Title: COLUMN 6

DATE: DECEMBER 2024	DRAWING No.
DESIGNED BY R.A & E.D	7 of 12
DRAWN BY R.A & E.D	
CHECKED BY M.Y & K.S	

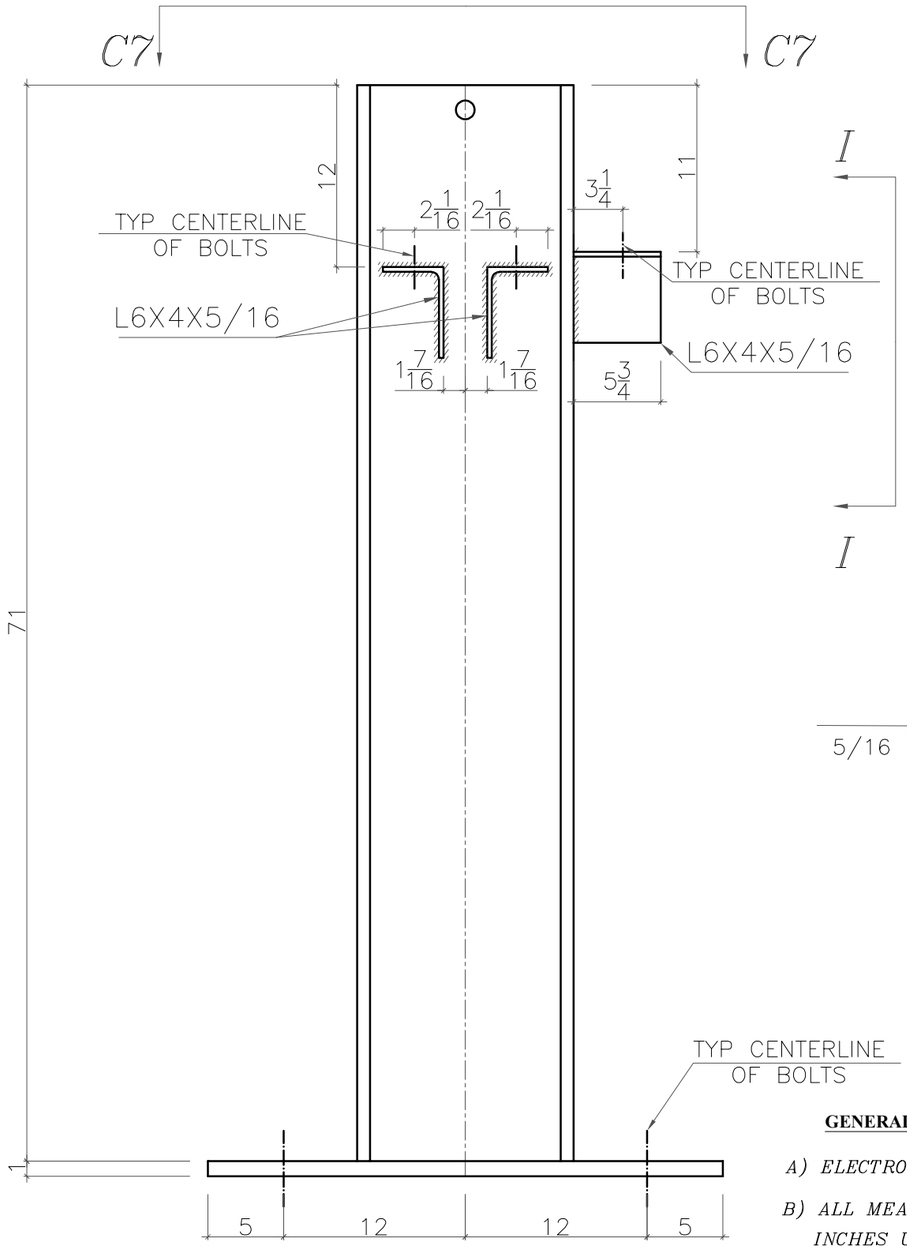

COLUMN 7 – W14X82

Scale 1:10

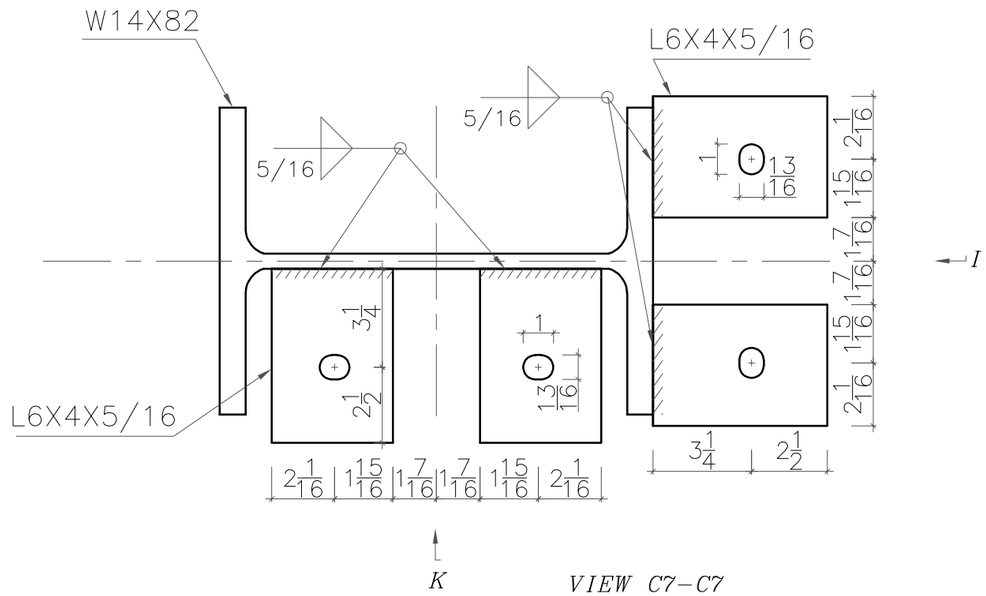

VIEW C7–C7

Scale 1:5

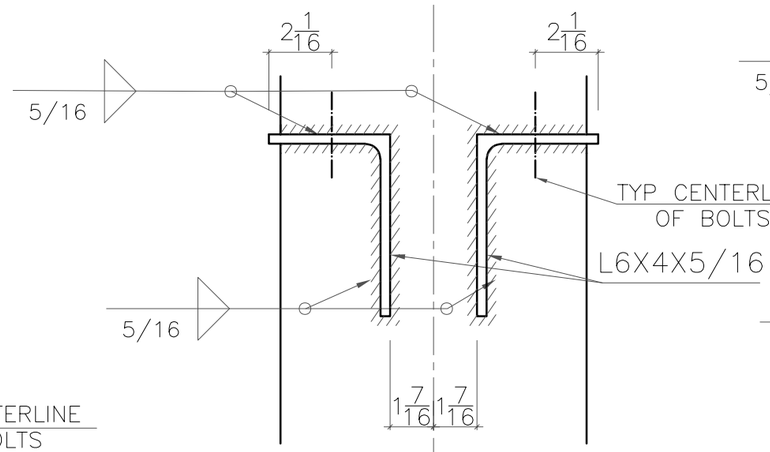

VIEW I–I

Scale 1:5

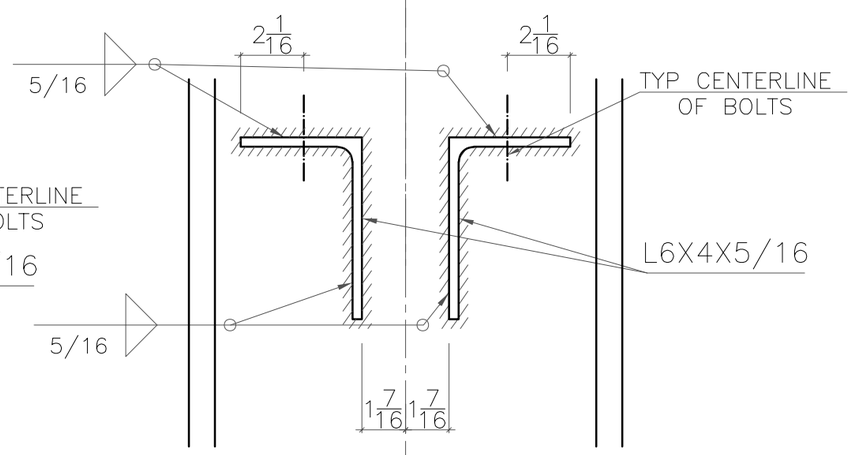

VIEW K–K

Scale 1:5

GENERAL NOTES

A) ELECTRODE TYPE IS E70.

B) ALL MEASUREMENTS ARE IN INCHES UNLESS SPECIFIED.

C) FOR ANGLES WITH UNEQUAL LEGS, THE LONGER LEG IS VERTICAL.

D) ALL STEEL TO BE UNCOATED BARE METAL

AUBURN UNIVERSITY
ADVANCED STRUCTURAL ENGINEERING LAB

PROJECT: AISC SPEED CONNECT: DROP–IN TOP FLANGE CONNECTION

Drawing Title: COLUMN 7

DATE: DECEMBER 2024

DESIGNED BY R.A & E.D

DRAWN BY R.A & E.D

CHECKED BY M.Y & K.S

DRAWING No. 8 of 12

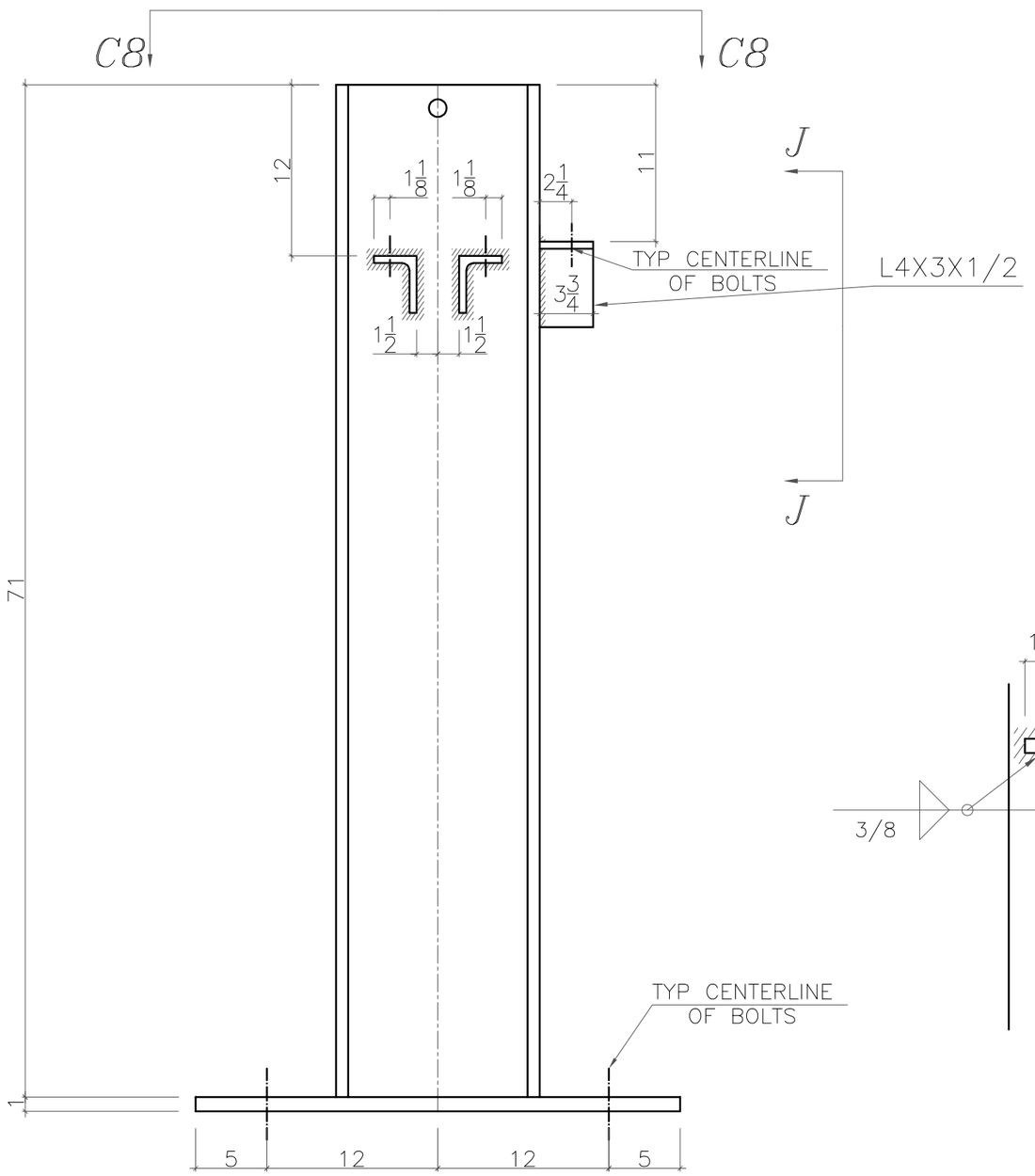

COLUMN 8 – W14X82

Scale 1:10

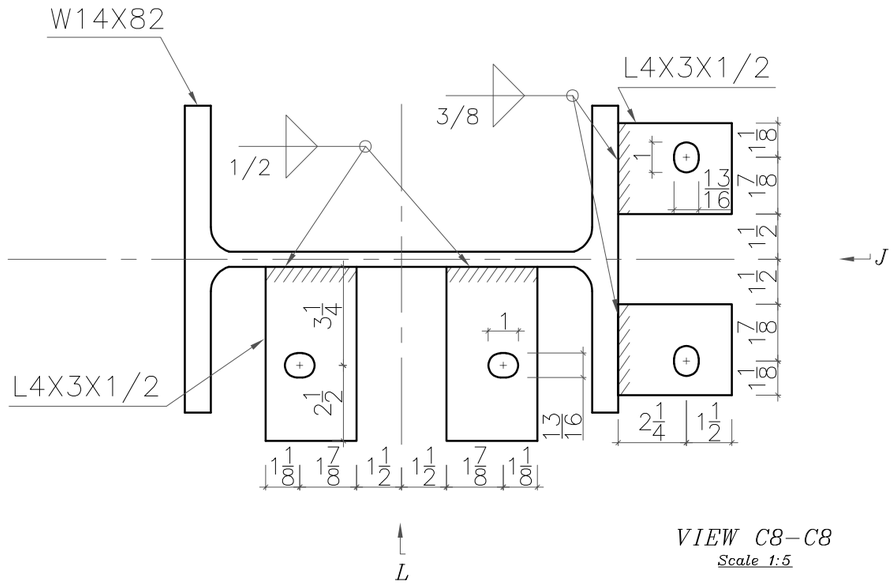

VIEW C8–C8

Scale 1:5

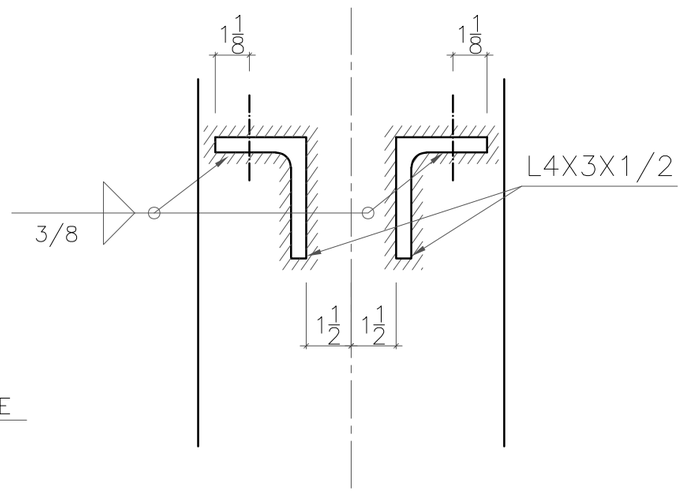

VIEW J–J

Scale 1:5

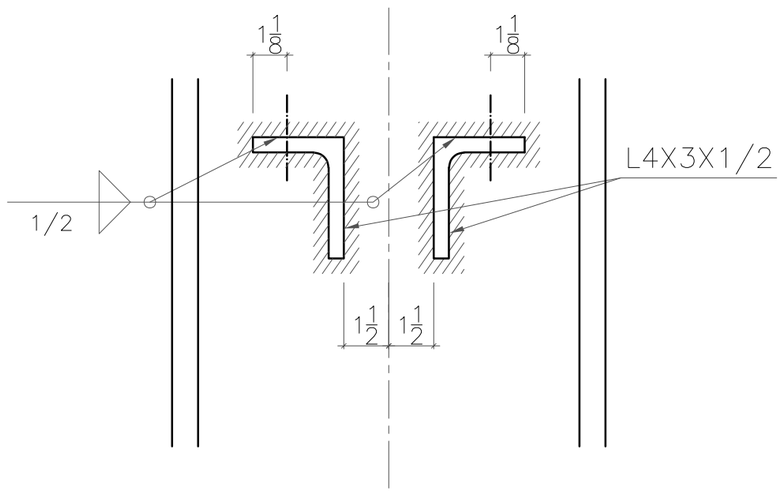

VIEW L–L

Scale 1:5

AUBURN UNIVERSITY
ADVANCED STRUCTURAL ENGINEERING LAB

PROJECT: *AISC SPEED CONNECT: DROP–IN TOP FLANGE CONNECTION*

Drawing Title: COLUMN 8

DATE: DECEMBER 2024	DRAWING No.
DESIGNED BY R.A & E.D	9 of 12
DRAWN BY R.A & E.D	
CHECKED BY M.Y & K.S	

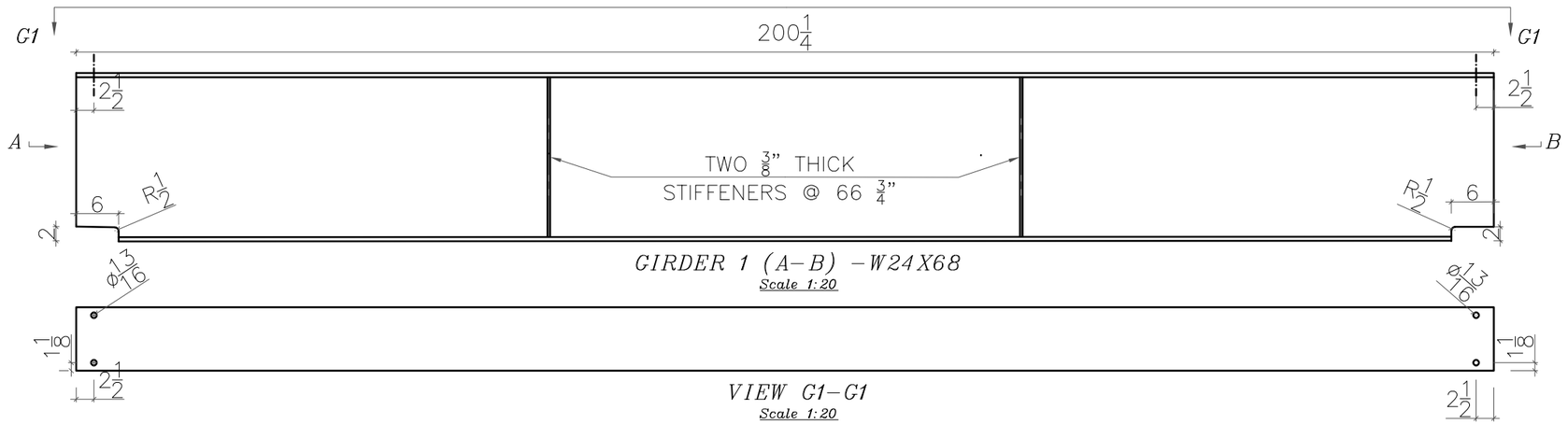

GIRDER 1 (A–B) –W24X68
Scale 1:20

VIEW G1–G1
Scale 1:20

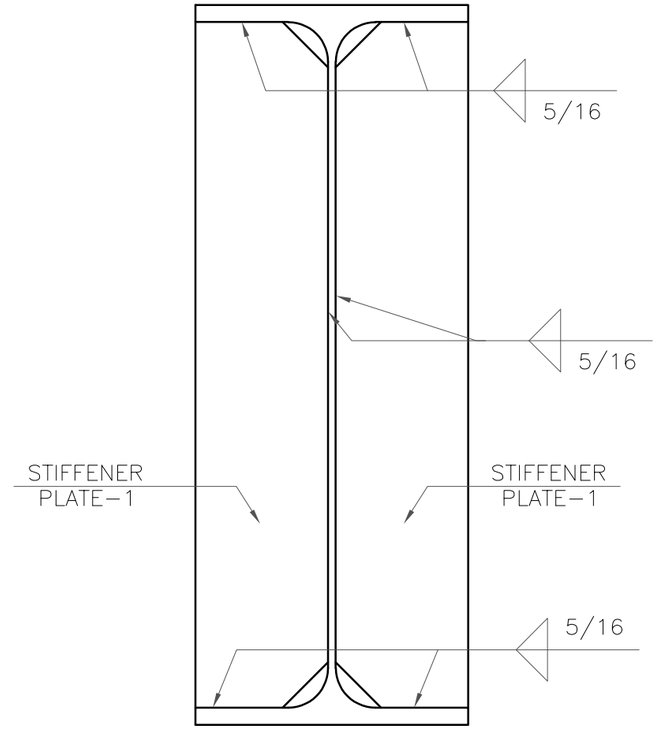

TYPICAL STIFFENER DETAIL FOR BEAMS 1 TO 5
Scale 1:5

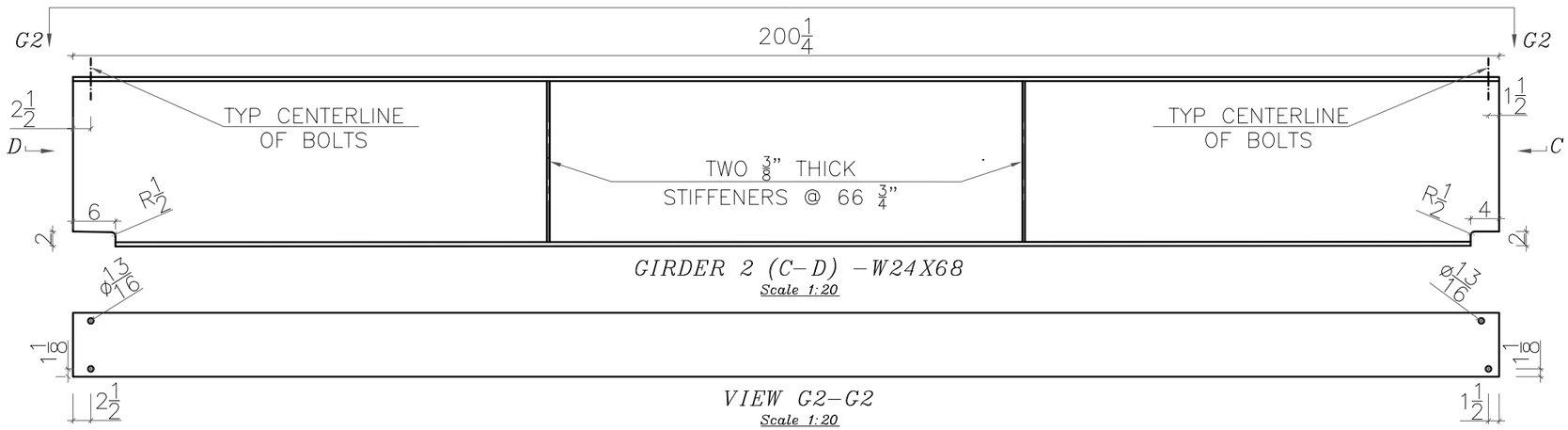

GIRDER 2 (C–D) –W24X68
Scale 1:20

VIEW G2–G2
Scale 1:20

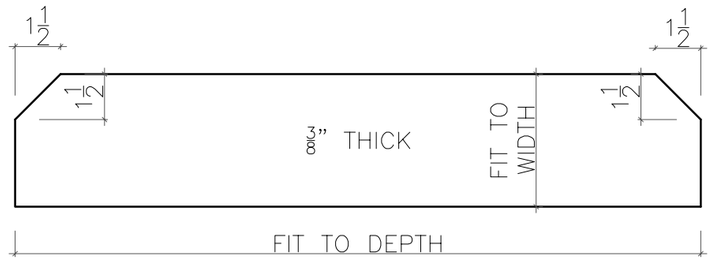

STIFFENER PLATE–1
(20 Pcs)
Scale 1:5

AUBURN UNIVERSITY
ADVANCED STRUCTURAL ENGINEERING LAB

PROJECT: *AISC SPEED CONNECT: DROP–IN TOP FLANGE CONNECTION*

Drawing Title: GIRDERS 1 & 2 AND BEAM STIFFENER DETAIL

DATE: DECEMBER 2024	DRAWING No.
DESIGNED BY R.A & E.D	10 of 12
DRAWN BY R.A & E.D	
CHECKED BY M.Y & K.S	

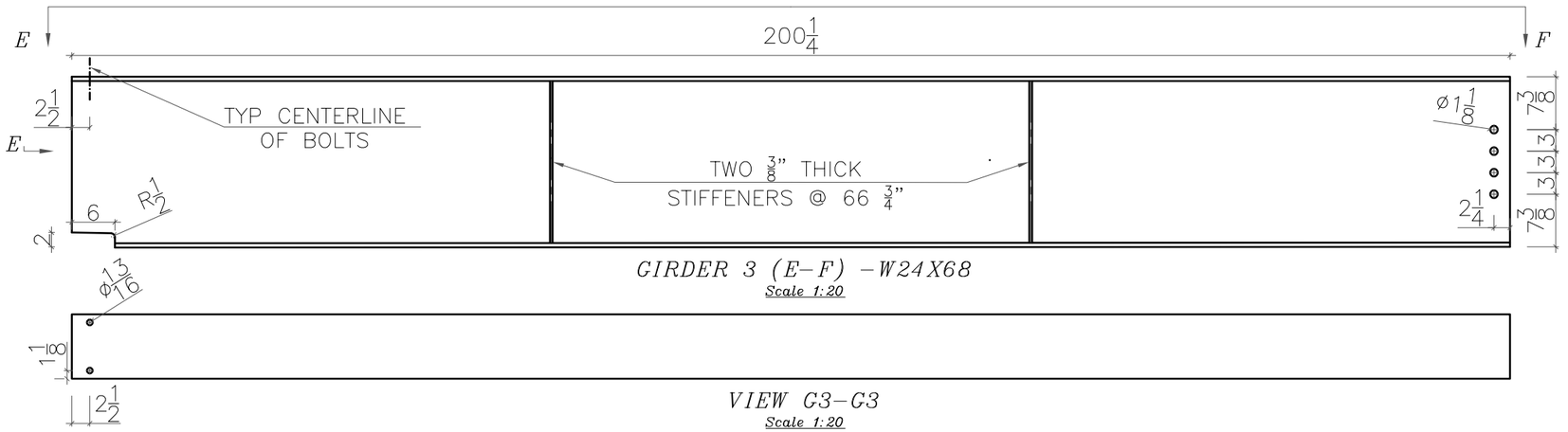

GIRDER 3 (E–F) –W24X68
Scale 1:20

VIEW G3–G3
Scale 1:20

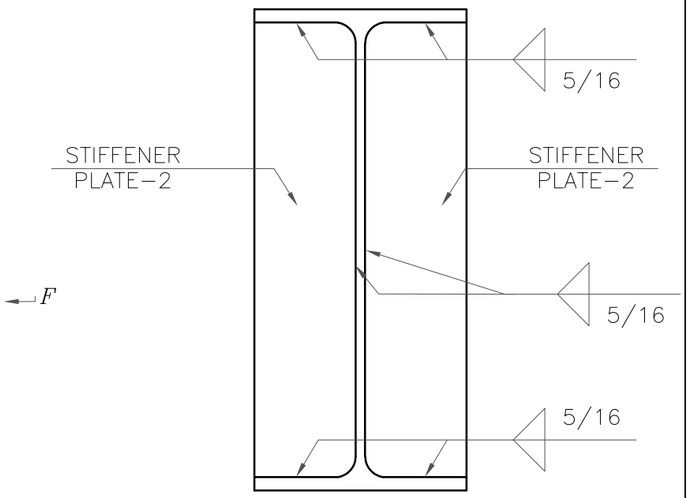

TYPICAL STIFFENER DETAIL FOR BEAM 6
Scale 1:5

GIRDER 4 (G–H) –W16X36
Scale 1:20

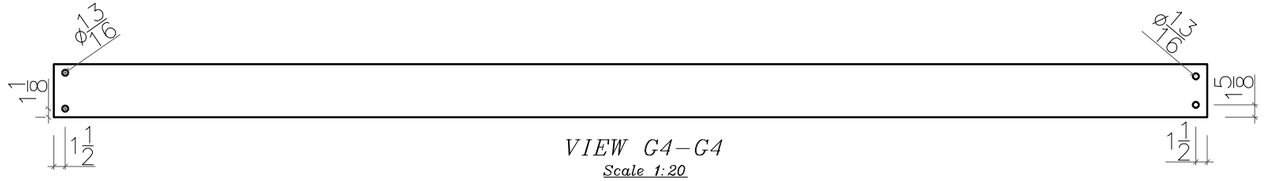

VIEW G4–G4
Scale 1:20

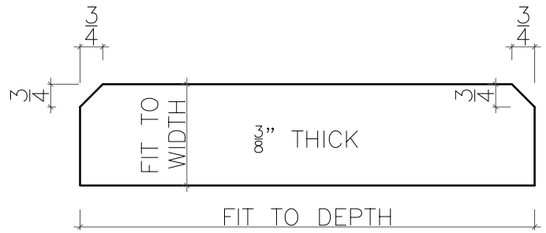

STIFFENER PLATE–2
(4 Pcs)
Scale 1:5

AUBURN UNIVERSITY
ADVANCED STRUCTURAL ENGINEERING LAB

PROJECT: *AISC SPEED CONNECT: DROP–IN TOP FLANGE CONNECTION*

Drawing Title: GIRDERS 3 & 4 AND BEAM STIFFENER DETAIL

DATE: DECEMBER 2024	DRAWING No.
DESIGNED BY R.A & E.D	11 of 12
DRAWN BY R.A & E.D	
CHECKED BY M.Y & K.S	

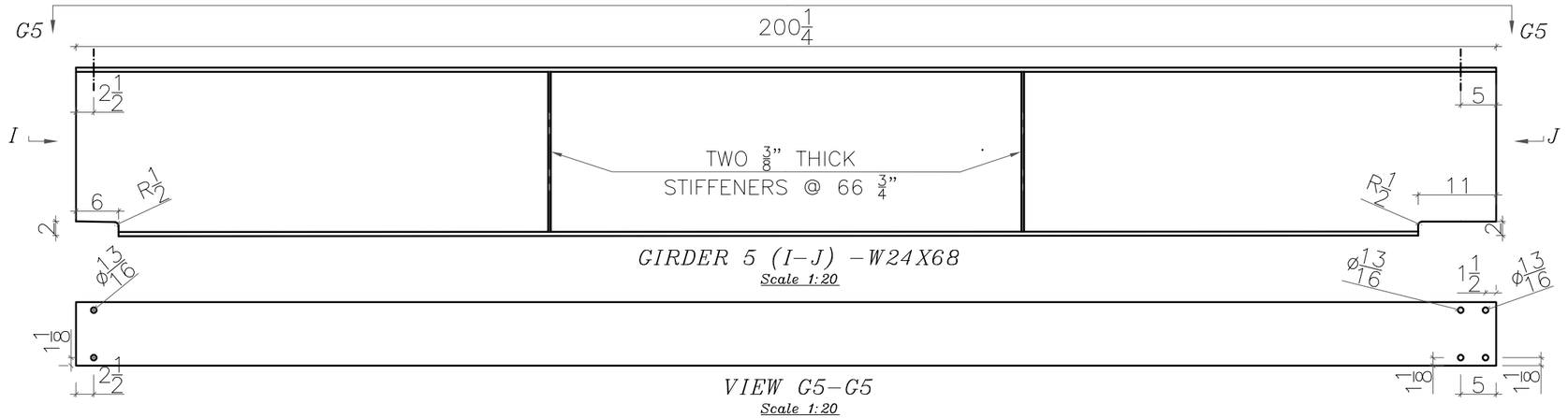

GIRDER 5 (I–J) –W24X68
Scale 1:20

VIEW G5–G5
Scale 1:20

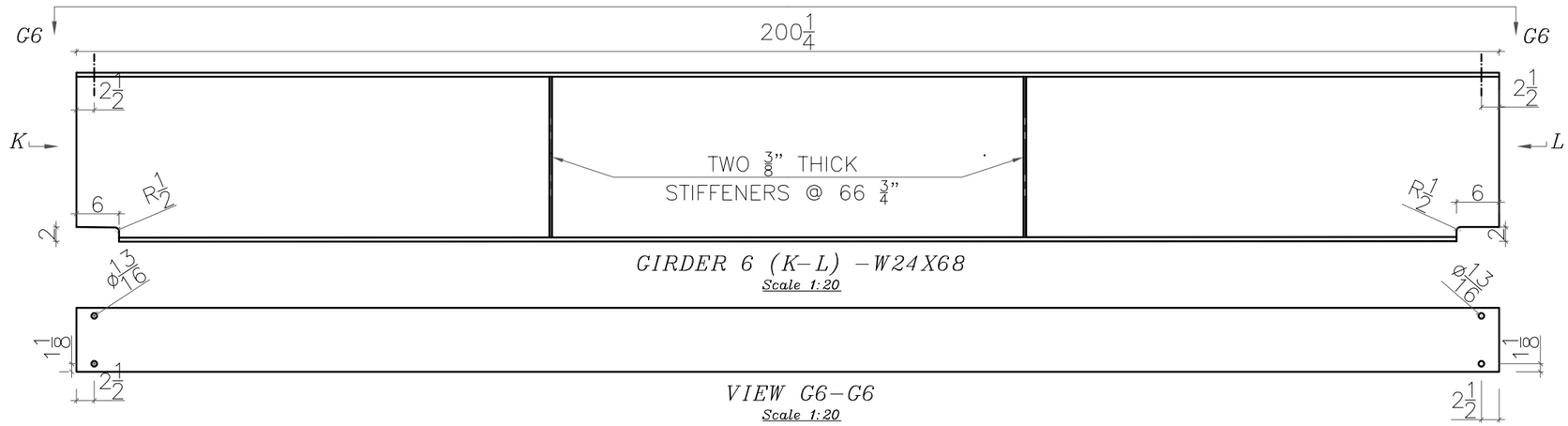

GIRDER 6 (K–L) –W24X68
Scale 1:20

VIEW G6–G6
Scale 1:20

AUBURN UNIVERSITY
ADVANCED STRUCTURAL ENGINEERING LAB

PROJECT: *AISC SPEED CONNECT: DROP–IN TOP FLANGE CONNECTION*

Drawing Title: GIRDERS 5 & 6

DATE: DECEMBER 2024	DRAWING No.
DESIGNED BY R.A & E.D	12 of 12
DRAWN BY R.A & E.D	
CHECKED BY M.Y & K.S	

Appendix C: Instrumentation Drawings

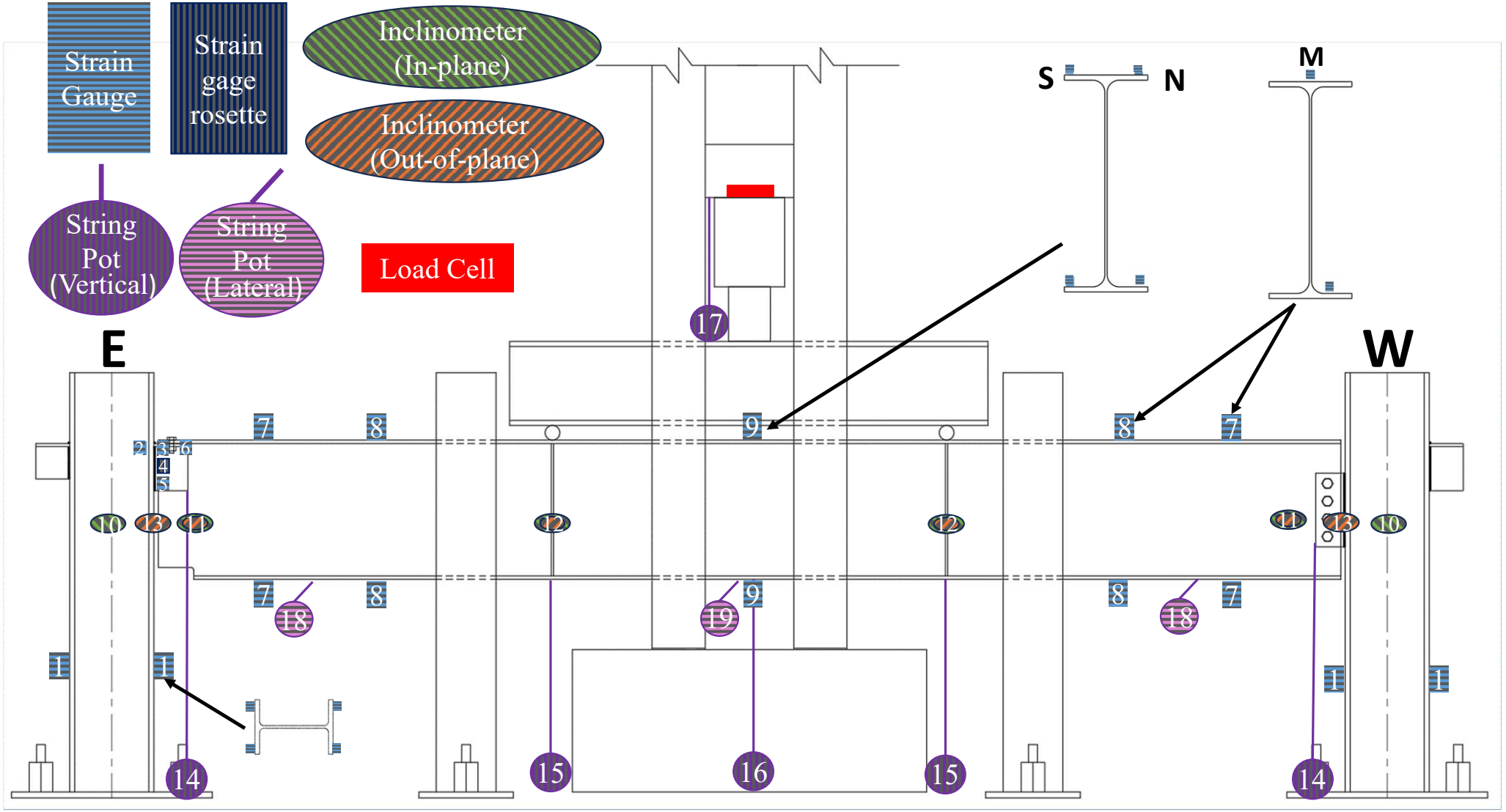

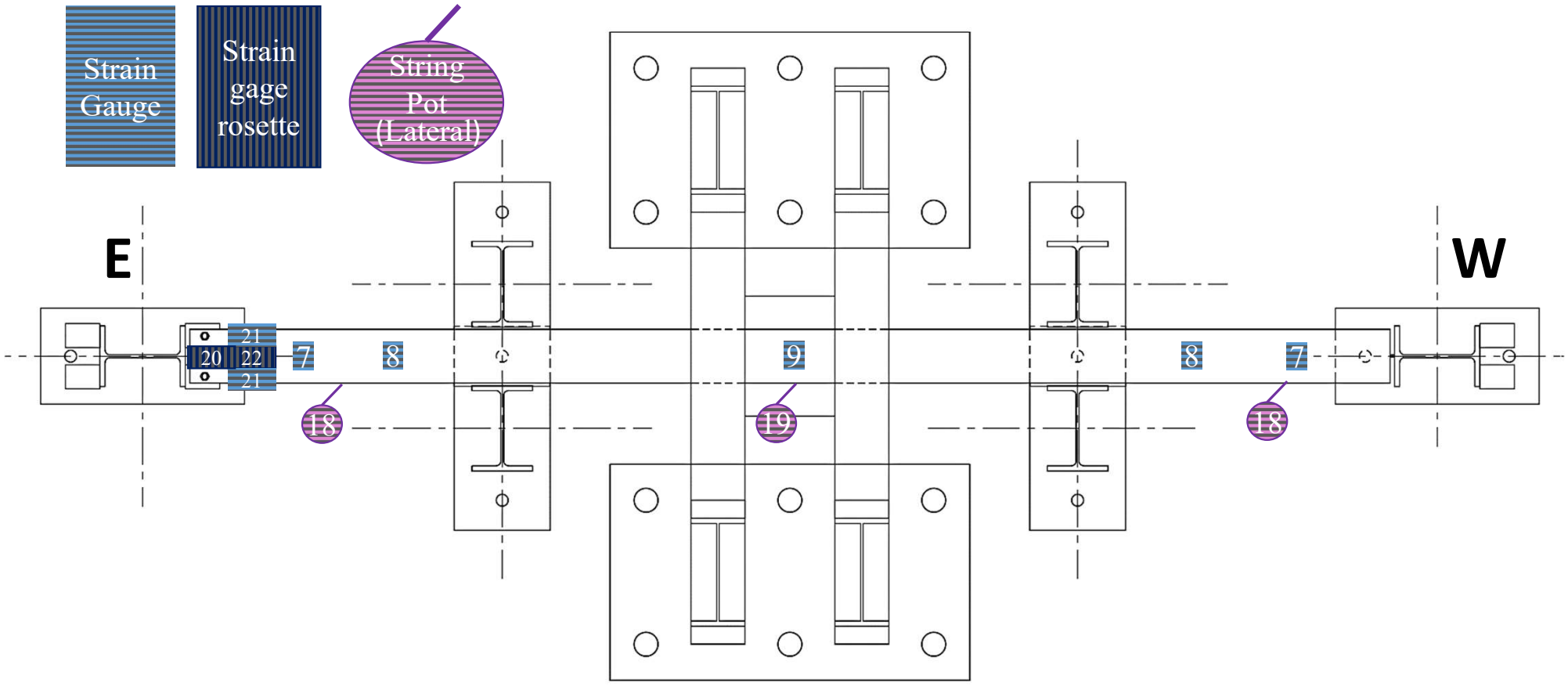
Strain Gauge
Strain gage rosette
String Pot (Lateral)
E
W
21
20
22
21
7
8
9
8
7
18
19
18

Appendix C: Instrumentation Drawings

All shown instrumentation is assumed to be present in all tests, unless noted otherwise.
[1] Located 2'-11" from top of baseplate and 1" from both North and South pointing flange edges
[2] Located approximately 4'-11" from top of baseplate (directly behind top of connection angle) and 1" from column web and 1" from column flange edge. Not present in Test-5.3 (Retrofit Connection) and Test-6 (Connection K and Connection L).
[3] Located 1" from bottom of top flange of angle and 1.5" from face of the column. Not present in Test-2.2 (Retrofit Connection) and Test-5.3 (Retrofit Connection).
[4] Located halfway between top and bottom of vertical leg and 1.5" from face of column. Not present in Test-2.2 (Retrofit Connection) and Test-5.3 (Retrofit Connection).
[5] Located 1" from bottom of angle and 1.5" from face of column. For 4" vertical legs, location is as close as possible to bottom of angle and 0.75" from face of column. Not present in Test-2.2 (Retrofit Connection)and Test-5.3 (Retrofit Connection).
[6] Located 1.5" from outside edge of angle and face of column for Test-1.1 and 1.2 (Connections A and B), Test-2.1 (Connections C and D), Test-3.1 and 3.2 (Connection E), Test-4.1 (Connections G and H), Test 4.2 (Connection G), Test-5.1, 5.2, and 5.3 (Connection I), and Test-6 (Connection K). Located 0.5" from outside edge of angle and 1" from face of column for Test-5.1 and 5.2 (Connection J) and Test-6 (Connection L). Not present in Test-2.2 (Retrofit Connection) and Test-5.3 (Retrofit Connection).
[7] Located 20" from end of girder/beam and centerline of top flange and 1 in. from centerline of bottom flange. Not present in Test-5.3(Retrofit Connection).
[8] Located 40" from end of girder/beam and centerline of top flange and 1 in. from centerline of bottom flange. Not present in Test-5.3(Retrofit Connection).
[9] Located at midspan of girder/beam and 1" from edge of flange.
[10] Located at midheight of girder/beam on centerline of column web. Not present in Test-2.1(Connections C and D) and Test-2.2(Retrofit Connection).
[11] Located 5" from end of girder/beam at midheight of girder/beam. In-plane inclinometer not present in Test-5.1, 5.2, and 5.3 (Connection J). Note that Connection J (Test-5.1, 5.2, and 5.3) and Connection L (Test-6.1) had in-plane inclinometer clamped to bottom flange at midspan. Out-of-plane inclinometer not present in Test-1.1 and 1.2 (Connections A and B),Test-2.1(Connections C and D), Test-2.2(Connection C), Test-3.1 and 3.2 (Connections E and F), Test-4.1 (Connections G and H), and Test-4.2 (Connection G). Neither in-plane or out-of-plane inclinometers present in Test-2.2(Retrofit Connection).
[12] Located at midheight of girder/beam at stiffener . In-plane inclinometer not present in Test-5.1, 5.2, and 5.3(Connections I and J) and Test-6.1(Connections K and L). Not present in Test-2.1 and 2.2 (Connections C and D) and Test-1.1 and 1.2 (A and B),
[13] Located on column flange edge at midheight of girder/beam. Only present in Test-5.1 and 5.2 (Connection I and J), Test-5.3 (Connection I), and Test-6.1 (Connections K and L).
[14] Located at midheight of vertical angle leg along edge. Not present in Test-2.2 (Retrofit Connection) and Test-5.3 (Retrofit Connection).
[15] Located on centerline of bottom flange at stiffener.
[16] Located on centerline of bottom flange at midspan of girder/beam.
[17] Located near actuator on bottom flange of header beam. Not present in Test-5.1,5.2,5.3, and Test-6.1.
[18] Located 25" from end of girder/beam on bottom flange edge. Not present in Test-2.1 (Retrofit Connection), Test-5.1 and 5.2 (Connections I and J), Test-5.3 (Connection I and Retrofit Connection), and Test-6.1 (Connections K and L).
[19] Located at midspan of girder/beam on both bottom and top flange edges. Both top and bottom are only present in Test-5.1 and Test-6.1. Only the bottom flange is present in Test-5.2 and 5.3
[20] Located directly on centerline of top flange between bolt holes. Not present in Test-1.1 and 1.2(Connection B), Test-3.1 and 3.2 (connection F), Test-4.1 (Connection H), Test-5.3 (Retrofit Connection).
[21] Located ¾" beyond transverse edge of angle and 1" from edge of top flange. Not present in Test-1.1 and 1.2 (Connection B), Test-3.1 and 3.2 (Connection F), Test-4.1 (Connection H), Test-5.1 and 5.2(Connection J), and Test 5.3 (Retrofit Connection).
[22] Located ¾" beyond transverse edge of angle and centerline of top flange. Not present in Test-1.1 and 1.2(Connection B), Test-3.1 and 3.2 (connection F), Test-4.1 (Connection H), and Test-5.3 (Retrofit Connection).

Appendix D: Drop-In Top Flange Connection Compatible Angles

Table 10-D provides geometrically compatible angles for W16 through W30 beam sections with a weight less than or equal to 100 lbs. per linear foot. Note the angles in this table only consider geometric constraints for erection and do not consider strength or ductility requirements (provided in a separate table).

The listed angles consider the supported beam's flange width (b_f), the angle's horizontal leg length (l_h), beam (k_1) and angle (k) fillet sizes, maximum fillet encroachment (E_n), entering and tightening (E&T) clearance, and required minimum transverse edge distance for the beam flange (l_{eb}) and angle (l_{ea}). Figure D-1 graphically illustrates the geometric constraints.

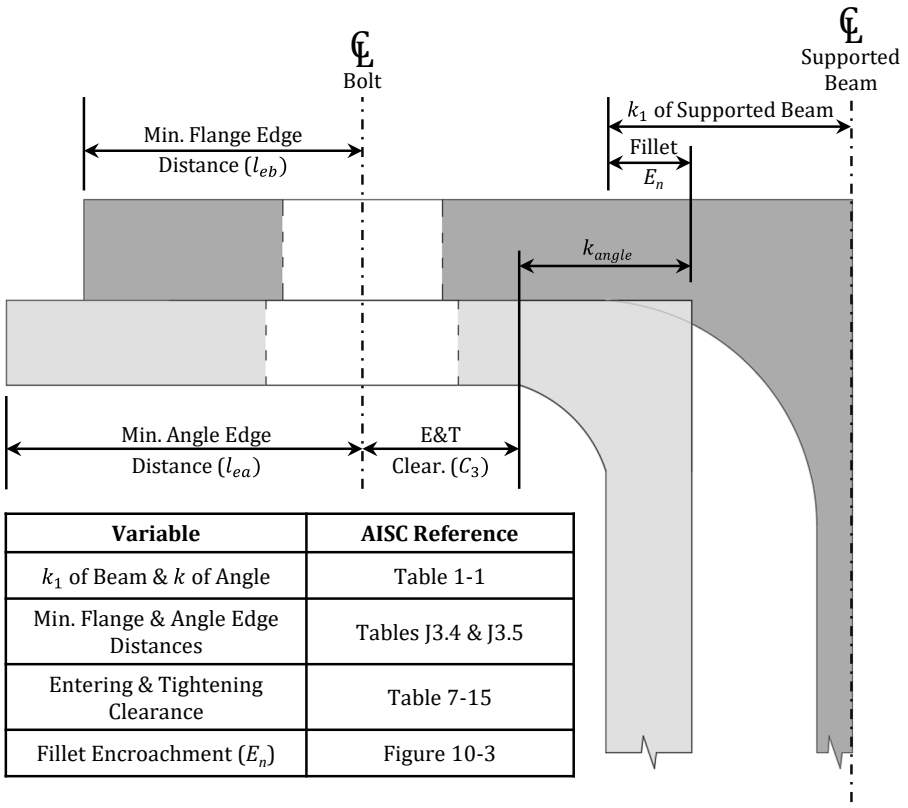

Variable	AISC Reference
k_1 of Beam & k of Angle	Table 1-1
Min. Flange & Angle Edge Distances	Tables J3.4 & J3.5
Entering & Tightening Clearance	Table 7-15
Fillet Encroachment (E_n)	Figure 10-3

Figure D-1: Geometric Constraints

Compatible angles are tabulated for A325-7/8 in. diameter bolts with an orientation in which the bolt head is seated on top of the supported beam flange. A bolt head placed on the underside of the angle will produce a greater range of compatible angle sections but is not considered in these tables. A standard hole is assumed to be utilized in the supported beam flange, while a standard short-slotted hole is in the angle (transverse to the longitudinal beam axis). The size of the bolt holes is as given in AISC Specification Table J3.3 (2022 edition).

Minimum edge distances are considered for both the supported beam and angle (defined according to AISC Specification Section J3.5). E&T clearance is considered to ensure adequate

room for field erection practices and assumes the maximum C3 value as noted in AISC Manual Table 7-15.

All listed angles in Table 10-D satisfy Equation 10-D1 to ensure adequate transverse edge distance of the angle according to the bolt diameter. The bolt centerline is determined from the left side of this equation.

$$l_h - k_{angle} - C_3 \geq l_{ea} \quad \text{(10-D1)}$$

where

l_h= horizontal leg dimension of angle, in.

k_{angle}= distance from the outer face of the angle's flange to the web toe of the fillet, in.

C_3= entering and tightening clearance (circular), in.

l_{ea}= minimum transverse edge distance for the angle, in.

A large percentage of the listed angles in Table 10-D satisfy Equation 10-D2 to ensure adequate transverse edge distance of the beam flange according to the bolt diameter. To provide more combinations, fillet encroachment is also considered. Angles in Table 10-D that are noted with an asterisk do not satisfy Equation 10-D2 but satisfy Equation 10-D3 utilizing encroachment. The maximum fillet encroachment is determined using the same approach as AISC Manual Figure 10-3 but in the horizontal direction.

$$\frac{b_f}{2} - k_1 - k_{angle} - C_3 \geq l_{eb} \quad \text{(10-D2)}$$

$$\frac{b_f}{2} - k_1 + E_n - k_{angle} - C_3 \geq l_{eb} \quad \text{(10-D3)}$$

where

b_f = width of supported beam top flange, in.

k_1 = distance from beam web centerline to flange toe of fillet, in.

l_{eb} = minimum transverse edge distance for the supported beam flange, in.

t_{wdet}= thickness of beam web used for detailing, in.

E_n= specified encroachment on the supported member fillet (see Table D-1), in.

Appendix D: Compatibility Tables

Table D-1: Fillet Encroachment (Riding the Fillet) (Units: Inches)

$k_1 - \frac{t_{wdet}}{2}$	E_n
5/16	1/8
3/8 to 1/2	3/16
9/16 to 13/16	1/4
7/8 to 1-1/4	5/16
1-5/16 to 1-3/8	3/8

The angles listed in Table 10-D assume that the minimum angle leg length is oriented horizontally for the drop-in top flange connect.

7/8-in. Bolts

W30x99

W30x90

Table 10-D

Drop-In Connection Compatible Angles

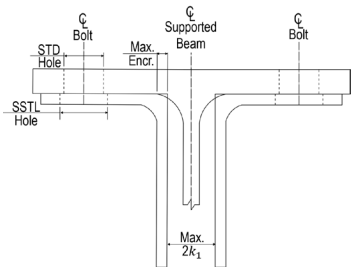

L12X12X1-1/4*	L7X4X3/4	L5X5X7/8	L4X4X3/4
L12X12X1-1/8*	L7X4X5/8	L5X5X3/4	L4X4X5/8
L12X12X1	L7X4X1/2	L5X5X5/8	L4X4X1/2
L10X10X1-1/4*	L7X4X7/16	L5X5X1/2	L4X4X7/16
L10X10X1-1/8*	L7X4X3/8	L5X5X7/16	L4X4X3/8
L10X10X1*	L6X6X1	L5X5X3/8	L4X4X5/16
L10X10X7/8	L6X6X7/8	L5X5X5/16	L4X4X1/4
L10X10X3/4	L6X6X3/4	L5X3-1/2X3/4	L4X3-1/2X1/2
L8X8X1-1/8	L6X6X5/8	L5X3-1/2X5/8	L4X3-1/2X3/8
L8X8X1	L6X6X9/16	L5X3-1/2X1/2	L4X3-1/2X5/16
L8X8X7/8	L6X6X1/2	L5X3-1/2X3/8	L4X3-1/2X1/4
L8X8X3/4	L6X6X7/16	L5X3-1/2X5/16	L4X3X1/2
L8X8X5/8	L6X6X3/8	L5X3-1/2X1/4	L4X3X3/8
L8X8X9/16	L6X6X5/16	L5X3X7/16	L4X3X5/16
L8X8X1/2	L6X4X7/8	L5X3X3/8	L4X3X1/4
L8X6X1	L6X4X3/4	L5X3X5/16	L3-1/2X3-1/2X1/2
L8X6X7/8	L6X4X5/8	L5X3X1/4	L3-1/2X3-1/2X7/16
L8X6X3/4	L6X4X9/16		L3-1/2X3-1/2X3/8
L8X6X5/8	L6X4X1/2		L3-1/2X3-1/2X5/16
L8X6X9/16	L6X4X7/16		L3-1/2X3-1/2X1/4
L8X6X1/2	L6X4X3/8		L3-1/2X3X1/2
L8X6X7/16	L6X4X5/16		L3-1/2X3X7/16
L8X4X1	L6X3-1/2X1/2		L3-1/2X3X3/8
L8X4X7/8	L6X3-1/2X3/8		L3-1/2X3X5/16
L8X4X3/4	L6X3-1/2X5/16		L3-1/2X3X1/4
L8X4X5/8			L3X3X1/2
L8X4X9/16			L3X3X7/16
L8X4X1/2			L3X3X3/8
L8X4X7/16			L3X3X5/16
			L3X3X1/4
			L3X3X3/16

Notes:
STD = Standard holes
SSTL = Short-slotted holes transverse to longitudinal beam axis
* = angle must encroach on beam fillet

7/8-in. Bolts
W27x94
W27x84

Table 10-D
Drop-In Connection
Compatible Angles

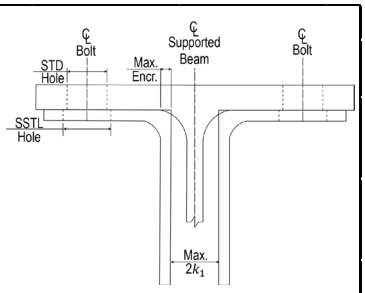

L12X12X1-1/8*	L7X4X3/4	L5X5X7/8	L4X4X3/4
L12X12X1*	L7X4X5/8	L5X5X3/4	L4X4X5/8
L10X10X1*	L7X4X1/2	L5X5X5/8	L4X4X1/2
L10X10X7/8*	L7X4X7/16	L5X5X1/2	L4X4X7/16
L10X10X3/4	L7X4X3/8	L5X5X7/16	L4X4X3/8
L8X8X1-1/8*	L6X6X1	L5X5X3/8	L4X4X5/16
L8X8X1*	L6X6X7/8	L5X5X5/16	L4X4X1/4
L8X8X7/8	L6X6X3/4	L5X3-1/2X3/4	L4X3-1/2X1/2
L8X8X3/4	L6X6X5/8	L5X3-1/2X5/8	L4X3-1/2X3/8
L8X8X5/8	L6X6X9/16	L5X3-1/2X1/2	L4X3-1/2X5/16
L8X8X9/16	L6X6X1/2	L5X3-1/2X3/8	L4X3-1/2X1/4
L8X8X1/2	L6X6X7/16	L5X3-1/2X5/16	L4X3X1/2
L8X6X1	L6X6X3/8	L5X3-1/2X1/4	L4X3X3/8
L8X6X7/8	L6X6X5/16	L5X3X7/16	L4X3X5/16
L8X6X3/4	L6X4X7/8	L5X3X3/8	L4X3X1/4
L8X6X5/8	L6X4X3/4	L5X3X5/16	L3-1/2X3-1/2X1/2
L8X6X9/16	L6X4X5/8	L5X3X1/4	L3-1/2X3-1/2X7/16
L8X6X1/2	L6X4X9/16		L3-1/2X3-1/2X3/8
L8X6X7/16	L6X4X1/2		L3-1/2X3-1/2X5/16
L8X4X1	L6X4X7/16		L3-1/2X3-1/2X1/4
L8X4X7/8	L6X4X3/8		L3-1/2X3X1/2
L8X4X3/4	L6X4X5/16		L3-1/2X3X7/16
L8X4X5/8	L6X3-1/2X1/2		L3-1/2X3X3/8
L8X4X9/16	L6X3-1/2X3/8		L3-1/2X3X5/16
L8X4X1/2	L6X3-1/2X5/16		L3-1/2X3X1/4
L8X4X7/16			L3X3X1/2
			L3X3X7/16
			L3X3X3/8
			L3X3X5/16
			L3X3X1/4
			L3X3X3/16

Notes:
STD = Standard holes
SSTL = Short-slotted holes transverse to longitudinal beam axis
* = angle must encroach on beam fillet

7/8-in. Bolts

W24x94

W24x84

Table 10-D

Drop-In Connection Compatible Angles

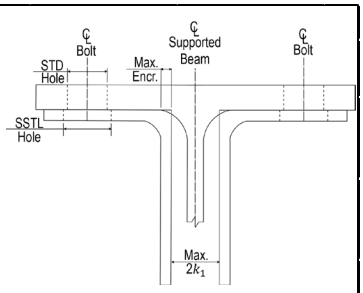

L8X8X3/4*	L7X4X3/4*	L5X5X7/8*	L4X4X3/4*
L8X8X5/8*	L7X4X5/8*	L5X5X3/4*	L4X4X5/8
L8X8X9/16*	L7X4X1/2	L5X5X5/8*	L4X4X1/2
L8X8X1/2*	L7X4X7/16	L5X5X1/2	L4X4X7/16
L8X6X7/8*	L7X4X3/8	L5X5X7/16	L4X4X3/8
L8X6X3/4*	L6X6X7/8*	L5X5X3/8	L4X4X5/16
L8X6X5/8*	L6X6X3/4*	L5X5X5/16	L4X4X1/4
L8X6X9/16	L6X6X5/8*	L5X3-1/2X3/4*	L4X3-1/2X1/2
L8X6X1/2	L6X6X9/16	L5X3-1/2X5/8	L4X3-1/2X3/8
L8X6X7/16	L6X6X1/2	L5X3-1/2X1/2	L4X3-1/2X5/16
L8X4X7/8*	L6X6X7/16	L5X3-1/2X3/8	L4X3-1/2X1/4
L8X4X3/4*	L6X6X3/8	L5X3-1/2X5/16	L4X3X1/2
L8X4X5/8*	L6X6X5/16	L5X3-1/2X1/4	L4X3X3/8
L8X4X9/16	L6X4X7/8*	L5X3X7/16	L4X3X5/16
L8X4X1/2	L6X4X3/4*	L5X3X3/8	L4X3X1/4
L8X4X7/16	L6X4X5/8*	L5X3X5/16	L3-1/2X3-1/2X1/2
	L6X4X9/16	L5X3X1/4	L3-1/2X3-1/2X7/16
	L6X4X1/2		L3-1/2X3-1/2X3/8
	L6X4X7/16		L3-1/2X3-1/2X5/16
	L6X4X3/8		L3-1/2X3-1/2X1/4
	L6X4X5/16		L3-1/2X3X1/2
	L6X3-1/2X1/2		L3-1/2X3X7/16
	L6X3-1/2X3/8		L3-1/2X3X3/8
	L6X3-1/2X5/16		L3-1/2X3X5/16
			L3-1/2X3X1/4
			L3X3X1/2
			L3X3X7/16
			L3X3X3/8
			L3X3X5/16
			L3X3X1/4
			L3X3X3/16

Notes:
STD = Standard holes
SSTL = Short-slotted holes transverse to longitudinal beam axis
* = angle must encroach on beam fillet

7/8 -in. Bolts

W24x76

W24x68

Table 10-D

Drop-In Connection Compatible Angles

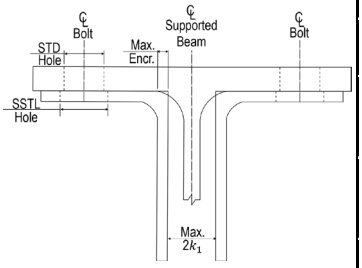

L8X8X5/8*	L7X4X3/4*	L5X5X3/4*	L4X4X3/4*
L8X8X9/16*	L7X4X5/8*	L5X5X5/8*	L4X4X5/8
L8X8X1/2*	L7X4X1/2	L5X5X1/2	L4X4X1/2
L8X6X3/4*	L7X4X7/16	L5X5X7/16	L4X4X7/16
L8X6X5/8*	L7X4X3/8	L5X5X3/8	L4X4X3/8
L8X6X9/16*	L6X6X3/4*	L5X5X5/16	L4X4X5/16
L8X6X1/2	L6X6X5/8*	L5X3-1/2X3/4*	L4X4X1/4
L8X6X7/16	L6X6X9/16*	L5X3-1/2X5/8*	L4X3-1/2X1/2
L8X4X3/4*	L6X6X1/2	L5X3-1/2X1/2	L4X3-1/2X3/8
L8X4X5/8*	L6X6X7/16	L5X3-1/2X3/8	L4X3-1/2X5/16
L8X4X9/16*	L6X6X3/8	L5X3-1/2X5/16	L4X3-1/2X1/4
L8X4X1/2	L6X6X5/16	L5X3-1/2X1/4	L4X3X1/2
L8X4X7/16	L6X4X3/4*	L5X3X7/16	L4X3X3/8
	L6X4X5/8*	L5X3X3/8	L4X3X5/16
	L6X4X9/16*	L5X3X5/16	L4X3X1/4
	L6X4X1/2	L5X3X1/4	L3-1/2X3-1/2X1/2
	L6X4X7/16		L3-1/2X3-1/2X7/16
	L6X4X3/8		L3-1/2X3-1/2X3/8
	L6X4X5/16		L3-1/2X3-1/2X5/16
	L6X3-1/2X1/2		L3-1/2X3-1/2X1/4
	L6X3-1/2X3/8		L3-1/2X3X1/2
	L6X3-1/2X5/16		L3-1/2X3X7/16
			L3-1/2X3X3/8
			L3-1/2X3X5/16
			L3-1/2X3X1/4
			L3X3X1/2
			L3X3X7/16
			L3X3X3/8
			L3X3X5/16
			L3X3X1/4
			L3X3X3/16

Notes:
STD = Standard holes
SSTL = Short-slotted holes transverse to longitudinal beam axis
* = angle must encroach on beam fillet

7/8 -in. Bolts

W24x62

W24x55

Table 10-D

Drop-In Connection Compatible Angles

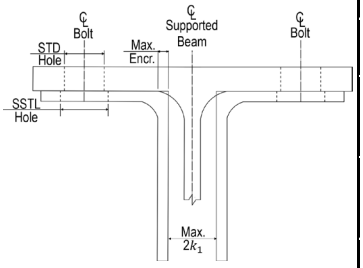

W24x62	W24x55
L5X3-1/2X1/4*	L5X3-1/2X5/16*
L5X3X1/4*	L5X3-1/2X1/4*
L4X4X5/16*	L5X3X5/16*
L4X4X1/4*	L5X3X1/4*
L4X3-1/2X5/16*	L4X4X3/8*
L4X3-1/2X1/4*	L4X4X5/16*
L4X3X5/16*	L4X4X1/4*
L4X3X1/4*	L4X3-1/2X3/8*
L3-1/2X3-1/2X5/16*	L4X3-1/2X5/16*
L3-1/2X3-1/2X1/4*	L4X3-1/2X1/4*
L3-1/2X3X5/16*	L4X3X3/8*
L3-1/2X3X1/4*	L4X3X5/16*
L3X3X5/16*	L4X3X1/4*
L3X3X1/4*	L3-1/2X3-1/2X3/8*
L3X3X3/16*	L3-1/2X3-1/2X5/16*
	L3-1/2X3-1/2X1/4*
	L3-1/2X3X3/8*
	L3-1/2X3X5/16*
	L3-1/2X3X1/4*
	L3X3X3/8*
	L3X3X5/16*
	L3X3X1/4*
	L3X3X3/16*

Notes:
STD = Standard holes
SSTL = Short-slotted holes transverse to longitudinal beam axis
* = angle must encroach on beam fillet

7/8 -in. Bolts
W21x93 W21x83
W21x73 W21x68
W21x62

Table 10-D
Drop-In Connection Compatible Angles

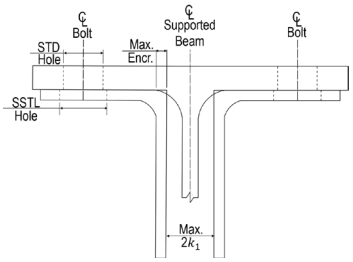

L8X8X7/8*	L7X4X3/4	L5X5X7/8*	L4X4X3/4
L8X8X3/4*	L7X4X5/8	L5X5X3/4	L4X4X5/8
L8X8X5/8	L7X4X1/2	L5X5X5/8	L4X4X1/2
L8X8X9/16	L7X4X7/16	L5X5X1/2	L4X4X7/16
L8X8X1/2	L7X4X3/8	L5X5X7/16	L4X4X3/8
L8X6X1*	L6X6X1*	L5X5X3/8	L4X4X5/16
L8X6X7/8*	L6X6X7/8*	L5X5X5/16	L4X4X1/4
L8X6X3/4	L6X6X3/4	L5X3-1/2X3/4	L4X3-1/2X1/2
L8X6X5/8	L6X6X5/8	L5X3-1/2X5/8	L4X3-1/2X3/8
L8X6X9/16	L6X6X9/16	L5X3-1/2X1/2	L4X3-1/2X5/16
L8X6X1/2	L6X6X1/2	L5X3-1/2X3/8	L4X3-1/2X1/4
L8X6X7/16	L6X6X7/16	L5X3-1/2X5/16	L4X3X1/2
L8X4X1*	L6X6X3/8	L5X3-1/2X1/4	L4X3X3/8
L8X4X7/8*	L6X6X5/16	L5X3X7/16	L4X3X5/16
L8X4X3/4	L6X4X7/8*	L5X3X3/8	L4X3X1/4
L8X4X5/8	L6X4X3/4	L5X3X5/16	L3-1/2X3-1/2X1/2
L8X4X9/16	L6X4X5/8	L5X3X1/4	L3-1/2X3-1/2X7/16
L8X4X1/2	L6X4X9/16		L3-1/2X3-1/2X3/8
L8X4X7/16	L6X4X1/2		L3-1/2X3-1/2X5/16
	L6X4X7/16		L3-1/2X3-1/2X1/4
	L6X4X3/8		L3-1/2X3X1/2
	L6X4X5/16		L3-1/2X3X7/16
	L6X3-1/2X1/2		L3-1/2X3X3/8
	L6X3-1/2X3/8		L3-1/2X3X5/16
	L6X3-1/2X5/16		L3-1/2X3X1/4
			L3X3X1/2
			L3X3X7/16
			L3X3X3/8
			L3X3X5/16
			L3X3X1/4
			L3X3X3/16

Notes:
STD = Standard holes
SSTL = Short-slotted holes transverse to longitudinal beam axis
* = angle must encroach on beam fillet

7/8-in. Bolts

W21x55

W21x48

Table 10-D

Drop-In Connection Compatible Angles

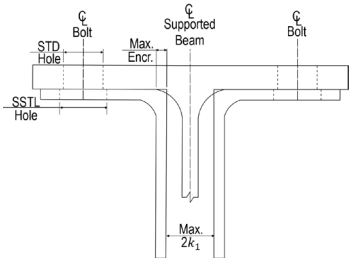

L8X8X7/8*	L7X4X3/4	L5X5X7/8*	L4X4X3/4
L8X8X3/4*	L7X4X5/8	L5X5X3/4	L4X4X5/8
L8X8X5/8	L7X4X1/2	L5X5X5/8	L4X4X1/2
L8X8X9/16	L7X4X7/16	L5X5X1/2	L4X4X7/16
L8X8X1/2	L7X4X3/8	L5X5X7/16	L4X4X3/8
L8X6X1*	L6X6X1*	L5X5X3/8	L4X4X5/16
L8X6X7/8*	L6X6X7/8*	L5X5X5/16	L4X4X1/4
L8X6X3/4	L6X6X3/4	L5X3-1/2X3/4	L4X3-1/2X1/2
L8X6X5/8	L6X6X5/8	L5X3-1/2X5/8	L4X3-1/2X3/8
L8X6X9/16	L6X6X9/16	L5X3-1/2X1/2	L4X3-1/2X5/16
L8X6X1/2	L6X6X1/2	L5X3-1/2X3/8	L4X3-1/2X1/4
L8X6X7/16	L6X6X7/16	L5X3-1/2X5/16	L4X3X1/2
L8X4X1*	L6X6X3/8	L5X3-1/2X1/4	L4X3X3/8
L8X4X7/8*	L6X6X5/16	L5X3X7/16	L4X3X5/16
L8X4X3/4	L6X4X7/8*	L5X3X3/8	L4X3X1/4
L8X4X5/8	L6X4X3/4	L5X3X5/16	L3-1/2X3-1/2X1/2
L8X4X9/16	L6X4X5/8	L5X3X1/4	L3-1/2X3-1/2X7/16
L8X4X1/2	L6X4X9/16		L3-1/2X3-1/2X3/8
L8X4X7/16	L6X4X1/2		L3-1/2X3-1/2X5/16
	L6X4X7/16		L3-1/2X3-1/2X1/4
	L6X4X3/8		L3-1/2X3X1/2
	L6X4X5/16		L3-1/2X3X7/16
	L6X3-1/2X1/2		L3-1/2X3X3/8
	L6X3-1/2X3/8		L3-1/2X3X5/16
	L6X3-1/2X5/16		L3-1/2X3X1/4
			L3X3X1/2
			L3X3X7/16
			L3X3X3/8
			L3X3X5/16
			L3X3X1/4
			L3X3X3/16

Notes:
STD = Standard holes
SSTL = Short-slotted holes transverse to longitudinal beam axis
* = angle must encroach on beam fillet

7/8 -in. Bolts

W21x57 W21x50
W21x44

Table 10-D
Drop-In Connection
Compatible Angles

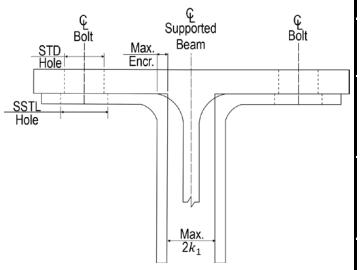

W21x57 and W21x50	W21x44
L5X3-1/2X1/4*	L4X4X1/4*
L5X3X1/4*	L4X3-1/2X1/4*
L4X4X5/16*	L4X3X1/4*
L4X4X1/4*	L3-1/2X3-1/2X1/4*
L4X3-1/2X5/16*	L3-1/2X3X1/4*
L4X3-1/2X1/4*	L3X3X1/4*
L4X3X5/16*	L3X3X3/16*
L4X3X1/4*	
L3-1/2X3-1/2X5/16*	
L3-1/2X3-1/2X1/4*	
L3-1/2X3X5/16*	
L3-1/2X3X1/4*	
L3X3X5/16*	
L3X3X1/4*	
L3X3X3/16*	

Notes:
STD = Standard holes
SSTL = Short-slotted holes transverse to longitudinal beam axis
* = angle must encroach on beam fillet

7/8 -in. Bolts

W18x97 W18x86 W18x76

Table 10-D

Drop-In Connection Compatible Angles

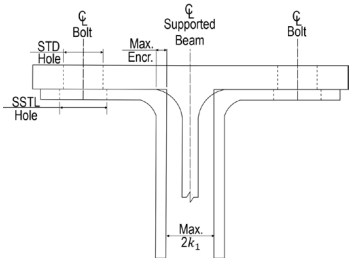

L12X12X1-3/8	L7X4X3/4	L5X5X7/8	L4X4X3/4
L12X12X1-1/4	L7X4X5/8	L5X5X3/4	L4X4X5/8
L12X12X1-1/8	L7X4X1/2	L5X5X5/8	L4X4X1/2
L12X12X1	L7X4X7/16	L5X5X1/2	L4X4X7/16
L10X10X1-3/8	L7X4X3/8	L5X5X7/16	L4X4X3/8
L10X10X1-1/4	L6X6X1	L5X5X3/8	L4X4X5/16
L10X10X1-1/8	L6X6X7/8	L5X5X5/16	L4X4X1/4
L10X10X1	L6X6X3/4	L5X3-1/2X3/4	L4X3-1/2X1/2
L10X10X7/8	L6X6X5/8	L5X3-1/2X5/8	L4X3-1/2X3/8
L10X10X3/4	L6X6X9/16	L5X3-1/2X1/2	L4X3-1/2X5/16
L8X8X1-1/8	L6X6X1/2	L5X3-1/2X3/8	L4X3-1/2X1/4
L8X8X1	L6X6X7/16	L5X3-1/2X5/16	L4X3X1/2
L8X8X7/8	L6X6X3/8	L5X3-1/2X1/4	L4X3X3/8
L8X8X3/4	L6X6X5/16	L5X3X7/16	L4X3X5/16
L8X8X5/8	L6X4X7/8	L5X3X3/8	L4X3X1/4
L8X8X9/16	L6X4X3/4	L5X3X5/16	L3-1/2X3-1/2X1/2
L8X8X1/2	L6X4X5/8	L5X3X1/4	L3-1/2X3-1/2X7/16
L8X6X1	L6X4X9/16		L3-1/2X3-1/2X3/8
L8X6X7/8	L6X4X1/2		L3-1/2X3-1/2X5/16
L8X6X3/4	L6X4X7/16		L3-1/2X3-1/2X1/4
L8X6X5/8	L6X4X3/8		L3-1/2X3X1/2
L8X6X9/16	L6X4X5/16		L3-1/2X3X7/16
L8X6X1/2	L6X3-1/2X1/2		L3-1/2X3X3/8
L8X6X7/16	L6X3-1/2X3/8		L3-1/2X3X5/16
L8X4X1	L6X3-1/2X5/16		L3-1/2X3X1/4
L8X4X7/8			L3X3X1/2
L8X4X3/4			L3X3X7/16
L8X4X5/8			L3X3X3/8
L8X4X9/16			L3X3X5/16
L8X4X1/2			L3X3X1/4
L8X4X7/16			L3X3X3/16

Notes:
STD = Standard holes
SSTL = Short-slotted holes transverse to longitudinal beam axis
* = angle must encroach on beam fillet

7/8 -in. Bolts

W18x71

Table 10-D
Drop-In Connection
Compatible Angles

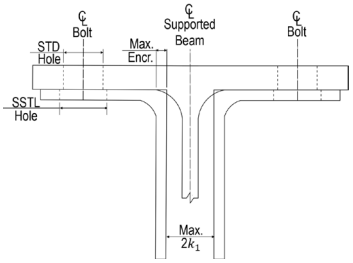

L8X8X9/16*	L7X4X5/8*	L5X5X5/8*	L4X4X3/4*
L8X8X1/2*	L7X4X1/2*	L5X5X1/2*	L4X4X5/8*
L8X6X5/8*	L7X4X7/16	L5X5X7/16	L4X4X1/2
L8X6X9/16*	L7X4X3/8	L5X5X3/8	L4X4X7/16
L8X6X1/2*	L6X6X5/8*	L5X5X5/16	L4X4X3/8
L8X6X7/16	L6X6X9/16*	L5X3-1/2X3/4*	L4X4X5/16
L8X4X5/8*	L6X6X1/2*	L5X3-1/2X5/8*	L4X4X1/4
L8X4X9/16*	L6X6X7/16	L5X3-1/2X1/2	L4X3-1/2X1/2
L8X4X1/2*	L6X6X3/8	L5X3-1/2X3/8	L4X3-1/2X3/8
L8X4X7/16	L6X6X5/16	L5X3-1/2X5/16	L4X3-1/2X5/16
	L6X4X5/8*	L5X3-1/2X1/4	L4X3-1/2X1/4
	L6X4X9/16*	L5X3X7/16	L4X3X1/2
	L6X4X1/2*	L5X3X3/8	L4X3X3/8
	L6X4X7/16	L5X3X5/16	L4X3X5/16
	L6X4X3/8	L5X3X1/4	L4X3X1/4
	L6X4X5/16		L3-1/2X3-1/2X1/2
	L6X3-1/2X1/2*		L3-1/2X3-1/2X7/16
	L6X3-1/2X3/8		L3-1/2X3-1/2X3/8
	L6X3-1/2X5/16		L3-1/2X3-1/2X5/16
			L3-1/2X3-1/2X1/4
			L3-1/2X3X1/2
			L3-1/2X3X7/16
			L3-1/2X3X3/8
			L3-1/2X3X5/16
			L3-1/2X3X1/4
			L3X3X1/2
			L3X3X7/16
			L3X3X3/8
			L3X3X5/16
			L3X3X1/4
			L3X3X3/16

Notes:
STD = Standard holes
SSTL = Short-slotted holes transverse to longitudinal beam axis
* = angle must encroach on beam fillet

7/8 -in. Bolts

W18x65

Table 10-D
Drop-In Connection
Compatible Angles

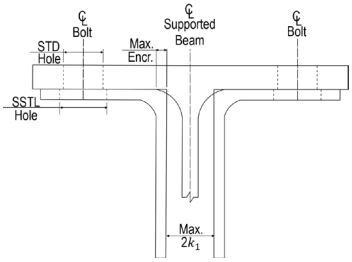

L8X8X1/2*	L7X4X5/8*	L5X5X5/8*	L4X4X3/4*
L8X6X5/8*	L7X4X1/2*	L5X5X1/2*	L4X4X5/8*
L8X6X9/16*	L7X4X7/16*	L5X5X7/16*	L4X4X1/2
L8X6X1/2*	L7X4X3/8	L5X5X3/8	L4X4X7/16
L8X6X7/16*	L6X6X5/8*	L5X5X5/16	L4X4X3/8
L8X4X5/8*	L6X6X9/16*	L5X3-1/2X5/8*	L4X4X5/16
L8X4X9/16*	L6X6X1/2*	L5X3-1/2X1/2*	L4X4X1/4
L8X4X1/2*	L6X6X7/16*	L5X3-1/2X3/8	L4X3-1/2X1/2
L8X4X7/16*	L6X6X3/8	L5X3-1/2X5/16	L4X3-1/2X3/8
	L6X6X5/16	L5X3-1/2X1/4	L4X3-1/2X5/16
	L6X4X5/8*	L5X3X7/16	L4X3-1/2X1/4
	L6X4X9/16*	L5X3X3/8	L4X3X1/2
	L6X4X1/2*	L5X3X5/16	L4X3X3/8
	L6X4X7/16*	L5X3X1/4	L4X3X5/16
	L6X4X3/8		L4X3X1/4
	L6X4X5/16		L3-1/2X3-1/2X1/2
	L6X3-1/2X1/2*		L3-1/2X3-1/2X7/16
	L6X3-1/2X3/8		L3-1/2X3-1/2X3/8
	L6X3-1/2X5/16		L3-1/2X3-1/2X5/16
			L3-1/2X3-1/2X1/4
			L3-1/2X3X1/2
			L3-1/2X3X7/16
			L3-1/2X3X3/8
			L3-1/2X3X5/16
			L3-1/2X3X1/4
			L3X3X1/2
			L3X3X7/16
			L3X3X3/8
			L3X3X5/16
			L3X3X1/4
			L3X3X3/16

Notes:
STD = Standard holes
SSTL = Short-slotted holes transverse to longitudinal beam axis
* = angle must encroach on beam fillet

7/8-in. Bolts

W18x60
W18x55

Table 10-D
Drop-In Connection Compatible Angles

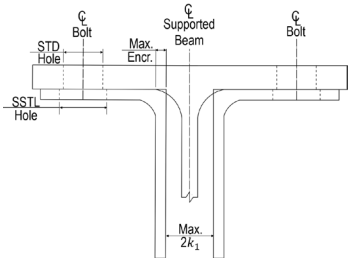

L8X8X9/16*	L7X4X5/8*	L5X5X5/8*	L4X4X3/4*
L8X8X1/2*	L7X4X1/2*	L5X5X1/2*	L4X4X5/8*
L8X6X5/8*	L7X4X7/16	L5X5X7/16	L4X4X1/2
L8X6X9/16*	L7X4X3/8	L5X5X3/8	L4X4X7/16
L8X6X1/2*	L6X6X5/8*	L5X5X5/16	L4X4X3/8
L8X6X7/16	L6X6X9/16*	L5X3-1/2X3/4*	L4X4X5/16
L8X4X5/8*	L6X6X1/2*	L5X3-1/2X5/8*	L4X4X1/4
L8X4X9/16*	L6X6X7/16	L5X3-1/2X1/2	L4X3-1/2X1/2
L8X4X1/2*	L6X6X3/8	L5X3-1/2X3/8	L4X3-1/2X3/8
L8X4X7/16	L6X6X5/16	L5X3-1/2X5/16	L4X3-1/2X5/16
	L6X4X5/8*	L5X3-1/2X1/4	L4X3-1/2X1/4
	L6X4X9/16*	L5X3X7/16	L4X3X1/2
	L6X4X1/2*	L5X3X3/8	L4X3X3/8
	L6X4X7/16	L5X3X5/16	L4X3X5/16
	L6X4X3/8	L5X3X1/4	L4X3X1/4
	L6X4X5/16		L3-1/2X3-1/2X1/2
	L6X3-1/2X1/2*		L3-1/2X3-1/2X7/16
	L6X3-1/2X3/8		L3-1/2X3-1/2X3/8
	L6X3-1/2X5/16		L3-1/2X3-1/2X5/16
			L3-1/2X3-1/2X1/4
			L3-1/2X3X1/2
			L3-1/2X3X7/16
			L3-1/2X3X3/8
			L3-1/2X3X5/16
			L3-1/2X3X1/4
			L3X3X1/2
			L3X3X7/16
			L3X3X3/8
			L3X3X5/16
			L3X3X1/4
			L3X3X3/16

Notes:
STD = Standard holes
SSTL = Short-slotted holes transverse to longitudinal beam axis
* = angle must encroach on beam fillet

7/8 -in. Bolts

W18x50

Table 10-D
Drop-In Connection
Compatible Angles

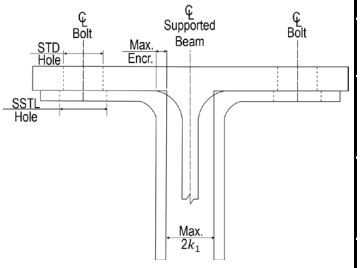

L8X8X1/2*	L7X4X5/8*	L5X5X5/8*	L4X4X3/4*
L8X6X5/8*	L7X4X1/2*	L5X5X1/2*	L4X4X5/8*
L8X6X9/16*	L7X4X7/16*	L5X5X7/16*	L4X4X1/2
L8X6X1/2*	L7X4X3/8	L5X5X3/8	L4X4X7/16
L8X6X7/16*	L6X6X5/8*	L5X5X5/16	L4X4X3/8
L8X4X5/8*	L6X6X9/16*	L5X3-1/2X5/8*	L4X4X5/16
L8X4X9/16*	L6X6X1/2*	L5X3-1/2X1/2*	L4X4X1/4
L8X4X1/2*	L6X6X7/16*	L5X3-1/2X3/8	L4X3-1/2X1/2
L8X4X7/16*	L6X6X3/8	L5X3-1/2X5/16	L4X3-1/2X3/8
	L6X6X5/16	L5X3-1/2X1/4	L4X3-1/2X5/16
	L6X4X5/8*	L5X3X7/16	L4X3-1/2X1/4
	L6X4X9/16*	L5X3X3/8	L4X3X1/2
	L6X4X1/2*	L5X3X5/16	L4X3X3/8
	L6X4X7/16*	L5X3X1/4	L4X3X5/16
	L6X4X3/8		L4X3X1/4
	L6X4X5/16		L3-1/2X3-1/2X1/2
	L6X3-1/2X1/2*		L3-1/2X3-1/2X7/16
	L6X3-1/2X3/8		L3-1/2X3-1/2X3/8
	L6X3-1/2X5/16		L3-1/2X3-1/2X5/16
			L3-1/2X3-1/2X1/4
			L3-1/2X3X1/2
			L3-1/2X3X7/16
			L3-1/2X3X3/8
			L3-1/2X3X5/16
			L3-1/2X3X1/4
			L3X3X1/2
			L3X3X7/16
			L3X3X3/8
			L3X3X5/16
			L3X3X1/4
			L3X3X3/16

Notes:
STD = Standard holes
SSTL = Short-slotted holes transverse to longitudinal beam axis
* = angle must encroach on beam fillet

7/8 -in. Bolts

W16x100

Table 10-D
Drop-In Connection
Compatible Angles

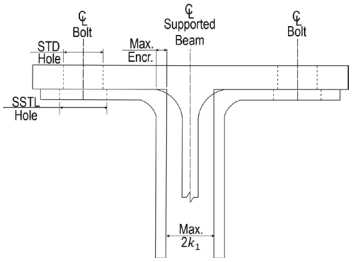

L12X12X1-3/8*	L7X4X3/4	L5X5X7/8	L4X4X3/4
L12X12X1-1/4	L7X4X5/8	L5X5X3/4	L4X4X5/8
L12X12X1-1/8	L7X4X1/2	L5X5X5/8	L4X4X1/2
L12X12X1	L7X4X7/16	L5X5X1/2	L4X4X7/16
L10X10X1-3/8*	L7X4X3/8	L5X5X7/16	L4X4X3/8
L10X10X1-1/4	L6X6X1	L5X5X3/8	L4X4X5/16
L10X10X1-1/8	L6X6X7/8	L5X5X5/16	L4X4X1/4
L10X10X1	L6X6X3/4	L5X3-1/2X3/4	L4X3-1/2X1/2
L10X10X7/8	L6X6X5/8	L5X3-1/2X5/8	L4X3-1/2X3/8
L10X10X3/4	L6X6X9/16	L5X3-1/2X1/2	L4X3-1/2X5/16
L8X8X1-1/8	L6X6X1/2	L5X3-1/2X3/8	L4X3-1/2X1/4
L8X8X1	L6X6X7/16	L5X3-1/2X5/16	L4X3X1/2
L8X8X7/8	L6X6X3/8	L5X3-1/2X1/4	L4X3X3/8
L8X8X3/4	L6X6X5/16	L5X3X7/16	L4X3X5/16
L8X8X5/8	L6X4X7/8	L5X3X3/8	L4X3X1/4
L8X8X9/16	L6X4X3/4	L5X3X5/16	L3-1/2X3-1/2X1/2
L8X8X1/2	L6X4X5/8	L5X3X1/4	L3-1/2X3-1/2X7/16
L8X6X1	L6X4X9/16		L3-1/2X3-1/2X3/8
L8X6X7/8	L6X4X1/2		L3-1/2X3-1/2X5/16
L8X6X3/4	L6X4X7/16		L3-1/2X3-1/2X1/4
L8X6X5/8	L6X4X3/8		L3-1/2X3X1/2
L8X6X9/16	L6X4X5/16		L3-1/2X3X7/16
L8X6X1/2	L6X3-1/2X1/2		L3-1/2X3X3/8
L8X6X7/16	L6X3-1/2X3/8		L3-1/2X3X5/16
L8X4X1	L6X3-1/2X5/16		L3-1/2X3X1/4
L8X4X7/8			L3X3X1/2
L8X4X3/4			L3X3X7/16
L8X4X5/8			L3X3X3/8
L8X4X9/16			L3X3X5/16
L8X4X1/2			L3X3X1/4
L8X4X7/16			L3X3X3/16

Notes:
STD = Standard holes
SSTL = Short-slotted holes transverse to longitudinal beam axis
* = angle must encroach on beam fillet

7/8-in. Bolts

W16x89

Table 10-D

Drop-In Connection Compatible Angles

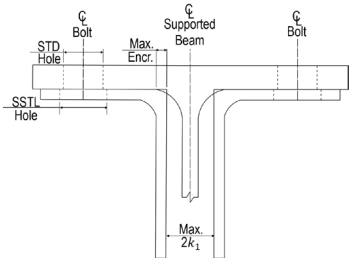

L12X12X1-3/8	L7X4X3/4	L5X5X7/8	L4X4X3/4
L12X12X1-1/4	L7X4X5/8	L5X5X3/4	L4X4X5/8
L12X12X1-1/8	L7X4X1/2	L5X5X5/8	L4X4X1/2
L12X12X1	L7X4X7/16	L5X5X1/2	L4X4X7/16
L10X10X1-3/8*	L7X4X3/8	L5X5X7/16	L4X4X3/8
L10X10X1-1/4	L6X6X1	L5X5X3/8	L4X4X5/16
L10X10X1-1/8	L6X6X7/8	L5X5X5/16	L4X4X1/4
L10X10X1	L6X6X3/4	L5X3-1/2X3/4	L4X3-1/2X1/2
L10X10X7/8	L6X6X5/8	L5X3-1/2X5/8	L4X3-1/2X3/8
L10X10X3/4	L6X6X9/16	L5X3-1/2X1/2	L4X3-1/2X5/16
L8X8X1-1/8	L6X6X1/2	L5X3-1/2X3/8	L4X3-1/2X1/4
L8X8X1	L6X6X7/16	L5X3-1/2X5/16	L4X3X1/2
L8X8X7/8	L6X6X3/8	L5X3-1/2X1/4	L4X3X3/8
L8X8X3/4	L6X6X5/16	L5X3X7/16	L4X3X5/16
L8X8X5/8	L6X4X7/8	L5X3X3/8	L4X3X1/4
L8X8X9/16	L6X4X3/4	L5X3X5/16	L3-1/2X3-1/2X1/2
L8X8X1/2	L6X4X5/8	L5X3X1/4	L3-1/2X3-1/2X7/16
L8X6X1	L6X4X9/16		L3-1/2X3-1/2X3/8
L8X6X7/8	L6X4X1/2		L3-1/2X3-1/2X5/16
L8X6X3/4	L6X4X7/16		L3-1/2X3-1/2X1/4
L8X6X5/8	L6X4X3/8		L3-1/2X3X1/2
L8X6X9/16	L6X4X5/16		L3-1/2X3X7/16
L8X6X1/2	L6X3-1/2X1/2		L3-1/2X3X3/8
L8X6X7/16	L6X3-1/2X3/8		L3-1/2X3X5/16
L8X4X1	L6X3-1/2X5/16		L3-1/2X3X1/4
L8X4X7/8			L3X3X1/2
L8X4X3/4			L3X3X7/16
L8X4X5/8			L3X3X3/8
L8X4X9/16			L3X3X5/16
L8X4X1/2			L3X3X1/4
L8X4X7/16			L3X3X3/16

Notes:
STD = Standard holes
SSTL = Short-slotted holes transverse to longitudinal beam axis
* = angle must encroach on beam fillet

7/8 -in. Bolts

W16x77

Table 10-D
Drop-In Connection
Compatible Angles

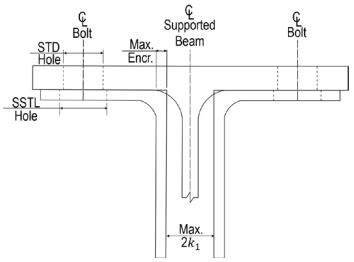

L12X12X1-3/8*	L7X4X3/4	L5X5X7/8	L4X4X3/4
L12X12X1-1/4	L7X4X5/8	L5X5X3/4	L4X4X5/8
L12X12X1-1/8	L7X4X1/2	L5X5X5/8	L4X4X1/2
L12X12X1	L7X4X7/16	L5X5X1/2	L4X4X7/16
L10X10X1-3/8*	L7X4X3/8	L5X5X7/16	L4X4X3/8
L10X10X1-1/4	L6X6X1	L5X5X3/8	L4X4X5/16
L10X10X1-1/8	L6X6X7/8	L5X5X5/16	L4X4X1/4
L10X10X1	L6X6X3/4	L5X3-1/2X3/4	L4X3-1/2X1/2
L10X10X7/8	L6X6X5/8	L5X3-1/2X5/8	L4X3-1/2X3/8
L10X10X3/4	L6X6X9/16	L5X3-1/2X1/2	L4X3-1/2X5/16
L8X8X1-1/8	L6X6X1/2	L5X3-1/2X3/8	L4X3-1/2X1/4
L8X8X1	L6X6X7/16	L5X3-1/2X5/16	L4X3X1/2
L8X8X7/8	L6X6X3/8	L5X3-1/2X1/4	L4X3X3/8
L8X8X3/4	L6X6X5/16	L5X3X7/16	L4X3X5/16
L8X8X5/8	L6X4X7/8	L5X3X3/8	L4X3X1/4
L8X8X9/16	L6X4X3/4	L5X3X5/16	L3-1/2X3-1/2X1/2
L8X8X1/2	L6X4X5/8	L5X3X1/4	L3-1/2X3-1/2X7/16
L8X6X1	L6X4X9/16		L3-1/2X3-1/2X3/8
L8X6X7/8	L6X4X1/2		L3-1/2X3-1/2X5/16
L8X6X3/4	L6X4X7/16		L3-1/2X3-1/2X1/4
L8X6X5/8	L6X4X3/8		L3-1/2X3X1/2
L8X6X9/16	L6X4X5/16		L3-1/2X3X7/16
L8X6X1/2	L6X3-1/2X1/2		L3-1/2X3X3/8
L8X6X7/16	L6X3-1/2X3/8		L3-1/2X3X5/16
L8X4X1	L6X3-1/2X5/16		L3-1/2X3X1/4
L8X4X7/8			L3X3X1/2
L8X4X3/4			L3X3X7/16
L8X4X5/8			L3X3X3/8
L8X4X9/16			L3X3X5/16
L8X4X1/2			L3X3X1/4
L8X4X7/16			L3X3X3/16

Notes:
STD = Standard holes
SSTL = Short-slotted holes transverse to longitudinal beam axis
* = angle must encroach on beam fillet

7/8 -in. Bolts

W16x67

Table 10-D

Drop-In Connection Compatible Angles

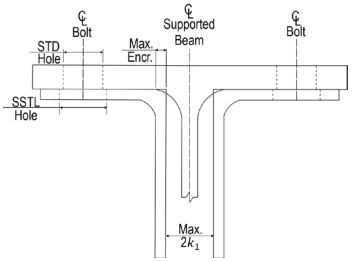

L12X12X1-3/8	L7X4X3/4	L5X5X7/8	L4X4X3/4
L12X12X1-1/4	L7X4X5/8	L5X5X3/4	L4X4X5/8
L12X12X1-1/8	L7X4X1/2	L5X5X5/8	L4X4X1/2
L12X12X1	L7X4X7/16	L5X5X1/2	L4X4X7/16
L10X10X1-3/8*	L7X4X3/8	L5X5X7/16	L4X4X3/8
L10X10X1-1/4	L6X6X1	L5X5X3/8	L4X4X5/16
L10X10X1-1/8	L6X6X7/8	L5X5X5/16	L4X4X1/4
L10X10X1	L6X6X3/4	L5X3-1/2X3/4	L4X3-1/2X1/2
L10X10X7/8	L6X6X5/8	L5X3-1/2X5/8	L4X3-1/2X3/8
L10X10X3/4	L6X6X9/16	L5X3-1/2X1/2	L4X3-1/2X5/16
L8X8X1-1/8	L6X6X1/2	L5X3-1/2X3/8	L4X3-1/2X1/4
L8X8X1	L6X6X7/16	L5X3-1/2X5/16	L4X3X1/2
L8X8X7/8	L6X6X3/8	L5X3-1/2X1/4	L4X3X3/8
L8X8X3/4	L6X6X5/16	L5X3X7/16	L4X3X5/16
L8X8X5/8	L6X4X7/8	L5X3X3/8	L4X3X1/4
L8X8X9/16	L6X4X3/4	L5X3X5/16	L3-1/2X3-1/2X1/2
L8X8X1/2	L6X4X5/8	L5X3X1/4	L3-1/2X3-1/2X7/16
L8X6X1	L6X4X9/16		L3-1/2X3-1/2X3/8
L8X6X7/8	L6X4X1/2		L3-1/2X3-1/2X5/16
L8X6X3/4	L6X4X7/16		L3-1/2X3-1/2X1/4
L8X6X5/8	L6X4X3/8		L3-1/2X3X1/2
L8X6X9/16	L6X4X5/16		L3-1/2X3X7/16
L8X6X1/2	L6X3-1/2X1/2		L3-1/2X3X3/8
L8X6X7/16	L6X3-1/2X3/8		L3-1/2X3X5/16
L8X4X1	L6X3-1/2X5/16		L3-1/2X3X1/4
L8X4X7/8			L3X3X1/2
L8X4X3/4			L3X3X7/16
L8X4X5/8			L3X3X3/8
L8X4X9/16			L3X3X5/16
L8X4X1/2			L3X3X1/4
L8X4X7/16			L3X3X3/16

Notes:
STD = Standard holes
SSTL = Short-slotted holes transverse to longitudinal beam axis
* = angle must encroach on beam fillet

7/8-in. Bolts

W16x57

Table 10-D

Drop-In Connection Compatible Angles

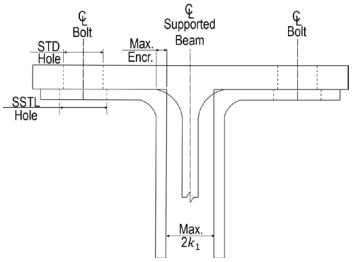

L7X4X3/8*	L4X4X1/2*
L6X6X3/8*	L4X4X7/16*
L6X6X5/16*	L4X4X3/8*
L6X4X3/8*	L4X4X5/16*
L6X4X5/16*	L4X4X1/4
L6X3-1/2X3/8*	L4X3-1/2X1/2*
L6X3-1/2X5/16*	L4X3-1/2X3/8*
L5X5X3/8*	L4X3-1/2X5/16*
L5X5X5/16*	L4X3-1/2X1/4
L5X3-1/2X3/8*	L4X3X1/2*
L5X3-1/2X5/16*	L4X3X3/8*
L5X3-1/2X1/4*	L4X3X5/16*
L5X3X7/16*	L4X3X1/4
L5X3X3/8*	L3-1/2X3-1/2X1/2*
L5X3X5/16*	L3-1/2X3-1/2X7/16*
L5X3X1/4*	L3-1/2X3-1/2X3/8*
	L3-1/2X3-1/2X5/16*
	L3-1/2X3-1/2X1/4
	L3-1/2X3X1/2*
	L3-1/2X3X7/16*
	L3-1/2X3X3/8*
	L3-1/2X3X5/16*
	L3-1/2X3X1/4
	L3X3X1/2*
	L3X3X7/16*
	L3X3X3/8*
	L3X3X5/16*
	L3X3X1/4
	L3X3X3/16

Notes:
STD = Standard holes
SSTL = Short-slotted holes transverse to longitudinal beam axis
* = angle must encroach on beam fillet

7/8 -in. Bolts

W16x50

W16x45

Table 10-D

Drop-In Connection Compatible Angles

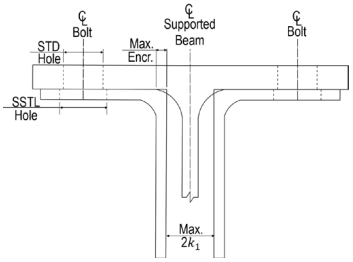

L8X6X7/16*	L7X4X7/16*	L5X5X7/16*	L4X4X1/2*
L8X4X7/16*	L7X4X3/8*	L5X5X3/8*	L4X4X7/16*
	L6X6X7/16*	L5X5X5/16*	L4X4X3/8*
	L6X6X3/8*	L5X3-1/2X1/2*	L4X4X5/16
	L6X6X5/16*	L5X3-1/2X3/8*	L4X4X1/4
	L6X4X7/16*	L5X3-1/2X5/16*	L4X3-1/2X1/2*
	L6X4X3/8*	L5X3-1/2X1/4	L4X3-1/2X3/8*
	L6X4X5/16*	L5X3X7/16*	L4X3-1/2X5/16
	L6X3-1/2X3/8*	L5X3X3/8*	L4X3-1/2X1/4
	L6X3-1/2X5/16*	L5X3X5/16*	L4X3X1/2*
		L5X3X1/4	L4X3X3/8*
			L4X3X5/16
			L4X3X1/4
			L3-1/2X3-1/2X1/2*
			L3-1/2X3-1/2X7/16*
			L3-1/2X3-1/2X3/8*
			L3-1/2X3-1/2X5/16
			L3-1/2X3-1/2X1/4
			L3-1/2X3X1/2*
			L3-1/2X3X7/16*
			L3-1/2X3X3/8*
			L3-1/2X3X5/16
			L3-1/2X3X1/4
			L3X3X1/2*
			L3X3X7/16*
			L3X3X3/8*
			L3X3X5/16
			L3X3X1/4
			L3X3X3/16

Notes:
STD = Standard holes
SSTL = Short-slotted holes transverse to longitudinal beam axis
* = angle must encroach on beam fillet

7/8-in. Bolts
W16x40
W16x36

Table 10-D
Drop-In Connection
Compatible Angles

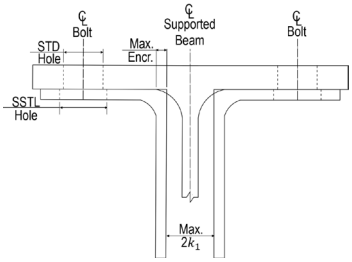

W16x40		W16x36	
L7X4X3/8*	L4X4X1/2*	L8X6X7/16*	L4X4X1/2*
L6X6X3/8*	L4X4X7/16*	L8X4X7/16*	L4X4X7/16*
L6X6X5/16*	L4X4X3/8*	L7X4X7/16*	L4X4X3/8*
L6X4X3/8*	L4X4X5/16*	L7X4X3/8*	L4X4X5/16
L6X4X5/16*	L4X4X1/4	L6X6X7/16*	L4X4X1/4
L6X3-1/2X3/8*	L4X3-1/2X1/2*	L6X6X3/8*	L4X3-1/2X1/2*
L6X3-1/2X5/16*	L4X3-1/2X3/8*	L6X6X5/16*	L4X3-1/2X3/8*
L5X5X3/8*	L4X3-1/2X5/16*	L6X4X7/16*	L4X3-1/2X5/16
L5X5X5/16*	L4X3-1/2X1/4	L6X4X3/8*	L4X3-1/2X1/4
L5X3-1/2X3/8*	L4X3X1/2*	L6X4X5/16*	L4X3X1/2*
L5X3-1/2X5/16*	L4X3X3/8*	L6X3-1/2X3/8*	L4X3X3/8*
L5X3-1/2X1/4*	L4X3X5/16*	L6X3-1/2X5/16*	L4X3X5/16
L5X3X7/16*	L4X3X1/4	L5X5X7/16*	L4X3X1/4
L5X3X3/8*	L3-1/2X3-1/2X1/2*	L5X5X3/8*	L3-1/2X3-1/2X1/2*
L5X3X5/16*	L3-1/2X3-1/2X7/16*	L5X5X5/16*	L3-1/2X3-1/2X7/16*
L5X3X1/4*	L3-1/2X3-1/2X3/8*	L5X3-1/2X1/2*	L3-1/2X3-1/2X3/8*
	L3-1/2X3-1/2X5/16*	L5X3-1/2X3/8*	L3-1/2X3-1/2X5/16
	L3-1/2X3-1/2X1/4	L5X3-1/2X5/16*	L3-1/2X3-1/2X1/4
	L3-1/2X3X1/2*	L5X3-1/2X1/4	L3-1/2X3X1/2*
	L3-1/2X3X7/16*	L5X3X7/16*	L3-1/2X3X7/16*
	L3-1/2X3X3/8*	L5X3X3/8*	L3-1/2X3X3/8*
	L3-1/2X3X5/16*	L5X3X5/16*	L3-1/2X3X5/16
	L3-1/2X3X1/4	L5X3X1/4	L3-1/2X3X1/4
	L3X3X1/2*		L3X3X1/2*
	L3X3X7/16*		L3X3X7/16*
	L3X3X3/8*		L3X3X3/8*
	L3X3X5/16*		L3X3X5/16
	L3X3X1/4		L3X3X1/4
	L3X3X3/16		L3X3X3/16

Notes:
STD = Standard holes
SSTL = Short-slotted holes transverse to longitudinal beam axis
* = angle must encroach on beam fillet

Appendix E: Design Table

Drop-In Top Flange Connections

A drop-in top flange connection is made when a supported member is seated on the bottom of the top flange, as illustrated in Figure E-1. In this connection, angles are shop welded to a steel element (e.g., column), as illustrated in Figure E-1 (Section A-A). The supported member is coped on the bottom flange to allow for a vertical drop-in erection. The final connection is made via vertical bolts, attaching the top flange of the supported member to the angles. Horizontal short-slotted holes are recommended for the angles.

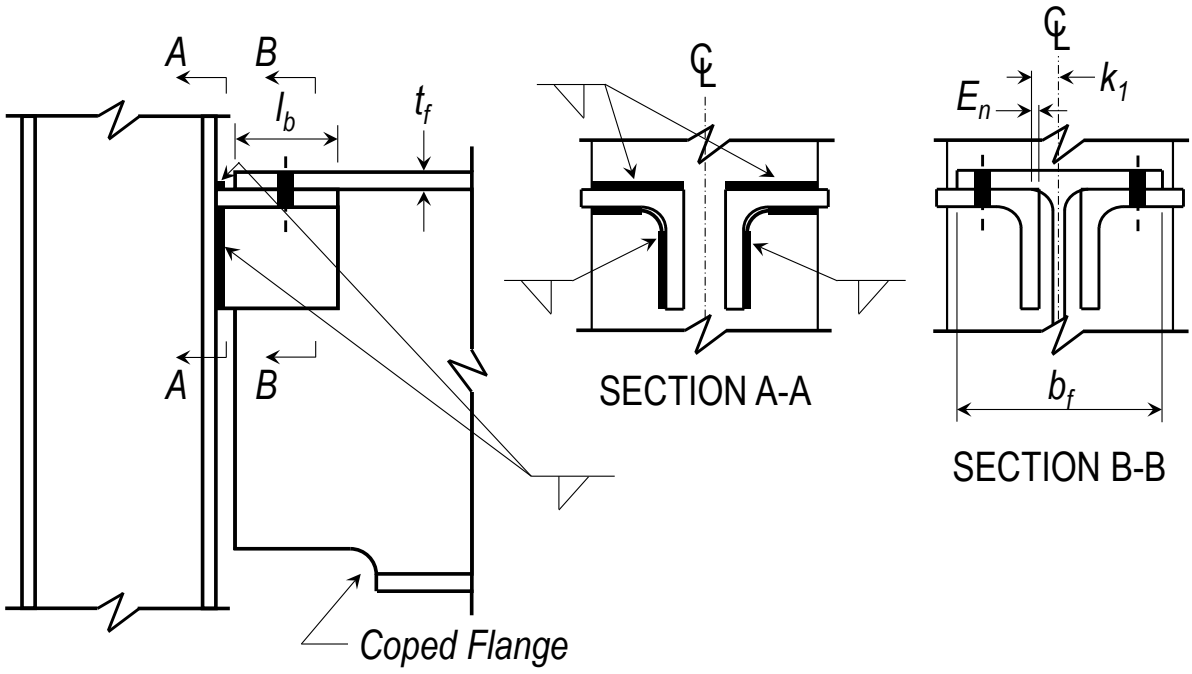

Figure E-1: Drop-In Top Flange Connection

Dimensional Limitations

1. The minimum flange edge distance for the bolt and the minimum angle horizontal edge distance (illustrated in Figure E-2) should satisfy AISC Spec. J3.4 and J3.5.
2. The entering and tightening (E&T) clearance for bolt installation adjacent to the vertical leg of the angle (illustrated in Figure E-2) should satisfy AISC Manual Table 7-15.
3. The horizontal proximity of the angle to the supporting member may encroach up to the values provided in AISC Manual Figure 10-3.
4. The supporting member flange thickness and depth should not exceed 1.0 in. and 30 in., respectively.
5. The supporting member bearing length (l_b) on the angles should range from 3.0 in. to 8.0 in.

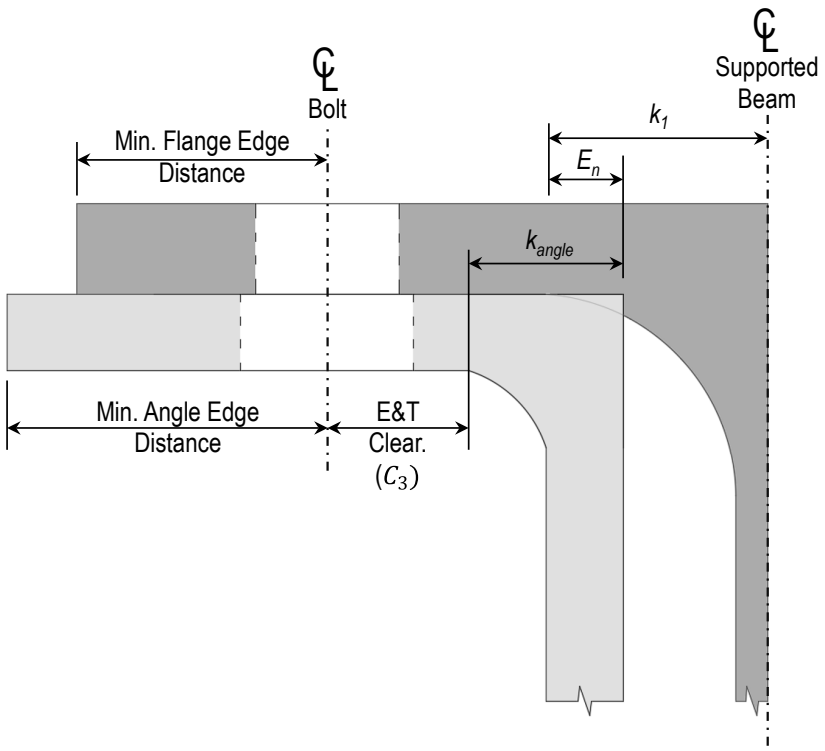

Figure E-2: Dimensional Limitations for Connection Assembly

Design Checks

1. Weld group available strength should be checked in accordance with AISC Spec J2 and Manual Part 8.
2. Flange bending available strength should be determined as follows.

$$R_{nFB} = \frac{{t_f}^2}{a} F_{yf} b \qquad \text{(E-1)}$$

where

t_f = thickness of flange, in.
F_{yf} = specified minimum yield stress of the flange, in.
a = $0.75k_1 - E_n$
k_1 = distance from the supporting member centerline to the toe of the fillet, in.
E_n = specified encroachment of the angles on the supported member fillet, in.
b = $l_b + 0.25b_f$
l_b = supporting member bearing length, in.
b_f = width of the flange, in.
ϕ = 0.90 (LRFD)
Ω = 1.67 (ASD)

3. Angle shear available strength should be checked in accordance with AISC Spec G3.
4. Supported member shear capacity should be checked in accordance with AISC Spec G, accounting for the coped flange.

5. Bolt available strength must be in accordance with AISC Spec J3 and Manual Part 7.
6. In all cases, the available strength, ϕR_n or R_n/Ω, must equal or exceed the required strength, R_r.

Design Table Discussion

Table 10-E is a design aid for drop-in top flange connections for conventional (not extended) configurations. Available strengths are provided for the supported member flange bending (left side) and the connection angles (right side). The flange bending available strength assumes the back corner of the angles are located at the toe of the supported member fillet (no encroachment). The flange bending available strength is provided for common W-shapes with a bearing length (l_b) of 4 in. or 8 in. Bearing lengths between these values can be linearly interpolated. The available strength of the angles is the combined shear capacity of both angles.

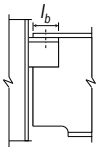

Table 10-E
Drop-In Connetions

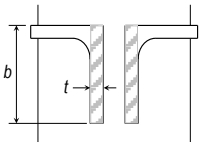

Flange Bending Available Strength, kips

Shape	l_b = 4 in		l_b = 8 in	
	ASD	LRFD	ASD	LRFD
W27X84	73.9	111.1	119.4	179.5
W24X84	103.0	154.8	168.9	253.8
W24X76	80.2	120.6	131.6	197.8
W24X68	59.3	89.2	97.3	146.3
W24X62	75.3	113.2	127.6	191.9
W24X55	58.6	88.0	99.3	149.2
W21X83	193.7	291.2	321.0	482.4
W21X73	151.8	228.1	251.7	378.3
W21X68	129.9	195.2	215.5	323.9
W21X62	112.6	169.3	186.9	281.0
W21X55	81.1	121.8	134.6	202.3
W21X48	54.8	82.4	91.2	137.0
W18X86	150.9	226.8	240.0	360.8
W18X76	117.3	176.3	186.8	280.7
W18X71	176.9	265.9	296.6	445.8
W18X65	151.3	227.5	254.0	381.8
W18X60	139.8	210.1	234.7	352.8
W18X55	114.7	172.4	192.7	289.7
W18X50	93.8	141.0	157.6	236.9
W16X89	189.9	285.4	304.9	458.3
W16X77	142.7	214.5	229.5	344.9
W16X67	115.6	173.8	186.2	279.9
W16X57	134.8	202.6	228.1	342.8
W16X50	112.5	169.0	190.5	286.3
W16X45	90.3	135.8	153.1	230.1
W16X40	72.0	108.3	122.2	183.6
W16X36	56.6	85.0	95.9	144.2
W14X82	179.2	269.4	289.1	434.5
W14X74	151.1	227.1	243.7	366.3
W14X68	126.6	190.3	204.5	307.4
W14X61	108.0	162.2	174.4	262.1
W14X53	104.6	157.2	174.2	261.8
W14X48	84.9	127.6	141.4	212.6
W14X43	67.3	101.1	112.1	168.5
W12X87	173.2	260.3	271.8	408.5
W12X79	142.6	214.3	223.8	336.3
W12X72	118.1	177.4	185.5	278.8
W12X65	102.3	153.7	160.7	241.6
W12X58	113.4	170.4	183.1	275.3
W12X53	91.5	137.5	147.8	222.2
W12X50	105.0	157.8	174.8	262.7
W12X45	84.6	127.2	141.0	211.9
W12X40	72.6	109.2	121.0	181.9
Beam			ASD	LRFD
F_y = 50 ksi			Ω = 1.67	ϕ = 0.90

Angles Available Strength, kips

Angle Vertical Leg		ASD	LRFD
b, in	t, in		
10	1	359.3	540.0
	7/8	314.4	472.5
	3/4	269.5	405.0
8	1 1/8	323.4	486.0
	1	287.4	432.0
	7/8	251.5	378.0
	3/4	215.6	324.0
	5/8	179.6	270.0
	9/16	161.7	243.0
	1/2	143.7	216.0
	7/16	125.7	189.0
7	3/4	188.6	283.5
	5/8	157.2	236.3
	1/2	125.7	189.0
	7/16	110.0	165.4
	3/8	94.3	141.8
6	1	215.6	324.0
	7/8	188.6	283.5
	3/4	161.7	243.0
	5/8	134.7	202.5
	9/16	121.3	182.3
	1/2	107.8	162.0
	7/16	94.3	141.8
	3/8	80.8	121.5
	5/16	67.4	101.3
5	7/8	157.2	236.3
	3/4	134.7	202.5
	5/8	112.3	168.8
	1/2	89.8	135.0
	7/16	78.6	118.1
	3/8	67.4	101.3
	5/16	56.1	84.4
4	3/4	107.8	162.0
	5/8	89.8	135.0
	1/2	71.9	108.0
	7/16	62.9	94.5
	3/8	53.9	81.0
3 1/2	1/2	62.9	94.5
	7/16	55.0	82.7
Angles		ASD	LRFD
F_y = 50 ksi		Ω = 1.67	ϕ = 0.90

Design Examples: Drop-In Top Flange Connection

Example F.1: Drop-In Connection (Conventional Girder-to-Column Flange)

Given:

Verify a drop-in top flange connection between an ASTM A992 W24×68 girder and an ASTM W14×82 column flange, as shown in Figure F.1, to support the following girder end reactions.

$R_D := 25\ \textit{kip}$ $R_L := 30\ \textit{kip}$

Use 70-ksi electrodes and an ASTM A572 Grade 50 angles.

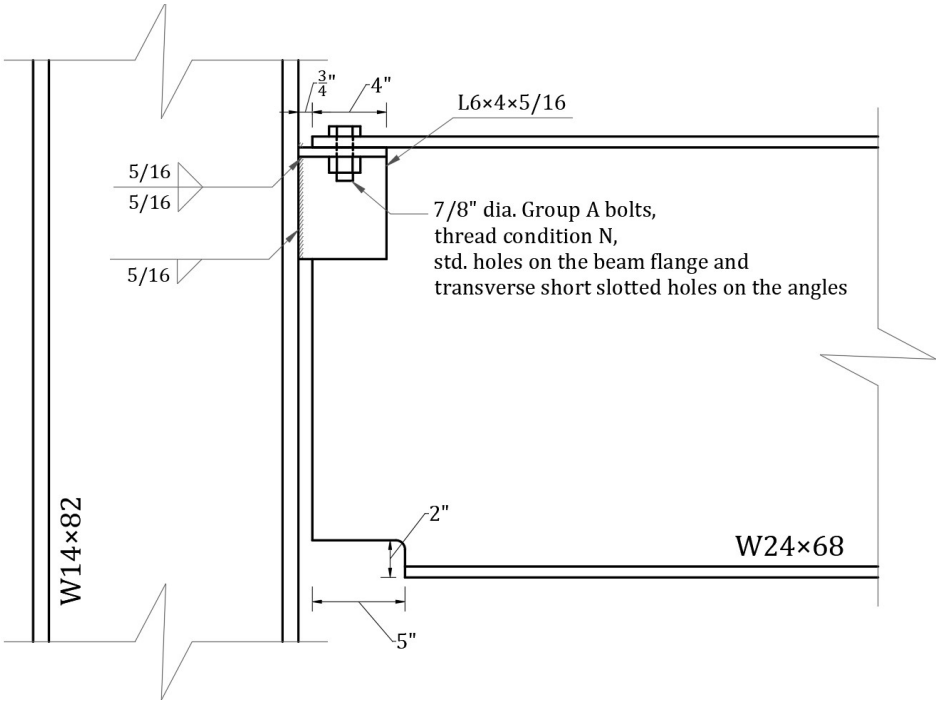

Fig. F.1. Connection geometry for Example F.1

Solution:

From AISC *Manual* Table 2-4, the material properties are as follows:

Beam and Column	Angles
ASTM A992	ASTM A572 Gr.50
$F_y := 50\ \textit{ksi}$	$F_y := 50\ \textit{ksi}$
$F_u := 65\ \textit{ksi}$	$F_u := 65\ \textit{ksi}$

From AISC *Manual* Table 1-1, the geometric properties are as follows:

Beam	Angles
W24×68	L6×4×5/16
$b_f := 8.97\ in$	$b := 6\ in$
$t_f := 0.585\ in$	$l_h := 4\ in$
$d := 23.7\ in$	$t := 0.3125\ in$
$t_w := 0.415\ in$	$k_{angle} := 0.8125\ in$
$k_1 := 1.4375\ in$	

The bearing length $l_b := 4.0\ in$

From ASCE/SEI 7, Chapter 2, the required strength is:

LRFD	**ASD**
$R_u := 1.2 \cdot R_D + 1.6 \cdot R_L$	$R_a := R_D + R_L$
$R_u = 78\ kip$	$R_a = 55\ kip$

Connection Selection

Phase 4 - Design guidance of the report includes checks for the compatibility, weld limit state, flange bending limit state, angle shear limit state, and girder shear limit state.

Compatibility Check

Check geometric compatibility between the angles and girder flange in accordance with Appendix D.

Entering and tightening clearance, AISC *Manual* Table 7-15 $C_3 := 0.875\ in$

Minimum transverse edge distance for the angle, AISC *Manual* Table J3.4 and Table J3.5 $l_{ea} := 1.25\ in$

Minimum transverse edge distance for the girder, AISC *Manual* Table J3.4 $l_{eb} := 1.125\ in$

No encroachment $E_n := 0\ in$

Ensure adequate transverse edge distance of the angle according to the bolt diameter, Equation 10-D1

$l_h - k_{angle} - C_3 = 2.313\ in$

$l_{ea} = 1.25\ in$

$l_h - k_{angle} - C_3 \geq l_{ea}$ **o.k.**

Ensure adequate transverse edge distance of the beam flange according to the bolt diameter, equation 10-D2 and 10-D3

$0.5 \cdot b_f - k_1 + E_n - k_{angle} - C_3 = 1.36$ *in*

$l_{eb} = 1.125$ *in*

$0.5 \cdot b_f - k_1 + E_n - k_{angle} - C_3 \geq l_{eb}$ **o.k.**

Alternatively, L6×4×5/16 is listed under W24×68 in Table 10-D, does not have an asterisk indicating that the angle and girder are geometrically compatible without the angle encroaching on the girder fillet.

Weld limit state

The design of the weld group for attaching the angles to the column flange should be in accordance with AISC Spec J2 and AISC Manual Part 8. The instantaneous center of rotation (ICR) method is utilized, also outlined in AISC Manual Part 8, using an eccentricity equal to the distance between the weld group and the bolt center line.

The weld length accounts for termination equal to the weld length at the ends of each weld line. The weld along the fillet is conservatively neglected in the calculations.

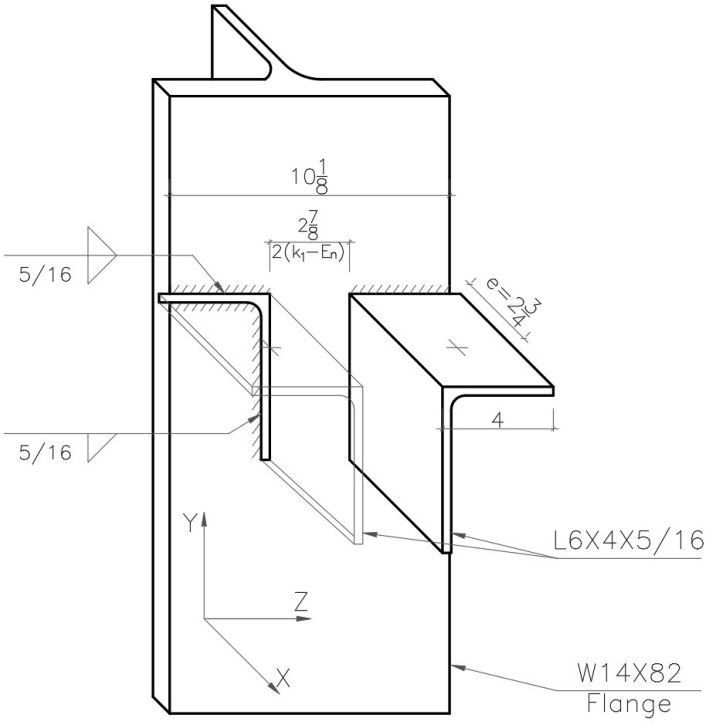

$l_{w\_Horizontal\_Top} := 2.9875$ *in*

$l_{w\_Horizontal\_Bott} := 2.1750$ *in*

$l_{w\_Vertical} := 4.5625$ *in*

It should be noted that the horizontal angle legs extend beyond the width of the column flange, and the horizontal weld lines end at the edge of the column flange.

The iterative solution of the ICR method at the final iteration step is shown in the table below. The variables listed in the table are defined in the AISC Manual Part 8. The vertical weld is divided into 20 equal-length elements, while the horizontal weld lines are divided into 10 equal-length elements.

Weld Position	Element number	Element coordinate y (in)	r (in)	θ (deg)	Δ_{ni} (in)	Δ_{ui} (in)	Δ_{ui} / r_i	Δ_i (in)	P_i	F_{nwi} (ksi)	A_{wei} (in²)	R_n (Kip)	R_{nx} (Kip)	R_{ny} (Kip)	M_{nIC} (Kip.in)
Vertical	1	0.11	4.49	78.12	0.0161	0.0191	0.0042	0.0191	1.19	62.09	0.10	6.26	6.13	1.29	28.14
	2	0.34	4.27	77.49	0.0161	0.0191	0.0045	0.0181	1.12	62.23	0.10	6.27	6.12	1.36	26.80
	3	0.57	4.05	76.79	0.0161	0.0192	0.0048	0.0172	1.06	62.22	0.10	6.27	6.11	1.43	25.40
	4	0.80	3.83	76.01	0.0162	0.0194	0.0051	0.0162	1.00	62.07	0.10	6.26	6.07	1.51	23.95
	5	1.03	3.61	75.13	0.0163	0.0195	0.0054	0.0153	0.94	61.78	0.10	6.23	6.02	1.60	22.47
	6	1.25	3.39	74.14	0.0163	0.0197	0.0058	0.0144	0.88	61.34	0.10	6.18	5.95	1.69	20.95
	7	1.48	3.17	73.01	0.0164	0.0198	0.0063	0.0134	0.82	60.74	0.10	6.12	5.86	1.79	19.40
	8	1.71	2.95	71.72	0.0165	0.0201	0.0068	0.0125	0.76	59.97	0.10	6.05	5.74	1.90	17.84
	9	1.94	2.73	70.22	0.0166	0.0203	0.0074	0.0116	0.70	59.02	0.10	5.95	5.60	2.01	16.27
	10	2.17	2.52	68.46	0.0167	0.0206	0.0082	0.0107	0.64	57.87	0.10	5.83	5.43	2.14	14.71
	11	2.40	2.31	66.39	0.0169	0.0210	0.0091	0.0098	0.58	56.48	0.10	5.69	5.22	2.28	13.16
	12	2.62	2.10	63.90	0.0171	0.0215	0.0102	0.0089	0.52	54.83	0.10	5.53	4.96	2.43	11.63
	13	2.85	1.90	60.87	0.0174	0.0221	0.0116	0.0081	0.46	52.87	0.10	5.33	4.66	2.59	10.14
	14	3.08	1.71	57.14	0.0177	0.0230	0.0135	0.0072	0.41	50.54	0.10	5.10	4.28	2.76	8.69
	15	3.31	1.52	52.46	0.0182	0.0241	0.0159	0.0064	0.35	47.76	0.10	4.82	3.82	2.93	7.32
	16	3.54	1.35	46.54	0.0189	0.0259	0.0192	0.0057	0.30	44.46	0.10	4.48	3.25	3.08	6.03
	17	3.76	1.19	38.96	0.0199	0.0286	0.0240	0.0050	0.25	40.55	0.10	4.09	2.57	3.18	4.87
	18	3.99	1.06	29.34	0.0217	0.0335	0.0315	0.0045	0.21	36.08	0.10	3.64	1.78	3.17	3.86
	19	4.22	0.97	17.52	0.0252	0.0436	0.0449	0.0041	0.16	31.23	0.10	3.15	0.95	3.00	3.06
	20	4.45	0.93	3.96	0.0369	0.0531	0.0573	0.0039	0.11	25.85	0.10	2.61	0.18	2.60	2.42
Horizontal (Top)	21	5.84	1.62	55.19	0.0154	0.0175	0.0108	0.0069	0.45	55.86	0.13	7.38	-6.06	4.21	11.96
	22	5.84	1.62	55.19	0.0154	0.0175	0.0108	0.0069	0.45	55.86	0.13	7.38	-6.06	4.21	11.96
	23	5.84	1.62	55.19	0.0154	0.0175	0.0108	0.0069	0.45	55.86	0.13	7.38	-6.06	4.21	11.96
	24	5.84	1.62	55.19	0.0154	0.0175	0.0108	0.0069	0.45	55.86	0.13	7.38	-6.06	4.21	11.96
	25	5.84	1.62	55.19	0.0154	0.0175	0.0108	0.0069	0.45	55.86	0.13	7.38	-6.06	4.21	11.96
	26	5.84	1.62	55.19	0.0154	0.0175	0.0108	0.0069	0.45	55.86	0.13	7.38	-6.06	4.21	11.96
	27	5.84	1.62	55.19	0.0154	0.0175	0.0108	0.0069	0.45	55.86	0.13	7.38	-6.06	4.21	11.96
	28	5.84	1.62	55.19	0.0154	0.0175	0.0108	0.0069	0.45	55.86	0.13	7.38	-6.06	4.21	11.96
	29	5.84	1.62	55.19	0.0154	0.0175	0.0108	0.0069	0.45	55.86	0.13	7.38	-6.06	4.21	11.96
	30	5.84	1.62	55.19	0.0154	0.0175	0.0108	0.0069	0.45	55.86	0.13	7.38	-6.06	4.21	11.96
Horizontal (Bottom)	31	5.22	1.16	37.34	0.0154	0.0175	0.0150	0.0049	0.32	51.70	0.10	4.97	-3.01	3.95	5.79
	32	5.22	1.16	37.34	0.0154	0.0175	0.0150	0.0049	0.32	51.70	0.10	4.97	-3.01	3.95	5.79
	33	5.22	1.16	37.34	0.0154	0.0175	0.0150	0.0049	0.32	51.70	0.10	4.97	-3.01	3.95	5.79
	34	5.22	1.16	37.34	0.0154	0.0175	0.0150	0.0049	0.32	51.70	0.10	4.97	-3.01	3.95	5.79
	35	5.22	1.16	37.34	0.0154	0.0175	0.0150	0.0049	0.32	51.70	0.10	4.97	-3.01	3.95	5.79
	36	5.22	1.16	37.34	0.0154	0.0175	0.0150	0.0049	0.32	51.70	0.10	4.97	-3.01	3.95	5.79
	37	5.22	1.16	37.34	0.0154	0.0175	0.0150	0.0049	0.32	51.70	0.10	4.97	-3.01	3.95	5.79
	38	5.22	1.16	37.34	0.0154	0.0175	0.0150	0.0049	0.32	51.70	0.10	4.97	-3.01	3.95	5.79
	39	5.22	1.16	37.34	0.0154	0.0175	0.0150	0.0049	0.32	51.70	0.10	4.97	-3.01	3.95	5.79
	40	5.22	1.16	37.34	0.0154	0.0175	0.0150	0.0049	0.32	51.70	0.10	4.97	-3.01	3.95	5.79

$R_{nW} := 126.4\ \textit{kip}$

$R_n = 126.4$ kip $\quad \Sigma F_x = 0.00$ kip

$I_{cx} = -0.926$ in. $\quad \Sigma F_y = 0.00$ kip

$I_{cy} = 4.513$ in. $\quad \Sigma M_{IC} = 0.00$ kip.in

LRFD	**ASD**
$\phi := 0.75$	$\Omega := 2.0$
$\phi \cdot R_{nW} = 94.8\ \textit{kip}$	$\frac{R_{nW}}{\Omega} = 63.2\ \textit{kip}$
$R_u = 78\ \textit{kip}$	$R_a = 55\ \textit{kip}$
$\phi \cdot R_{nW} > R_u$ **o.k.**	$\frac{R_{nW}}{\Omega} > R_a$ **o.k.**

Flange Bending Limit State

Calculate the distance between the pairs of yield lines 'a' using Equation 4-1

$a := 0.75 \cdot k_1 - E_n = 1.078$ ***in***

Calculate the 'b' dimension of the yield lines using Equation 4-2

$b. := l_b + 0.25 \cdot b_f = 6.243$ ***in***

Calculate the flange bending capacity using Equation 4-7

$R_{nFB} := \frac{t_f^{\,2}}{a} \cdot F_y \cdot b. = 99.1$ ***kip***

LRFD	**ASD**
$\phi := 0.9$	$\Omega := 1.67$
$\phi \cdot R_{nFB} = 89.2$ ***kip***	$\frac{R_{nFB}}{\Omega} = 59.3$ ***kip***
$R_u = 78$ ***kip***	$R_a = 55$ ***kip***
$\phi \cdot R_{nFB} > R_u$ **o.k.**	$\frac{R_{nFB}}{\Omega} > R_a$ **o.k.**

Alternatively, using Table 10-E:

$\phi \cdot R_{nFB} = 89.2$ ***kip***

$\frac{R_{nFB}}{\Omega} = 59.3$ ***kip***

Angle Shear Limit State

Calculate the shear capacity of the angles in accordance with AISC Spec G3:

$k_v := 1.2$

$E := 29000$ ***ksi***

$$C_{v2} := \text{if } \frac{b}{t} \le 1.1 \cdot \sqrt{\frac{k_v \cdot E}{F_y}} \quad \| \quad 1.0 \quad \text{else if } \frac{b}{t} \le 1.37 \cdot \sqrt{\frac{k_v \cdot E}{F_y}} \quad \| \quad \frac{1.1 \cdot \sqrt{\frac{k_v \cdot E}{F_y}}}{\frac{b}{t}} \quad \text{else} \quad \| \quad \frac{1.51 \cdot k_v \cdot E}{\left(\frac{b}{t}\right)^2 \cdot F_y} = 1.0$$

$R_{nAV} := 2 \cdot \left(0.6 \cdot F_y \cdot b \cdot t \cdot C_{v2}\right) = 112.5$ ***kip***

LRFD	**ASD**
$\phi := 0.9$	$\Omega := 1.67$
$\phi \cdot R_{nAV} = 101.3$ ***kip***	$\frac{R_{nAV}}{\Omega} = 67.4$ ***kip***
$R_u = 78$ ***kip***	$R_a = 55$ ***kip***
$\phi \cdot R_{nAV} > R_u$ **o.k.**	$\frac{R_{nAV}}{\Omega} > R_a$ **o.k.**

Alternatively, using Table 10-E:

$\phi \cdot R_{nAV} = 101.3$ ***kip***

$\frac{R_{nAV}}{\Omega} = 67.4$ ***kip***

Girder Shear Limit State

Calculate the shear capacity of the girder in accordance with AISC Spec G2 or Equation 4-8

Depth of cope $d_c := 2.0$ ***in***

Beam depth at the cope $h_c := d - d_c = 21.7$ ***in***

$C_{v1} := 1.0$

$R_{nBV} := 0.6 \cdot F_y \cdot h_c \cdot t_w \cdot C_{v1} = 270.17$ ***kip***

LRFD	ASD
$\phi := 0.90$	$\Omega := 1.67$
$\phi \cdot R_{nBV} = 243.15$ ***kip***	$\frac{R_{nBV}}{\Omega} = 161.78$ ***kip***
$R_u = 78$ ***kip***	$R_a = 55$ ***kip***
$\phi \cdot R_{nBV} > R_u$ **o.k.**	$\frac{R_{nBV}}{\Omega} > R_a$ **o.k.**

Bolt Tension, Including Prying Action

Calculate the maximum bolt tension corresponding to the flange bending limit state and compare it with the available tensile strength per bolt.

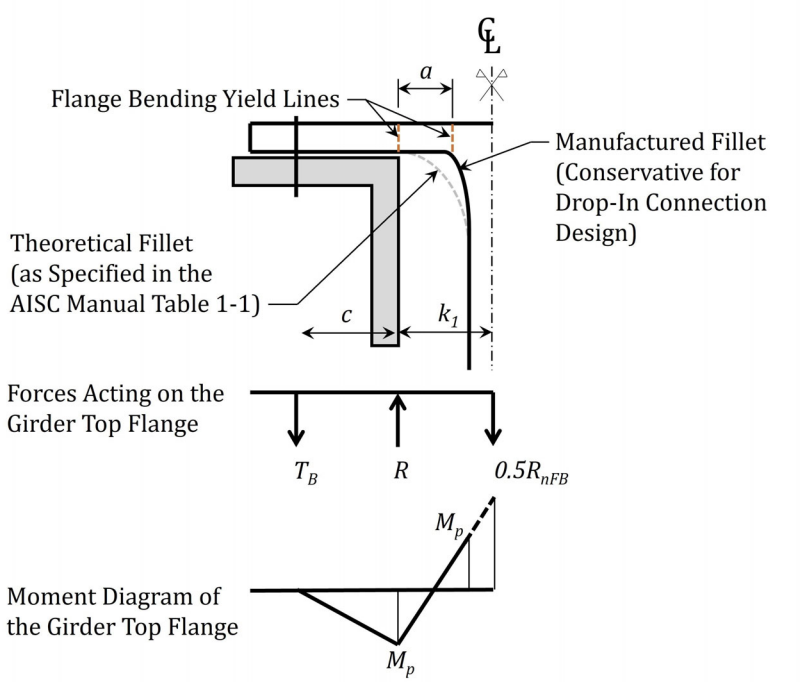

It should be noted that angle encroachment is not shown in the diagram.

The distance from the bolt center line to the face of the angle:

$$c := \left(0.5 \cdot b_f\right) - l_{eb} - k_1 - E_n = 1.92 \text{ in}$$

$$M_p := \frac{t_f^{\,2}}{4} \cdot F_y = 4.28 \text{ kip} \cdot \frac{\text{in}}{\text{in}} \qquad \text{Equation 4-6}$$

Tension force per bolt when flange bending limit state is reached:

$T_B := \frac{M_p \cdot b}{c} = 13.35$ ***kip***

$R_{u\_TB} := T_B = 13.35$ ***kip***

$R_{a\_TB} := R_{u\_TB} \cdot \frac{R_a}{R_u} = 9.41$ ***kip***

Nominal tensile strength of group A bolts (e.g., A325), AISC Spec. Table 3.2

$F_{nt} := 90$ ***ksi***

Area of 7/8" bolt, AISC Table 7-17

$A_b := 0.601$ ***in***^{2}

$R_{nBT} := F_{nt} \cdot A_b = 54.09$ ***kip***

Check if the bolt has sufficient strength to support the load corresponding to the flange bending limit state.

LRFD	**ASD**
$\phi := 0.75$	$\Omega := 2.00$
$\phi \cdot R_{nBT} = 40.57$ ***kip***	$\frac{R_{nBT}}{\Omega} = 27.05$ ***kip***
$R_{u\_TB} = 13.35$ ***kip***	$R_{a\_TB} = 9.41$ ***kip***
$\phi \cdot R_{nBT} > R_{u\_TB}$ **o.k.**	$\frac{R_{nBT}}{\Omega} > R_{a\_TB}$ **o.k.**

Conclusion

The connection is found to be adequate as given for the applied loads.

Example F.2: Drop-In Connection - Structural Integrity Check

Given:

Verify the drop-in top flange connection from Example F.1, as shown in Figure F1, for the structural integrity provisions of AISC *Specification* Section B3.9. The connection is verified as a beam and girder end connection and as an end connection of a member bracing a column. Note that these checks are necessary when designing for structural integrity is required by the applicable building code.

Solution:

From AISC Specification Section B3.9(b), the required axial tensile strength is:

LRFD	ASD
$T_u := \max\left(\frac{2}{3} \cdot R_u, 10\ \textit{kip}\right) = 52\ \textit{kip}$	$T_a := \max\left(R_a, 10\ \textit{kip}\right) = 55\ \textit{kip}$

Bolt Shear

From AISC *Specification* Section J3.6, the nominal bolt shear strength is:

$F_{nv} := 54\ \textit{ksi}$ AISC Specification Table J3.2 (Group A bolts)
$n := 2$ Number of bolts
$A_b = 0.601\ \textit{in}^2$ Area of 7/8" bolt

$T_{n1} := n \cdot F_{nv} \cdot A_b = 64.9\ \textit{kip}$

Bolt Bearing and Tearout

From AISC Specification Section B3.9, inelastic deformations of the connection are permitted to satisfy structural integrity requirements; therefore, AISC Specification Equations J3-6b and J3-6d are used to determine the nominal bearing and tear-out strength. By inspection, bolt bearing and tearout will control the angle.
For bolt bearing on the angle:

$d_{bolt} := \frac{7}{8}\ \textit{in}$

$T_{n2} := n \cdot 3.0 \cdot d_{bolt} \cdot t \cdot F_u = 106.6\ \textit{kip}$ (from Spec. Eq. J3-6b)

For bolt tearout on the angle:

From AISC *Specification* Table J3.3, the hole diameter in the direction of loading for a 7/8-in. diameter bolt with a short slot in the transverse direction is:

$$d_h := \frac{15}{16}\ in$$

$$l_c := \left(0.5 \cdot l_b\right) - \left(0.5 \cdot \left(d_h + \frac{1}{16}\ in\right)\right) = 1.5\ in \qquad \text{(from Spec. Eq. J3-6d)}$$

$$T_{n3} := n \cdot 1.5 \cdot l_c \cdot t \cdot F_u = 91.4\ kip$$

Block Shear Rupture

By comparison of the seat angle length and flange width, block rupture of the beam flange will control. The block shear rupture failure path is shown. From AISC *Specification* Section J4.3, the available block shear rupture strength of the beam flange is determined as follows (account for a possible 1/4-in. beam underrun.)

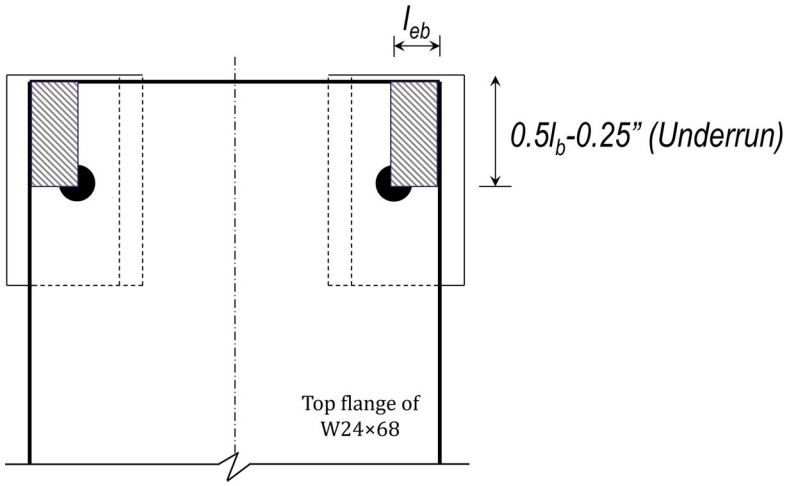

$$A_{gv} := 2 \cdot \left(\left(0.5\ l_b\right) - 0.25\ in\right) \cdot t_f = 2.05\ in^2 \qquad \text{gross area subject to shear}$$

$$A_{nv} := 2 \cdot \left(\left(0.5\ l_b\right) - 0.25\ in - \left(0.5 \cdot \left(d_h + \frac{1}{16}\ in\right)\right)\right) \cdot t_f = 1.46\ in^2 \qquad \text{net area subject to shear}$$

$$A_{nt} := 2 \cdot \left(l_{eb} - \left(0.5 \cdot \left(d_h + \frac{1}{16}\ in\right)\right)\right) \cdot t_f = 0.731\ in^2 \qquad \text{net area subject to tension}$$

$$U_{bs} := 1.0$$

$$T_{n4} := min\left(\left(0.6 \cdot F_u \cdot A_{nv}\right) + \left(U_{bs} \cdot F_u \cdot A_{nt}\right), \left(0.6 \cdot F_y \cdot A_{gv}\right) + \left(U_{bs} \cdot F_u \cdot A_{nt}\right)\right) = 104.6\ kip$$

Weld Strength

From AISC Specification Section J2.4, the nominal tensile strength of the weld is determined as follows:

$F_{EXX} := 70\ ksi$

$\theta := 90\ deg$ Angle between longitudinal axis of weld and the direction of resultant force.

$F_{nw} := 0.6 \cdot F_{EXX} \cdot \left(1 + 0.5 \cdot \sin\left(\theta\right)^{1.5}\right) = 63\ ksi$ (*Spec.* Eq. J2-5)

$w := \frac{5}{16}\ in$ weld size

$l_w := 19.45\ in$ total length of weld accounting for termination equal to the weld size on each weld line.

The throat dimension is used to calculate the effective fillet weld

$A_{we} := \frac{w}{\sqrt{2}} \cdot l_w = 4.298\ in^2$

$T_{n5} := F_{nw} \cdot A_{we} = 270.8\ kip$

Nominal tensile Strength

The controlling nominal tensile strength is the minimum of the previously calculated:

$T_n := min\left(T_{n1}, T_{n2}, T_{n3}, T_{n4}, T_{n5}\right) = 64.9\ kip$

LRFD		**ASD**	
$T_u = 52\ kip$ $T_n = 64.9\ kip$		$T_a = 55\ kip$ $T_n = 64.9\ kip$	
$T_n > T_u$	**o.k.**	$T_n > T_u$	**o.k.**

Column Bracing

From AISC *Specification* Section B3.9(c), the minimum axial tension strength for the connection of a member bracing a column is equal to 1% of two-thirds of the required column axial strength for LRFD and equal to 1% of the required column axial for ASD. These requirements are evaluated independently from other strength requirements.

The maximum column axial force this connection is able to brace is determined as follows:

LRFD	ASD
$T_n \geq 0.01\left(\frac{2}{3} P_u\right)$	$T_n \geq 0.01\left(\frac{2}{3} P_u\right)$
Solving for the column axial force:	Solving for the column axial force:
$P_u \leq 100\left(\frac{3}{2} T_n\right)$	$P_a \leq 100\ T_n$
$100\left(\frac{3}{2} T_n\right) = 9736\ \boldsymbol{kip}$	$100\ T_n = 6491\ \boldsymbol{kip}$

As long as the required column axial strength is less than or equal to the above P_u or P_a, this connection is an adequate column brace.

130 E Randolph St, Ste 2000
Chicago, IL 60601
312.670.2400
www.aisc.org

Research Report No. AISC-IRR-NFS-2025-01